SMALL HYBRID SOLAR THERMAL ELECTRIC PLANTS WITH GAS TURBINES: "MINI" POWER TOWER (2-4 MWE) VS. DISH/BRAYTON

Theodore Caplow Jr.

PU/CEES Report No. 308

June 1998

A Thesis presented to the Faculty of Princeton University in partial fulfillment of the Master of Science Degree

Center for Energy and Environmental Studies
School of Engineering and Applied Science
Princeton University
Princeton, NJ 08544-5263

Financial support for this research was provided by the W. Alton Jones Foundation, the Energy Foundation, and the Link Foundation.

SMALL HYBRID SOLAR THERMAL ELECTRIC PLANTS WITH GAS TURBINES:
"MINI" POWER TOWER (2-4 MWE) VS. DISH/BRAYTON

Theodore Caplow Jr.

A THESIS PRESENTED TO THE
FACULTY OF PRINCETON UNIVERSTY
IN PARTIAL FULFILLMENT OF
THE MASTER OF SCIENCE DEGREE

JUNE 1998

ABSTRACT:

A solar thermal electric plant (STEP) contains a collector which gathers sunlight, a receiver which transforms it into heat, and an engine which produces electricity. Devices in this study share the following characteristics: high solar concentration, a gas turbine co-fired by natural gas, no thermal storage, and relatively small size. Two systems are examined in detail: a 25 kWe dish/engine system and a 2-4 MWe "mini power tower" (MPT). The latter design is presented here for the first time, although it borrows components from existing systems.

Dish / engine systems direct sunlight to the focus of a parabolic dish, where a small, durable engine produces electricity. A new initiative by Allied Signal focuses on a recuperated Brayton cycle engine. This Allied Signal dish / Brayton system (ASDB) is adapted here to share the same collector modules as the MPT.

A "power-tower" includes a field of "heliostats": mirrors which track the sun on two axes, reflecting sunlight up to a receiver mounted on a central tower. In the MPT, a gas turbine is also located on the tower, either recuperated or attached to a cogeneration system for absorption chilling/heating. The MPT owes its high efficiency to small size, a secondary concentrator (TERC), and a windowed (DIAPR-type) receiver. Heliostats for the MPT are based on a modular drum-type design.

The solar fraction, net solar-to-electric efficiency, and levelized energy cost (LEC) is calculated for both the ASDB and the MPT at four locations in the USA. A gas-only case is included. The MPT appears cheaper than the ASDB, although less versatile. Cogeneration benefits are dependent upon climate; in favorable locations cogeneration may be cheaper than recuperation. MPT solar fraction is 15-30% vs. ASDB 25-32%; MPT net efficiency is ~20% vs. ASDB ~22%. LEC (in cents/kwh) can be as low as 4.15 for the MPT, 4.37 for the ASDB, and 3.87 for a 2-4 MWe gas-only system (gas price of $10/MWht; somewhat below today's prices.). The MPT system begins to break even with gas-only systems at a gas price of $13.50/MWht with base case assumptions. An experience-curve analysis shows that the cost of buying down the MPT to economic parity with gas could be as low as $50 million. A bonus for small-scale (distributed) production is considered, but *not* included in these figures.

ACKNOWLEDGMENTS:

The author wishes to express his appreciation to Robert Socolow of Princeton's CEES, for his encouragement and support as an academic advisor. Thanks are also due at CEES to Robert Williams, for his general expertise as well as his emphasis on R&D price targets; to Joan Ogden, for support of investigations in solar geometry and absorption chilling; and to Tom Kreutz and Eric Larson, for their valuable assistance with gas turbines. Stefano Consonni, formerly a student here and now a professor at the Politecnico di Milano, also provided indispensable gas turbine advice. Beyond Princeton, this study owes a debt to Mike Thompson at The Trane Company for data and experience with chiller units; to Richard Wenglarz at the Allison Engine Company for operating and cost parameters for gas turbines; to Tom Mancini at Sandia Labs for fundamental input on the ASDB model and SAIC heliostats; to Jacob Karni at the Weizmann Institute for information on the DIAPR receiver and SCOT system; and, with particular emphasis, to Ari Rabl at the Ecole des Mines in Paris for his terrific book and helpful reviewing. Above all, the author wishes to recognize the forbearance and constant support of his wife, Pascale.

Research for this thesis was conducted with support of a Link Foundation Graduate Energy Fellowship, which is gratefully acknowledged. In addition, the author's first year at Princeton was supported by a Guggenheim Fellowship within the Department of Mechanical and Aerospace Engineering.

This thesis carries the number **3026-T** in the records of the Department of Mechanical and Aerospace Engineering.

CONTENTS:

LIST OF TABLES:

LIST OF FIGURES:

PRINCIPLE ACRONYMS AND ABBREVIATIONS:

STEP	Solar Thermal Electric Plant; e.g. D/E, LDA, or CR system
D/E	Dish / Engine System; e.g. Dish / Stirling or Dish / Brayton
ASDB	Allied Signal's Dish/Brayton System, currently under commercial development
CR	Central Receiver System; e.g. Solar Two
PT	Power Tower; another term for a central receiver system.
MPT	Mini Power Tower, a CR proposed here in a hybrid configuration producing 2-4 MWe
LDA	Linked-Dish Array; e.g. closed-cycle methane or open cycle direct Brayton.
OLAA	Open Loop Air Array; an LDA using air as a heat transfer fluid; the air is not recycled
GT	Gas Turbine
RGT	Regenerated Gas Turbine
CC	Combined Cycle; i.e. a GT with a downstream steam generator and ST.
SF	Solar Fraction, the percentage of electrical output which originated as solar radiation
CF	Capacity Factor, the output of a system divided by its output at a constant 100% load
Cogen	Cogeneration, referring to a plant in which waste heat is recovered for another purpose
Recup	Recuperation, referring to an engine in which waste heat displaces some of the fuel
Hybrid	Co-fired by two different fuelss; here, this refers to a STEP co-fired with natural gas
Solar-Assisted	Another way of describing a hybrid plant
Gas-Assisted	Another way of describing a hybrid plant

CHAPTER 1:
INTRODUCTION TO SOLAR THERMAL ELECTRIC PLANTS

I.1 Solar Power and Solar Thermal Electric Plants

The pace at which the renewable energy market share grows may in part determine the degree to which humanity is able to maintain a safe habitat for itself. Certain fossil-fueled pollution processes, including global warming, may be non-linear or possess non-linear feedback mechanisms. By the time the effects are visible, it may be too late to undo the damage through commensurate changes in the relative prices of fossil and renewable fuels. Thus there is a mandate within the community of concerned citizens to drive the advance of renewable technologies as quickly as possible. While most forecasters see important roles for a broad variety of these technologies, solar power seems destined to be the leading "green" energy source in the 21st century.

"Solar power" in this context refers to those technologies which seek to extract electricity, heat, and chemical energy directly from the sun's rays, without relying upon a short-term (e.g. biomass) or long-term (e.g. fossil fuel) ecological conversion, or upon geophysical processes (e.g. wind). Solar is the leading candidate for widespread renewable energy use for one principal reason: the resource (sunlight) is larger, more accessible, and more evenly distributed than any other. Despite this abundance, however, solar power is currently unable to compete economically with fossil fuels on a large scale. Rather than passively awaiting the uncertain hour when the price of a barrel of oil is pushed upward by supply instability (due to political causes and/or resource scarcity), or the equally uncertain (but probably nearer) hour when society agrees to charge the true cost of pollution back to its producers, the solar power community is making every effort to bring the price of a barrel of sun power down. To do this as quickly as possible, we must build machines which are both cheaper and more efficient than today's generation

of solar collectors. The current study examines this challenge within the corner of the renewable energy world occupied by solar thermal electric plants.

In its basic form, a solar thermal electric plant (STEP) seeks to convert sunlight into heat and then into electricity. As such, it may be distinguished from a photovoltaic power plant, in which sunlight is converted directly to electricity in special materials at the molecular level, or from a solar heating plant, in which the heat derived from sunlight is itself the desired output. Another type of solar device, the solar chemical plant, stores the light energy in chemical bonds, producing a fuel which may then be used in a variety of applications, including the reversal of the original solar-driven reaction. If this application is chosen, and the heat released thereby is used to produce electricity, then this chemical plant is really a STEP with a closed-loop chemical circuit within it. There may be a number of reasons why this configuration is desirable; prominent among these is the ability to store the solar energy in the fuel until it is needed. Stored energy allows the heat engine to run at full-load for a longer period of time, simultaneously increasing capacity factor and reducing performance penalties associated with part-load operation. Furthermore, the heat engine which must be constructed for a given solar installation may be smaller if storage is used to defer conversion of any excess energy to a later time. Many of the operating characteristics of plants with chemical storage also apply to plants with thermal storage, whether in a liquid (e.g. molten salt) or solid (e.g. rocks) medium.

This study is concerned with a class of STEPs known as *hybrids*, in which a fuel is combusted to lend additional heat. This fuel may be a fossil resource (natural gas, coal, diesel oil, etc.) or another renewable resource such as biomass feedstock. For the cases considered here, natural gas (also referred to here as just "gas") is the fuel. Gas possesses several properties which together create excellent compatibility with STEPs; these include ready abundance, growing popularity, low prices, and combustion properties which lend themselves to use in a Brayton cycle.

The design requirements for gas-hybrid STEPs are very similar to those for solar-only versions, with a few important changes in priority.[1] First, the heat engine efficiency must be as high as possible, especially when the plant is running mostly or entirely on the supplementary gas. In a solar-only STEP, a lower heat engine efficiency may be compensated for by higher optical efficiency – as is somewhat the case for dish / engine systems (see below) – but in a hybrid system, the gas-fired fraction of the total energy output is unaffected by the optical efficiency. The large size of this fraction (50% - 90%) mandates that top priority be given to the heat engine efficiency; hybrid systems with heat engine efficiencies far below those found in gas-only electrical plants will offer poor competition to those plants regardless of their environmental credentials. Fortunately, the high temperatures reached by certain types of STEPs, combined with advances in gas turbines over the last several decades, allow the design of hybrid plants with competitive heat engine efficiencies. In traditional power generation, the larger the heat engine, the more efficient it becomes. This trend is not so clearly exhibited by STEPs, however, and one goal of this study is to show that effective hybrid designs are possible without the necessity of building at a very large scale.

As a second consequence of hybridizing a STEP design, thermal storage becomes relatively unimportant. Any deficiencies in solar flux are filled in by gas combustion. Thus the part-load characteristics of the heat engine are not a factor, and the only effect of thermal storage is to boost the solar fraction (fraction of the total energy output which began as sunlight). Storage creates such a boost because the amount of sunlight collected can be larger than the amount used, with the excess used at night. However, with gas available as a backup, such an arrangement is advantageous only if the gas is *more* expensive to burn than the solar energy is to collect and store. At current cost levels, gas is cheaper than solar energy, and storage is not considered in the systems presented here. However, the cost analysis of this study seeks to identify certain price targets for solar equipment which, when reached, will push the price of solar energy below the price of

[1] In addition to the operational differences in the text, it should also be noted that hybrid plants require access to a supply line of natural gas; thus deployment in remote areas may incur significant or even unacceptable costs depending upon local conditions.

gas. When solar system prices reach such levels, the addition of storage capabilities to hybrid plants may prove advantageous. In the meantime, the objective is to create a hybrid plant within which the cost of solar energy is as close as possible to the cost of gas, while offering considerable environmental and risk-avoidance benefits. These hybridization considerations are discussed in more detail in section **I.2.2**.

I.1.1 Components of a Solar Thermal Electric Plant

Schematically, a STEP must have the following elements:

Collector, by means of which solar light rays are intercepted and (for all STEPs considered here) concentrated onto a smaller target than the collector itself

Receiver, in which the light is converted into heat, and in some cases, chemical energy. The heat and/or chemical energy is carried away from the receiver by a working fluid. Designs discussed or mentioned here use all of the following as a working fluid: air, steam, oil, syngas, molten salt, methane, carbon dioxide, hydrogen, helium. However, the primary focus is on systems employing methane, syngas, and air.

Transport, by which the heat energy or chemical energy in the working fluid is carried from the receiver to the heat engine. This allows more fluid to be heated in the receiver. After passage through the heat engine (and through any of the three "optional" elements listed in the next section), the transport system returns the working fluid to the receiver, if the system is of the "closed-loop" type. In an "open-loop" STEP, the working fluid is discarded downstream of the heat engine (or waste heat recovery unit in cogen applications). The designs modeled here are all open loop.

Heat Engine, in which the working fluid (or a second heat carrying fluid into which the energy from the first fluid has been transferred) is expanded to produce work in the form of motive force. In this study, the heat engines are gas turbines.

Generator, in which the motive force from the heat engine is used to produce electricity.

In addition, some of the STEPs considered here contain some or all of the following "optional" elements:

Secondary Collector, mounted between the primary collector and the receiver, and typically much smaller than the primary collector. The secondary collector provides additional focusing of the sun's rays, allowing the aperture of the receiver to be reduced.

Heat Exchangers, in which the working fluid gives up some or all of the sensible heat acquired in the receiver to another working fluid, or to a thermal storage medium.

Thermal Storage, in which the thermal energy is stored in sensible form until it is needed. Thermal storage may consist of the working fluid itself in a container, or it may consist of another material which is sequentially heated and cooled by the working fluid.

Supplementary Burner, in which a fuel is combusted to add heat to the working fluid before it is passed to the heat engine. Certain STEP designs may have separate working fluids for the solar and fuel inputs, as when solar energy is used to supplement the heat recovery steam generators on a combined cycle plant but is not used to heat the turbine inlet air. Arrangements of this kind are not practical at the small scales considered in this study, and for all systems considered here, the same working fluid (air) is used to carry energy derived from both solar and fuel sources. The burner is always downstream of the solar receiver, because the efficiency of the latter is higher at lower temperatures whereas the efficiency of the former is largely insensitive to (or even increases with) temperature.

Chemical Storage, in which the energy is stored in chemical form until it is needed. Chemical storage must be preceded by an endothermic chemical reaction in which energy is absorbed. When the energy is needed to produce electricity, the working fluid is passed through a reactor where a reversing, exothermic reaction takes place.

Chemical Reactors, in which energy is exchanged between thermal and chemical forms. In a closed-loop chemical STEP, one reactor is incorporated into the receiver, resulting in a chemical conversion of the working fluid as it passes through. A second chemical reactor is necessary to reverse this process and release the stored heat.

Figure I-1:
Components of a Solar Thermal Electric Plant
Optional elements indicated by italics

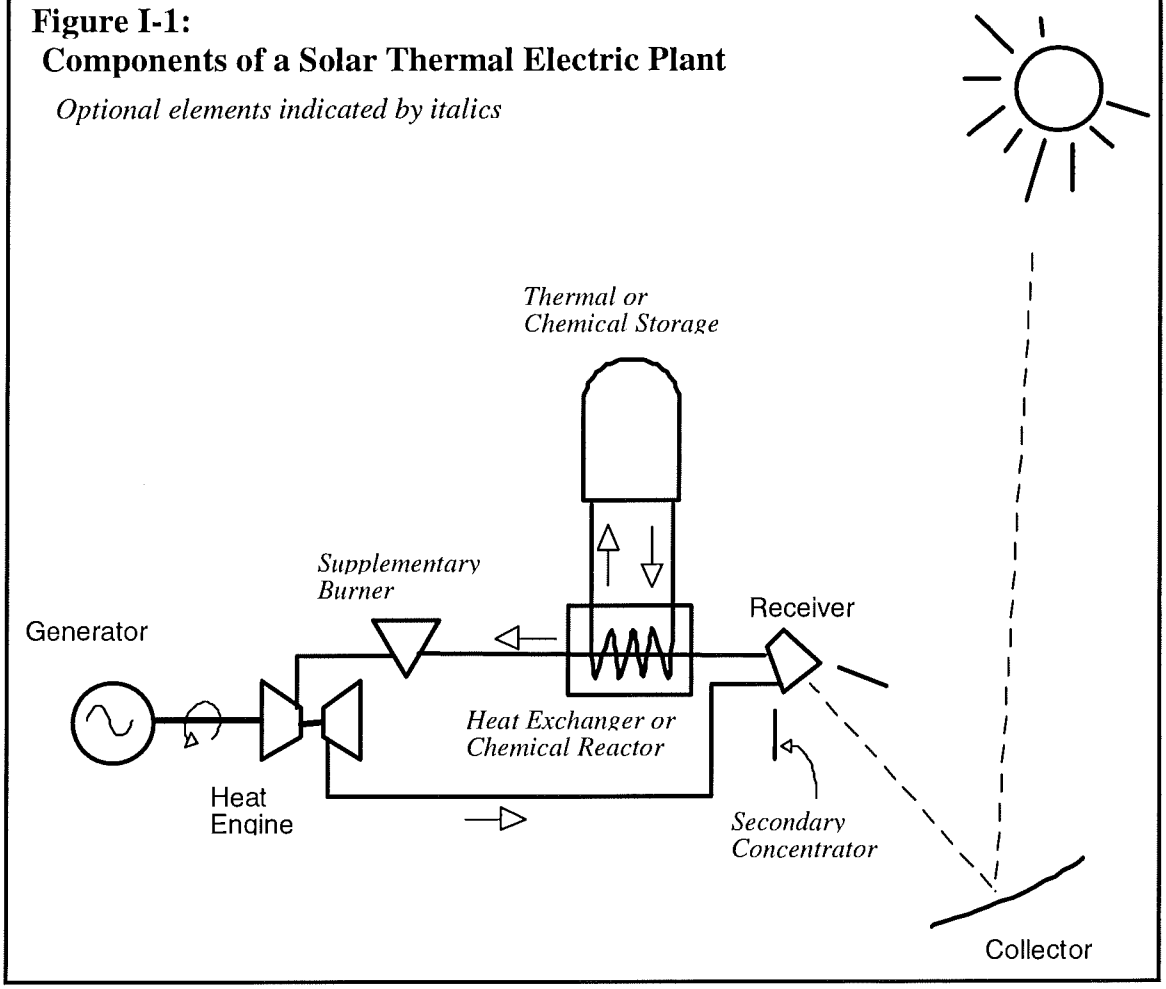

I.1.2 Variety of STEP Designs

STEPs are usually divided into three categories according to their collectors: parabolic trough, heliostat field, and parabolic dish. All of these designs must track the sun along either one (troughs) or two (dishes; heliostats) axes. The trough is a two-dimensional concentrator in which the working fluid flows axially within a tube located along the line of focus. Trough systems operate at lower temperatures and efficiencies, and are not covered here due to their incompatibility with hybrid gas turbines plants.[2] The heliostat field is three-dimensional concentrating system which acts as a giant fresnel reflector, redirecting sun rays to a centrally located tower. The parabolic dish is the most optically efficient; these units are always pointed directly at the solar disk and redirect its rays to a "point" focus (more accurately, a small region of space near the focal point of the paraboloid). In most dish designs currently under development, an integrated receiver / heat engine is placed in this focal region, and the system has no transport as defined above (the only energy transported off-dish is already in electrical form). The linked-array design considered briefly herein modifies this configuration by replacing the dish-mounted heat engine with a much larger (and potentially more efficient) centrally located heat engine. This change requires the addition of a thermal transport network to bring the heated (or chemically charged) working fluid to the central location, and (if necessary) to return the recycled working fluid to the dish. Implicit in this idea is an "array" of multiple dishes all linked together into a single power plant.[3]

By contrast, photovoltaic systems are substantially different, both technically and operationally, from STEPs, and thus are mentioned here only briefly. However, this study is undertaken with a keen awareness that PV yields the same end product and offers

[2] Although troughs could be used with gas turbines, their low temperatures would require a large amount of gas boosting to reach turbine inlet conditions. This boosting would lower the daytime solar fraction significantly; when combined with nighttime operation, the annual solar fraction might be so low as to make the solar portion of the plants nearly irrelevant. Furthermore, existing large scale trough systems use oil or water as a heat transfer fluid; in order to employ a gas turbine, a heat exchanger would be necessary, adding further costs and thermal losses. The SEGS trough systems in California use steam turbines.

greater flexibility of plant scale and application area. Indeed, the galloping advances in the PV field threaten to put STEPs out of business entirely, unless STEP systems can demonstrate a concrete advantage to justify their operating complexity. The capability for cogeneration could provide such an advantage in certain applications. Nonetheless, net conversion efficiency may be decisive in the long run. The linked-dish array (LDA) was included here because, in theory, it can yield net solar-to-electric conversion efficiencies well beyond those foreseen for commercial PV modules in the next several decades. Upon analysis, the advantages of the LDA appear unlikely to materialize in practice, both of the other systems modeled (dish / Brayton and mini power tower) appear to offer sufficiently high solar conversion efficiencies at low enough costs to justify the continued pursuit of solar thermal irrespective of current PV advances.

I.1.3 Dish / Engine Systems

Dish / engine (D/E) systems include one dish and one engine as a complete system for electric production. Several such units may be combined together in one place to create a "field" of D/E systems so as to benefit from economies in construction, land acquisition, maintenance, and electric power processing. These fields should not be confused with the linked-dish array (LDA) concept which is considered (but not pursued; see below) in this study. (In the LDA, the dishes are physically linked by a thermal transport system and a central heat engine replaces the engine at each dish.)

I.1.3.1 Choice of Heat Engine for Dish Systems

The R&D on D/E systems is currently divided into two approaches based upon the choice of heat engine; the engine chosen then dictates the form of the receiver and minor components. Stirling motors (usually four cylinders with a variable swashplate, but

[3] The "linked" moniker for the LDA indicates that the dishes are interdependent and that power is produced centrally; as opposed to a dish / engine field, which is simply a collection of independent D/E systems arranged in one place.

several designs exist) and miniature Brayton cycle regenerated gas turbines are both under active development. Although various steam and organic Rankine cycles have been evaluated, these are currently not part of mainstream R&D for D/E systems.

The leading heat engine for D/E applications is the Stirling motor. Dedicated and optimistic commercialization campaigns have been underway for at least fifteen years, but have encountered numerous difficulties, leading to a rash of program cancellations, reinstatements, and re-definitions. Nonetheless, very promising development efforts are currently nearing maturity in the United States (led by SAIC, Inc.), Germany, and Japan. This technology may be marketed commercially within two years (see, e.g., Beninga *et al* 1995).

An open, regenerated, Brayton cycle gas turbine offers comparable (or slightly lower) efficiency and two potential operating advantages when compared with the Stirling motor for D/E applications. First, it is believed that operating and maintenance (O&M) costs for the gas turbine will be lower. This view is grounded partly in recognition of the long lifetime enabled by the gas turbine's non-reciprocating motion and few moving parts, and partly in the perception that worldwide expertise and tooling are better adapted to the gas turbine than to the Stirling motor. The second Brayton cycle advantage stems from its ready adaptation to fuels other than sunlight. To an increasing extent, the solar thermal industry is looking to hybrid plants (as used here, "hybrid" means solar co-fired with fossil fuels or biogas) as a stepping stone to the future. This alliance is necessitated by the intermittent availability of the solar resource: a turbine burning natural gas at night can produce between three and four times as much energy per year as a solar-only turbine. Solar hybrid plants can be conceptualized as fossil fuel plants with "solar assistance'; seen this way, the solar energy is a fuel saving device, reducing the specific fuel consumption (and output of CO2 and other pollutants) by up to 25% in baseload plants without thermal storage; in plants with thermal storage or in peaking plants, this fuel reduction (called the "solar fraction") is unlimited.

Table I-1:
Typical Efficiency and Part-Load Efficiency of Stirling vs. Brayton Engines

	Stirling (20-40 kWe)		Micro Brayton (20-60 kWe)	
Load	*Efficiency Correction*	*Part-load Efficiency*	*Efficiency Correction*	*Part-load Efficiency*
100%	1.00	.370	1.00	.330
90%	.99	.366	.95	.352
80%	.98	.363	.88	.326
70%	.97	.359	.81	.300
60%	.96	.356	.72	.266
50%	.95	.352	.63	.233
40%	.94	.348	.54	.200
30%	.93	.344	.46	.170

Source: for Stirling: Schiel *et al* (1994); *for Brayton:* Gallup & Kesseli (1994)

The advantages of the Brayton cycle have not yet been conclusively demonstrated in practice, and Sandia laboratories in the United States is currently pursuing both Stirling cycle and Brayton cycle D/E programs. Proponents of the Stirling design point to the engine's somewhat higher efficiency and considerably better part-load performance (see table **I-1** above), and maintain that reliability and operating life has been greatly extended over the past decade to the point that these areas are no longer an obstacle. Moreover, the receiver of the Stirling engine has been fitted with a special shutter which, when closed, allows natural gas (or similar clean, gaseous fuel) to be burned in the receiver cavity, thus allowing hybrid operation. Proponents of the gas turbine note that the Stirling engine efficiency on gaseous fuel will not be equal to that of the turbine, which may be readily fitted with a conventional in-line combustor. Perhaps of greater importance is the compatability of this combustor with non-gaseous fuels such as diesel or biodiesel, a flexibility not incorporated into the current leading Stirling design. Hybrid operation on diesel may be critical for dissemination of these systems in remote, off-grid markets. As the next section seeks to demonstrate, small and single-dish installations in this market, where natural gas is less available than diesel, may have a much greater chance of success for D/E technology than large, grid-tied, plants co-fired on natural gas. In this latter market, a central receiver should have the competitive edge.

I.1.3.2 Relative Spheres of Advantage for Different Dish Systems

As the field matures, solar R&D is unlikely to converge to "a one design fits all" system. Different systems tailored for two distinct applications can be expected to emerge: grid-tied and off-grid. Similarly, a minimum of two designs will be required to satisfy different fueling modes: solar-only and hybrid. All four of these "modes" are distinct from one another:

Table I-2: General Application Modes for STEPs

	Solar Only	*Hybrid*
Grid Tied	?	?
Off-Grid	?	?

Over the long term, it is very unlikely that a single system design can be competitive in more than one of these four areas at once. This specialization is somewhat unique to STEPs; off-grid photovoltaic (PV) modules, for example, resemble their on-grid counterparts. (This flexibility results in part because PV modules are not subject to the same scale economies that STEPs are.) Thus while both of the current front-running U.S. D/E projects list *all four* of these application modes as possibilities, in reality the prototype designs of these systems are more promising in certain areas and less promising in others. The dish / Stirling concept may be competitive in the grid-tied solar only market or in the off-grid solar-only market, while the dish / Brayton cycle is promising for the off-grid solar-only market and the off-grid hybrid market. The Stirling motor is inappropriate for the off-grid hybrid market because it does not run as efficiently on non-gaseous fuels (e.g. diesel) as the Brayton engine. Conversely, the Brayton engine is unlikely to compete with the Stirling in the grid-tied solar only market, because of its poor part-load performance. (This deficiency is not an issue when the turbine is co-fired, because maximum load can be maintained) Note, however, that the Brayton engine may be competitive in the off-grid solar-only market, where its supposed longer lifetime and greater ease of use may outweigh its slightly inferior efficiency.

Table I-3: Most Promising Application Modes for Dish / Engine Systems

	Solar Only	*Hybrid*
Grid Tied	Stirling (good at part load)	Brayton? (see chaps. 3-5)
Off-Grid	Stirling (good at part load) Brayton (reliable; long-lived)	Brayton (easily hybridized)

Neither D/E system is perfectly suited for widespread deployment in the grid-tied hybrid market, because of the low efficiency with which D/E systems, either Stirling or Brayton, burn natural gas. By contrast, the mini-power tower (MPT) system introduced in the following section will use gas at a somewhat higher efficiency, and may therefore be preferable to D/E systems in the grid-tied hybrid market. In theory, the direct-air linked-dish array (LDA) design proposed here shares this advantage, but upon further analysis, various operational complications (discussed in sections **I.1.5** and appendix **D**) remove it from further consideration. However, chapters 3, 4 and 5 present modeling and results for both dish / Brayton and MPT systems.

I.1.4 Central Receivers (Power Towers) and the MPT

In the central receiver (CR), or power tower, design, the collection system and the receiver are not physically connected. The solar flux is redirected by a large number of mirrors ("heliostats") mounted on tracking supports and distributed over the ground near the base of a tower. The receiver is mounted at the top of the tower, or in the case of a two-stage system under development in Israel, at the base of the tower (a reflecting mirror is placed at the top to redirect the flux down to the receiver). CR designs do not track the sun as efficiently as dishes do,[4] because the heliostats and the receiver are stationary with respect to one another. Thus, while the heliostats have the same two-axis tracking

[4] The difference in sun-tracking ability between dishes and central receivers does not have to be as large as it is with current CR designs. The MPT design introduced here is substantially more optically efficient, nearly erasing the dish advantage. See section **V.5.4** for details.

equipment as a dish, they are *not* always pointed at the sun; rather, the normal to the mirrors must be pointed so as to exactly bisect the angle between the sun and the receiver as perceived at the mirror's surface. Only in this orientation will the flux, which is of course reflected at its angle of incidence, strike the receiver. When the sun is not high in the sky, the flux "sees" a fraction of the total mirror area; this fraction is equal to the cosine of the half-angle between the sun and the receiver. These "cosine losses" are important because heliostat cost is a large part of total cost, and is largely a function of the mirrored area.

I.1.4.1 Heliostats

The heliostats in a CR system may be of several designs, but in all cases the mirrors are mounted on short pedestals via a two-axis motorized tracking mechanism controlled by a central computer. Each heliostat consists of one or more "facets", which may in turn be composed of several separate, flat mirrors. The facets themselves may have a slight curvature (depending upon their size) so as to minimize their image at the receiver, but the primary focusing of the heliostat is achieved by "canting" the various facets so that together they form a concave lens.

The heliostats at Solar Two are of two similar types (Jones *et al* 1995), having 5 to 8 facets arranged on either side of the central pedestal; each facet consists of 3 or 4 flat mirrors. An alternative design with round facets is under active development by Science Applications International Corporation (SAIC 1997a). The SAIC heliostat has 22 round facets,[5] each of which is slightly concave, but once again the critical focusing step is the canting of the facets relative to the supporting base. The round facets consist of a thin stainless sheet stretched like a drum on either side of a steel hoop. The interior is evacuated; each facet is equipped with a control valve and a vacuum pump is

[5] SAIC is also developing an alternative heliostat with two giant round facets, one on either side of a central pedestal (Beninga 1997).

Figure I-2: SAIC Heliostat and Solar Two Heliostats

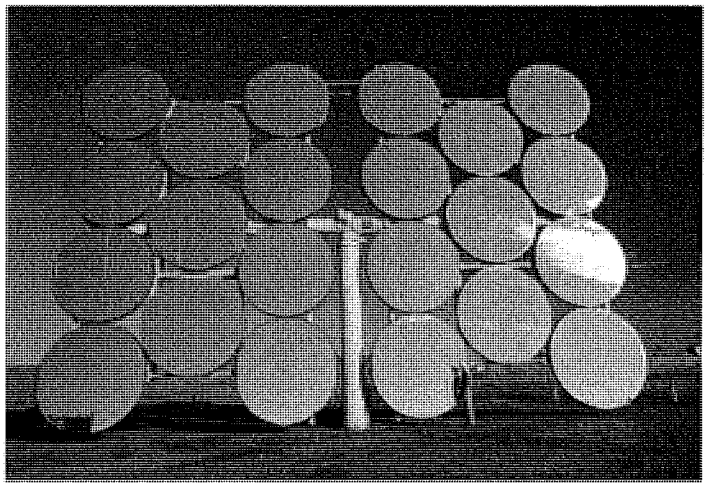

SAIC 22 Facet Drum-Type Heliostat
(Facets are ~3 meters in diameter)

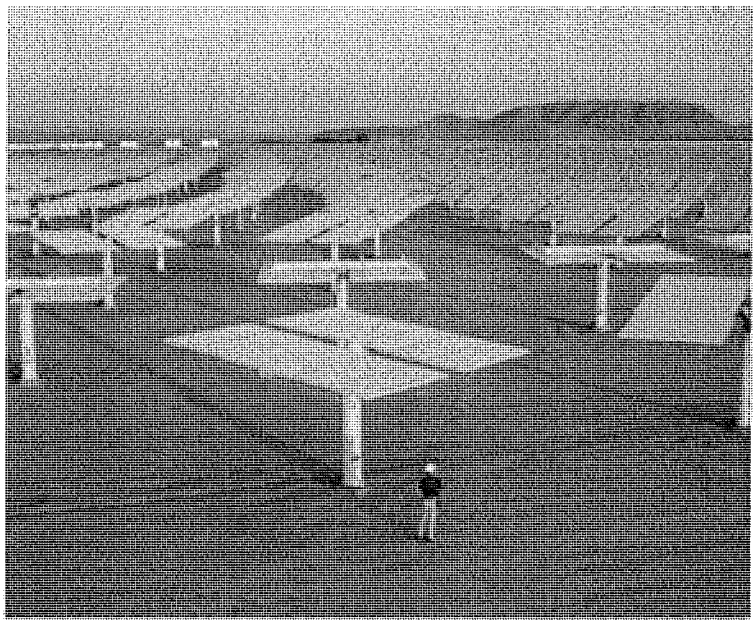

Solar Two Type Heliostats

incorporated into the heliostat support structure. Small (approximately 40 cm square),[6] thin mirrors are laminated to the front of each drum; these are flexible enough to allow the facets to focus.

In the effort to reduce heliostat costs, several similar round, stretched drum designs are under development in other parts of the world, particularly at Schlaich, Bergermann & Partner in Germany (Weinrebe *et al* 1996). A major current goal of R&D in this area is to dramatically reduce costs by eliminating the flat mirrors and using the surface of the drum itself as the reflecting surface. It is important that this step be achieved without a significant loss in reflectivity. Current average heliostat reflectivity is around 90%.

There are a variety of mechanical methods for canting heliostats; see Jones *et al* (1995) for details. The accuracy of the procedure becomes more and more important as the receiver becomes smaller. In a large 360-degree field such as Solar Two, the canting is less critical than in a small field system like the MPT, because at Solar Two the heliostats are smaller relative to the receiver. Regardless of how the heliostats are canted, they will only achieve their designed focus at one particular sun location. The simplest and most common arrangement is to cant the heliostats so that they are perfectly focused when the sun is directly behind the receiver; this is known as "on-axis" canting. It is possible to optimize the focus for other sun positions, but the net effect on optical performance is not large (Jones *et al* 1995). As the sun moves to locations other than the cant location, astigmatic effects will act to broaden the heliostats image on the receiver target plane; this effect is minimized by the MPT design geometry but is unavoidable (unless the heliostats are dynamically canted, an impractical scheme which has not been proposed for any of the major CR systems). Heliostat performance is discussed further in chapters 3 (modeling) and 5 (modeling results).

[6] This is a visual estimate made by the author August 1997 at Sandia Lab.

I.1.4.2 Rim Angle for a Power Tower

The layout of the heliostat field determines the "rim angle", an important parameter in receiver design (see figure **I-3**). For a solar concentrator, the rim angle is the angle seen at the midpoint of the absorber between the center of the concentrator and its extreme element or edge section. In a CR context, the rim angle is defined by the heliostats at the edge of the collector field (for a 360-degree system, the rim angle is not meaningful). In some field layouts, the rim angle will not be rotationally uniform; for example, as seen from the tower, the angle subtended by the extreme north and south heliostats (this is twice the rim angle in this direction) may not equal the angle subtended by the extreme east and west heliostats (again, twice the rim angle in that direction.) Strictly speaking, the rim angle is the maximum of such measurements, but if the receiver geometry is circular, there will be a loss of efficiency if the rim angle is not rotationally constant. This loss occurs because a receiver designed to accept rays from the maximum rim angle will have some wasted capacity (the optical system "sees" blank space on the ground) at all other rotational angles. The MPT system avoids this loss by using a constant rim angle all around the edge of the field; the resulting shape on the ground is neither a circle nor a wedge, but a distended oval. (See chapter 3 for further detail.)

Figure I-3: Rim Angle

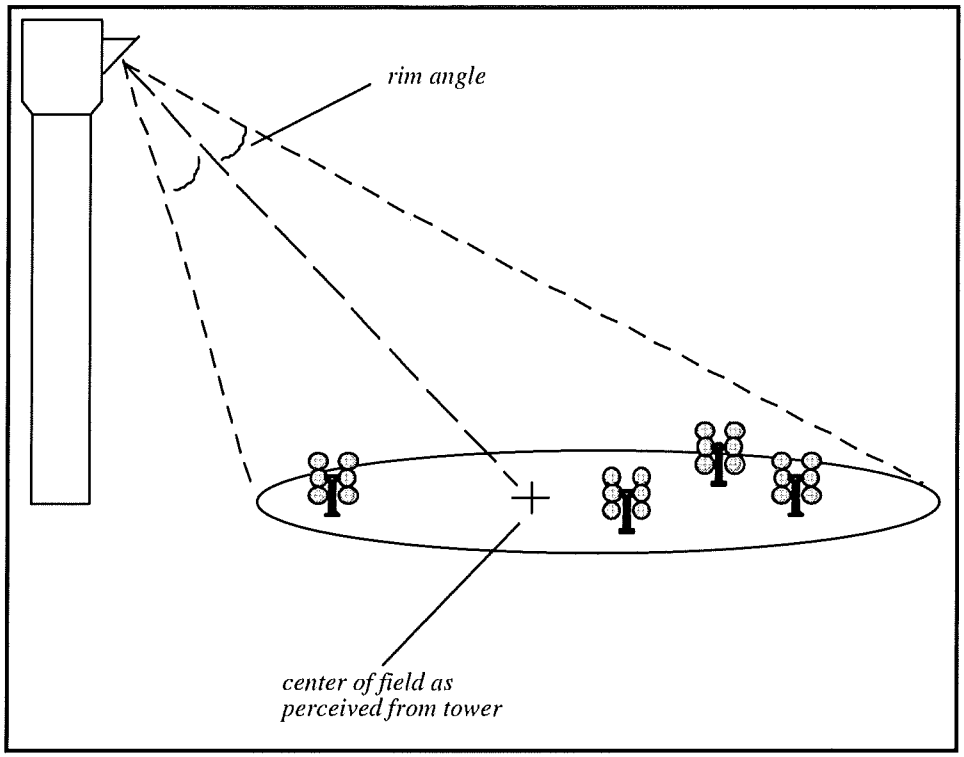

Note: The center of the field as seen from the tower is displaced from the true center of the field because of differential foreshortening; i.e. the half of the field which is closest to the tower appears to take up more space than the half further from the tower. This effect is also responsible for the final shape of the field when it is constructed in such a way that the rim angle is constant around its perimeter. The MPT fields are constructed in this fashion (see chapter 3) and have a distended elliptical form similar to that which appears if a flashlight is shone upon a wall at an angle of about 45 degrees from the perpendicular. See figure **V-1d** for field layouts as they would appear from directly overhead; when seen from the tower, these layouts appear as circles.

I.1.4.3 Power Tower Receivers

The receiver may be a vertical cylinder designed to accept flux from all directions (as at Solar Two), or a cavity aimed in one particular direction (as in the MPT design in chapter 3). Other possibilities exist as well: in the "Phoebus" design (see chapter 2), the receiver is one-directional but consists of a flat, approximately circular plate instead of a cavity. The advantage of the cylindrical layout is that a greater number of heliostats may be used without increasing their distance from the tower, because the field may surround the tower on all sides. However, there are two significant drawbacks: First, the heliostats on the south side are less optically efficient than those on the north, because the usual

location of the sun in the southern sky increases the cosine losses of south-field mirrors (for the northern hemisphere; the converse is true in the southern hemisphere). Second, the outer surface of the cylinder is exposed to a very large *vertical* sweep of earth and sky, of which only a small fraction is occupied by heliostats. This fraction, the heliostat "view factor" for the receiver, is critical in determining the radiation losses from the latter.[7] In a cylindrical design of this kind, it is impossible for the receiver's surface to reach very high temperatures without incurring unacceptable radiation losses; if the view factor were larger, then the ratio of incoming flux to re-radiated flux would likewise be larger. In a CR system integrated with gas turbines, higher temperatures (700-800 C) are desirable to ensure a reasonably high solar fraction (i.e. to reduce the amount of booster gas which must be used in daylight hours). As a result of their poor view factors, 360-degree receivers are restricted to lower temperature applications, and are better suited to very large layouts.

The means of heat absorption are somewhat dependent on the receiver's shape. A cavity receiver may employ both "volumetric" absorption (evenly distributed over a fluid's volume) as well more conventional irradiated-tube or irradiated-plate absorption. In addition, any cavity may, in theory, include a window (see below). However, a cylindrical receiver cannot easily incorporate a pressure-resistant window, and is not readily configured for volumetric absorption. At Solar Two, the heat transfer fluid (molten salt) is carried within vertical tubes which collectively make up the wall of the cylinder.

The MPT design presented here was constructed with a number of priorities in mind, but chief among these were high efficiency, high temperatures, and small size. This combination clearly mandated a cavity-type receiver, a choice which offers higher efficiency and temperature at the expense of heliostat field size, an easy sacrifice to make in light of the original desire to explore smaller CR designs. Both windowed and non-windowed designs are considered in the analysis of the MPT, and a secondary

[7] In theory, a 360 degree cavity receiver is possible, but the design would be awkward and no examples of this configuration are apparent in the literature.

collector is also considered. In this case, the secondary takes the form of a TERC (tailored edge ray concentrator) attached to the receiver's aperture.

Incoming rays from the heliostats are aimed so as to strike either the TERC (shaped like a truncated cone) or the aperture itself; those which strike the TERC are redirected into the aperture. The net effect is to increase the concentration of the solar flux; seen another way, the TERC allows the size of the aperture to be reduced without losing any of the solar flux. *This reduction in aperture size makes a critical impact upon both the cost and performance of the whole system.* The smaller the aperture, the smaller the radiation losses. In the MPT, the aperture has been so effectively reduced that re-radiation losses become nearly negligible.[8] Secondary concentrators of this kind might not be practical on larger power towers, because of weight, wind resistance, and manufacturing demands. Even on the MPT, the TERCs are 10-15 meters across and 5-10 meters deep – large enough that size reduction becomes a design priority (see section **V.3.2**).

I.1.4.4 Timeliness of the Mini Power Tower

A number of broad current developments encourage the pursuit of the MPT design at this time, despite substantial differences from Solar Two (the current focus of U.S. power tower research). These advantages may be summarized as follows:

Development of Windowed Receivers

Karni *et al* (1995) introduce the DIAPR, or Directly Irradiated Annular Pressurized Receiver, developed at Israel's Weizmann Institute (see figure **III-6**). This cavity-type design employs a fused-quartz window (2.25mm thick) in the shape of a truncated cone to withstand pressures up to 30 bar and temperatures over 1000 C. Behind the glass, air is blown over a unique "porcupine" absorber composed of small alloy[9] bars (2 x 3 x 30 mm)

[8] Two other design factors also contribute in a major way to the low radiation losses of the MPT: hybrid operation, which allows a much lower receiver temperature, and the receiver window, which traps heat.
[9] Alumina or alumina-silica.

arranged on a plate and pointed directly towards the glass; the combination of material, coating, and orientation means that very few incoming rays are rejected. The short length and free-standing arrangement of the bars reduces thermal expansion concerns. The temperature of the window itself is reduced by ducting the incoming air against the back side of the glass; this cooling reduces both material stress as well as re-radiation from the outer side. Furthermore, the entire geometry may be optimized (as in, e.g., Kribus 1994) to minimize the net ray rejection for a given field size (rim angle); when correctly configured, the window's net reflectance is below 3%. The DIAPR prototype tested in 1995 featured an aperture diameter of 125.5 mm; the window was in the shape of a truncated cone tapering to a final diameter of 65 mm after a length of 210 mm.

A scaled-up version of the DIAPR is the best candidate for a windowed power tower receiver in the size range of the MPT (2-4 MWe), but other designs (developed for the dish application) exist as well, such as the German VOBREC (Heller *et al* 1994). The DIAPR is at the heart of the Israeli SCOT system now under development (see section **II.2.2**) for applications ranging from 600 kWe to 34 MWe. The individual units will be scaled up as far as the window will allow (it is currently unclear precisely how large the windows can become); for systems requiring a larger aperture, individual DIAPR units will be arranged in a tight bunch, with their air duct plumbing connected in parallel. Gaps between adjacent receivers will be filled with small tertiary concentrators[10] which will redirect the solar flux into the apertures on either side (Kribus *et al* 1997). The MPT designs presented in this study require an aperture diameter of approximately 1.8 meters (1800 mm); this represents a 14:1 scale up of the original DIAPR prototypes. However, it should be noted that the prototypes can withstand 30 bar and 1000 C, while the MPT receiver need only withstand 10 bar and 800 C.

[10] Probably CPCs (compound parabolic concentrators).

Development of the TERC

Gordon & Ries (1993) discuss this innovation, which is ideally suited for a smaller power tower such as the MPT. The "tailored edge-ray concentrator" replaces the compound parabolic concentrator as the secondary of choice for fields with rim angles between about 25 degrees and 50 degrees. Below this range, the CPC is still superior (it becomes ideal in the limit of zero rim angle – collimated radiation), while above this range, there is not as much to be gained by using a secondary concentrator. (In effect, a secondary concentrator increases the rim angle and decreases the aperture; the product of these is call etendue and is a conserved quantity in any optical system if no rays are lost. If the rim angle is already quite large, then there is little possible improvement left.)

A TERC concentrator is shaped roughly like a truncated cone fanning out from the aperture – but only a certain portion of the TERC may be manufactured as a cone without introducing unacceptable approximation (Gordon & Ries 1993). The heliostat aiming strategy must be slightly modified as follows: instead of aiming each heliostat directly at the center of the aperture and allowing the secondary to collect any spillage (as is the strategy for a CPC), each heliostat is aimed at a slightly different point on the side of the TERC closest to that heliostat. This allows a unique solution to the edge-ray principle of non-imaging optics, which requires that the edge ray (extreme ray) from incoming beam (from the heliostat in this case) must be reflected onto the edge of the outgoing beam (onto the edge of the absorber in this case). This principle determines the slope of the TERC at any given point and guides its construction. If the edge rays from two different heliostats (one on either side of the field) were to strike the same point on the TERC, the edge ray principle could not be satisfied (because the incident angles would not be the same). Thus, the aiming strategy must be modified as an integral part of TERC implementation; however, this should be (and is assumed in this model to be) trivial to achieve in practice.

The MPT is particularly well suited for a TERC because its cavity receiver mandates a smallish rim angle (25-50 degrees) and because its small size allows the TERC to be relatively large in relation to the overall geometry (and thus effective), without being large in an absolute sense. With the very large (100 or even 300 MWe) CR schemes currently contemplated for the cylindrical salt receiver (e.g. Kolb 1997), the TERC would have to be gigantic (on the order of 100 meters wide and 50 meters deep).

Changes in the Electricity Industry

The spread of gas turbines (and of natural gas) into primary electric production in the United States and elsewhere is well recognized. Thus the time is ripe for a hybrid STEP with a gas turbine. Furthermore, the ongoing deregulation of the electric power sector in the U.S. has increased competition and enhanced the opportunities for smaller systems (such as the MPT). The new climate enables small independent power producers to compete, while larger utilities are beginning to recognize the very high value of "distributed" production. Indeed, some studies (Smith 1994) have shown that building quite small plants located near the point of consumption will save up to $750 in distribution costs, per kW installed, when compared with building a large central station plant.[11] These benefits are mostly due to decreased transmission costs and enhanced reliability. Finally, the advent of consumer choice (and power source disclosure) will allow renewable technology to compete in the marketplace without establishing complete cost parity (as traditionally measured; societal and environmental costs are not addressed here). Taken together, the trends above suggest increased opportunity for systems deployed in a "distributed" fashion, as opposed to the traditional "centralized production" model.

[11] Of course, the economies of scale for the central plant may outweigh this distribution benefit and are not included in the calculation; the figure of $750/kwe refers only to the avoided distribution costs.

Cogeneration and Recuperation at a Small Scale

There have been two inter-related barriers blocking scale reductions in CR designs. First, low operating temperatures restricted these systems to steam turbines, thus favoring a larger size to exploit the scale economies associated with these power plants. We have seen how the MPT receiver design and hybrid operating strategy open the door for gas turbines. However, a second restriction arises with gas turbines: the most efficient gas turbine electric cycles are "combined cycles" (CC), in which a steam bottoming cycle recovers heat lost in the turbine exhaust. Without the bottoming cycle, conventional gas turbines are not nearly as efficient, although they can be built at small (1 MWe) or even micro (50 kWe) scales.

There are two strategies by which a small gas turbine may be used as a source for efficient electricity production without a bottoming cycle: cogeneration and recuperation. Both of these scenarios are modeled here with the MPT. (For the dish / Brayton system, recuperation is the standard configuration.) The recuperation scenario offers a large (~50%) efficiency improvement but makes the most demands on the MPT plant design: a lower pressure turbine is necessary[12] (2-4 bar instead of the 8-10 which might otherwise characterize an open cycle machine in this size range), and a recuperator (air to air heat exchanger) must be added. The former modification may affect receiver design (lower pressure eases window requirements, but lower density reduces heat transfer), and the latter may increase the turbine cost (but this increase will be offset by less stringent material requirements due to lower turbine inlet temperatures). Nonetheless, this configuration has the advantage of flexibility: it requires neither a water source nor a suitable cogen site (but does of course need a gas line).

[12] For a standard open-cycle gas turbine engine, a higher pressure ratio (10-20 bars is typical) is desirable because it increases the cycle efficiency. However, a recuperated turbine must have a lower pressure ratio (2-4 bars is typical) because the turbine exhaust stream must be significantly hotter than the compressor exhaust stream for heat transfer to take place. However, if the pressure ratio is too high, the compressor exhaust will be too hot (and the turbine exhaust too cool).

In the cogeneration scenario used here, the turbine exhaust stream is used to heat pressurized water for circulation through a system of absorption chillers (in summer) and heaters (in winter) for building climate control. This type of system is becoming increasingly popular, and offers more flexibility than "industrial" cogeneration applications in which higher temperatures or higher pressures are often required. An appropriate location is assumed: perhaps a small university, high school campus, shopping mall, or corporate headquarters. The heat produced is equivalent to a savings in natural gas if it is further assumed that gas would have been burned directly if the turbine exhaust were not available. By this accounting system, the net effect of cogeneration is to reduce the gas used and thereby increase the efficiency of the system *in toto*.

I.1.4.5 Characterizing the MPT

The MPT is not a typical power tower. It is smaller, the heat engine is located on the tower, and the receiver design offers much higher performance than many current designs. The heliostat field is located only on the north side of the tower (for northern hemisphere applications), and is confined to a small elliptical area designed to ensure that the TERC and/or receiver window are used at maximum efficiency. (The field layout is discussed in detail in chapter 3.) As a result of this configuration, the impact of the traditional "cosine losses" has been substantially reduced; in fact, these losses fall to less than 10% when the system is optimized (see figure V-3). At the same time, the tightly focused geometry leads to a very high receiver efficiency, particularly in light of the high operating temperatures. For a system using a TERC but no window, the annualized receiver efficiency (accounting for both aperture misses and re-radiation, but neglecting convection losses[13]) reaches 94%; for a system using both a TERC *and* a window, this figure reaches 96%. (System optimization and more complete results are addressed in chapter 5; see especially figs. V-3a and V-3c.)

[13] Convection losses are not expected to be very significant: the receiver can be well insulated on all sides except the aperture, which offers an apparent surface area of about 3 m^2 (in reality, the cavity geometry

In comparison with a design such as Solar Two, the MPT is much more efficient and operates at higher temperatures. Part of this achievement is due to smaller size, and part is due to design priorities, but a substantial fraction relies on the use of new and/or unproved technology such as the cavity receiver (windowed or not) and the TERC. Nonetheless, even if these improved devices were not to function perfectly, it appears that the MPT would still outperform Solar Two on a simple efficiency basis. This comparison is something of an apples vs. oranges exercise: the MPT is a hybrid system, relying on natural gas to enable the efficient around-the-clock use of a gas turbine, while Solar Two is a solar-only system built to explore thermal storage possibilities.

I.1.5 Linked Dish Arrays

The solar R&D field is thus divided between a configuration which favors heat engine performance (central receiver) and one which favors collector performance (dish / engine). How can we achieve the best of both worlds? A system combining dish collectors and central power generation, referred to here as the linked-dish array (LDA), provides a theoretical answer, at least at the macroscopic level. In an LDA, sunlight is transported either thermally or thermo-chemically from a highly efficient dish network to a highly efficient central heat engine. The latter, as already mentioned, is critical for the success of large-scale hybrid STEPs, while the former assures that mirrors, support structures, and drive mechanisms within the solar field are used to collect as much light energy as possible.

I.1.5.1 Approaches to LDA design

Past efforts at an effective LDA design (see chapter 2) include both steam and oil as working fluids. Compared with the proposal here, these systems operated at lower

---

should provide some additional insulation effect) at an average temperature of about 600 C. (compare with

temperatures, had less sophisticated receivers, and were not designed as aggressively for long-term competition with mainstream electric power. The LDA design considered here uses compressed air as a working fluid, operates at temperatures up to 700 or 800 C, and includes temperature-boosting with natural gas. Advances in receiver design will allow the solar-to-thermal performance of each individual dish to reach the high levels enjoyed by modern dish / engine systems (75% - 95% depending upon configuration and operating temperature).

In the LDA pursued here (OLAA: open loop air array), ambient air is taken from the surroundings and compressed at the power plant for delivery to the outer edge of the dish field. The dishes are arranged in series of three to six dishes. Many such series may be included in a single installation, but the optimum arrangement in all cases is for the last dish in each series to be as close to the heat engine as possible. The flow is piped in one direction through the line of dishes, gaining heat in each receiver. After passing through the final dish, the airflow from each series is combined with others and ducted to the central power generating module, where it enters a gas combustion chamber. Sufficient gas is burned to bring the flow up to turbine inlet conditions (this amount will vary throughout the day and year with the solar flux), and then the hot air is passed through a gas turbine (and in the case of a combined cycle plant, through a steam generator). The exhaust air is not returned to the dishes; this layout is "open-loop".

The driving motivation behind this system is the combination of high efficiency dish optics with high efficiency centralized gas turbines. The latter enables the competitive use of natural gas to co-fire the solar airflow. (In fact, natural gas will be the dominant fuel in this plant; solar fraction is discussed in more detail in later chapters.) Dish collectors are 40-50% more efficient than conventional heliostat / power tower arrangements (such as Solar Two), and 15-20% more efficient than the highly optimized mini power tower proposed in this study, but their use introduces a thermal transport challenge. Each dish in the field must be linked with the next dish in series by an insulated duct through which

---

an average thermal flux through the device on the order of 4-6 MWt). See chapter III for more discussion.

the hot air passes. As a further complication, the receiver of the dish moves to follow the sun, and must be connected to the piping network through a length of flexible hose. This connection must also be insulated and capable of withstanding high temperatures. Despite these concerns, the serial / parallel arrangement for the OLAA which is presented here does offer three major mitigating advantages:

1. Because the dishes are arranged in series, the pipe from each dish needs only to lead to the next dish in series, not all the way back to the central station. The flow rate is the same anywhere along the series; this is in contrast to a field in which each dish adds incrementally to the flow rate. Thus each dish unit only adds a small increment to the total piping demand; typically about ten meters.

2. A further advantage of the series arrangement is that the fluid is only heated gradually as it moves towards the heat engine. Thus the lengths of pipe between dishes early in the series require less insulation.

3. Co-firing allows great flexibility in the operating temperatures in the field, allowing reduction of thermal transport losses as necessary. In fact, the field could operate at nearly any temperature, and gas can be co-fired to raise this temperature to turbine inlet conditions. Of course, the lower the exit temperature from the field, the lower the solar fraction. Field operating temperature might be lowered in one of two ways: either by increasing the flow rate to the dishes, or by shortening the length of the dish series. The former adjustments can even be made after the plant is built, by adjustment of valves controlling the amount of air which bypasses the dish array and goes straight to the combustion chamber.

The challenges associated with LDAs lie in the transport problem: to what extent is it possible to transfer thermal energy across open spaces between dishes, and between the dish field and the central station? How much energy will be lost in this process? If a chemical energy carrier is used instead of a purely-thermal one, can the energy by

transferred into and out of the chemical form without unacceptable losses? What sort of maintenance demands are created by the array which do not exist for the dish itself? Finally, how will such a system compare to current dish / engine systems, in terms of performance and, ultimately, levelized cost of energy? Some of these questions are addressed in appendix **D**, where their resolution is judged sufficiently problematic to discourage further investigation of the LDA concept (within the confines of this study).[14]

I.2 Design Priorities

I.2.1 Component Efficiencies of STEPs

The efficiency of a STEP may be broken into four major components: collection efficiency, conversion efficiency, transport efficiency, and heat engine efficiency. The first of these, collection (or optical) efficiency, is a measure of the amount of sunlight

---

[14] A second LDA concept, incorporating closed loop chemical heat transfer via CO2 reforming of methane, was also considered briefly. In this design, which is patterned after experiments at Israel's Weizmann Institute (and elsewhere), CO_2 and CH_4 are piped through reactors in the receivers (which may or may not be in series) where a catalyst enables the highly endothermic production of a syngas (containing H_2 and CO, along with some of the original reactants). The sensible heat which is absorbed in this process (about 1/3 of the total energy absorbed) is passed via a heat exchanger to the incoming reactant flow, while the syngas (still fairly hot – about 400 C) is ducted to the central facility, where the chemical energy is unlocked in an exothermic methanation step. Heat exchangers must again be used, to transfer the heat of the reaction to a working fluid for the heat engine. For a solar-only application, this engine must be a steam turbine, as operating temperatures for the methanator do not enable the effective use of a gas turbine. The methanator products (mostly CO_2 and CH_4) are returned to the dish field.

A critical feature of the closed-loop LDA is the possibility for integral energy storage. After the syngas leaves the dish field, it can be stored indefinitely in tanks near the methanator unit, thus allowing the methanator to run even when the sun is down. Of course, the syngas contains sensible heat as well as chemical heat, and if this can not be used in real time, some of it will be lost while the syngas waits in storage to be used. It may even be necessary to reheat this gas for the methanator if the storage tanks are not insulated.

A closed-loop solar-only LDA of this kind coupled to a steam generator represents a direct alternative to the central receiver / molten salt configuration of Solar Two: both systems would operate at similar temperatures (and thus similar heat engine efficiencies), and both would incorporate energy storage. There are numerous small differences, of course, but in broad strokes the LDA replaces the heliostat field of Solar Two with more efficient parabolic dishes, but introduces the possibility of greater thermal losses during energy transport. Although it seems possible that the dish advantage might prove decisive in the long run as the costs of materials falls, it is also true that the closed-loop methane cycle has only been partly validated by laboratory experience, and has never been demonstrated on a large scale at all. Moreover, many of the critical components (methanator, reformer, heat exchangers) are difficult to price.

which is collected per unit of collector area. To be meaningful, this measurement must be averaged over a full range of operating conditions; usually a single, typical year of insolation data is sufficient (a discussion of solar flux modeling appears in chapter 3). Once the light is collected, it must be converted into heat (or chemical energy) in the receiver and then transported to the heat engine; both of these processes have associated efficiencies. Finally, a conventional heat engine thermal efficiency determines how much of the captured solar energy can be converted into electricity. At many points along this path, of course, there may be additional minor pieces of equipment with their associated efficiencies (e.g. heat exchangers, pumps, and chemical reactors). By assimilating these pieces into one or another of the four major components listed, we can define the net solar-to-electric efficiency ("Es-e") as follows:

$$E_{s\text{-}e} = E_{col} * E_{con} * E_{tran} * E_{he}$$

The explicit definitions for these components will vary according to system; for the MPT, "collection" occurs at the heliostat field and secondary reflector, "conversion" (from radiation to thermal energy) occurs in the receiver, and "transport" occurs between the receiver and the gas turbine (the "heat engine").

To see why an LDA makes theoretical sense, consider the approximate component efficiencies of the current front-runners in the STEP field, presented in table **I-4**. (Solar trough systems are neglected here and throughout this study. Their lower operating temperatures and geometric collection inefficiency are generally expected to prevent troughs from making a large contribution to *electric* generation in the mid- to long-term future.) Except for the MPT and LDA estimates, these efficiencies are design point maximums for actual systems currently operating or under development, and while not necessarily fully optimized, dramatic improvement is not expected within the constraints of current designs. (The figures in bold are borrowed from chapter 5 of this study; the figures indicated with a question mark are highly uncertain.) It is of utmost importance to recognize that some of these efficiencies (e.g. those for the CC/PT design) may only be

reached under hybrid operation; nonetheless, they are still solar-to-electric efficiencies: they represent the amount of energy produced from the sunlight relative to the energy carried in the sunlight.

Table I-4: Approximate Component Efficiencies of Major STEP Designs: (ranked by net conversion efficiency)

System	Size, MWe	E_{col}	E_{con}	E_{tran}	E_{he}	E_{s-e}
big LDA	30	**.85**	**.88**	.75?	.55	.31?
dish / Stirling	.025	**.85**	**.88**	.99	.35	.26
CC/PT	100-300	.60	.75	.95	.55	.24
dish / Brayton	.025	**.85**	**.88**	**.99**	**.30**	**.22**
Recuperated MPT	2	**.69**	**.99**	**.99**	**.32**	**.22**
small LDA	2	**.85**	**.88**	.80?	.32	.19?
Solar Two	10	.60	.75	.95	.35	.15

Source: see text

The D/E, LDA, and MPT systems are already familiar, but the two remaining CR designs require clarification: Solar Two uses a molten salt collection system and salt-to-steam heat exchanger to drive a conventional steam turbine. The system currently operates as a solar-only plant. By contrast, the CC/PT design by Bohn *et al* (1995) employs a salt-to-air heat exchanger and a supplementary burner in order to reach high enough temperatures for a combined cycle plant (gas turbine with steam bottoming cycle). The substantially better efficiency of the CC plant relative to steam-only plants has led to the widespread introduction of this design into the electric power industry in recent years; this trend is expected to continue.

What they lose in collection efficiency, conventional central receiver STEPs regain in heat engine efficiency and/or through benefits related to storage. In the case of Solar Two, the steam turbine is not substantially more efficient than either the Stirling or Brayton engines of the D/E systems, and the E_{s-e} is lower. However, this CR STEP includes integrated thermal storage in large tanks holding molten salt; this storage allows the power producing elements of the plant, including the steam turbine, to be used at a higher capacity factor (CF) than is possible on direct sunlight (sunlight is limited to a CF of about .30 annually, even in a very sunny region such as southern California.) Storage has

a second benefit at Solar Two: solar power can be stored throughout the day for dispatch in the evening, at a time when the price paid for grid power is higher but sunlight is no longer available. The combined capacity and dispatch advantages of this type of STEP allows it to compete with D/E systems despite its lower efficiency. However, over the long term, it is not clear that low-efficiency designs can prevail, particularly if the cost of PV modules continues to fall, or if an effective thermal storage system is contrived for D/E systems.

Note that the MPT, due to its technical innovations and small size, considerably outperforms other CR designs (Solar Two; CC/PT) with regard to collection and conversion. Overall efficiency is about the same as the much larger CC/PT, because of the loss of efficiency with gas turbine size. However, the much smaller scale of the MPT is a major advantage.

I.2.2 Co-firing with Natural Gas

Many experts in the solar field believe that an alliance with the natural gas industry would be mutually beneficial. This proposed symbiosis forms the motivation for most current solar R&D on hybrid systems (with the exception of some smaller-scale ideas, e.g. the use of non-gaseous fuels such as diesel in off-grid dish / Brayton systems). As developed by Bohn *et al* (1995) and others, this argument maintains that:

- Solar energy will benefit from inclusion in natural gas plants because of the economic power and expected market dominance of natural gas companies in the 21st century. Although the solar fraction of the resulting hybrid plants may be quite low (10-30%), even a handful of commercial plants would vastly expand the solar thermal market share, resulting in extensive cost reductions through learning processes in manufacturing, economies of scale in production, and R&D experience.

- The natural gas industry will benefit from the addition of "fuel-saving" solar plants to existing and future natural gas plants (usually assumed to be CC) because of the reduced risk achieved by diversifying the fuel base. (Although solar power may not reach economic parity with gas plants for some time, the long-term trend is in that direction.) Moreover, current and future legislation requiring that a minimum percentage of power generation originate in a renewable resource can be satisfied with hybrid plants. The Clinton Administration's "Comprehensive Electricity Competition Plan" (DOE 1998) proposes a renewable portfolio standard (RPS) which would reach 5.5% by the year 2010. Adoption of this measure would require electricity sellers to cover 5.5% of their sales with *non-hydroelectric* renewables, subject to a cost cap. Retail sellers could trade credits with other vendors to meet the RPS requirements.

There is a major sticking point, however, barring the introduction of natural gas co-firing into a CR plant such as Solar Two: the steam turbine , chosen because its operating temperature matches the temperature of the working fluid in Solar Two, is not efficient enough to compete with a modern natural gas plant. Dish / engine systems, including Allied Signal's new dish / Brayton design, will burn gas at similarly non-competitive efficiencies (see table I-4). Thus burning any sizable amounts of gas at Solar Two or in current D/E systems would inevitably result in a waste of gas.

The most desirable arrangement would use the gas to raise the temperature of a working fluid (air) high enough to allow efficient utilization of a modern combined cycle (CC) plant. In the CC/PT concept, the molten salt from the Solar Two design is used to heat an air stream which is then further heated in a gas burner before expanding through a high-temperature gas turbine. Exhaust gas from the turbine is used to raise steam and drive a ST bottoming cycle. The total heat engine efficiency in this case is much higher, around 55%, and gas burned in *this* plant is used as effectively as gas burned anywhere. Plants of this type can be expected to be of interest to natural gas power companies, while those operating at lower, Rankine cycle, temperatures and efficiencies cannot be considered competitive (in the absence of perverse tax benefits or similar legislative effects).

The CC/PT concept, while a good one, appears not to have caught on yet. This reluctance probably derives in part from some technological issues, such as the expense and performance of the air/salt heat exchanger, and in part from the U.S. solar industry's current commitment to the Solar Two design, which, while inefficient, does not require co-firing.

I.2.3 System Scaling

The ongoing evolution of the electric power industry, in tandem with the growing need for village power in the developing world, has highlighted the need for plants designed at the intermediate scale: from a fraction of a megawatt up to several megawatts. Yet solar thermal technology does not currently boast a system optimized to this size range. (Photovoltaics, of course, can be scaled up to any size.) The largest dish / engine designs are about 25 kWe and can also be combined in fields, but their performance is not fundamentally different in this configuration. By contrast, power towers which follow the Solar Two model are believed to reach their optimum size above 100 MWe; the current prototype is 10 MWe and is considered too small. The scale ratio between power towers and dishes is thus about 400:1!

At present, the intermediate size range is occupied by other renewable energies, primarily wind power. Most modern turbines are manufactured in the 100 kWe to 750 kWe size range, and these are often combined in small clusters. There are many areas where the solar resource is more abundant than wind, and in these applications the MPT should offer advantages comparable to those of a small wind farm: manageable project scale, limited land requirements, and nearly stand-alone operation (in the recuperated scenario). The modest financial commitment required for such a plant (approximately $5 million; see chapters 4 and 5) is more compatible with the risks inherent in new technology than is the massive outlay which a scaled-up Solar Two will require. In particular, a 2-4

megawatt plant is a much more appropriate for many developing countries, where capital is scarce and current demand intensity is well below U.S. levels. In this context, MPT systems could be deployed over a wide area, not only reducing transmission problems but also spreading technology and jobs to a larger population segment. Regardless of location, if early generation MPTs are successful, it will be easy to enlarge the design somewhat, or (if necessary) to build multiple systems side by side.

I.3 Summary of Appropriate Applications for STEPs

The table which follows summarizes the discussion thus far by assigning the STEP (and PV) systems to the modes of application in which they seem likely to make the greatest contribution.

Table I-5: **Most Appropriate Application Modes for Solar Power Technologies**

	Solar Only	Hybrid
Grid-Tied	Power Tower (Solar Two type) Dish / Stirling Linked-Dish Array (chemical) PV	Mini Power Tower Power Tower (CC/PT type) Dish / Brayton Linked-Dish Array (air cycle)
Off-Grid	Dish / Brayton Dish / Stirling PV	Dish / Brayton

Note: no meaning is attached to the ordering of systems

CHAPTER 2:
A BRIEF REVIEW OF SOLAR THERMAL ELECTRIC PLANTS

Note: This is a thumbnail sketch of solar thermal developments; many more exhaustive descriptions can be found in the literature, including the chapter "Solar-thermal Electric Technology", by De Laquil et al, *in the indispensable sourcebook* Renewable Energy *(1993). There are several other similar sources, including some which focus more on a particular branch of the technology, but this chapter owes a particular debt to the comprehensive De Laquil article.*

II.1 Prior Efforts

In 1896, a patent was issued for the first solar thermal plant recognizable as such by modern standards: a central receiver arrangement in which the mirrors were mounted on railroad cars surrounding the tower. (This idea was never implemented, but in 1957 a group of Russian researchers revived the concept for the design of a gigantic layout requring 1,293 railroad flatcars! A model was built, but the project never reached fruition.) Solar thermal power was first used commercially in 1912 to run a steam pumping plant in Egypt. This trough-type plant generated 45 kWe from an area of 1200 m^2, and operated for two or three years, until a decline in the prices of conventional fuels made it obsolete (De Laquil *et al* 1993).

After these early efforts, there was little interest in solar thermal until the oil crisis of the 70's encouraged a wide array of renewable energy initiatives. These included trough systems, central receiver systems, and dish systems. Notable achievements in each of these areas are as follows:

- **SEGS plants**: The world's largest solar thermal facility (354 MWe) is comprised of the nine SEGS (solar electric generating system) plants in California's Mojave desert. The first of these trough collector plants, SEGS I, was built in 1984; the last plant, SEGS IX, in 1990 (De Laquil *et al* 1993). Outputs range from 15 to 88 MWe, and all of the plants are hybrid; i.e. they are assisted with natural gas. The plants only operate when the sun is shining (CF ≈ .25) and the gas is used as a topping fuel to boost cycle temperatures, contributing about 18% of the total energy (solar fraction ≈ 82%). Although the exact configurations vary from plant to plant, all of the plants use a steam turbine as the prime mover; steam is raised by heat transfer from a flow of hot oil which circulates through the long rows of trough collectors. Solar to electric efficiencies hover around 10-12%, with "gas mode electrical conversion efficiency" of 37-39%. (Note: This latter figure compares well with the MPT presented in this study, but the former figure is much lower than the predicted net solar efficiency of the MPT.) The SEGS plants continue to operate commercially as of this writing, although their original builder, the Luz corporation, has failed financially. Levelized costs calculated by the company ranged from 8.9 cents/kwh for SEGS VIII to 26.5 cents/kwh for SEGS I (De Laquil *et al* 1993).

- **Solar One**: Constructed in 1982 as a joint venture between the DOE and several utilities, Solar One was the largest of several central receiver ("power tower") designs built around the world during the 1980's. Unlike the SEGS plants, Solar One operated as a solar-only plant, incorporating oil/rock storage in an effort to increase the capacity factor of the steam turbine. Unfortunately, the oil/rock system only operated up to about 300 C, limiting turbine efficiency when storage was used. (The directly generated solar steam reached 510 C; compare this figure with the 800 C air in the MPT and ASDB systems presented in later chapters of this study.) Solar One used a cylindrical, 360-degree field of view receiver located 80 meters above the ground; receiver panels contained vertical pipes about 14 meters long. As a result of its enormous surface area, receiver losses were crippling: net solar-to-electric efficiency

was predicted to reach 8% over time, but the plant was deactivated (later to be revived as Solar Two; see below) before its efficiency exceeded 5-6% (De Laquil *et al* 1993).

- **Other Early Power Towers**: Other power tower efforts which were actually built include the 1 MWe Eurelios (Sicily), the 1 MWe CESA-1 (Spain), the 2.5 MWe Themis (France), the 5 MWe C3C-5 (USSR), and the 1 MWe Sunshine (Japan). All of the early plants used a steam turbine, but a few (e.g. Themis) used a salt solution in the receiver instead of raising steam directly. Although the use of salt requires a heat exchanger (steam generator), it allows for integral thermal storage by installing a buffer tank in between the receiver outlet and the steam generator. In none of the receivers (whether salt or water cooled) could temperatures exceed about 520 C. All of the plants suffered from long start-up times and significant turbine-efficiency losses from transient outages (e.g. cloud passages, although this problem was mitigated at plants with salt receivers, which have a built-in buffering capability). Heliostat costs fell throughout the decade, from around \$1,000 / m^2 (installed cost) prior to 1980 to about \$150 / m^2 (manufactured cost) for stretched membrane prototypes in the early 1990's (De Laquil *et al* 1993). Designs for modern power towers seek continued heliostat price reductions in conjunction with more efficient receivers, higher-temperature storage, and the introduction of gas turbines. See section **I.2.2** (and the MPT design in chapter 3) for more information.

- **Shenandoah Solar Total Energy Project**: This system, constructed in Georgia in 1982, was one of the few of the linked-dish type: hot oil circulated through 114 parabolic dish collectors before passing to a supplementary burner. The plant produced electricity (from a steam turbine), air conditioning (from an absorption chiller), and process steam. Over time, the solar components only supplied about 20% of the thermal input, and thermal losses in transport were unacceptably large (De Laquil *et al* 1993).

- **Vanguard I**: This fully automated stand-alone dish / Stirling prototype holds the current world record for solar to electric conversion – 29.4% maximum and 22.7% annual average. The 25 kWe system was built and operated (from 1984 and 1985) in California by DOE and the Advanco Corporation (De Laquil *et al* 1993). The Stirling engine was built by United Stirling, and was of the "kinematic" type, in which the pistons are mechanically joined to a rotating power shaft (a newer design allows for a magnetically driven linear alternator and free-floating pistons – see section **II.2.3** below). The Vanguard I collector consisted of a large number of small, square, flat mirrors bonded to a parabolic support structure. This arrangement was expensive and required precise alignment of each mirror, but once constructed it provided high concentration and good durability (Stine and Diver 1997). However, the Vanguard I engine was not durable enough for long-lasting electricity generation (where lifetimes -- or periods between major overhaul – need to be on the order of 5-10 years), and much of the subsequent research in this area has been devoted to increasing the lifetime of the Stirling engine.

- **Other Early Dish / Engine Systems**: Significant dish / engine systems were built during the 1980's in Saudi Arabia (3 German SBP dishes with United Stirling 50 kWe engines), the United States (6 McDonnell Douglas Dishes with United Stirling 25 kWe engines), Germany (various prototypes, SBP dishes, various engines) and Japan (Aisin Seiki Stirling engines). The dishes built by Schlaich, Bergermann und Partner (SBP) in Germany are of the stretched-membrane design, in which a large sheet of metal or plastic is stretched over a drum with a slight vacuum. The front surface is either directly reflective or provides a mounting surface for thin, flexible mirrors which are bonded to it. For a large concentrator, vacuum pressure does not provide a sufficient focus, so pre-forming the membrane (often with water pressure) has been attempted as an alternative (Stine and Diver 1997). Another design, currently under active development by SAIC in the U.S., breaks the membrane up into a number of smaller modules, all of which are attached to a common support frame – this is the design chosen for the ASDB system presented in chapters 3-5.

- **Warner Springs**: This 5 MWe plant was completed in California by the LaJet Energy Company in 1984, and was of the linked-array type. 700 dish concentrators were used to generate steam, which circulated through the field. The receivers incorporated a salt heating fluid as a thermal buffer between the sunlight and the steam. The dishes were composed of small stretched-membrane facets, the unexpected deterioration of which eventually killed the project (De Laquil *et al* 1993).

II.2 Current State of the Art

This section is a continuation of the prior one, in that it lists some of the major solar thermal electric projects under way in the world today. Important areas of R&D are also outlined. The material presented is in no way exhaustive; this is a fast-moving and very international field, and the major players are constantly changing. Furthermore, the reader should be aware that the more commercial technologies are often considered proprietary by their developers.

II.2.1 Overview

Although the SEGS (trough-style) plants are commercially operating today, the original operating company (Luz) was driven to bankruptcy by cost overruns, unanticipated reductions in fossil fuel costs, and withdrawal of public incentives. The trough technology, which tracks the sun in one axis instead of two, is limited to much lower temperatures than dishes or central receivers. Lower temperatures have limited these plants to steam turbine cycles, whereas the modern electricity industry is turning more and more to gas turbines (or, as an even-more advanced step, to fuel cells[15]). While a

[15] There are possible synergies between fuel cells and solar power, in that methane might be refined in a solar reactor to produce hydrogen for fuel cells. There are a number of experimental solar

hybrid, gas-assisted trough plant powering a modern gas turbine is certainly a possibility, such an arrangement would create heat transfer difficulties between the fluid in the troughs (usually an oil circulating in closed loop) and the air necessary for the Brayton gas turbine cycle. Receiving the solar energy directly into air, obviating the need for such heat transfer, will be much more readily adapted to the dish or the central receiver. Finally, the low trough temperatures would reduce the solar fraction in a hybrid plant to very low levels (less than 10%).

To summarize, the trough suffers from the following disadvantages: low optical efficiency, low temperature, a separate heating oil flow loop[16], and low solar fraction if hybridized. In light of these drawbacks, it is generally recognized in the industry that trough plants will play a secondary role in the solar thermal installations of the next century. Ongoing research at the SEGS plants focuses on techniques for operations monitoring and associated O&M expense reductions; it is expected that this research will contribute to future projects, regardless of collector type, across the solar thermal industry (Cohen *et al* 1997).

Power tower technology claims the lion's share of current solar thermal research, attracting the interest of the largest companies and the biggest spenders. Power towers are generally perceived as vary large central-station equivalents of interest to large utilities with operations in desert areas. By contrast, dish technology, while supported with equal vigor, attracts the interest of somewhat smaller companies with a more diverse set of potential applications in mind, ranging from large utility contracts to remote off-grid locations or even individual or corporate customers on the edges of a distribution network.

---

hydrogen-reforming projects under way around the world; some of these ideas are listed in sections **I.2.2** and **I.2.3**.

[16] Steam has been considered as a heat carrying fluid in the troughs, and could be directly piped to the turbine. However, steam has a lower (and variable) density, which will give rise to many of the transport problems which face the LDA (which uses air instead of steam); e.g. significant heat and pressure losses. See appendix **D** for a further discussion of transport problems in the LDA.

II.2.2 Current Power Tower Projects

- **Solar Two**: This 10 MWe installation, sponsored by DOE, Southern California Edison, Bechtel, and several regional utilities, is a direct descendant of Solar One, sharing the same site, most of the original (~2,000) heliostats, the original (~100 m) tower, and the original steam turbine (Sunlab 1996). The critical addition at Solar Two is a new receiver using molten salt instead of steam, and an associated network of salt pipes and thermal storage tanks. The salt, which reaches a maximum temperature of 550C, circulates during the day from a cold storage tank, through the receiver, and into a hot storage tank. Some of the salt passes directly to the steam generator; in the evening, the salt in the hot tank is used to keep the steam turbine running for up to three more hours. Downstream of the steam generator, the salt returns to the cold storage tank. Solar Two is currently online and operational, but considerable problems were encountered at many points along the development path; the vast majority of these related to the age of the original heliostats or to the salt piping system and receiver. If the salt is allowed to freeze at night, pipe damage, blockages, and leaks occur, so a heat trace was added to the entire piping network; in addition, the pumps are cycled throughout the night whenever the salt temperature falls too low (Gould *et al* 1996). Once, the rupture of a receiver tube allowed a large quantity of hot salt to spill out onto the ground. Overcoming these problems has pushed the project's price tag beyond initial expectations; Solar Two has cost about $40 million, not including equipment and land inherited from Solar One and estimated at $140 million! (DOE 1997a).

- **PHOEBUS**: This design, a 30 MWe air receiver power tower designed by a consortium of nine European companies for deployment in the Wadi Rum area of Jordan, has not been built because the Gulf War disrupted planning. The engineering study for this plant concluded that an air receiver was "equal or superior" to a salt/steam configuration, and that the resulting levelized energy cost (LEC) would be

lower. Both co-firing and thermal storage were included in the design; the latter was to rely upon "cowper technology" borrowed from the steel industry (Grasse 1991). Despite moving to an air receiver and gas boosting, PHOEBUS retains a steam turbine instead of a gas turbine. It is in this respect that the CC/PT (see below) or the MPT (see chapters 3-5) are most distinct from the current generation of power towers.

- **Combined Cycle Power Tower (CC/PT)**: This design is heavily dependent upon hybrid operation in order to boost overall efficiency, but the system retains the salt receiver and thermal storage system from the Solar Two design (Bohn *et al* 1995). Heat from the salt is used to preheat the air upstream of the burner in what is otherwise a conventional combined cycle layout; selection of an engine with low compressor exit and turbine inlet temperatures is desirable in order to maximize the solar fraction. (The instantaneous solar fraction, regardless of storage capacity, will be bounded by the maximum salt temperature – 550 C – relative to the turbine inlet temperature; additional heating will be provided by the gas burner. Bohn *et al* propose a turbine such as the Navy's WR-21, a 20 MWe, inter-cooled, recuperated unit which could be modified to a more efficient combined cycle by replacing the recuperator with a steam generator.) The CC/PT design is very flexible, in that the solar field size is independent of the plant size; a smaller field will still fulfill the same function, but the annual solar fraction will be lower. In comparison with the MPT presented in chapters 3-5, the CC/PT is much larger (due to scale economies of combined cycles), includes storage, and relies upon existing (instead of next-generation) receiver technology.

- **SCOT**: This Israeli system, sponsored by the Weizmann Institute and its industrial partners, is closer to the MPT than any other active design currently in the literature. The SCOT (Solar Concentration Off-Tower) mounts a bank of DIAPR air receivers (see section **II.2.3**) on the ground; these units are flanked by CPC tertiary concentrators and are connected to a gas turbine. Sunlight is reflected to this plant from a hyperboloid secondary mirror located on the tower; the heliostat field is

distributed around the tower in an essentially one-sided pattern (Kribus *et al* 1997). This system simplifies the tower enormously, but incurs multiple reflection losses because of the more contorted optical path.

II.2.3 Current Dish / Engine Systems

- **SAIC Dish / Stirling**: The Science Applications International Corporation has developed a 25 kWe dish / Stirling system which is near the point of commercial roll-out (SAIC 1997b). The dish for the system, consisting of 16 stretched-membrane drum facets, is the basis for modeling in the text, and is discussed in detail in chapters 3-5. The engine, an STM 4-120 built by Stirling Thermal Motors and de-rated to 30 kWe for long-life applications, uses a variable-angle swashplate to couple the (four) pistons to the power shaft and boasts a design-point thermal efficiency of 42% and a projected MTBO[17] of 60,000 hours (SAIC 1997b). The receiver is of the "directly-irradiated" type, in which the engine working gas (helium at about 20 Mpa and 720 C) circulates through thin metal tubes arranged in coils just behind the receiver aperture. This arrangement, while functional and a direct descendant of Vanguard I, is very demanding on the tube material and engine, particularly during cloud transients. Use of a heat pipe to buffer the heat transfer is a subject of very active research and is addressed below.

- **Heat Pipe Receivers for Dish / Stirling**: Heat pipes are under active investigation at Sandia national labs, at several companies (such as Thermacore), and in Germany at DLR. There are two basic designs; in both cases the solar flux is absorbed on a thin metal plate in the receiver. At the back of this plate, sodium is vaporized by the heat and rises by convection up a short tube to the engine heating heads, where it condenses back to its liquid form and flows back to the receiver. In the "pool-boiler", the back surface of the receiver is immersed in a pool of sodium; in the newer wick

[17] Mean Time Between (major) Overhauls.

designs, the sodium is drawn up from a small sump to wet the absorber (Stine & Diver 1997). Finding a durable material for the wick has presented an ongoing challenge, but this arrangement involves a smaller quantity of sodium while simultaneously avoiding some of the start-up problems associated with the pool boiler (see e.g. Noble *et al* 1995).

- **Kinematic Engines for Dish / Stirling**: Uncertainty about the effects of piston/driveshaft coupling (and shaft sealing) upon the lifetime of the kinematic (directly coupled) Stirling engine has encouraged efforts to develop a "free-piston" Stirling engine. In this design, the power piston forms an alternator with components clapped on to the outside of the unit; thus the engine is hermetically sealed. The pistons bounce back and forth between springs (gas or mechanical), and the engines operate at a natural frequency determined by the mass of the pistons and the power of the springs (Stine & Diver 1997). Two years ago, a small (9 kWe) engine of this kind was nearing commercialization under a program sponsored by DOE and Cummins Power Generation; Cummins has since dropped the program, but the "free-piston" engine remains a promising technology.

- **VOBREC Receiver for Dish / Brayton**: The German Aerospace Research Establishment (DLR) has focused its recent (since the early 1990's) efforts in solar thermal upon the development of a small air receiver for dish systems, the VOBREC. The aperture is surrounded by a secondary concentrator and covered by a domed window. Inside, air at about 3 bar is pulled through a ceramic mesh absorber located behind the window. Finding the proper material for this mesh is difficult, because it must withstand repeated and rapid thermal cycling to high temperatures (to 870 C) without crumbling or releasing any dust which could collect on the window. The VOBREC receiver has reached efficiencies of 80-85% in tests (Buck *et al* 1996; see also Heller *et al* 1994), and although it operates at lower temperatures and pressures than the Israeli DIAPR (see below), it is a promising alternative.

- **DIAPR Receiver**: The Directly Illuminated Annular Pressurized Receiver is similar to the German VOBREC (see above), except that the entire unit has a tapered frustum shape, and the absorber consists of a "porcupine" arrangement of metal rods which line the entire inner surface of the cone. The DIAPR's design allows operation at higher pressures (because the window's shape is very strong) and temperatures (because the heating surface is not isothermal) than any other air receiver yet designed. A 50 kWt DIAPR prototype, appropriate for dish / engine systems, has been tested at 1130 C and 19 bar (Karni *et al* 1995), and a scaled up version is included in the SCOT power tower design. The DIAPR forms the basis for much of the receiver modeling in chapters 3-5; see figure **III-6** for a rough schematic.

- **Allied Signal Dish / Brayton**: In 1997, a new dish / Brayton project between Allied Signal and Sandia Labs was initiated. This system, dubbed ASDB throughout this text, is the subject of extensive modeling in chapters 3-5; a complete description is available there.

II.2.4 Current Interest in (Chemical) Linked Dish Arrays

There are currently no system-level designs for LDA's in the mainstream solar thermal literature. (The challenges associated with LDA's are detailed in chapter 1 and in appendix **D**.) The projects listed below are not explicitly LDA designs, but the technology under development (specifically, dish mounted chemical reactors) requires a central power plant and thus implies a linked dish array with chemical energy transport. (An LDA with sensible heat transport is a more direct arrangement but the transport issues are unresolved; see section **I.1.5**.).

- **CAESAR**: The Catalytically Enhanced Solar Absorption Receiver project began in the early 1990's as a joint effort between Sandia Labs in the U.S. and DLR in

Germany (Muir *et al* 1994; see also Buck *et al* 1994). The receiver unit is scaled for dish deployment (100 kW_{chem}), and is quite similar to an air-receiver of the VOBREC type with two important differences: first, the working fluid which enters the receiver is a mixture of carbon dioxide and methane. Second, the solar-heated absorber matrix contains a rhodium catalyst which allows the reforming reaction (CH4 + CO2 <> 2CO + 2H2) to take place as the gas passes through. Careful adjustment of the catalyst density, temperature, and flow rate are necessary to create conditions which favor the forward reaction and thus result in the highest possible H2 concentration in the exhaust gases. In a complete system, the syngas could be combusted immediately at a central turbine, stored for later combustion, or purified and pumped off-site. A descendant of CAESAR was tested at the Weizmann solar tower in Israel in 1995 as part of their closed thermo-chemical loop (see below). Under the right conditions, the receiver converts up to 84% of the methane in the flow stream, but at some cost to efficiency, in this high-conversion run, 87% of the solar energy was absorbed into the gas, but only 34% as chemical energy (the rest was heat). In an alternate configuration, the unit reached 91% absorption of solar energy with 59% in chemical form, but only 61% of the methane was converted (Abele *et al* 1996).

- **Israeli Closed Thermo-Chemical Loop**: Researchers at the Weizmann Institute have been trying to create a highly efficient and flexible arrangement in which a methanator is coupled to a carbon dioxide reforming solar receiver (such as the CAESAR, above, or an Israeli alternative featuring a directly-irradiated metal pipe – see e.g. Levy *et al* 1992). In the closed loop, the reactor products are ducted to a methanator where the reaction (see above paragraph) reverses itself at somewhat lower temperatures, again in the presence of a catalyst (Levitan *et al* 1991). The heat which is released is measured with a calorimeter in the experimental setup, but could be used to raise steam or possibly preheat air for a gas turbine burner (a hybrid arrangement). Inline storage can easily be added to the system. Control issues are delicate throughout, because both reactions will only operate efficiently under the

right conditions; in general, high receiver efficiency is more important that high chemical conversion efficiency. Net energy-transport efficiency (i.e. one reforming process and one methanating process) for the closed-loop system has reached 85% (Segal & Levy 1993); this figure reflects the energy lost in adjusting the temperature of the gas stream and in adding steam (if necessary); it does *not* include receiver efficiency, which is quite low for the Israeli model. Recent advances on this system include the introduction of ruthenium catalysts, prompted by sharp price increases for rhodium (Berman *et al* 1996).

CHAPTER 3: PERFORMANCE MODELING METHODOLOGY

III.1 General STEP Modeling Considerations

III.1.1 Solar data and the direct solar beam

The sunlight which reaches the surface of the earth can be divided into two components: the direct solar beam, which travels in a straight line (except for atmospheric prismatic effects), and the diffuse (or scattered) radiation, which strikes the surface from all directions. If a collection system concentrates sunlight, then the direct beam is dominant: most of the diffuse radiation strikes the concentrating element at angles larger than those which are transmitted to the absorbing element. (The maximum angle, measured from the center of the solar disk to the point in the sky from which a ray appears to emanate, for which a ray is transmitted to the absorber is the system's *acceptance angle*. See figure **III-0** below.) As the degree of concentration increases, the acceptance angle becomes smaller and smaller, and the diffuse radiation becomes less and less significant. For the systems considered here only the direct beam is accepted.

There are a few subtleties about the direct beam which are worth bearing in mind. First, as noted, the direct beam may actually be bent by the edge of the atmosphere, and at extreme zenith angles (degrees away from straight up), the beam will be separated into its component colors. In addition, even at noonday, the direct beam is not restricted to the precise region of the solar disk but instead "leaks" off the edge somewhat as a result of mild atmospheric scattering; this expanded region often appears as a slight "halo" around the sun. For the purposes of solar power engineering, the direct beam is taken to include light emanating from this halo, but is not concerned with atmospheric light splitting: during early morning and evening when bending becomes an issue, the sun is not strong enough for most solar systems to operate effectively.

Figure III-0: Acceptance Angle and the Direct Beam

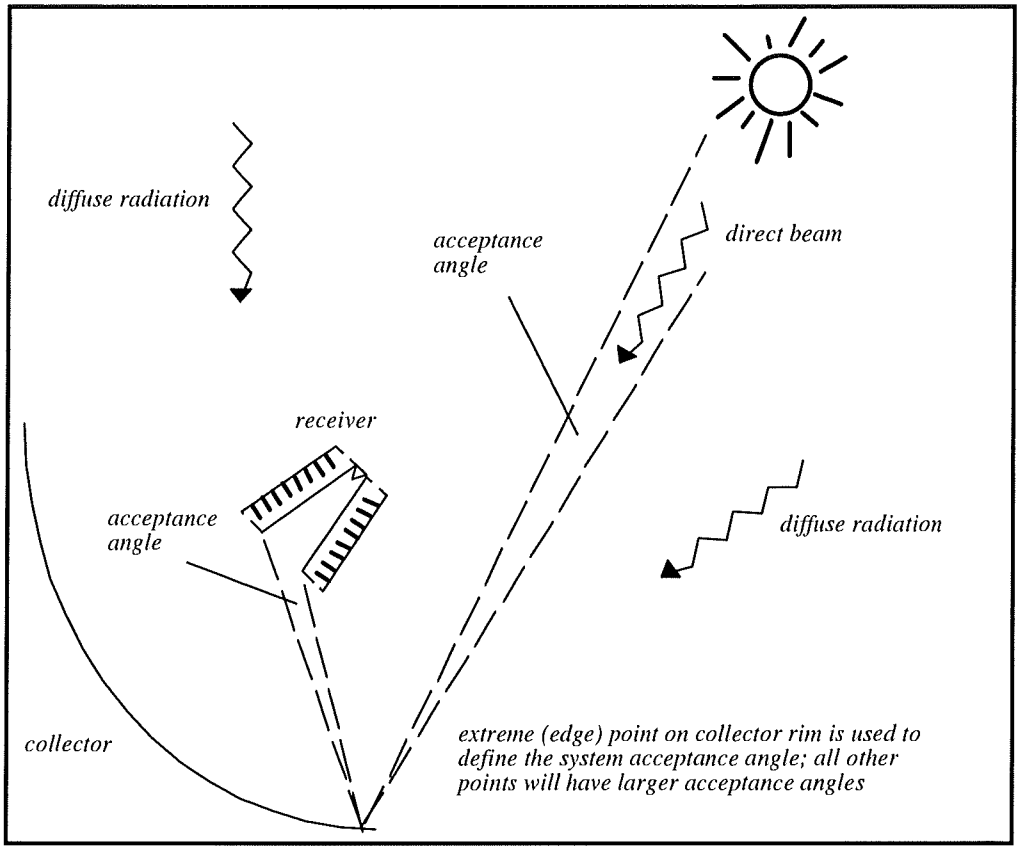

In dry, sunny locations with little cloud cover, the direct beam will contain a very large fraction of the total annual radiation; in more typical conditions, it will be about 70-80% of the annual total. For most systems in most locations, concentration increases the overall efficiency by an amount sufficient to justify discarding the diffuse radiation. Non-concentrating PV systems are the major exception to this rule. For STEPs, however, concentration is very important, working simultaneously to reduce system size and material, raise attainable system operating temperatures, and reduce re-radiation losses from the absorbing element.

At any moment in time, the direct solar beam is characterized in this study by four parameters: power, elevation, azimuth, and solar half-angle. The elevation and azimuth angles locate the solar disc and are calculated by a purely geometric model, depending only upon the hour of the day, day of the year, and latitude. The power is found by

combining the geometric model with measured data. The solar-half angle is nominally the sum of the angular radius of the solar disc (as seen from earth), mirror slope errors, mirror tracking errors, and mirror alignment errors, and is kept constant across all modeling runs for all systems. More detailed descriptions follow:

III.1.1.1 Elevation and Azimuth

A simple set of geometric formulas (adapted from Rabl 1985 pp.31-33) is used for the sun's elevation and azimuth:

$$\textbf{Declination, } \delta = \arcsin\left(-\sin 23.45^\circ * \cos\left(\frac{360^\circ * (n + 10)}{365.25}\right)\right)$$

...where n = the day of the year, a number from 1 to 365;

$$\textbf{Azimuth, } \theta = 360^\circ * (t / 24)$$

...where t = hour of the day, a number from 1 to 24;

$$\textbf{Elevation, } \phi = 90^\circ - \arccos(\cos\lambda * \cos\delta * \cos\theta + \sin\lambda * \sin\delta)$$

...where λ is the latitude, a number from 0 to 90

Note that the calculations depend upon the latitude (λ). This figure must be input as part of the model configuration, and before the STEP models are run, an "annual solar table" is constructed by the MS-Excel program (see appendix **B**). The axis of this table contains 5-degree intervals of azimuth, and the abscissa contains 5-degree intervals of elevation. Each cell of the resulting table contains a number which represents the fraction of daylight hours during the year for which the sun appears in the corresponding altitude and azimuth ranges. The table is normalized so that the fractions add to 1.0; note the basis for the fractions is 4380 (daylight) hours, not 8760 (total) hours. There are various conventions and possibilities for referencing these angles; throughout this study, the solar elevation is called PHI(s) and is measured in *degrees above the horizon with 0 at the*

horizon, while the solar azimuth is called THETA(s) and is measured in *compass degrees with 0 at due north.*

For example, at a latitude of 35 degrees, a figure of .004451 appears at the intersection of 175 degrees azimuth and 52.5 degrees elevation. Thus the sun appears in this region of the sky (a 5 degree by 5 degree region just east of south, and slightly above half-way up) for (.004451 * 4380 =) 19.5 hours each year. Compiling a table of this kind vastly speeds convolution of the STEP model over a year's worth of data (at the cost of an insignificant loss in resolution), because model results need only be calculated once for each cell in the table, rather than for each hour (or each minute, depending upon the precision of the convolution). In the above example, 19.5 hours are rolled into one calculation, even though these hours occur on different days in different months throughout the year. In fact, the annual solar table is constructed with quarter-hour temporal resolution, so the time savings for this particular region are almost 80:1. (Note that this removes the possibility of using a dynamic ambient temperature, but the savings in model execution are worth the minor inaccuracies thereby introduced.)[18]

III.1.1.2 Power

The solar flux is expressed in watts per square meter, and is approximately equal to 1350 W/m^2 (*SOLCON*) just outside the earth's atmosphere, with a percentage or two of seasonal variation due to the earth's eccentricity; these variations may be neglected for current purposes. The power remaining in the solar beam when it reaches the surface is a function of the quantity and composition of the atmosphere it has passed through. For a sunbeam, the atmosphere's thickness is equal to the thickness straight overhead divided by the sin of the solar elevation. It is not necessary, however, to model this thickness

[18] There are at least three model areas in which a dynamic ambient temperature could have come into play: gas turbine efficiency, receiver re-radiation calculations, and cogeneration capacity factor calculations. The first two areas are handled by using an average ambient temperature; see section **III.2.6.3.2** for further discussion of the cogeneration model.

explicitly. Rather, the solar model is calibrated through a quick recursive process as follows:

1. A maximum solar flux (*EARTH*) is chosen to represent conditions as if the sun were directly overhead. For example, in Dagget, California, 970 W/m^2 is an appropriate value.

2. The base atmospheric attenuation coefficient (ATTBASE) is calculated:

ATTBASE = EARTH/SOLCON (0.718 in our Dagget example).

3. For other elevations, the attenuation must be raised to a power representing the ratio between the perceived thickness and the minimum (straight overhead) thickness:

ATT = ATTBASE ^ (1 / sin (PHIS))

where *PHIS* = phi(solar) = the solar elevation. (These are the actual variable names from the model, and are used here to ensure consistency with the appendices.) To continue our Dagget example, at an elevation of 50 degrees, the attenuation will be 0.649.

4. The solar insolation at any time is equal to the solar constant times the new attenuation:

INSOL = SOLCON * ATT (876 W/m^2 at 50 degrees in our Dagget example)

5. The average insolation is calculated for each month (in this case, day by day and hour by hour; the annual table compilation method described above is *not* used), and compared to measured data published by the National Renewable Energy Laboratory (NREL 1997). Based on the comparison, a new noonday ground-level solar flux (EARTH) is chosen, and steps 2-6 are repeated. Three iterations is usually sufficient if a reasonable initial value is chosen.

In the example outlined, we began with the correct figure of 970 W/m^2 to match the NREL data for Dagget, California. Table **III-1** shows a month by month comparison of the measured data and the calibrated model. These values are in very close agreement; variation in the measured data from year-to-year for any given month's average may be up to 1 kwh / day, and the calibrated model is well within this limit for all 12 months. It is possible to detect some seasonal differences between fall and spring in the measured data which are not represented in the modeled data, but these trends will not have an important effect on annualized STEP performance. These Dagget calculations are exactly similar to those carried out on data from other locations to derive the results presented in chapter 5. Solar and climate data for all locations appears in appendix **B**.

Table III-1:
Comparison of Measured and Calculated Insolation Data at Dagget, California

Month	*Average kwh/day, Calculated by Model*	*Average kwh/day ±1 Measured by NREL*
Jan	4.9	5.4
Feb	6.0	5.9
Mar	7.6	6.9
Apr	8.5	8.1
May	9.7	8.9
Jun	9.7	9.7
Jul	9.6	9.0
Aug	9.2	8.7
Sep	7.8	8.2
Oct	6.6	7.3
Nov	5.2	6.0
Dec	4.7	5.4

III.1.1.3 Solar Half Angle

The modeling here follows standard practice in that a single half-angle parameter is used to represent a variety of factors which together determine the *minimum size* to which the solar beam can be focused. The primary such factor is the radius of the sun itself: at any point on earth, some of the sunbeams will come from the exact center of the solar disk while some will come from the edge of the disc; the angle between these rays is 4.7 milliradians. This angle will be preserved as the rays are concentrated onto the absorber: the incoming light cannot span less than 4.7 milliradians.

In real systems, even this limit is unachievable, because a host of tracking, alignment, and mirror-surface errors will spread the incoming light out even further (moreover, a small amount of sunlight in the "halo" comes from beyond 4.7 milliradians). Prediction of the precise value of these errors is extensive and subject to inaccuracy; it is common to roll them up together with the solar disk half-angle into an *effective* solar half angle (*SHA*). A value of .01 radians is typical for central receiver systems and is used here in the mini-tower system. The dish / Brayton system is modeled here without reference to a solar half-angle, because the receiver efficiency is stated explicitly in the source material. (Unlike central receiver systems, the geometric optics of a dish system is not a function of the solar position; thus, for the accuracy required here, one set of average specifications will suffice for all operating times and conditions. The mini-tower, by contrast, presents a different geometry at every sun position because the heliostats and receiver are fixed in place and do not follow the sun in the same sense that the dish does.)

The solar half-angle is a critical parameter in a central receiver system because it determines the lower limit on absorber size. (The smaller the absorber, the lower the re-radiation losses). In the ideal case represented by a perfectly focused heliostat pointed directly at the receiver, the radiation will be spread out to a diameter of 2*sin(SHA)*L, where L is the distance from the heliostat to the receiver. For example, if the heliostat is 100 meters away, then the image will be 2.0 meters across and any aperture smaller than

this will lose some of the light. In real systems, both focusing errors and astigmatic spread must be added to this width. For the mini-towers presented here, the spread from the solar half-angle may be responsible for anywhere from about 40% to 90% of the final heliostat projected image size. The modeling of image size and aperture acceptance is discussed in more detail in section **III.2.2**.

III.1.2 Concentration ratio and Efficiency

Another way to think of the solar half angle (SHA) is as a limit upon the maximum concentration ratio, which is the ratio between the aperture area (adjusted for any cosine viewing angle losses) and the absorber area. A high concentration ratio is desirable in order to reach high temperatures and correspondingly higher heat engine efficiencies. However, radiation is lost as a function of the fourth power of the absorber temperature, and many materials will melt under extreme solar flux, so the optimum operating point may not be at maximum temperature. In practice, reductions in absorber temperature are better achieved by increasing the flow rate of the coolant (often the heat engine working fluid), rather than by sacrificing concentration.

In theory, an absorber under maximum concentration "sees" only the surface of the sun, and therefore could reach thermal equilibrium (approximately 5700 K) with the sun if it were placed in outer space. In reality, this temperature range is not of interest and the concentration ratio is used only to calculate the absorber size (or vice versa) and the re-radiation losses; the theoretical maximum temperature is not approached. Furthermore, the SHA would have to be 4.7 milliradians, and as we have seen above, this limit is not realistic.

The thermodynamic limit on concentration is found through the conservation of optical *etendue*, or the aperture times the view factor (in finite systems, these quantities must be integrated – see, for example, Gordon and Ries 1993). The "view factor" is the fraction of

the total space (e.g. a hemisphere for a flat surface) above an object which is occupied by another object. The "view factor" of the solar disk is the solid angle which it subtends, equal to $\sin(.0047)^2 * \pi$ steradians. To minimize the aperture, the view factor must be maximized; the logically maximum possible view factor is π steradians; thus the aperture must be reduced by a factor of $1/(\sin^2(SHA))$. Thus the maximum solar concentration in 3-dimensions is:

$$Cmax = 1 / \sin^2(SHA).$$

For the ideal SHA of 4.7 milliradians, Cmax is equal to 45,270, but for the more realistic SHA of 10 milliradians which is used here, Cmax = 10,000. For example, a heliostat field with a solar aperture of 20,000 m^2 can never be concentrated onto an absorber with an area smaller than 2 m^2 without losing some of the light.

Dish systems are mildly hampered by the shading caused by the receiver and engine unit, but well-constructed units may approach these concentration limits. However, it is impossible for a real-world central receiver system to come anywhere near this limit, for two equally important reasons:

Blocking and Shading Restrict Ground Coverage. The thermodynamic limit assumes that the reflector (the heliostat field) is continuous; therefore, the aperture area is also equal to the mirrored reflector area. In practice, significant space must be left between heliostats, or else each heliostat will be shaded by its neighbors closer to the sun (if the sun is not directly overhead), and blocked by its neighbors closer to the tower. The mini tower model explicitly calculates these losses for each heliostat and part of the optimization procedure is to place heliostats closer and closer together until the losses outweigh the gains. (Of course, if heliostats are extremely tightly bunched, maintenance and repair access become critical as well.)

Finite Heliostats Lead to Astigmatic Losses. Under the limiting assumption, the reflector is a smoothly curved parabola rather than a fresnel system with heliostats of finite size. In reality, the finite sized heliostats, even if focused perfectly upon the receiver, will generate image spread in addition to that caused by SHA. This spread is due to the astigmatic focusing properties of a circular lens (or a parabolic lens – there is no meaningful difference at the minute curvatures required for heliostat focusing).

When the heliostats are installed in the field, they are "canted" by one of several methodologies (Jones *et al* 1995) so that the entire heliostat (which may be composed of several facets) is focused as a concave lens upon the receiver in the tower.[19] Thus when the sun is almost behind the receiver (as seen from the heliostat), the heliostat would focus parallel radiation to a point at the receiver. The solar radiation is not parallel but rather characterized by the SHA, so the image at the receiver has a width of 2*SHA*(the distance to the receiver), as previously mentioned.

However, if the sun is *not* directly behind the receiver, then the heliostat is *not* pointed directly at the tower but is instead pointed so that it's surface normal bisects the angle between the sun and the receiver. In this position, the angles of incidence (to the sun) and reflection (to the receiver) are equal, but the image is *not* focused to point, even for parallel radiation. Rather, the "tangential" rays (lying in the same plane as the heliostat, sun, and receiver) focus in front of the target, and the "sagittal" rays (lying perpendicular to this plane) focus at another point behind the target. The receiver will be located between these points, at the plane of least projected area, provided that the heliostats were correctly canted.

[19] Various canting and focusing systems exist, including heliostats which are not canted at all, but are simply left as flat reflectors. This practice only makes sense if the receiver aperture is substantially larger than the individual heliostats. Another system, devised theoretically at the Weizmann Institute in Israel, arranges the rotational axes of the heliostats so that one of these always points at the receiver. As a result, the heliostats can have a permanent correction for astigmatism built into their canting; conventional heliostats cannot do this because the orientation of their axes is always changing with regard to the receiver. Despite the elegance of the Israeli proposal, the benefits turn out to be marginal. (Zaibel *et al* 1995)

A full explanation of this effect can be found in most optics texts; Rabl (1985) is particularly lucid. In the mini tower model, the heliostat canting is assumed to be imperfect (see section **III.2.2**). The adjusted heliostat focus, as well as the tangential and sagittal foci, are explicitly calculated so as to determine the dimensions of the ellipse which actually strikes the receiver plane. (SHA spread is also added at this point.).

As a final note, the focusing of the individual mirror facets is ignored. (At Solar Two these facets are rectangular, while for the mini-tower a circular facet is used as explained below.) In the base-case mini-tower model, there are 6 facets on each heliostat, and even if these were completely flat, they would still generate less image spread than the heliostat as a whole. Moreover, it is expected that the round facets can be focused fairly accurately.[20]

III.2 Mini Power Tower System

This section presents the system modeling methodology for the MPT system. The goal has been to achieve sufficient accuracy to ensure useful comparisons across systems and to predict performance results for a typical year. The model is not exhaustive in breadth: there are many other power tower configurations which have not been considered. Different heliostat designs, alternative receivers, and power cycles based on different principles are all possibilities. However, the choices made here are believed to represent the best configuration for the MPT within certain external constraints: namely, that the system make use of a gas turbine, that it operate in a hybrid fashion, and that it be small (2-4 megawatts). As discussed in chapter 1, this set of priorities led to the choice of a cavity receiver (with a secondary concentrator and/or a window), a one-sided field, and a rotationally constant rim angle (oval heliostat field).

[20] If the facets actually have a *negative* focus (i.e. they are convex on the reflective side), then the image spread will rapidly become a very grave problem. However, there is no difficulty in ensuring a fairly accurate, concave curvature for the SAIC type round facets.

All of the systems (MPT, D/B, and LDA) are modeled in MS-Excel on a personal computer with a Pentium processor. The Excel spreadsheets and programs are presented in the appendices. The input and output sections of the these sheets are frequently self-explanatory; in any event, the relevant results are discussed completely in the text. Where an italicized, capitalized title appears in this section in parentheses following the description of a parameter, it indicates that the parameter exists as a variable (input or output) in the spreadsheet model, and the titles will be consistent throughout the text and the appendices.

Figure III-1:
Mini Power Tower System Components

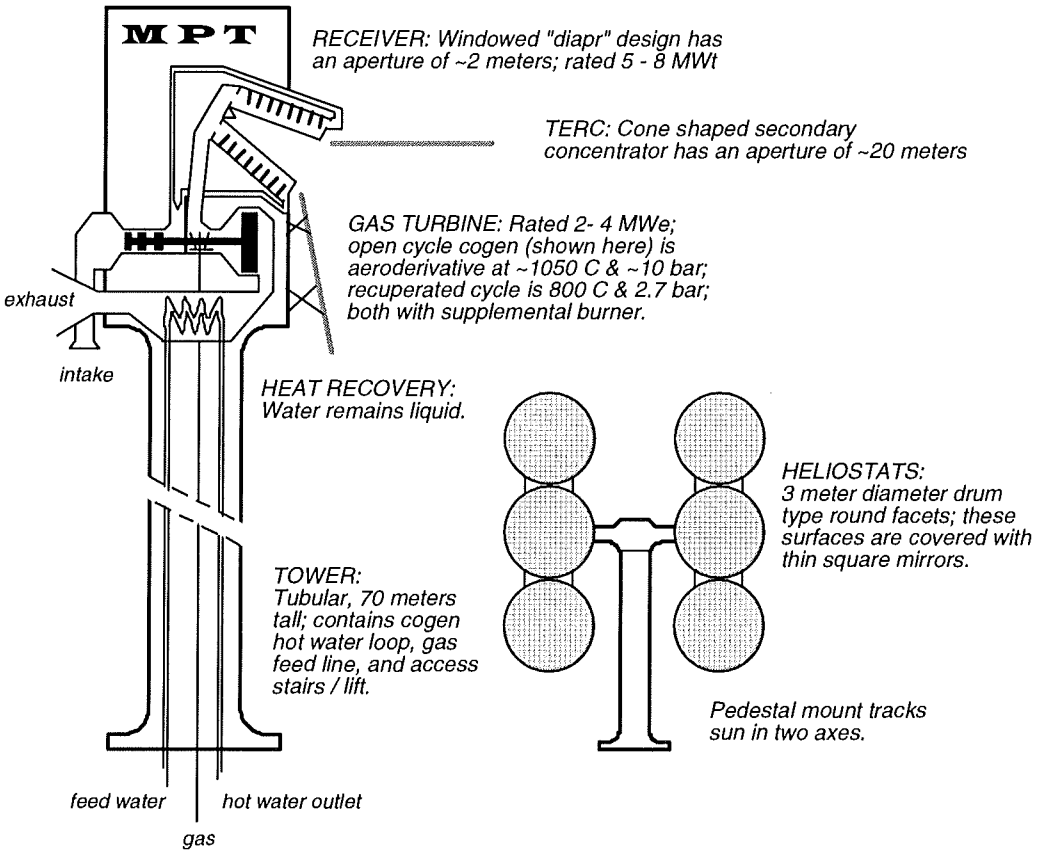

III.2.1 Tower

The field definition process begins by defining the tower height (*THEIGHT*) and mean half-width (*MTHW*). For modeling purposes, these parameters fully define the tower. At relatively modest heights, the taller the tower, the more optically efficient the field (because the average angle between the sun and the tower, as seen by the heliostats, is reduced). However, as the tower reaches a certain level, the growing distance between the heliostats and the receiver (at the top of the tower) begins to counteract the beneficial effects of tower height, as image spread (which increases with distance) becomes a problem. However, this effect is much less pronounced (happens at a much greater height) for configurations which include a TERC, as do most of systems explored here. Optimization of tower height is discussed in further detail in chapter 5, and the selection of a constant tower height of 70 meters is explained. Tower height also has important implications on rim angle and field size; these are discussed in section **III.2.3**, which addresses field layout.

The width of the tower is not critical so long as the tower is fairly narrow. As the sun swings across the southern sky, the tower casts its shadow across the heliostat field, shading a number of heliostats at any one time. These losses are calculated in the model (see below) assuming that the tower is a perfect cylinder of uniform (or average) width. Although real towers will be slightly broader at the base and at the top (where the receiver equipment and the turbine require extra space), the average width is adequate for modeling the relatively minor tower shading losses. It helps that this shading effect is reduced when the sun is high in the sky, a characteristic trend for heliostat fields: all of the major loss mechanisms (with the exception of re-radiation) are less acute at the times of maximum insolation, but in early morning and evening, the performance falls off dramatically.

The gas turbine is located at the top of the tower. The small physical dimensions and relatively light weight of aeroderivative (and even some of the lighter industrial-type)

turbines (see section **III.2.6**) make this possible. Furthermore, the maintenance needs for the turbine are minimal and it is expected that a stairway within the tower will be all that is required. Finally, placing the turbine in the tower removes any need for a separate exhaust stack. A gas line will need to run up the tower, and in the case of the cogeneration system, a loop of pressurized water pipe see section **III.2.6.3.1**).

Placement of the turbine on the ground was considered as an alternative configuration, but rejected because of the large exposure to thermal and pressure losses which would be created by long (70 meters) air ducts within the tower, as well as the increased expense incurred by these ducts. A hybrid solution, in which the turbine was on the tower, but the exhaust gases were ducted to ground level for the cogeneration application, was likewise rejected. The greater density, ease of compression, and heat capacity of the water all suggest that it is the appropriate heat carrier for the length of the tower.[21]

III.2.2 Heliostats

The heliostat design has only limited effect on system performance and is determined more by cost and maintenance considerations. The design modeled here is based upon a prototype developed by SAIC (SAIC 1997a). Round, drum-type facets are fastened in rows on either side of the central pedestal shaft. The front face of each facet consists of mirrors bonded to the steel skin of the drum. The focus of each individual facet is maintained by a vacuum system within the drum, and all of the facets on each heliostat are collectively canted so as to reach their minimum focus at the receiver aperture. In addition to the cost reductions expected to result from adoption of drum-type heliostats, there was an additional motivation for the choice of SAIC facets: these units are exactly the same as those used in the SAIC dish, vastly facilitating direct comparison between the *other* characteristics of the dish / Brayton and MPT systems: aside from minor differences in the support structure, an SAIC dish is roughly equivalent, in technology and cost per

[21] Many thanks to Tom Kreutz of Princeton CEES for his helpful comments in this area

square meter, to an SAIC heliostat. These collecting elements are among the most influential in a solar plant, by equalizing them, this study allows a much clearer comparison of the other elements (e.g. geometric optics, receiver performance, gas turbine efficiency).

The SAIC facets in the model are each 3.0 meters in diameter (*MDIAM*), just as they are in reality (SAIC 1997a, SAIC 1997b, SAIC 1997c, Beninga 1997; note that these are the exact same facets used in the dish model; see section **III.3.1**).[22] However, the heliostats have been reduced from 22 facets each (155 m^2) to 6 facets each (42 m^2). The original design is intended for use in much larger fields, in which the size of the individual heliostats is much smaller relative to the size of the receiver. However, in the smaller MPT field, reduced heliostat size is necessary to ensure that the receiver size remains unaffected by *facet* focusing and that *heliostat* focusing ("canting") remains dominant. Of course, further size reductions would further increase optical efficiency, until at the theoretical limit the heliostat field could be independently aligned at every point. However, this degree of miniaturization is impractical and unnecessary; the returns are diminishing as heliostats shrink, while the cost (of extra pedestals and drive mechanisms) increases. The choice of 6 facets is somewhat arbitrary but was chosen because it allows an adequately tight focus without raising serious questions of practicability. Furthermore, the 6-facet heliostat presents a nearly square finished shape (two vertical rows of three facets, with a large gap in between for the pedestal mount and drive mechanism), which considerably eases a number of field modeling areas (particularly blocking and shading).

The MPT model allows the user to define the diameter (*MDIAM*) of the facets and the number of facets on each heliostat (*MNUM*). These figures are used to layout the heliostat in a rectangular shape, as square as possible. The width (*HX*), height (*HY*), and area (*HAREA*) of the rectangle are computed for use in the rest of the model; these are

[22] There are some minor but perplexing discrepancies in the SAIC reference materials concerning facet diameter. Beninga (1997) and SAIC (1997c) state 2.8 meters, while SAIC (1997a) states 10.5 feet (3.2 meters), and SAIC (1997b) implies 3.06 meters by specifying 16 facets with a total area of 118 m^2. It appears that several prototype sizes have been constructed, or else the information sheets are simply careless. In either case, a diameter of 3 m, used here, adequately represents all of the specifications.

particularly important in determining the heliostat focus (see below), blocking, and shading (see section **III.2.7.2**).

Heliostat Focus

Each heliostat in the field is modeled separately. The heliostat is placed automatically (see section **III.2.3**) and then the angle between the sun and the tower is calculated geometrically. One-half of this angle, a critical parameter for this unit throughout the rest of the model, is dubbed "epsilon". The solar flux impinging on the heliostat is equal to the current solar beam (see "Solar Data" above) times cosine(epsilon), minus any shading losses from the tower or other heliostats. This flux is relayed to the receiver, minus reflection and blocking losses ("blocking" refers to other heliostats between the heliostat and the tower). The characteristics of the relayed beam are used to determine the amount of this radiation which actually passes the aperture of the receiver (or of the TERC secondary, if one is used).

Heliostat focus is not assumed to be perfect, but a lack of data prevented reconstruction of a typical focal error distribution; even if this were available for one of the few existing installations, it would not necessarily apply to the SAIC units. Instead, each unit was focused 5% short of the receiver,[23] this becomes the design specification for MPT fields as follows: in a real installation, each heliostat would be focused exactly on the receiver aperture, and then after some time the real foci could be measured. The model assumes that the distribution of errors found would have effects less severe than a 5% reduction

[23] The 5% error is taken in the direction of the heliostats (that is, the focus is too short rather than too long) because this direction results in a larger astigmatic error. In an astigmatic situation, the sagittal focus is behind the focal plane while the tangential focus is in front of it. As a result of coming to a shorter focus, the tangential rays are diverging at the receiver plane (plane of minimal image area) faster (with a greater slope away from the normal) than the sagittal rays are converging. By moving the receiver plane back (equivalent to a shorter focal length), the focal area is increased (it becomes an ellipse as the sagittal spread reduces and the tangential spread increases) according to this greater, tangential diversion. This results in a larger ellipse than would be found if the focal plane were moved the same distance forward.

across the board; this seems a safe assumption.[24] Note that this is a focal length error, not an aiming error; each heliostat is assumed to be aimed correctly (at the dead center of the aperture unless a TERC is used, in which case each heliostat has a slightly different aim point). The aiming errors are included in the solar half-angle (*SHA*) as is customary in STEP modeling; the value of 10 milliradians (.010 rads) used here is standard.

The heliostat image size at the receiver, and the fraction of light admitted, are estimated as follows: first, the heliostats are assumed to be round reflectors of equivalent area to the real, multifaceted, rectangular shape, accelerating the calculation of tangential and sagittal foci (see section **III.1.2** for an explanation of these terms). The facets are assumed to be canted so that the adjusted focus is 5% short of the receiver, as described above. The tangential and sagittal foci are determined separately, and the difference between these lengths and the actual distance to the receiver (called the "slant range" in CR parlance) are used to find the height and width of the ellipse which reaches the receiver. At this point, these dimensions represent the astigmatic effects of a point source; solar half-angle effects must be added to both axes of the ellipse, increasing the total dimension considerably. The total area of the resulting ellipse is calculated and compared with the receiver's aperture. The formulas are as follows (adapted from Rabl 1985 pp. 177-182):

[1] $f_S = f_0 / \cos \varepsilon$

...where f_S is the sagittal focus, f_0 is the nominal focal length (set 5% short of the receiver as explained above), and ε is epsilon, the half angle between sun and receiver, as defined above;

[2] $f_T = f_0 \cos \varepsilon$

...where f_T is the tangential focus;

[24] It is not as simple as defining the average error to be 5%, because the relationship between focal length error and radiation accepted is in no sense linear and depends upon the heliostat size and position, the sun position, and the receiver diameter.

[3] $h_T = (D - f_T) * w * \cos \varepsilon / f_T$

...where h_T is the length of the tangential axis of the image ellipse at the receiver plane, D is the slant range (actual distance to the receiver) and w is the (mean) heliostat diameter;

[4] $h_S = (f_S - D) * w / f_S$

...where h_S is the length of the sagittal axis of the image ellipse at the receiver plane. Together, h_T and h_S define the area of the image ellipse, which can then be compared with the aperture.

Although the elliptical image thus produced is exact (for the SHA, focal length, and heliostat shape approximations) and located *at* the plane of the aperture, it is not *in* the plane of the aperture; rather, the aperture is tilted away from the heliostat by an angle equal to the individual rim angle for this unit. A completely rigorous model would then project this ellipse onto the receiver's aperture plane *first determining the orientation of the sagittal and tangential axes relative to the direction of projection.* Although the area of the new image can be calculated easily from the rim angle, the shape is far more complex, as the sagittal and tangential axes will be lengthened by different factors depending upon their orientation. In fact, the resulting image may not even be defined by the tangential and sagittal axes; in some cases an intermediate diameter of the ellipse will become the largest diameter in the projection. After determining this image, the overlap with the circular aperture must be calculated, using calculus or, more probably, numerically. The grand result, the fraction of flux admitted to the aperture, will still be compromised by the estimates of heliostat shape, focal length, and solar half-angle.

Figure III-2:
Tangential and Sagittal Foci

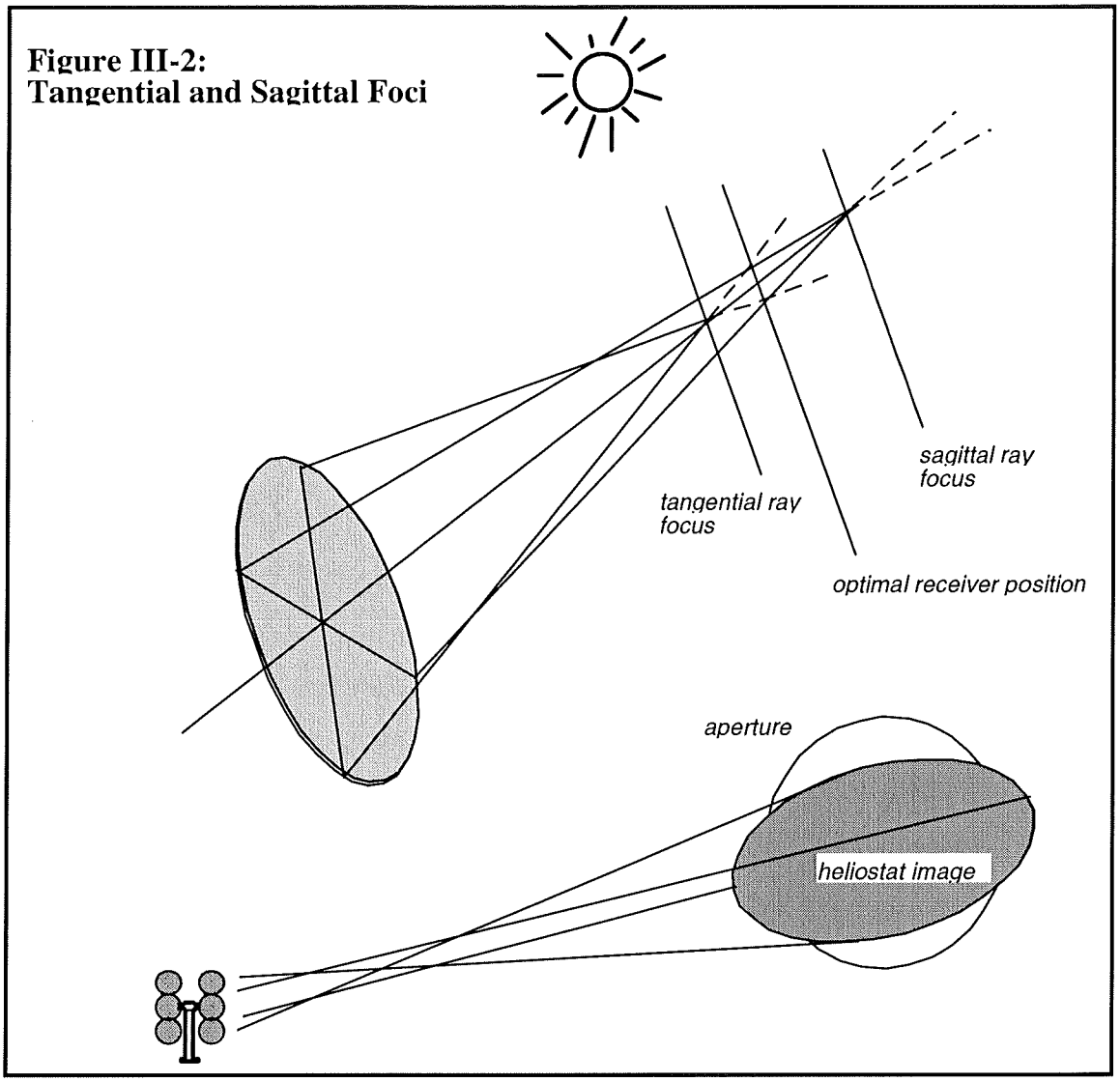

In order for the model to run at reasonable speeds on the fastest machine available (a 300 MHz Pentium II lent for this purpose by an off-campus source), this level of rigor had to be abandoned. Fortunately, the rim angles of interest for the MPT are small, and thus the distortion to the ellipse upon projection is not severe. Consider a field with a rim angle of 35 degrees: for the worst-case heliostats, the extension of any single ellipse diameter can be at most (1 / cos(35) - 1 =) 22%. In most cases, this maximally extended chord will *not* be the actual maximal diameter of the ellipse (the sagittal axis, in the case of a shortened focus). Rather, the distortion to the maximal axis will vary from 0% to 22% according to a sin curve, with an average lengthening of (2 / π * .22 =) 14%. For a heliostat closer to

the center, at the average rim angle for this field of 25 degrees, the average lengthening of the maximum (or any other) ellipse axis is only 6.6%.

The distortions for the heliostat images are handled on this average basis. For each heliostat, the average diameter lengthening factor is calculated as [1 + (2 / π) * (1 / cos(RA) - 1)] where RA is the rim angle of the individual heliostat (see example in above paragraph for derivation). This factor is applied to *both* the tangential and the sagittal axes (as calculated in equations [3] and [4], above), to create a new, average ellipse.[25] For a given heliostat, the lengthening factor will be the same regardless of solar position; this approximation must be followed in some cases by another: If the new axes are both greater than the diameter of the aperture, then area of the aperture as a fraction of the area of the ellipse becomes the "acceptance" for this heliostat.[26] If the new axes are both shorter than the aperture diameter, then the acceptance is 100%. However, if one axis is larger than the aperture and one is smaller, then the overlap is calculated through a "rectangular" approximation: the ellipse is transformed into a rectangle with the same height and width, and the circular aperture into a square; the fraction of the rectangle which overlaps the square is easily calculated, as is the portion of the square which overlaps the rectangle on its longer sides. This approximation avoids the need for a numerical solution. Note that these calculations are performed on each heliostat for each sun location in the sky (5 degree squares; see section **III.1.1.1** above).

---

[25] The special case in which the new ellipse will have neither the tangential nor the sagittal axes as a maximum are ignored, because this peculiar situation will only occur for the most central heliostats where rim angles, and images, are small.

[26] Even this is not entirely accurate. The real heliostat image is not covered by uniform flux, but is stronger in the middle and fades towards the edges, because these regions only receive flux from the edges of the sun, whereas the middle of the image contains rays from all points of the sun. The constant-flux modeled here is conservative, because it overestimates the losses incurred if the edges of the image do not pass the aperture.

III.2.3 Field Layout

The heliostat field is generated automatically by the MPT program, and a large variety of configurations can be examined within this single model. In the completed field, each heliostat is represented by a location in (x,y) coordinates with the tower located at the origin. The shape, placement, and composition of the field is determined by six parameters: the tower height (*THEIGHT*), the maximum field radius (*FRAD*), the plant radius (*PRAD*), the construction rim angle (*CRA*), and the heliostat spacing in the north-south (*YFOOT*) and east-west (*XFOOT*) directions. The size of the heliostat modules, represented by their height (*HY*) and width (*HX*), is also important.

The maximum field radius (*FRAD*) determines the distance between the tower and the most distant heliostat, which is labeled #1 in the spreadsheet and is always placed due north of the tower. This heliostat is located at the construction rim angle (*CRA*) as seen from the tower, thus the angular center of the field (rim angle = 0) is located at the point (0,*YCENT*) where *YCENT* is calculated based on *THEIGHT, FRAD,* and *CRA*. The rest of the field is constructed in rows below the first heliostat, with the following constraints:

1. No heliostat can have a rim angle greater than *CRA*.

2. Each heliostat is a distance *YFOOT* from its neighbors (if any) to the north and south, and a distance *XFOOT* from its neighbors (if any) to the east and west.

3. Each successive row is staggered by (*XFOOT*/2), like seats in a movie theater, so that each reflector will have a minimally obstructed view of the receiver.

4. No heliostat can be closer to the base of the tower than the distance *PRAD*, which defines a clear area where power plant components must be located. If the field is located far enough to the north, *PRAD* may not come into effect at all because the rim angle at (0,*PRAD*) may be larger than *CRA*.

Chapter 5, figure **V-1d**, contains heliostat field layouts for various locations and power cycles.

If *FRAD* is large enough and *CRA* is small enough, the entire field will be located to the north of the tower, but this is not necessarily so. (For example, if *THEIGHT* is equal to *FRAD*, then a *CRA* of 45 degrees defines a completely circular field.) Heliostats deep behind the tower may be blocked by the tower itself, and this is not allowed in the model. Therefore, in the examples presented here, *FRAD* is much larger than *THEIGHT*, *CRA* is usually 45 degrees, and the field is therefore almost entirely in front (to the north) of the tower. This location aids optical efficiency for temperate zone latitudes; the ideal location for the field at any point in time is directly down-sun from the tower, so that the receiver's shadow strikes the heliostat located at (0,*YCENT*). At the latitudes modeled here (between 30 and 40 degrees north) this suggests a field located substantially to the north of the tower.

III.2.4 Receiver

The MPT receiver is more dependent on technological innovation than any of the other system elements. Although an air receiver has been developed for a one-sided field as part of the PHOEBUS system (see chapter 2), this receiver is not appropriate for the MPT because it does not use pressurized air. Moreover, the PHOEBUS receiver is not a cavity design, and is thus not optimum for the small rim angles which are achievable in the MPT (due to small overall size). Apart from PHOEBUS, a number of small scale air receivers are relevant for the MPT modeling, these are the Allied Signal dish / Brayton (ASDB) receiver, and the directly irradiated annular pressurized receiver (DIAPR) developed at the Weizmann Institute and introduced in chapter 1. Both of these receivers are of the cavity type.

The ASDB receiver is used for the dish / Brayton model, and is discussed in detail in section **III.3.2**. This type does not use a window, but allows for pressures above ambient because the air is physically separate from the cavity. By contrast, air flows directly into the cavity of the DIAPR, which is protected from the outside by a fused quartz window.

The MPT receiver is neither a DIAPR nor an ASDB, but rather a generic cavity receiver with feasibility considerations and performance characteristics based upon both ideas. The relatively modest size of the MPT makes the scale-up of these receivers less problematic than it would be for a full-scale power tower. For example, the DIAPR design has been physically validated at the 50 kWt scale (Karni *et al* 1995), and the MPT only requires about 3 MWt or less; this is equivalent to a scale-up factor between 8:1 (for the aperture diameter) and 4:1 (for cavity dimensions).

The MPT receiver has the following characteristics:

1. The receiver aperture diameter (*DIAPE2)* is variable and is defined by user input. When a TERC is used, then the program chooses both *DIAPE1*, the aperture of the TERC, as well as *DIAPE2*, based upon the achievable concentration ratio for the TERC (see section **III.2.5**).

2. The air outlet temperature at maximum flux (*TMAX*) is variable and is defined by user input. An outlet temperature of 800 C was used to produce most of the results presented in the current study, but this figure can be reduced as necessary.

3. The airflow is calibrated to the maximum temperature and maximum flux and is kept constant, so the outlet temperature floats with the solar flux. This is more efficient than varying the air flow and keeping the temperature fixed (reduced radiation losses).

4. The air outlet temperature (*RECTEMP*) is calculated dynamically once flow is calibrated.

5. The re-radiation losses are calculated dynamically based on the aperture area and the (fourth-power corrected) average of the air inlet and air outlet temperatures. The air inlet temperature (*CRET*) is determined in the gas turbine model and is equal to compressor exit conditions or recuperator exit conditions (for the RGT case.) The emissivity is assumed to be 1.0, which is a conservative but not unrealistic choice for a cavity receiver.

6. Receiver pressure is determined by inputs to the gas turbine model.

7. The total pressure drop in the receiver is five percent (5%) of the compressor (or recuperator) outlet pressure. This drop *only* applies in solar mode; when the MPT is running gas-only, it is assumed that the receiver is shut off and the air is ducted directly to the gas burner without significant losses. The figure of 5% is intended as a conservative (overestimated) approximation of the receiver pressure drop.[27] The effect of this pressure drop on plant performance is discussed below in section **III.2.7.5**.

8. A window is optional. If a window is specified, a small amount of flux is reflected at the window (see **section III.2.7.3**), but the dramatic reduction in re-radiation losses dwarfs the reflections. The window is cooled by the incoming air stream (as in the DIAPR) and therefore is not itself a source of significant radiation. Long-wave heat radiation emanating from the inside of the cavity is determined as in the non-windowed case, but the window (fused quartz) only transmits 38.2% (*WTFEED*).[28] The rest is absorbed (or reflected) at the window and passed back into the cavity.

---

[27] The justification for this figure is as follows: Allied Signal (1997) indicates a drop of 2% for the much smaller ASDB receiver, while Grasse (1991) implies a drop of just under 5% for the much larger PHOEBUS receiver (it is acknowledged that these designs are very different and cannot be directly compared). In light of these data points, it seems reasonable to suppose that a receiver can be constructed for the intermediate scale MPT with a pressure drop of 5% or less.

[28] Incropera & De Witt (1990) present data which suggest that the transmissivity of fused quartz is very near 100% for shortwave (e.g. solar) radiation and continues at near 100% up to a certain region of the spectrum,

The modeling properties above define the MPT receiver. Its materials and structure are not explicitly addressed here, and thus the receiver is the most important area for future R&D on the MPT system. Nonetheless, the behavior of the windowed receiver is very much within expectations for a scaled up DIAPR, and the non-windowed version does not present an insuperable set of conditions, particularly if the ASDB receiver, currently under development, lives up to expectations. In this latter case, it is *essential* to realize that the temperature in the MPT is a variable quantity, and can be reduced if material limits or heat transfer failures require such de-rating when the ASDB unit is scaled up (the DIAPR is expected to handle the 800 C range easily). Unlike a solar-only system, the hybrid MPT suffers a loss in solar fraction but *no loss* in efficiency when *TMAX* is reduced.

III.2.5 Secondary Concentrator (TERC)

The tailored edge-ray concentrator (TERC) is a relatively new idea for a secondary solar concentrator, introduced by J.M. Gordon and Harald Ries (1993). There does not appear to be anything particularly difficult about its construction; the main innovation, as discussed in chapter 1, is in revising the heliostat aiming strategy so that each edge ray strikes a unique point on the secondary. The TERC itself consists of two segments: an

---

within which it falls very rapidly to nearly 0%. The cut-off region appears to be around $\lambda = 4$ microns. (Data for the particular material in use at the Weizmann Institute is not available).

A computer program was constructed in MS-Excel to calculate (based on the Planck distribution) the fraction of blackbody radiation at a given temperature which would pass through a material having the following property: transmissivity of 100% for waves shorter than 4 microns, and transmissivity of 0% for waves longer than 4 microns. The program accepts as input two temperatures, representing the extremes of a spatially linear temperature distribution along the emitting material (in this case, the inlet and outlet temperatures for the receiver cavity). The range between these extremes is divided into a number of temperature "zones" and the program calculates the net transmittance (through the 4-micron-cutoff material) for each zone; the results are summed. The net effect is an integrated calculation of net window transmittance for a linear temperature distribution in the receiver.

The program was constructed as a function which could be called dynamically in Excel by passing the receiver inlet and outlet temperatures, which vary with insolation, degree of recuperation, etc. However, invoking this function (which contains a double integral, first over the Planck spectrum and then over the temperature distribution) had an unacceptable impact upon code execution, so the dynamic function was replaced with the result for the temperature range 600-1000 K, representing fairly "average" receiver

inner ring shaped in a parabolic form, and an outer, much larger, ring shaped approximately like a cone. The concentrator can be optimized to the heliostat field so that it is not excessively large, and is capable in most practical installations of increasing the concentration to 60 or 70% of the thermodynamic maximum. This increase may also be expressed as a reduction in the receiver aperture size: for the MPT systems analyzed here, the outer TERC aperture may be 3-10 times the size of the receiver aperture. Nearly all of the rays which pass the outer aperture are redirected to the receiver; some are absorbed or scattered by the TERC, which is modeled here with a reflectivity (*TROE*) of 93%.[29]

A complete set of equations for constructing the TERC was not available, and in any case, theoretical developments in this area are still ongoing. Fortunately, Gordon & Ries (1993) present results for two TERCS, one of which is an appropriate choice for the rim angles of interest in the MPT. In all cases, choosing a TERC for a given rim angle is not straightforward, because the secondary must actually be designed for a field with a much *larger* rim angle field and then truncated. This is because the complete TERC always physically terminates at the edge of the field itself; that is, it is a mirror the size of the entire heliostat field! Not only is this structure absurd in size, but it would shade all of the mirrors. However, as heliostats at the edges of the field are removed, the edges of the TERC are no longer used, and it shrinks very rapidly. This process is continued until the TERC reaches a chosen depth (distance from the receiver aperture plane to the TERC aperture plane), and until the field rim angle reaches a desired value. Care must be taken to ensure that both of these requirements are satisfied.

The principal TERC used here is one designed for a rim angle of 49.6 degrees and presented in Gordon & Ries (1993). (This happens to be the maximum rim angle for which a TERC can collect 100% of the incoming rays, but smaller angles are possible.)

---

conditions. When called with this range, the function returns a net transmissivity of 38.2%. Appendix **A** contains a chart which shows results for a broad variety of temperature ranges from 400 K to 1100 K.

[29] Note that the heliostat reflectivity is only 90%. It is assumed that greater care and quality would be used on the more critical secondary mirrors. The figure of 93% is not at all unrealistic; the "Carissa Plains" modules used to replace some of the heliostats at Solar Two measured a mean reflectivity of 94% (Jones *et al* 1995).

This TERC is the right choice for real field rim angles in the 35-45 degree range, because the depth becomes quite shallow: 2% of the slant range to field center at 35 degrees rim angle; 4% at 40 degrees rim angle. Furthermore, a high degree of concentration is maintained: 63% of the thermodynamic maximum at 35 degrees rim angle, and 78% at 40 degrees. Note that this TERC has the same *inner* (receiver) aperture regardless of whether it is truncated for use with a 35 degree field or a 40 degree field. With the 40 degree field the TERC is about twice as deep (and more than twice as large in mirrored area because it spreads out like a cone), and the concentration ratio is naturally better because the inner aperture is fixed while the field has grown.

For narrower rim angles below about 30 degrees, a TERC designed for a rim angle of 35 degrees could be used instead; results for this version are also presented in Gordon & Ries (1993). Performance is similar but the TERC is a little larger relative to the field: at 25 degrees rim angle, the concentration is 62% of the thermodynamic maximum and the depth is 4% of the slant range to field center; at 30 degrees, concentration is 73% and depth is 10% of slant range. The MPT designs actually selected for final analysis all have rim angles above 35 degrees, and all of them use the first (50 degree) TERC. Although this TERC cannot be 100% optimal for each different rim angle, its performance is very representative of what these secondaries can accomplish. The curve of concentration ratio as a function of TERC depth (which is locked to rim angle) is very shallow in the range of interest (see fig **III-3**); thus further TERC optimization is not expected to alter results.

Figure III-3:

Relationship Between TERC Depth, Rim Angle, and Concentration

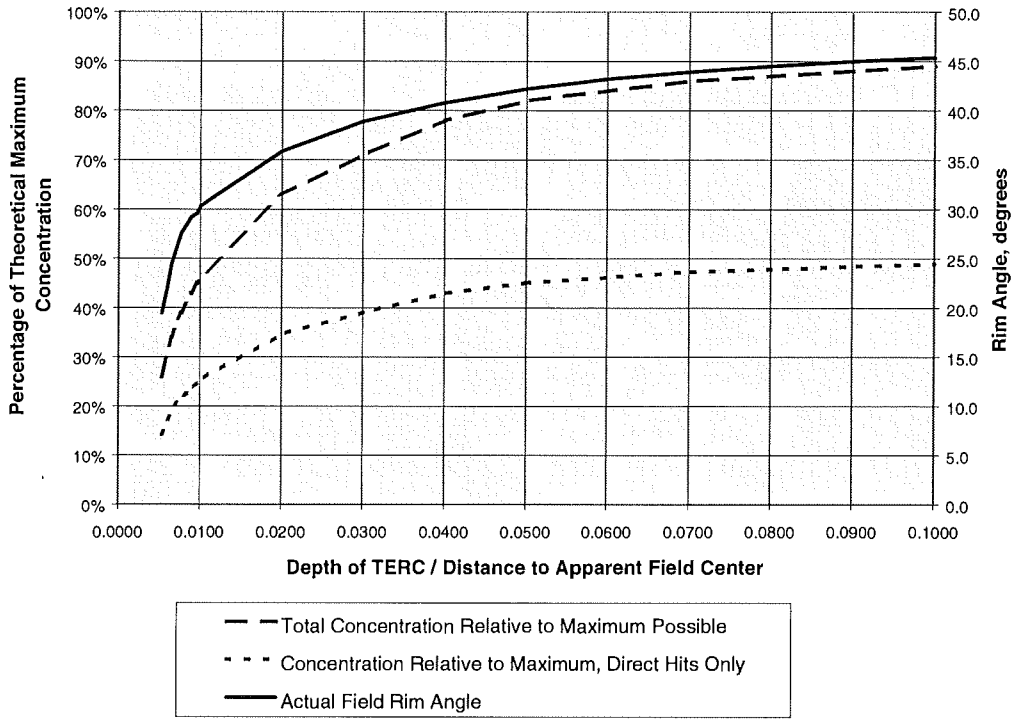

Source: Adapted from Gordon & Ries (1993). Bumpiness of lines is an artifact; they ought to be smooth, as these are theoretical calculations only.

Each TERC design in Gordon & Ries is accompanied by a graph giving the net concentration ratio as a fraction of the thermodynamic concentration limit; the ratio is plotted as a function of field rim angle. Before applying these figures, the MPT spreadsheet first calculates the thermodynamic limit on concentration for a heliostat field of the given rim angle (*CRA*), according to the formula (adapted from, e.g., Gordon & Ries 1993):

$$\sin^2\phi / (2 * \cos\phi * \sin^2\theta * (1 - \cos\phi))$$

...where ϕ is the field rim angle (*CRA*) and θ is the effective solar half-angle (*SHA*).

Note that this concentration is *geometric*, not *energetic*: because there are spaces between the heliostats, this degree of energy concentration cannot be achieved; rather this represents the ideal ratio between the field area and the area of the aperture receiver. (It is advantageous to have the heliostats as closely spaced as possible so as to approach the geometric ratio. However, if they are too close blocking and shading will become a problem; see section **III.2.7.2**) The maximum concentration ratio is used with the TERC performance data to determine the achievable concentration ratio, but this figure is reduced by 20% to allow for gaps between the secondary and the aperture. The resulting actual concentration ratio is combined with the apparent field area ($= \pi L^2 \tan^2 \phi$) to yield the receiver aperture.[30]

The MPT model handles the TERC as an optional add-on. If a TERC is added, then the user-inputted aperture diameter (*DIFEED*) becomes inactive. The receiver aperture (*DIAPE2*) is then calculated as described above, and the *outer* TERC aperture (*DIAPE1*)[31] is determined by the size and shape of the TERC, which are specified in Gordon & Ries. (The MPT spreadsheet looks up the TERC properties in a table.) The reflectivity of the TERC (*TROE*) is used to calculate the reflectance losses (*ETREF*) in the secondary; a ratio of direct hits to reflected hits from Gordon & Ries (1993) is also necessary for this calculation. *ETREF* is usually 3-5%. Finally, the total surface area of the TERC (*SCONA*) is calculated geometrically by using a conical approximation; *SCONA* is used to estimate TERC costs in chapter 4. This approximation is quite valid: Gordon & Ries suggest that the outer portion (the majority) of the TERC could actually be constructed as a simple cone without incurring significant losses, as long as greater care was used on the smaller CPC section adjacent to the receiver.

[30] Mirror surface errors, however, are already accounted for in the conservatively estimated solar half angle (*SHA*); see section III.1.1.

[31] If no TERC is selected, then *DIAPE2* = *DIAPE1*.

III.2.6 Gas Turbine & Power Plant

The objective of the MTP model is to demonstrate the feasibility and expected performance of a high-efficiency hybrid solar thermal system incorporating a gas turbine. Extensive theoretical gas turbine modeling is not a part of this objective; much of the modeling is simplified in any case by the hybrid operation, which ensures full-load around the clock. The turbine modeling is intended to simulate performance with sufficient accuracy to ensure that none of the results will be gross misrepresentations of reality. For example, compressor outlet temperatures must be accurate within 10 or 15 degrees C, but not to within 1 or 2 degrees. Pressure drops in the recuperator must be within the range of those experienced in real machines. System efficiency must be accurate within two or three percentage points. Precision beyond these levels is neither necessary nor meaningful, as constant advances in turbine engineering will give rise to many incremental improvements over the course of MPT development.

III.2.6.1 Simple Open Cycle Gas Turbine

Table **III-2** lists manufacturers specifications, collected from a variety of sources, for twelve turbines in the size range of interest for the MPT.

Table III-2: Manufacturer's Turbine Specifications Listed by Output

Manufacturer	*Model*	*Size, MWe*	*Press,. Bar*	*TIT C*	*TOT C*	*Weight kg/kWe*	*Cost $/kWe*	*Weight kg*	*Net Eff,%*
Turbomeca	Makila T	1.1	9.6	n/l	505	8.2	833	9,000	25.4
Solar	Saturn	1.2	6.5	n/l	516	8.3	740	10,000	24.4
Kawasaki	M1A-11	1.3	9.3	910	459	5.1	n/l	6,650*	23.4
EGT	Hurricane	1.7	9.2	1134	610	7.8	610	13,200	24.7
Pratt & Whitney	ST18	2.0	13.1	n/l	536	2.7	n/l	5,350*	30.5
Nuovo Pignone	PGT2	2.1	12.5	n/l	550	5.7	n/l	12,000	25.0
Allison	501KB3	2.8	9.3	n/l	566	2.7	n/l	7,600*	26.0
Solar	Centaur	3.5	9.7	n/l	437	7.8	455	27,300	27.9
Allison	501KB5	3.9	10.1	n/l	549	2.7	450	10,350*	28.7
EGT	Typhoon	4.2	13.0	1049	510	7.1	400	30,000	30.0
Solar	Taurus	4.9	11.7	n/l	481	5.6	400	27,300	30.3
Nuovo Pignone	PGT5	5.2	9.2	n/l	548	5.4	425	28,000	26.9

Sources: GTW (1994); GTW (1997); Gas-Turbines.com (1997a,b); GEC (1997); ICGTI (1997a,b).
Notes:
**For these models, turbine weight is listed in GTW 1996-1997 without a generator; information from another manufacturer (IES 1997) was used to derive a rough rule of thumb for the additional gearbox, generator, and skid weight: 2.5kg per kWe. This factor was added to the engine-only weights (3400 kg for the Kawasaki MIA-11, but only 600 kg for the Allison and 350 kg for the Pratt & Whitney aeroderivatives!) to yield the figures in the table.*
All Costs include the generator, but are in no sense "installed" costs; see chapter 4.
Weight includes the generator
Efficiency is open-cycle, LHV, and includes the generator (95% efficient)
"n/l" = not listed. The information was not available in the sources which were searched

In figure **III-4**, the specific weight, specific cost, and net efficiency are plotted for the turbines in table **III-2**. All three of these specifications are important in selecting an appropriate turbine model for the MPT system. The object of the model is to develop a turbine which closely resembles a real turbine (and is easily within the bounds of modern technology), but which has been parameterized in order to enable various modifications (including pressure losses in the receiver and variations in ambient temperature) and to establish certain specialized results (e.g. solar fraction).

Turbine Weight

There are three highly aeroderivative turbines in the data, a 2.0 MWe model manufactured by Pratt & Whitney, and two Allison engines at 2.8 and 3.9 MWe. The weight of these turbines is less than half of their industrial counterparts, an attribute which is viewed here as being critical to their usefulness in a tower-mounted design.

Fortunately, these engines also boast high efficiency and reasonable cost, making them the apparent first choice for the MPT.

Figure III-4: Specific Weight, Cost, and Efficiency of Very Small Gas Turbines

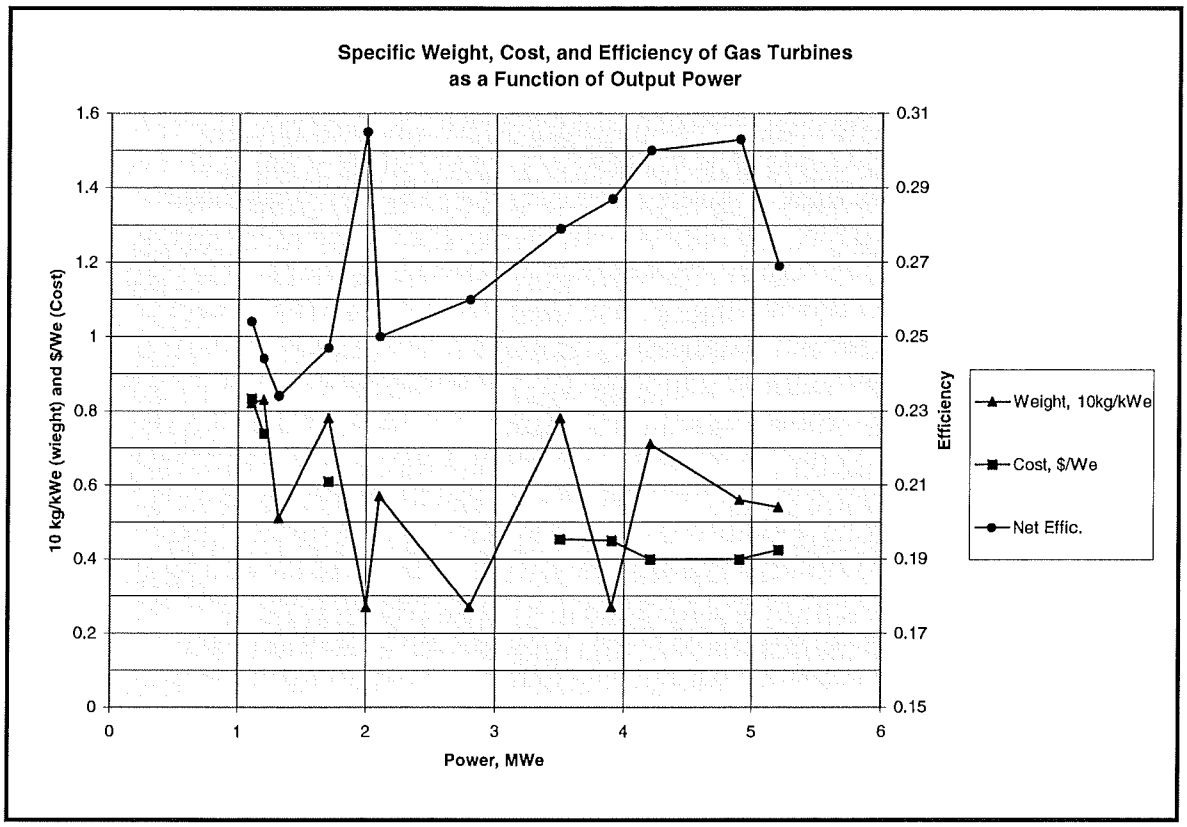

Turbine Cost Optimization

Even at this extreme small end of the turbine-generator market, certain trends are evident as a function of scale; these include higher efficiency and lower cost. However, the scale effect upon cost is *not* included explicitly in the MPT model optimization, because it is not purely monotonic but rather dips somewhat up and down depending upon the turbine manufacturer. Nonetheless, it is clear from figure **III-4** that below about 2 MWe, severe cost penalties will be felt. Above this point, the specific cost levels out considerably such that it is no longer a critical determinant of MPT scale. Of course, if consideration were open to much larger systems (20MWe and up), then cost would drop still lower.

However, this study is dedicated to exploring the smallest effective power tower systems; hence the "mini" part of the MPT designation. The MPT turbine cost optimization takes the simplified form of a requirement that the turbine output be above the apparent cost inflection point of 2 MWe.

Cost data is missing for the lower-power Allison engine (the 2.8 MWe 501KB3) and for the Pratt & Whitney ST18. To fill in this gap, a very conservative linear extrapolation has been made between the smaller EGT Hurricane (1.7 MWe, $610/kWe) and the larger Allison 501KB5 (3.9 MWe, $450/kWe), resulting in a formula for this part of the graph of -$73 per kWe per MWe. This approximation yields $588/kWe for the Pratt & Whitney and $530/kWe for the smaller Allison. This latter estimate, while not explicitly verified, is not inconsistent with the experience of system packagers at Allison.(Wenglarz 1997) To further ensure internal consistency, and in view of its unexpectedly high efficiency specification, the Pratt & Whitney ST18 has been dropped entirely, and **the two Allison turbines form the basis of the MPT turbine model.**

The use of two Allison turbines from the same family allows some moderate optimization of system scale. In chapter 5, this optimization will be explored in more detail: in all cases the MPT systems have been modified until the turbine output closely matches (within 1-2%) the rating of one or the other of the two Allison turbines. Thus the cost, weight, and efficiency of the relevant turbine can be included in the model and the effect of scale over this admittedly limited range (essentially 3 MWe vs. 4 MWe) can be examined. Although small, this range has been carefully chosen to represent a sort of "practical minimum", below which affordability and efficiency fall off much more steeply.

The Allison 501 turbine possesses two other attributes which make it very suitable for the MPT: the engine requires little personal attention (an essential quality for tower mounting), and it may be readily adapted to incorporate a solar receiver. Wenglarz (1997) estimates the frequency of scheduled maintenance as twice a year, and notes further that

even cogeneration packages incorporating these engines are designed to run unattended. With regard to solar receiver ducting, Wenglarz views the necessary modifications as "feasible" for the 501 because they are similar to changes which were undertaken several years ago as part of an experimental D.O.E coal combustion program. The coal-burning engine requires the addition of flanges which duct the air off of the compressor to a separate, external coal combustor and then return it to the power turbine; something of the same sort will be required in the MPT.

Modeling Methodology

The Allison specifications cannot simply be lifted off the manufacturer's data sheets and plugged into the spreadsheet model, because the model includes variations in temperature and pressure drop. Furthermore, it is necessary to estimate the turbine inlet temperature (*TIT)* in order to calculate the solar fraction, because the receiver's maximum output temperature will be fixed below this level and the difference made up by burning gas. The TIT is not published in the manufacturer's specifications, but an educated estimate has been substituted.

All of these needs are solved by constructing a thermodynamic model of the gas turbine(s), based on equations contained in Appendix **A**. The model includes parameters for ambient temperature (*AT*), compression ratio (*PR*), isentropic compressor (*CN*) and turbine (*TN*) efficiencies, turbine inlet temperature (*TIT*), recuperator effectiveness (*REGEN*), and hot side (*RPDROP1*) and cold side (*RPDROP2*) pressure drops in the recuperator (if applicable). Specific heat was allowed to vary but average temperatures in each process were used to determine its value. Air was used as the fluid throughout without allowance for combustion products and other gases. The net efficiency (*GASEFF*) from table **III-2,** above, was used to "reverse engineer" the turbine:

The isentropic efficiencies of both the compressor and the turbine are not listed in the manufacturer's data, but these figures are the key to accurately modeling the gas turbine. Fortunately, they can be calculated if the compression ratio, ambient temperature, turbine outlet temperature, and *either* compressor outlet temperature or, more commonly, the turbine inlet temperature, are known. This is the procedure followed in the model to simulate the performance of the Allison 501 engines.

Table **III-3** gives the complete specifications for the two open-cycle gas turbine engines used in the model. These have been designated GT3 and GT4, but they are intended to closely represent the real-world performance of the Allison 501KB3 and 501KB5.[32] The table represents performance in gas-only mode, *without* a pressure drop between the compressor and the turbine. In solar operation, the model includes a 5% pressure drop (see section **III.2.7.5**) to allow for circulation through the receiver, resulting in a slight rise in turbine exit temperature and a commensurate loss in turbine efficiency. Without the thermodynamic turbine modeling, it would not have been possible to account for this effect, leading to significant overestimates of performance in solar-mode.

Table III-3:
Open-Cycle Gas Turbine Specifications Used In the Model, Ambient = 15 C

Name	*Comp. Isen. Eff.*	*Turb. Isen. Eff.*	*Sizet MWe*	*Press., bar*	*TIT C*	*TET C*	*Weight kg/kWe*	*Cost $/kWe*	*Weight kg*	*Net Eff,%*
GT3	.700	.800	2.8	9.3	1016	566	2.7	530	7,600	26.0
GT4	.700	.800	3.9	10.1	1077	549	2.7	450	10,350	28.7

III.2.6.2 Recuperated Gas Turbine

Modeling the recuperated gas turbine is complicated by the lack of commercial archetypes at this scale (2-4 MWe). The solution which has been pursued is a scale-up of

[32] Note that this model does not make explicit allowances for blade cooling, although at least the first blade is cooled in most of the real world turbines listed in table **III-2**. Rather, the blade cooling effects, which are minor, are rolled into the turbine's isentropic efficiency. Regardless, the overall conversion efficiency comes out correctly and matches the real-world turbines.

the much smaller (25 kWe) Allied Signal dish Brayton turbine, which is highly recuperated and already adapted for use with the solar resource.

Following suggestions of Sefano Consonni[33], the following informal method was used: the polytropic efficiencies for the components in the Allied Signal turbine were calculated, and then three percentage points were added to both the compressor and turbine efficiencies. The *RTIT* (recuperated version TIT) and *REGEN* (regenerator effectiveness) were left unchanged at 817 C and 90% respectively, and the new isentropic efficiencies (*RCn* and *RTn*) were devised.

Note that this method produces an apparent anomaly which does not significantly impact the net outcome: the compressor efficiency appears very low in relation to the expander efficiency. This mismatch comes about because the compressor efficiency actually includes pressure losses and temperature rises associated with the inlet ducting and air filtering, just as the turbine efficiency included blade cooling in the open cycle case. The recuperated turbine requires no blade cooling at these low temperatures. (A further advantage of a low *RTIT* is a higher solar fraction, because the receiver in this MPT model has been limited to 800 C).

The pressure drops in the recuperator are based upon figures **for somewhat smaller recuperators** in (**ref from TK**); the model uses 3% pressure drops on each side. These drops are slightly less than those in the Allied Signal specifications, but seem more typical for larger recuperators.

The turbine scale is variable under the RGT scenario and is not limited to 2.8 or 3.9 MWe as are the open cycle machines; this relaxation acknowledges that, unlike GT3 and GT4, the RGT cannot be considered a near-exact simulation of a real-world turbine. Nonetheless, the RGT systems presented in chapter 5 are adjusted until the scales are almost all identical, facilitating direct comparison across different locations.

---

[33] Stefano Consonni is a former student with the CEES research group and an expert on gas turbines.

After optimization, a pressure ratio (*RPR*) of 2.7 was chosen for the RGT. The following complete specifications are produced by the thermodynamic model:

Table III-4:
Recuperated Gas Turbine (2-4 MWe) Specifications Used In Model. Ambient = 15 C

Parameter	*Model Name*	*Value*	*Source*
Compressor Pressure Ratio	RPR	2.7	*Optimized*
Isentropic Comp. Eff.	RCn	73.2%	*Consonni's method*
Compressor Exit Temp, C	CRIT	144	*Model (15 C ambient)*
Recuperator Effectiveness	REGEN	90%	*ASDB engine*
Recup. Cold Side Press. Drop	RPDROP	3%	***(ref from TK)***
Recuperator Exit Temp, C	ENGCRET	559	*Model*
Recuperator Exit Temp, C, ***Solar Mode***	CRET	569	*Model*
Recuperator Exit Pres., bars	CREP	2.62	*Model*
Turbine Inlet Temp, C	RTIT	817	*ASDB engine*
Isentropic Turbine Eff.	RTn	93.4%	*Consonni's method*
Turbine Exit Temp, C		616	*Model*
Turbine Exit Temp, C, ***Solar Mode***		605	*Model*
Recup. Hot Side Press. Drop	RPDROP2	3%	***(ref from TK)***
Turbine Pressure Ratio		2.54	*Model*
Turbine Pressure Ratio ***Solar Mode***		2.41	*Model*
System Exit Temp, C		190	*Model*
System Exit Temp, C, ***Solar Mode***		191	*Model*
Net Thermal Efficiency, LHV	GASEFF	35.4	*Model*
Net Thermal Efficiency, LHV, ***Solar Mode***	GTEFF	32.9	*Model*

Notes:
1. In Solar Mode, there is a pressure drop (TOWDROP = 5%) in the receiver; this is the only difference effecting turbine performance, but as the table demonstrates, it is significant. See section ***III.2.7.5.***
2. The open cycle turbines discussed in the previous section also have separate sets of specifications for solar and gas-only modes, but the solar efficiencies are left out for clarity. Thus, it is appropriate to compare the gas-only (larger) efficiency from the RGT case with "GT3" and "GT4" from above.
3. A 95% electric generator efficiency is included in GASEFF and GTEFF, as described in the text.

Both the open and recuperated turbines are static in the MPT modeling. With the exception of a choice between the 3 or 4 MWe open cycle gas turbine, the engines are not part of the optimization process in chapter 5, which is concerned only with the *solar* part of the system. One of the specification sets in the tables above is used *throughout* each MPT scenario. These specifications represent reasonable facsimiles of power plants which can be built with today's technology. The turbines are not advanced technology; their inlet temperatures are only high enough to ensure competitive efficiency for natural gas combustion, provided that either recuperation or cogeneration is included.

A generator efficiency of 95% is assumed for all operations. In chapter 5, the solar-to-thermal efficiency (*STEFF*) for the MPT is reported along with the overall solar-to-electric (*HEFF*) and energy-to-electric (*HADJEFF)* efficiencies. The gas turbine efficiency (including the generator) is equal to *HEFF / STEFF;* all that is necessary to examine the effect of alternative gas turbine efficiencies is to multiply *STEFF* by a different figure.

III.2.6.3 Open Cycle with Cogeneration

Cogeneration is only modeled here without a recuperator. This dichotomy is not meant to imply that an RGT could not also benefit somewhat from cogeneration, and that in such a case even more gas would be saved. However, the beauty of the RGT is that once the recuperator has been added, the MPT becomes a stand-alone package. Without adding the constraint of cogeneration, the gas conversion efficiency of this package is high enough to compete in the distributed electricity market. Thus cogeneration, which sharply restricts application sites, has been reserved only for the case where it is most "needed": the simple open cycle RGT, in which the conversion efficiency may be too low to offer a viable alternative to centrally produced gas power. (Of course, all decisions based upon "competitiveness" are subject to change, as addressed in chapters 4 and 5.)

III.2.6.3.1 Absorption Chilling

The suitable cogeneration schemes are a function of the turbine exhaust temperature. By restricting the analysis to the non-recuperated turbine, a broader range of cogeneration options are possible, including industrial and commercial processes running on both

water and steam.[34] There is no intention here to examine this full range of alternatives; rather, a single application has been chosen in order to illustrate the substantial economic improvements which cogeneration can bring to the MPT. This application is absorption chilling (with heating in the wintertime) for building climate control. However, the MPT's small size and high visibility as an environmental icon should open up other possibilities, particularly in the corporate environment.

The absorption cooling cycle is best conceived as the standard vapor compression cycle with a chemical loop replacing the engine-driven compressor. The most common refrigerant is water; after flashing into steam upon exposure to low pressure and thereby absorbing heat from the surroundings, the water is re-compressed by a two-step process: first, it is taken up by an "absorbent" fluid; this is most commonly lithium bromide. The solution is then pumped to a "desorber" where it is heated to high temperatures, either by direct fuel combustion or by heat exchange from a circulating hot water or steam loop. (For the cogeneration application, this hot water or steam is reheated by a heat recovery system in the turbine exhaust.) As the temperature rises, the water boils out of the lithium bromide, and is carried to a condenser and then to the evaporator, where it flashes back to vapor and the cycle begins again.

[34] In some cases, the same process is simply more efficient at higher temperatures. This is the case for absorption chillers, in which the double-effect devices, which are only possible if a recuperator is not fitted (Thompson 1997), are 40-50% more efficient than lower temperature single-effect machines.

Figure III-5: Single and Double Effect Chillers

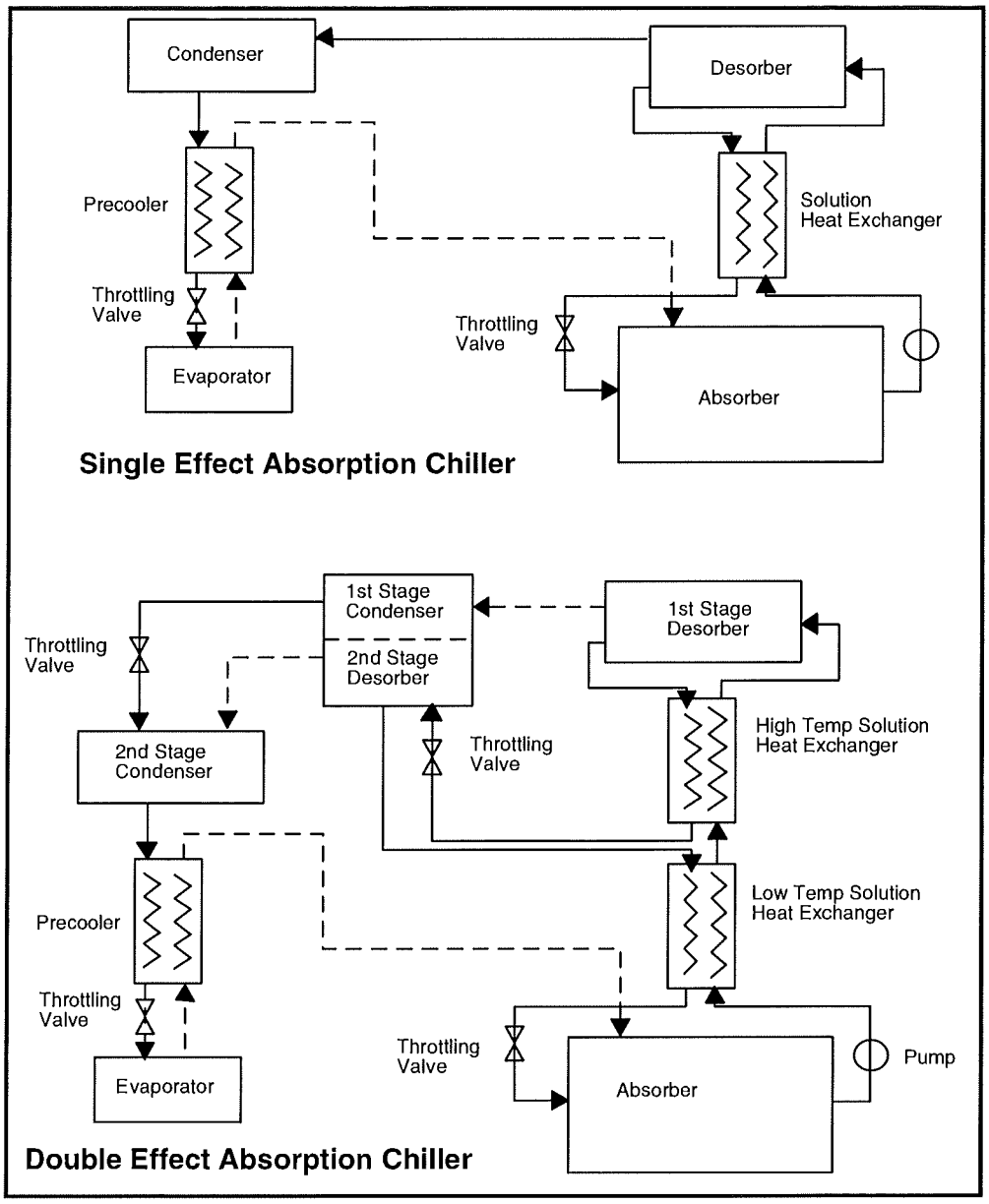

Source: Adapted from RCLSGI (1997)

Two heat exchangers may be used to improve the efficiency: one in which the vapor coming from the evaporator pre-cools the water going into the evaporator, and another in which the hot absorbent coming from the desorber is used to preheat the refrigerant/absorbent mixture about to enter the desorber. Viewed as a black box, the chiller absorbs heat from the environment and from the circulating hot water/steam line (or gas burner for direct-fired units), and rejects an equal amount of heat into the

condenser cooling water. (Chillers require a cooling tower, water source, or other form of heat sink.) The coefficient of performance (COP) is the standard measure for evaluation of refrigeration cycles. The cycle just described is called a "single-effect" cycle and commercial chillers of this type typically have a COP of 0.7 (e.g. Yazaki 1984; Carrier 1997; Thompson 1997), meaning that the amount of heat which is removed from the environment is equal to 70% of the amount of heat which is supplied by the circulating feed line or gas burner.

Single-effect chillers require a heat supply line at about 135 C (Thompson 1997). If a higher heat source is available (190 C), a more intricate technology is available in the form of the double-effect chiller. These machines have two desorbers and either two condensers or two absorbers; the stages are coupled in series so as to transfer heat to one another (see figure **III-5**). The net effect of this complicated plumbing is a COP as high as 1.2 (e.g. Carrier 1997; Trane 1996). This is such a dramatic improvement (70%) over the single-effect machines that the double-effect chillers were selected for the MPT cogeneration model.

Double-effect chillers, like single-effect versions, can be fired either directly or remotely. The remote-fired chillers would be used in an MPT cogeneration plant. It is further assumed that if the MPT were not there, then natural gas would be burned at the site of the MPT to heat a circulating hot water (or steam) system.[35] It is recognized that this may not be the most effective scheme for all sites. Particularly for new installations, it may be more effective to use direct-fired chillers and heaters and have a gas distribution network instead of a water network. For sites with an existing water piping network, however, the central burner scenario will be more appropriate. In any case, it would be impossible to

[35] According to Thompson (1997), the chillers will work equally well on hot, pressurized water or on steam. The choice of circulating fluid will depend on site specifics in most applications; for the MPT, water is strongly preferred over steam because it will be much easier to circulate through the tower, and will considerably reduce the size of the heat recovery system in the turbine exhaust. A large cogen hot-water system at the same temperature and similar pressures is currently in place at Rutgers university (Rutgers 1997).

provide a site-independent estimate of gas savings for the MPT if the alternative were direct-fired chillers; the indirect models have been used in all cases.

The turbine's location on top of the receiver tower creates a special situation for hot water circulation. Thompson (1997) specifies hot water at 370 F for the double-effect chillers, and Rutgers (1997) has an installed cogen system using water, also at 370 F. Some allowance for thermal losses in transit must be made, so the temperature exiting the heat recovery system, which is located in the turbine exhaust stream, might be as high as 200-205 C (allowing for a thermal drop of about 10% towards ambient in transit). At these temperatures, the pressure must be on the order of 15-17 bars to avoid vaporization. In the MPT system, this pressure must be maintained at the tower top; thus for the tallest tower modeled here (70 meters), a ground-level pressure of 22-24 bars will be necessary. This rise is a ~45% increase over the requirement without a tower, but fortunately the chillers are designed to work with water pressures up to 27 bar (Thompson 1997). By operating without steam, a great advantage is preserved: because the system is sealed, the suction of the descending water column will do almost all of the work required to raise the ascending column, and only thermal buoyancy forces between the hot and cold columns must be overcome. A high-volume, high pressure-head pump will not be needed and can be replaced by a pump which only generates a modest head at full flow. (If the system needs to be charged after draining, the flow rate can be much less, or an alternate pump can be employed). By contrast, if the water were flashed to steam at the tower top, then the heat recovery unit would act as a siphon break, and a 7-8 bar booster pump would be in constant operation to overcome the vertical pressure head.

III.2.6.3.2 Cogeneration Modeling

The cogeneration model does *not* need to consider the total price of the chillers themselves, nor the expenses of installation, piping, ducting, or cooling towers. Rather, the benefits of cogen will be expressed in gas savings, and these will be credited back to

the MPT plant and thus reduce its operating cost and the levelized cost of electricity. An assumption is necessary to simplify this calculation: *the effectiveness of heat transfer from the turbine exhaust to the water is equal to the burner efficiency of the natural gas alternative*. This leveling allows a one-to-one matching of the available heat in the exhaust with the available heat in the displaced natural gas.

The available heat in the turbine exhaust (usable for heating water which is initially at temperature WIT), in megawatts thermal, is:[36]

[(1 - GTEFF / GREFF) / (GTEFF / GREFF)] * GTRATING * (TET - WIT) / (TET - AT)

where *GTEFF* is the gas turbine efficiency (*including* the generator, and thus must be divided by the generator efficiency *GREFF* to yield the heat remaining in the exhaust), *GTRATING* is the gas turbine rating (in MWe), *TET* is the turbine exhaust temperature, *WIT* is the water inlet temperature, and *AT* is the ambient temperature. This formula maintains the adiabatic engine approximation and simply assigns the energy not converted into work to the turbine exhaust. This energy is in the form of sensible heat measured relative to the ambient temperature; the available fraction depends upon the temperature of the incoming water. *TET* is taken directly from the gas turbine model (without a recuperator), while *WIT* is calculated by assuming a 10% temperature drop (vs. ambient) on the return line from the chillers. For example, Thompson (1997) gives a chiller exit temperature (*CHILLOUT*) for water of 165 C (439 K). Thus if the ambient temperature (which is fixed at the annual daytime average for each location) is 15 C (for example), *WIT* is set to 150 C (423 K).

---

[36] Non-constant Cp will introduce a slight inaccuracy in this simplified formula. Consistent with other parts of the MPT model, the available heat is actually corrected in the spreadsheet by two functions derived from graphical combustion data in Cohen *et al* (1996). These functions are named COMBUSTO (for the open-cycle thermal regime) and COMBUSTR (for the regenerated-cycle operating regime). Each function takes as input an upper and lower temperature and outputs the heat energy necessary to raise air from the lower input to the higher input, assuming that the heat addition takes place in the climate of a gas turbine's combustion chamber. COMBUSTO and COMBUSTR are used throughout the MPT, and the complete functions appears in Appendix **A**.

Finally, and most importantly, the chiller capacity factor (CF) must be included; this is usually expressed in equivalent full-load hours per year (EFLH) in the HVAC industry (Ogden 1988). Dividing this figure by 8760 hours per year yields the chiller CF, which may fall between 10-50% depending upon climate. In the geographic scenarios chosen in chapter 5, the cooling loads for the southwest (Dagget, California) site are of course much greater than those for the northeast (New Jersey) site.

Before the gas savings at full load is reduced by the chiller CF, the flip side must be considered: in the winter months, it is assumed that the circulating hot water is used for heating, and that it displaces direct-fired heating in analogous fashion to the cooling model. This is reasonable in light of the fact that many of the double-effect chillers on the market can be used as heating units (e.g. the 16DF model from Carrier). The *combined* heating and cooling capacity factor (*CCF*) determines the total gas savings which can be credited back to the MPT. Of course, this credit as presented here will be approximate because the true gas savings for any given installation will depend upon the physical layout of the buildings, the ambient temperatures, the piping insulation, building insulation, hours of operation, and climate control strategy, and the make and model of chiller chosen. The MPT model approaches the *CCF* as follows:

Data from NREL (1997) gives the following monthly data for each of the sites considered in chapter 5:

- Average and extreme high temperatures for each month

- Average and extreme low temperatures for each month

- Total heating degree-days (HDD) for each month. A heating degree-day in this data is when the average high minus the average low is one degree below a reference temperature of 18.3 C. If the average is two degrees below, then that day counts as 2 HDD, and so on.

- Total cooling degree days CDD for each month. The converse of HDD. Note that both HDD and CDD are calculated based on a 24 hour day and a 7 day week.

There are a variety of ways in which this data could be used to calculate the equivalent full-load hours per year for heating and cooling combined. For example, a capacity based upon the most extreme temperatures will yield a much lower annual CF than one based upon average temperatures. Data in Ogden (1988) presents a broad range for equivalent full-load hours for cooling systems, even at the same geographical location. For example, the EFLH for New Jersey sites range from 500 to 1000 hours per year; this range reflects differences in building usage (hours of operation in particular) and in the density of cooling coverage (e.g. cooling tons installed per 1000 square feet).

The desired calculation method for EFLH will be based upon the NREL monthly data (and thus portable to many locations in the U.S.) but will be in agreement with the Ogden range. The upper part of the range is most appropriate for 24-hour applications such as a university campus or housing development, and less appropriate for a purely commercial setting. For the current model, the upper part of the range is desired, because this is first and foremost a *feasibility* study, in which it is necessary to consider the more favorable, 24-hour applications first.

The chiller units must be sized and installed so as to meet a reasonable maximum thermal demand. Because this application is for both heating and cooling, both modes must be examined to see which poses the larger full-load requirement. In warmer climates, full-load will be defined by cooling; in cooler climates, by heating. The machines are assumed to be sized to meet this requirement, and the capacity factor in the relevant mode (heating or cooling) is determined. The capacity factor in the opposite mode is then inferred.

Maximum differences between the ambient (inferred from the NREL data) and the desired (set to 18.3 C, following the NREL data) temperatures are calculated for both heating and cooling. An efficiency correction factor must be applied to allow direct comparison. The necessary efficiency correction is equal to the COP, reflecting the fact that the heating content of the hot water (or steam) when it arrives at the chiller is unity in comparison to its cooling ability, determined by the chiller's COP, or coefficient of performance. A typical COP for double effect chillers is 1.2 (see above); thus the temperature difference (desired - ambient) at full load heating is only (1 / 1.2 =) 83% of the temperature difference (ambient - desired) at full-load cooling. This correction must be taken into account when determining which application "sizes" the system.

For clarity, the following development assumes that *cooling* is the sizing application, and describes how the combined capacity factor (CCF) is derived:

Full-load cooling is determined in the model by taking the average high temperature during the hottest month of the year, and averaging it with the record high for that month. The resulting figure is taken to be the high temperature on a "design-point" day: a day in which the temperature does not establish a record, but is nonetheless well above average. The low for this day is assumed to be the same number of degrees above the average low that the high is above the average high. The design-point high and low are then averaged, and 18.3 degrees is subtracted to find the degree days for the design-point day. The result is multiplied by 365 to find the total annual degree days at full-load, or "design-point" (dpACDD); the actual annual CDD (from the NREL data) is divided into this figure to yield the cooling CF. This CF can be multiplied by 8760 to yield the EFLH.

The heating CF must be based upon the same machines; thus it cannot follow the same procedure as above. Furthermore, the HDD cannot be used as stated in the data to represent the heating potential, because on some of the days it might be so cold that the chillers, which have been sized to match the *cooling* load, may not be large enough to provide the full range of heating. Instead, the "eligible heating degree-days" (EHDD) are

calculated month by month in the spreadsheet by assuming a quick triangular temperature distribution approximation (in which the temperature is equal to the average monthly low at midnight and the average monthly high at noon). In addition to the EHDD, which represents the actual time spent heating, the full-load heating capacity is needed. This figure, dubbed dpAHDD, is equal to the design-point annual cooling degree days (dpACDD), which is derived in the paragraph, times the efficiency correction (COP) for cooling vs. heating. Finally, the heating CF is equal to the actual heating time (EHDD) divided by the annual potential time (dpAHDD):

EHDD = HDD modified by checking for very cold days which exceed design-point capacity

dpAHDD = dpACDD * COP ; this represents the total annual heating capacity

heating CF = EHDD / dpAHDD

Example: Calculating the Combined Heating and Cooling Capacity Factor

Consider Dagget, CA. According to the NREL data, the hottest month of the year is July, with an average high of 39.9 C. The record high in July is 46.7 C; these two figures are averaged to find the design-point high, 43.3 C. The average low in July is 23.3 C; the design-point low is the same distance above this as the high is above the average high: (23.3 + (43.3 - 39.9)) = 26.7 C. Averaging the high (43.3) and the low (26.7) and subtracting 18.3 from the result yields 16.7 cooling degree days for this design-point day. Multiplying by 365, we have 6,096 degree days per year at full load. The actual CDD per year is 1,659 (again from the NREL data), so the cooling CF is (1659 / 6096 =) 27.2%. (Converting to EFLH yields 2,384 hours. If this procedure were followed in Atlantic City, the EFLH comes out to 1,020, which is near the top end of the range from the Ogden data, as desired.)

The heating CF is found through the calculation derived above, after noting that the EHDD in Dagget is 1106 (it turns out that in Dagget, the EHDD and the HDD are the same), and the dpACDD is 6096, as derived above:

dpAHDD = 6096 * 1.2 = 7315

heating CF = (EHDD / dpAHDD) = (1106 / 7315) = 15.1

The combined Dagget heating and cooling capacity factor (CCF) is (.272 + .151 =) 42.3%.

With the CCF and the available heat formula, the effects of cogeneration may be obtained. The first step determines the full-load cogeneration gas replacement efficiency (*FLCGREFF*); that is, the gas saved (in energy units) as a fraction of the energy in the turbine exhaust (relative to ambient temperature), assuming that the chiller system is operating at full-load:[37]

$$FLCGREFF = (TET - WIT) / (TET - AT)$$

where *TET* is the turbine exit temperature, *WIT* is the water inlet temperature at the turbine exhaust heat recovery system (as defined above), and *AT* is the ambient temperature. The usual average-basis specific heat correction is applied in the actual model but omitted here for clarity.

The annual cogeneration gas replacement efficiency (*CGREFF*) must include the capacity factor:

$$CGREFF = FLCGREFF * CCF$$

CGREFF expresses how much heat is "saved" from the turbine exhaust; a typical figure (for the Dagget example above, with the GT4 4 MWe gas turbine) is 32.4% (see chapter 5 for complete results). The annual gas savings (*AGS*) are found as follows:

$$AGS = TOTHEAT * (1 - \text{average GT efficiency}) * CGREFF$$

where *TOTHEAT* is the total annual heat requirement at the turbine inlet (computed from the peak solar delivered megawatts *PKDMW*, after accounting for the difference in temperature between the receiver outlet maximum and the turbine inlet), *CGREFF* is the net cogeneration capacity factor as developed above, and the average GT efficiency is an

[37] see previous note

expression which accounts for the fact that the efficiencies in hybrid and gas-only modes are somewhat different (due to pressure losses in the former from tower ducting; see **section III.2.7.5**).

To find the advantage gained through cogeneration, *AGS* is simply deducted from the annual gas requirements, also in MWt, before the latter is converted into dollars and applied to the LEC. The annual evaluation and LEC computation is discussed further below and in chapter 4.

III.2.7 Loss Mechanisms

This section collects a brief description of all of the energy losses along a complete pathway through the MPT system, and how they are computed. Stairstep diagrams of these losses are presented with the final results in chapter 5.

III.2.7.1 Geometric Losses

The cosine angle losses of the MPT heliostat field, versus an ideal two-axis tracker such as a D/E system, have already been introduced, along with the methodology for calculating the solar collection from each heliostat. The total light which would have fallen on the heliostat *had they been perfect trackers* (pointed directly at the sun) is labeled *EMW* in the model. *EMW* is an instantaneous value, in MWt, and is summed over the course of the year to produce *ANNEMW*, in MWht. Note that the basis for this summation is not the total number of hours in a year, but rather the hours of system operation (*HOURS*). *HOURS* is determined dynamically: as the model runs over the course of the year, receiver conditions are checked to see if net positive heat flow is possible. When this is the case, the instant values are added to the annual totals, and HOURS is incremented. If the receiver losses are too great, the solar part of the system is

assumed to be shut down (probably by means of a shutter over the receiver aperture). *All* of the annual results are calculated on this basis.

The light which would be available to the heliostats, without counting any blocking or shading, but accounting for mirror reflectance (equal to 90% throughout), is labeled *TBBMW*, (transmitted before blocking, in megawatts. The annual version is *ANNTBBMW*). The annual geometric efficiency, useful for theoretical comparison with dish systems, is found by dividing *ANNTBBMW* into *ANNEMW*ROE*. This quantity is calculated by the model and is labeled *ANNUAL* in the results.

III.2.7.2 Blocking and Shading

The dish vs. heliostat comparison is not completed by examining the annualized cosine losses (*ANNUAL*). Prominent among the additional loss terms are the blocking and shading losses caused by the physical proximity of the system components.

Tower Shading

Tower shading is calculated at each heliostat by determining what fraction (if any) of the horizontal (*HX*) dimension of the heliostat overlaps a rectangular shadow stretching directly down-sun from the base of the tower. The length of the shadow is determined by the solar elevation (*PHIS*), and the direction by the solar azimuth (*THS*). This approximation is quite accurate, especially because the heliostat will be pointed directly at the tower if the sun is directly behind; thus no oblique cosine factor is necessary in computing the overlap. No attempt is made to account for a partially vertically-covered heliostat at the very tip of the shadow; a heliostat is either within the shadow's reach or it is not.

Heliostat Shading

Heliostat shading occurs when the incoming sunlight to a particular mirror is intercepted by another heliostat before it reaches its target. This light is reflected to the tower, but an equivalent amount of light which *could* have been collected by the shaded heliostat is lost; thus part of the mirrored surface is wasted. The MPT model takes advantage of the regularity of the field construction, and the fact that the sun is in the same direction from every heliostat, to create a single matrix for heliostat blocking. This matrix includes only four neighboring heliostats,: one on the left, one on the right, and two to the south. The field is constructed (see section **III.2.3**) in the form of a brick wall, so that these two southern heliostats are spaced evenly one on either side of the N-S mid-line of the heliostat above. Although it is theoretically possible for heliostats further away to cause shading which is not duplicated by one of these closer heliostats, it is rare and insignificant. Note that heliostats to the north need not be considered in the latitudes modeled here, because the sun is never coming from that direction.[38]

The matrix computes the horizontal *and the vertical* overlap for each of the generic neighboring heliostats in the matrix. For each heliostat in the field, this matrix is checked and the overlaps are summed, *provided* that the respective neighbor actually exists in the field. (Heliostats on the east, west, and southern edges do not have a full set of neighbors. Note that it is very rare for a heliostat to be shaded by two neighbors at once). The resulting shading is placed in the spreadsheet in the same column as the tower blocking; the maximum of the two numbers is used. This approximation excludes cases of both tower and neighbor shading, but is justified because tower shading, if it occurs, means that the sun is directly behind the tower: any heliostat shading is likely to be contained already within the tower shading.

[38] Even in tropical latitudes, shading from the northern heliostats could be neglected, because the sun is very high when it is in the northern half of the sky.

Blocking

Blocking occurs when the light which is reflected from a heliostat intercepts the back of another heliostat before it strikes the tower. As with heliostat shading, blocking could only be eliminated by creating a field with unacceptably low heliostat density. Blocking is more difficult to model than shading, because the vector to the tower is different for each heliostat and will therefore intercept a different set of neighbors despite the regularity of the field. No universal matrix is possible; instead the model contains a program which combs through the field and identifies, for each heliostat, all other heliostat which are within a critical radius; beyond this radius, no blocking can occur regardless of solar angle.

The potentially blocking heliostats occasionally number four or five, but are more often zero or one. The number increases with distance to the tower, because the angle to the receiver becomes more acute. Unlike shading, the light path does not change with sun position, and thus the blockers must be considered under all solar conditions. However, the blocking factor is dependent upon the *angle* of the heliostats with respect to the ground; this is equal to the average (angle to the midpoint) of the solar elevation (*PHIS*) and the angle to the receiver, determined from the tower height (*THEIGHT*) and heliostat position (*X,Y*). This heliostat tilt angle is used to dynamically calculate the projected vertical overlap for each of the blockers; the horizontal overlap is calculated in a separate step and does not change. These figures must be calculated for *each* heliostat on the "blocking list" of each heliostat in the field. A final step is necessary: the overlaps from separate blockers on the list cannot be summed, because there is a good chance that they duplicate one another, especially when the sun is low in the sky. Therefore a quick numerical scan across the horizontal view of the primary heliostat is conducted, and at each point, the blockers are all examined to find the greatest vertical overlap (if any). Thus a blocker duplicated by another, closer (and therefore seemingly higher) blocker

will not be counted. The final blocking total of each heliostat is placed in a separate column on the spreadsheet.

Summation

The blocking and shading cannot be summed, because there will be cases of overlap between the two. Nor was it practical, in the interests of modeling resources, to examine each heliostat for this kind of overlap; such examination would require detailed tracking of the two-dimensional region on the heliostat's surface which was shaded, so as not to count this area as blocked. Instead, an averaging method was used which, over the course of the solar year, is not expected to differ markedly from a more minutely rigorous approach. The method is founded on the following principles and assumptions, beginning after the program has already calculated the percent blocked (%B) and the percent shaded (%S) of each heliostat. This method is applied separately to each heliostat at each solar position:

1. If only one loss (%B or %S) is greater than zero, then it is included in its entirety and the calculation is complete. If both %B and %S are greater than zero, then the larger is included in its entirety, and...

2. The smaller of the two is only partially included, because in many cases the blocking and shading will be redundant;

3. The redundancy (overlap) is approached on a horizontal basis, because both effects will begin at the bottom edge of the heliostat and extend upward to varying degrees;

4. The mean horizontal obstruction (MHO, called *AVHZBS* in the spreadsheet) is calculated by dividing the heliostat width (*HX*) into the average heliostat spacing, which is 1/6 * (4 * ($XFOOT^2$ + $YFOOT^2$)^.5 + 2 * *XFOOT*). This formula follows

logically from the brick-like construction pattern of the field: at each heliostat, there are 4 other heliostats located diagonally and 2 other heliostats located to the east and west ("x"-direction). For example, a typical MHO might be 50%;

5. The MHO gives a rough figure for the average horizontal (one-dimensional) obstruction between heliostats, but %B and %S refer to the total (two-dimensional obstruction) at one particular heliostat, so...

6. A simple integrate-and-average method is used to find the mean *redundancy* (extent to which the horizontal region of the smaller obstruction is already obscured by the larger). It is first assumed that the larger effect (blocking or shading) is present with a horizontal coverage equal to MHO. The second effect, which will be smaller in *vertical* extent but *not* necessarily in horizontal extent, is also of (mean) width MHO but "slides" around behind the first coverage. By integrating over all possible positions of the first and second coverages, the average amount of the second coverage which is "seen" past the first one can be determined.

7. The average amount of the second coverage which is *not* redundant turns out to be equal to (1-MHO)/(3 * MHO). This rather startlingly simple result (which is only valid as long as MHO > 50%) is derived in Appendix **A**.

8. It is acknowledged that this method only applies to overlaps of heliostat shading and blocking caused by heliostats, and not to shading caused by the tower. Fortunately, tower shading is an infrequent effect which is very dominant when it occurs; thus any errors in how the blocking is handled when tower shading is present are of minimal importance.

For example, assume that a heliostat is 23% blocked and 14% shaded, both by other heliostats. The model will calculate the total blocking and shading as follows:

Total Reduction = Larger + (1-MHO)/(3 * MHO) * Smaller

...in this example, with MHO = 50%, the total reduction would be 27.7%. On average, the larger obstruction in this field will obscure 66.6% of the smaller one. In a more densely packed field with MHO = 75%, the larger obstruction will obscure 88.9% of the smaller one.

The energy transmitted after blocking and shading are counted is labeled *TMW* (transmitted megawatts); the annual sum is *ANNTMW*. By dividing *ANNTMW* by *ANNTBBMW*, we get *ANNBEFF*, the annual blocking and shading efficiency. Typical values are around 80%, but depend sharply upon heliostat spacing, and upon field size relative to tower height.

III.2.7.3 Aperture Acceptance

Although *TMW* represents the light transmitted up to the receiver, not all of this energy is actually admitted. The heliostat canting and solar half-angle spread calculations are used to determine the fraction of the beam from each heliostat which is admitted to the receiver (see section **III.2.2**). As described, if a TERC is used then the flux is further reduced by reflections off the TERC, although the aperture size is also reduced. If a window is used, the flux is reduced by window reflections. Aperture size (or TERC aperture if one exists) is *by far* the dominant parameter; the window losses are in the range of 1% and the TERC losses are in the range of 1 to 3%, but if the aperture is not large enough a great fraction of the flux can miss entirely. However, some loss is desirable: the projected heliostat images become larger when the sun is in the east or the west (and thus at a large angular distance from the receiver). If the aperture were made

large enough to capture all of the incoming rays at these times, then it would be *too* large during the critical midday hours, generating unnecessary re-radiation losses. Aperture size is discussed further in chapter 5.

Window Reflectance

The window reflectance is modeled after Kribus (1994), in which a DIAPR type conical quartz window is analyzed by ray tracing. Transmittance is given as a function of rim angle, allowing for easy translation to the MPT system. Furthermore, the results[39] were close enough to linear to allow for a single transmittance figure based on the median field rim angle (*ARA*).[40] Beyond a certain angle (designated as the "full-acceptance" angle), the linear relationship ends and the transmittance becomes very close to 100%, before falling off sharply at extreme angles beyond the range of interest in the MPT.[41] The spreadsheet finds the reflectance at the median rim angle, and then reduces this to account for the near-perfect transmission of that part of the field lying beyond the full-acceptance angle. The result is labeled *EWREF*, or effective window reflectance, and is a constant for any given window and field.

TERC Reflectance

The TERC reflectance (*ETREF*) is distinct from the TERC reflectivity (*TROE*) and refers to the *net* loss resulting from non-specular (scattered) reflections off of, and absorption at, the TERC surface. This loss is not simply (1 - *TROE*), because many of the rays strike the aperture directly. Gordon & Ries (1993) present data which reveal that the fraction of direct hits (no TERC involvement) is about 55% and 35% in the 50 degree and 30 degree TERCs, respectively (see section III.2.5). This fraction is multiplied by (1 - *TROE*) to find

---

[39] Kribus (1994) gives several window geometries; the optimum configuration for fields with rim angles in the range of the MPT was chosen. The differences are not large.

[40] The median rim angle is equal to the square root of one-half of the square of the maximum rim angle: $ARA = ((CRA*CRA) / 2)^{0.5}$.

[41] This property *appears* to resemble a feature possessed by most dialectrics (Brewster's angle), for which the effect is usually limited to those rays which have the correct polarization. In this case, however, the effect is due to the special geometry off the conical window.

the effective TERC reflectance, *ETREF*. The result is 3.15% for the more standard, 50 degree TERC. (*TROE* is always 93%, and 1-*TROE* is thus 7%, as presented in section **III.2.5**.)

Summation

The radiation which actually enters the receiver is designated *RMW* (received megawatts); the annual total is *ANNRMW*. The output *APEEFF* contains the annual "aperture efficiency" and is equal to *ANNRMW/ANNTMW*. The calculation of *RMW* is performed as follows:

RMW = (*TMW* - light which misses the aperture) * (1 - *EWREF*) * (1 - *ETREF*)

EWREF and *ETREF* are set to 100% if the respective component (window or TERC) is missing. Note that absorption is neglected in both the window and the TERC.

III.2.7.4 Re-radiation

Re-radiation losses keep the aperture size in check. Emissivity is 100%, and the receiver is treated as a blackbody cavity. The power emitted is designated *RADMW* and is calculated as follows:

$$RADMW = \pi * (DIAPE2 / 2)^2 * EWTRA * \sigma * T4AVG^4(RECTEMP, CRET)$$

...where *DIAPE2* is the receiver aperture, *EWTRA* is the effective window transmittance *in the lower (infrared) temperature bands*, σ is the Stefan-Boltzmann constant, *RECTEMP* is the receiver *exit* temperature, and *CRET* is the recuperator exit temperature on the high-pressure side (compressor exit temperature if no recuperator is fitted). *T4AVG(x,y)* is a spreadsheet function created for and used throughout this project to find the correct base temperature to express T^4 losses in an object assumed to have a linear temperature distribution from *x* to *y*:[42]

$$T4AVG = [\ 1 / (y\text{-}x) * \int_x^y t^4\, dt\ ]^{.25} \quad = \quad [\ 1 / 5(y\text{-}x) * (y^5 - x^5)\ ]^{.25}$$

Although *T4AVG* is used for more rigorous accuracy, it should perhaps be noted that the difference between *T4AVG(x,y)* and the usual average of *(x,y)* is probably well within the bounds of error created by the original linear temperature assumption. For example, in a receiver heating air from 500 C (773 K) to 800 C (1073 K), the average temperature is 650 C and *T4AVG*, only slightly greater, is 662 C. (Of course, this difference of 1.3% in absolute temperature becomes a difference of 5.3% when the fourth power losses are calculated.)

RECTEMP is solved iteratively based on the incoming flux. Before the model runs over the solar year, a maximum receiver temperature (*TMAX*) is specified. The program calibrates the receiver airflow (implicitly, but the effect is the same) so that *TMAX* is just reached when the sun is in a position for maximum flux. For every other solar position, this airflow remains the same and the new *RECTEMP* is calculated based upon the energy flow into the receiver (*RMW*) and the energy losses from radiation (*RADMW*). Note that convection losses, expected to be much smaller than *RADMW*, are neglected.

EWTRA (transmittance) is *not* the converse of *EWREF* (reflectance), because the latter is the reflectance for solar energy (temperature 5800 K), and the former is the transmittance

[42] No other reasonable assumption is possible without an entire finite element study devoted to modeling the flow path and heat transfer inside of the receiver.

for heat energy (typical temperature approximately 900 K). Section **III.2.4** (see in particular note[28]) specifies an average value of 38.2% for the transmittance of fused quartz in the relevant wavelengths; this value is used in the model without any attempt to account for angular distribution.[43]

III.2.7.5 Minor Effects on Turbine Efficiency

Ambient Temperature

In a real MPT installation, turbine efficiency will be somewhat affected by the ambient temperature, assuming that turbine inlet temperature remains the same. Lower ambient temperatures will mean a greater spread between the heat source and the heat sink, and therefore the potential for higher thermodynamic efficiency. Furthermore, the receiver may be operated marginally colder (on the order of 10-20 degrees C) in the wintertime without sacrificing additional solar fraction; an alternative would be to operate at the same temperature and raise solar fraction slightly. These effects are expected to be small and have been neglected in favor of a constant year-round ambient temperature determined as a function of location only. (Recall from section **III.1.1** that the solar year model relies on a solar-position table; thus each day is not modeled explicitly and a dynamic temperature is not practical.) It is expected that this method will result in a slight efficiency exaggeration in the summer and a slight understatement in the winter, and that these will tend to cancel each other on an annual basis.

[43] Examination of the DIAPR geometry (or that of any conical windowed receiver) reveals that the window is more or less parallel to the heat-emitting surfaces.

The ambient temperature (*AT* in the model) is found from the NREL degree day data (see section **III.2.6.3.2**) by subtracting the heating degree days (HDD) from the cooling degree days (CDD) and dividing the result by 365 days to find the average daily difference from the base temperature of 18.3 C. Thus:

$$AT = (CDD\text{-}HDD) / 365 + 18.3$$

As an example, in Dagget, CA, the HDD is 1106, the CDD is 1659, and the *AT* is 19.8 C.

Pressure Drops

The pressure drop in the receiver is set conservatively to 5% of the compressor exit temperature, as discussed in section **III.2.4**. This pressure drop is present *only* during solar operation; at night time, the air is ducted directly from the compressor (or recuperator) to the gas burner and *does not enter the receiver.* The recuperated turbine (RGT) involves pressure losses in both the cold (high-pressure) and the hot (low-pressure) sides of the recuperator. These drops are always present in the RGT system.

Table III-5: Pressure Losses in the MPT System:

Description	*Model Name*	*Time of Effect*	*Typical Value*	*Source*
Receiver	*TOWDROP*	Daylight	5%	Sec **III.2.4**
Recuperator Cold Side	*RPDROP*	Always on RGT	3%	**ref TK**
Recuperator Hot Side	*RPDROP2*	Always on RGT	3%	**ref TK**

Although incremental, all of these pressure losses have an effect on heat engine thermal efficiency, often amounting to a percentage point or two. In the case of the RGT losses, these drops are easily accounted for, because they are present at all times. However, the tower and receiver losses require the introduction of two separate net gas turbine efficiency variables in the model: *GTEFF,* which is the efficiency in solar mode, and *GASEFF*, which is the efficiency in gas-only mode. Both figures already include *GREFF*, the generator efficiency. When calculating a number of annualized parameters which

cover both daytime and nighttime operation, a time-average of these figures must be used. For example, in section **III.2.6.3.2** above, the expression for annual gas savings was:

$$AGS = TOTHEAT * (1 - \text{average GT efficiency}) * CGREFF$$

The full formula for average GT efficiency relies upon *HOURS*, the number of hours during the year during which the plant is operating in solar mode. Note that the turbine efficiencies must also be divided by the generator efficiency *GREFF* for this particular application:

$$\text{Avg GT Eff} =$$
$$(GASEFF/GREFF) * (1 - HOURS/8760) + (GTEFF/GREFF) * (HOURS / 8760)$$

For the Dagget, CA ambient temperature (see above) and the GT4 (4 MWe Allison-based) turbine described in section **III.2.6.1**, *GTEFF* is **28.5%** while *GASEFF* is **30.0%.**

III.2.7.6 Summary of MPT Annual Calculations

Efficiency

The sections above have presented all of the MPT losses and their associated, annual efficiency calculations. When it comes time for system evaluation, several of these efficiencies will be of interest, in addition to the usual levelized cost of energy calculation (discussed in chapter 4). In particular, the output *STEFF* (annual solar to thermal efficiency) contains the net product of all of the various loss mechanisms, and represents the MPT performance exclusive of the gas turbine. For example, *STEFF* may be compared with *ASDBSTEFF* (see the section **III.3.4** on D/E systems) to grasp the optical differences between heliostat fields and power towers. Chapter 5 will examine issues of this kind, but the component efficiencies are summarized here:

Table III-6: Component Annual Efficiencies of the MTP

Model Designation	Description	Range
ROE *	(Heliostat Mirror Reflectivity)	90%
ANNUAL *	(1 - Annual Cosine Losses)	90-95%
ANNBEFF *	(Blocking and Shading Efficiency)	90-95%
APEEFF *	(Aperture Efficiency)	85-95%
RECEFF =	(Receiver Efficiency)	85-95%
STEFF	(Net Solar to Thermal Efficiency)	55-75%
STEFF *	(Net Solar to Thermal Efficiency)	55-75%
GTEFF =	(Gas Turb. + Gen. Effic. in Solar Mode)	23-38%
HEFF	(Heliostat Solar to Electric Efficiency)	12-28%

The MPT solar fraction (*HSF*) is also a very significant output; this figure measures the fraction of total heat *entering the turbine* which came from a solar source. Thus *HSF* reveals the portion of the annual electric yield which was produced by sunlight. Note that the annual efficiency figures and average power output (see below) are bases upon *HOURS*, the number of hours during the year for which the receiver is able to generate a net positive heat flow. However, *HSF* is based upon the entire year's plant operation.

HADJEFF is the final annual efficiency output, representing the net total efficiency of energy conversion from both sunlight and gas *combined.* This figure is found by dividing the total electricity output by the sum of the gas and solar inputs. (Note that there are two turbine efficiencies: *GASEFF*, which represents the thermal efficiency when the solar portion of the system is shut off, and *GTEFF*, the thermal efficiency is hybrid mode. *GASEFF* is higher that *GTEFF* because no pressure losses (*TOWDROP*) are incurred in the receiver or its ducts.)

HADJEFF can be found directly from the efficiencies and from *HOURS*, the time spent in solar hybrid mode. If one defines the amount of energy entering the turbine as equal to one unit, the electric output is:

$$\text{Electric Output} = E_{out} = GASEFF * (1 - HOURS / 8760) + GTEFF * (HOURS / 8760)$$

...and the gas portion of the total input is:

$$\text{Gas Input} = G_{in} = (1 - HSF)$$

...recalling that *HSF* is the MPT solar fraction. The solar portion of the total input is:

$$\text{Solar Input} = S_{in} = HSF / STEFF.$$

...recalling the *STEFF* is the solar to *thermal* efficiency. Thus:

$$HADJEFF = E_{out} / (G_{in} + S_{in}) =$$
$$[\ GASEFF * (1 - HOURS / 8760) + GTEFF * (HOURS / 8760)\ ] /$$
$$[\ (1 - HSF) + HSF / STEFF\ ]$$

Note that the overall efficiencies are calculated on a **mirror area basis**. That is, *STEFF* represents the thermal energy passed to the gas turbine as a fraction of the light energy which would strike this same set of heliostats if they were always pointed directly at the sun and suffered no shading losses. All subsequent efficiencies are affected by this definition.

Power

The efficiency figures can be viewed on their own as an accurate description of the MPT, but they contain no information about the absolute quantity of power produced. A second set of figures is used to determine the gas turbine rating, in MWe. First, the number of megawatts thermal delivered by the receiver is tracked throughout the year, and the peak value (*PKDMW*) is used in conjunction with the receiver maximum temperature (*TMAX*, reached at *PKDMW*), the turbine inlet temperature (*TIT*), the compressor (recuperator)

exit temperature (*CRET*) and the gas turbine efficiency **in solar mode** (*GTEFF*) to determine the gas turbine rating (*GTRATING*). The formula is:[44]

$$GTRATING = PKDMW * ((TIT - CRET) / (TMAX - CRET)) / GTEFF$$

This process may result in a gas turbine rating which may not precisely match the rating for one of the commercially available models upon which it is based. However, the turbine is an exact match for the heliostat field. A considerable effort has been made to match the turbine rating to existing machines by adjusting the field size, and the ratings of the model cases are within 1-2% of the ratings of the real world turbines. (This matching only applies to the open-cycle machines; in the recuperated case, no exact real-world analog has been selected.) Of course, when an MPT is built, it will be necessary either to match the field size with an existing turbine or to build (or de-rate) a turbine to match the *GTRATING* specification.

Table **III-7** summarizes the power outputs for the MPT:

Table III-7: Annual Power Outputs of the MTP

Model Designation	Description	Range
HGTRATING	Gas Turbine Rating	2.0 - 3.9 MWe
PKDMW	Peak Solar Heat Delivered to Turbine Inlet	6 - 9 MWt
ANNEMW	Annual Avg. Heat on Flat Mirrors Pointed at Sun	5 - 9 MWt
ANNTBBMW	Annual Avg. Heat on Actual Mirrors	4.5 - 7.5 MWt
ANNTMW	Annual Avg. Heat after Blocking & Shading	4 - 6 MWt
ANNRMW -	Annual Avg. Heat Accepted by the Aperture	3 - 5.5 MWt
ANNRADMW =	Annual Avg. Heat Re-Radiated	0.02 - 0.04 MWt
ANNDMW	Annual Average Solar Heat Delivered to Turbine Inlet	3 - 5.5 MWt

Note: Annual Averages based on HOURS, the time when the system is actually operating in solar mode.

[44] The spreadsheet model corrects the formula for variable specific heat (using customized combustion fucntions), but this detail is omitted here for clarity. See **note 36** and Appendix **A** for more detail.

III.3 Dish / Brayton System

The Allied Signal Dish Brayton (ASDB) system is modeled here for comparison with the MPT. This system is currently under development as a joint project between Allied Signal, Inc., and Sandia National Labs. Delivery of system components to Sandia and initial on-sun testing are planned for 1998. The ASDB design was chosen because it is the only dish / Brayton initiative sponsored by major institutions in the United States at this time. Other efforts are underway in Germany, and possibly in Israel (although the main focus at the Weizmann Institute appears to be a solar tower.)

The modeling methodology is immensely simplified. Rather than constructing an installation from scratch, the planning-phase ASDB specifications were obtained from sources at Allied Signal and Sandia National Laboratory. The spreadsheet model uses these specifications, but convolves the dish over the course of the exact same solar year, in the same locations, as the MPT system.

III.3.1 Parabolic Dish

The choice of a dish for inclusion with the real-world ASDB system has not been completed as of this writing. Some latitude still exists for this part of the design; therefore the choice has been made to model the system with an SAIC-type dish so as to facilitate comparison with MPT. The SAIC dish is composed of round drum type facets mounted on a steel truss frame. An arm is attached to the frame which projects up to the focal point and holds the receiver and engine (in this case, the ASDB receiver and RGT engine). The entire assembly is mounted on a pedestal mount with two-axis tracking, in a fashion very similar to the SAIC heliostat (see MPT model). The facets are distributed fairly tightly over the surface of the support structure, while avoiding shading by the receiver support

Figure III-6:
Allied Signal Dish / Brayton System Components

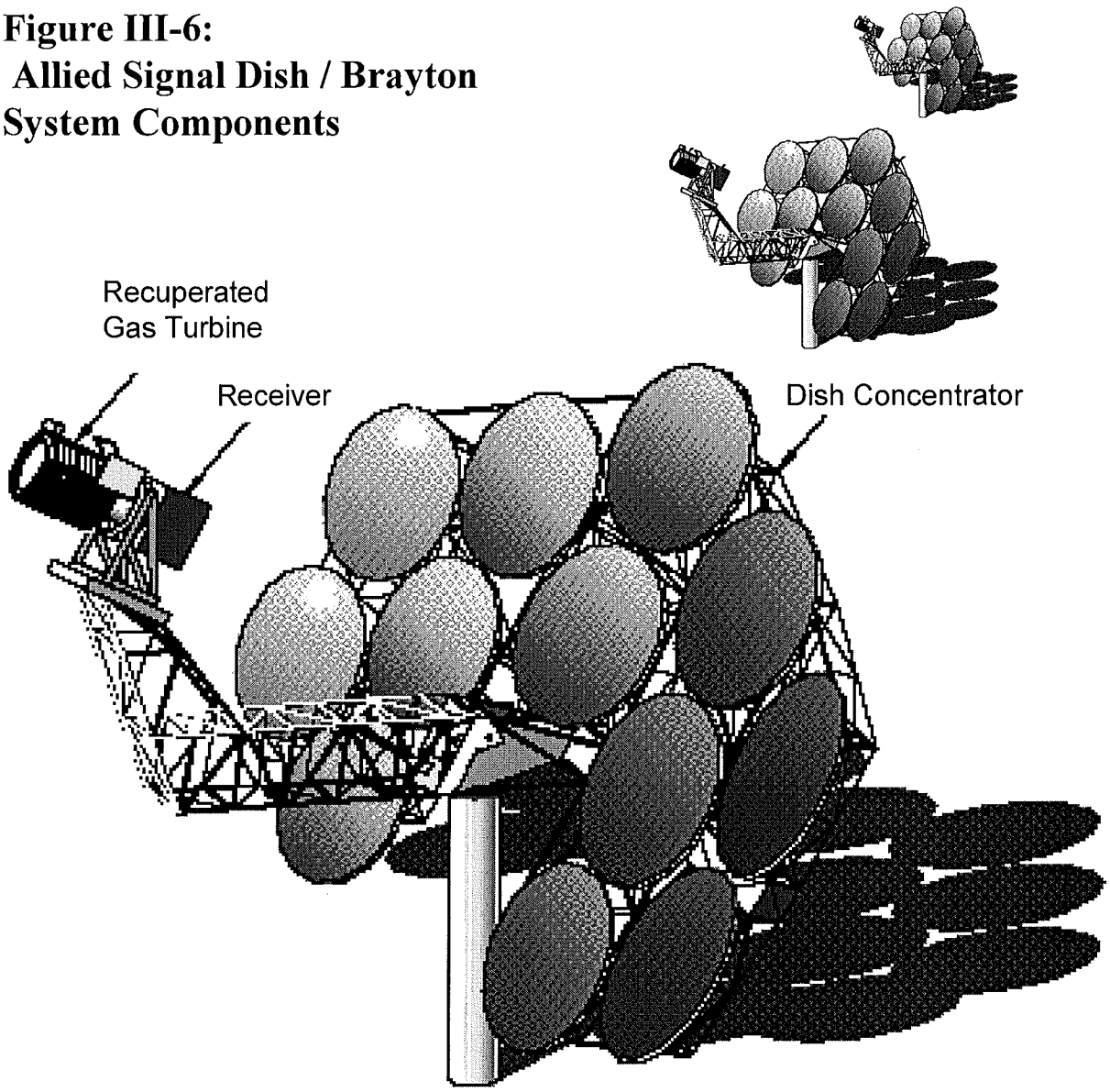

DIAPR-Type
Windowed Receiver

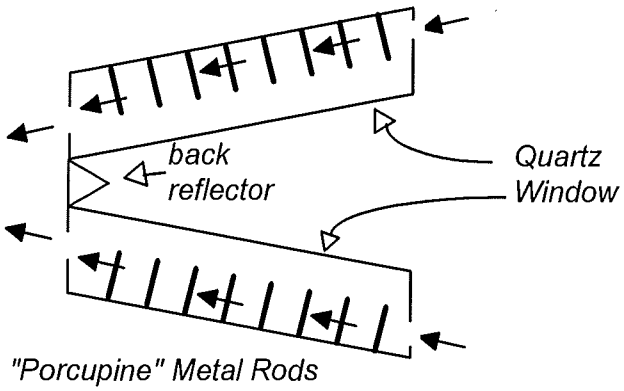

Shell and Can
Receiver

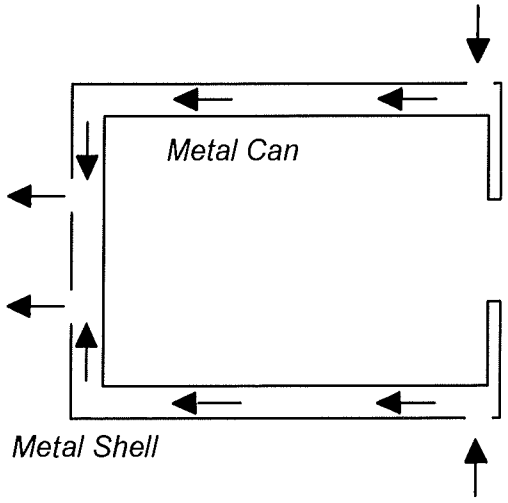

strut and module. As in the MPT model, the round facets are 3.0 meters in diameter. SAIC dish / Stirling systems with these facets are currently being manufactured.

With the dish technology selected, the modeling methodology switches to the ASDB design specifications obtained privately from Sandia. The system calls for 90 kWt of solar flux under full-load. "Full-load", or "design point", flux is usually 1000 Watt/m^2 for solar thermal devices. Maintaining the same mirror reflectivity of 90% as in the MPT model, the flux specification implies a dish aperture (*DAPE*) of 100 square meters. However, the mirrored area is somewhat more than this, because the dish is concave. A spherical approximation is valid at this slight degree of curvature and was used by the model to find the true mirror area (*DAREA*). A radius of 7.0 meters and a focal length of about 7.5 meters is used for this calculation. These values, which are not atypical for dish systems (see, e.g. Beninga 1997), were chosen because they result in an integer number of 3.0 meter drum facets while leaving sufficient room for the circular facets to be arranged on the surface of the dish: the resulting *mirror* area of 106.1 m^2 is composed of 15 drum facets arranged over the surface of a 163.4 m^2 dish.

The above construction may at first appear to be a bit cavalier, but it is critical to realize that the receiver's optical performance is *already* specified in the Sandia materials and does *not* depend upon the above figures, which represent reverse engineering. Furthermore, the SAIC dishes currently under construction do not necessarily have the same number of facets (15) as the dish constructed here (instead, 16 seems to be a typical number). However, this is the correct number needed to match the ASDB specifications, which may or may not be matched to a dish of this kind in the future. The dish created here is thus *representative* of a drum-type dish matched to the ASDB receiver, but is not a unique solution.[45] This dish is only used for cost calculations, with a single exception: the relationship between the dish aperture (*DAPE*, which is really the summed aperture of the mirrors rather than the whole dish form) and the dish area (*DAREA*) is used to

[45] The dish is matched in terms of optical power. However, angular acceptance for the ASDB receiver is not available, so the dish is not matched in this sense. However, it is unlikely that a gross mismatch would occur, since the ASDB receiver is designed with a dish of this general size in mind.

estimate the optical cosine losses for a dish this size. Unlike the heliostat case, these losses are constant because the sun is always in the same position relative to the dish. The geometric efficiency of the ASDB dish is (100 / 106.1 =) 94.3%.

III.3.2 Receiver

The ASDB receiver is a can-and-shell design, in which the air flows over the outside surface of a can which forms the wall of the cavity. The air flow is trapped against the can by an outer shell, and the passage through which it flows is filled with heat exchange fins attached to the inner can. There is no window and no secondary receiver. The materials for the can are not specified, but its maximum operating temperature of about 815 C suggests that special alloys (e.g. Inconel) may be included. The primary challenges in developing the prototype of this receiver will probably relate to its structural integrity under thermal loading. The high pressure side of the cavity is at approximately two atmospheres, and it is critical that no leaks form in the can. As with the MPT receivers, the hybrid operation mode allows a reduction in receiver operating temperature if material constraints so require. Chapter 5 contains a test case for both the ASDB and the MPT at reduced receiver temperatures to examine the impact on solar fraction, efficiency, and LEC.

The spreadsheet model treats the ASDB receiver in much the same fashion as the MPT unit: a linear surface temperature gradient is assumed and the *T4AVG* function is used to facilitate the calculation of receiver losses. These are based on the high-pressure recuperator outlet temperature (*ASDBCRET*) and the receiver temperature (*ASDBRECTEMP*); the latter must be solved for iteratively. The output variable *ASDBRECEFF* contains the instant receiver efficiency (a function of solar flux but usually in the range of 85%-90%), while *ANNASDBREFF* contains the annualized figure. As with the MPT, the system only operates in solar mode when the net heat flow in the

receiver is positive; when the losses become greater than the gains, a shutter is assumed to close over the aperture.

III.3.3 Recuperated Gas Turbine

The ASDB gas turbine is a low-pressure (2.3 bar) recuperated machine with an overall thermal to electric efficiency around 31%. The model follows a similar strategy to that for the MPT: a set of thermodynamic parameters is reverse-engineered until the performance specifications are met. In the case of the ASDB engine, the specifications from Allied Signal were nearly complete; the only parameters which could be back-calculated were the isentropic efficiencies for the turbine and compressor. This was done is such a way that all of the temperatures throughout the cycle matched the specifications exactly, and the overall efficiency was likewise an exact match (within one-tenth of a percentage point). Although the engine model is not really necessary with the specifications on hand (except to test a few variations), this exercised verified its validity, an important consideration when the same model is used on the MPT.[46]

The following table presents the specifications from Allied Signal along with their counterparts in the spreadsheet. It is clear that the engine has been accurately re-produced, and can be used to explore variations in these parameters if desired. A few such variations are experimented with in chapter 5, but the baseline ASDB model leaves the engine unchanged.

[46] There is one caveat concerning this model when applied to the open-cycle MPT engine, having to do with blade cooling corrections. This caveat is noted in the relevant section within the MPT model description.

Table III-8:
ASDB Recuperated Gas Turbine (25 kWe) Specifications In Model. Ambient = 15 C

Parameter	*Model Name*	*Value*	*Source*
Compressor Pressure Ratio, bars	ASDBHP	2.33	*Allied Signal*
Isentropic Comp. Eff.	ASDBCn	70.5%	*Model*
Recuperator Effectiveness	ASDBREGEN	90%	*Allied Signal*
Recup. Cold Side Pressure Drop, bars	ASDBRPDROP	0.084	*Allied Signal*
Turbine Inlet Temp, C	ASDBTIT	817	*Allied Signal*
Isentropic Turbine Eff.	ASDBTn	90.5%	*Model*
Recup. Hot Side Pressure Drop, bars	ASDBRPDROP2	0.029	*Allied Signal*
Net Thermal Efficiency, LHV, Solar Mode	ASDBGTEFF	30.4	*Allied Signal or Model*

***Note**: A 95% electric generator efficiency is included in the ASDBGTEFF result, as described in the text*

III.3.4 Summary of ASDB Annual Efficiency Calculations

The annual results for the ASDB system are somewhat simpler than those of the MPT system, because there are no blocking, shading, or aperture losses.[47] The annual averages and efficiencies are all based upon *ASDBHOURS*, the number of hours during which the dish can generate a net positive heat flow. For the rest of the year (8760 - *ASDBHOURS*), it is assumed that the shutter is closed and that the turbine is 100% gas-fueled. As with the MPT, the solar fraction (*ASDBSF*) represents the portion of total heat *at the turbine inlet* which is generated by sunlight, while the adjusted efficiency (*ASDBADJEFF*) represents the net energy conversion efficiency for both sunlight and gas combined.

Tables **III-9** and **III-10** present the annual efficiencies and power ratings for the ASDB system. As opposed to the MPT case, where system configuration can vary widely, the dish system is a fixed design with the **exception of a few experimental changes covered in chapter 5**. Thus the bulk of variance in the ranges of these values is due to changes in solar flux from site to site.

[47] An actual dish will have small, but nonzero, aperture losses (light which fails to be admitted), because at a certain diameter the increased radiation loss will overcome the diminishing returns of increased acceptance angle (this point will be in the corona around the sun). However, for the ASDB system, these losses are neglected.

Table III-9: Component Annual Efficiencies of the ASDB

Model Designation	Description	Range
ROE *	(Dish Facet Mirror Reflectivity)	90%
DAPE/DAREA =	(1 - Annual Cosine Losses)	94.3%
DEFF;	(Dish Efficiency)	85%
DEFF *	(Dish Efficiency)	85%
ANNASDBREFF =	(Receiver Efficiency)	85-90%
ASDBSTEFF;	(Net Solar to Thermal Efficiency)	73-77%
ASDBSTEFF *	(Net Solar to Thermal Efficiency)	73-77%
ASDBGTEFF =	(Gas Turb. + Gen. Effic.)	29-31%
ANNASDBEFF	(ASDB Solar to Electric Efficiency)	21-24%

Table III-10: Annual Power Outputs of the ASDB (Single Dish)

Model Designation	Description	Range
ASBHEATPROV /	(Heat Provided by Sunlight, MWht)	180 - 240
ASDBHEATREQ =	(Heat Required by Turbine, MWht)	600 - 800
ASDBSF	(ASDB Solar Fraction)	23%-33%
ANNASDBDMW	(ASDB Average Delivered MWt)	.045 - .065
ASDBPKDMW	(ASDB Peak Delivered MWt)	.078 - .080
ASDBGTRATING	(ASDB Gas Turbine Rating, MWe)	.023 - .024

CHAPTER 4: COST MODELING

IV.1 General Approach to Cost

This study acknowledges at the outset that the cost modeling is not as precise as the performance modeling. Some of the technology under investigation is still in the experimental stage of development, and there is extensive cost uncertainty within the industry itself. However, it is often a consideration of cost which balances a technical presentation and permits the document's scope to extend from engineering into the realm of policy. Such is the hope and intention of the current analysis.

IV.1.1 Relative vs. Absolute Estimates

There are two purposes in compiling cost information for the systems modeled here. First, a direct comparison can be made between the two small-scale gas turbine STEPs which have been selected as most promising: the MPT and the ASDB. Second, an attempt is made to determine how economical these systems will be within the larger energy market, under various assumptions concerning the price of natural gas and STEP materials.

The first comparison, system-to-system, will be the most accurate, largely because of the effort made to make the system scale and components as similar as possible. The most costly component, the mirrors, are the same in both systems. Both systems appear to be technically feasible within the next several years, although the ASDB, which is actually under development, may have a lead in this regard over the MPT, which contains several more experimental components (the TERC e.g.). To achieve equivalent system scale, the individual ASDB systems are pooled together in sufficient number that their combined output is equal to the output of the MPT with which they are being compared, although their greater modularity must be acknowledged.[48] Finally, the benefits of the

[48] Of course, the number of ASDB systems must be an integer, so the match will not be exact in all cases, but nonetheless will be close enough to allow meaningful direct comparison of capital costs.

cogeneration application for the MPT have been accounted for in terms of gas savings so that direct economic comparison is possible with dish systems lacking cogeneration.

IV.1.2 Cost Targets

The second type of cost comparison, that between the STEPs and conventional power generation systems (e.g. centrally located coal and gas plants), is accomplished implicitly by calculating the levelized energy cost (LEC) under a variety of assumptions. Some of this variance relates to the price of gas and the value of distributed production, but the most interesting figures are the R&D cost targets for solar plant components, particularly heliostats and to a lesser extent, receivers. For example, in addition to assigning a single fixed "base case" price to the cost of mirrors, the net LEC is also graphed against a variable mirror cost. Ultimately, by choosing scenarios for the cost of gas and other system components, an "R&D price target" can be established for mirrors at which the STEP LEC becomes equal to the conventional power LEC. The component costs and calculation methodology are established in this chapter; the actual comparisons are presented in chapter 5.

A summary of component costs for all systems is presented below in section **IV.5.4**.

IV.1.3 Environmental Costs and Benefits

Environmental costs and benefits are not directly addressed here. However, in section **V.8.2**, which addresses the buy-down costs for making the MPT competitive, a carbon tax scenario is included. The tax level represented is $50 / ton carbon. As illustrated in figure **V-6b**, this level of tax would make a very significant impact upon the financial appeal of the MPT, and would vastly speed progress down the experience curve.

Qualitatively, the reader should be aware that, in its requirement for large areas of relatively unobstructed land (up to 20 hectares), the MPT may be considered to have an environmental cost. This "cost" will depend strongly upon local conditions, and must be weighed against the carbon (and other emissions) displaced by solar radiation.

IV.2 Mini Power Tower Component Costs

IV.2.1 Land

Including the capital cost of land with the other MPT component costs introduces an undesirable degree of site-specificity into the results. Possible application sites range from a desert environment (negligible land cost) to a college campus to the roof of a shopping mall[49] or even an apartment complex. Hopefully, sites can be selected so that land cost will be small or negligible. A 4 MWe MPT with cogeneration in Dagget, CA requires on oval plot of land with a long axis of about 350 meters and a short axis of about 200 meters (see fig **V-1d**). This represents about 17 hectares. Land costs have been left out of the LEC calculations for both the MPT and the ASDB, and this should be duly noted.

IV.2.2 Tower

Requirements: The tower must be relatively modest but strong enough to support the weight of the gas turbine, generator, receiver, and TERC secondary. The 3.9 MWe Allison 501-KB5, which represents a typical turbine for the MPT, weighs about 10,000 kg (with generator) and measures 2.5 m long by 1 m wide by 1 m high (GTW 1997). (These figures do not include the generator, but after it is added the set will still be very compact.) Neither the receiver nor the secondary is expected to be nearly this heavy, and

[49] The shopping mall application may be particularly promising. The owners of such complexes are often in need of a special element to differentiate them from the competition, and the very futuristic appeal of an MPT installed on the roof might provide just such an element.

a tower top capacity of 15,000 kg (15 metric tons) seems adequate to cover all components. In order to minimize shading, it is desirable to support this weight with as narrow a structure as possible, while still allowing convenient access to the machinery, meaning here stairs (or an elevator) instead of a ladder, and a large working platform surrounding the turbine, which is located just below the receiver.

The tower data which was collected does not permit a meaningfully accurate optimization of field performance versus tower cost as functions of tower height.[50] An alternative approach has been taken: a region of "reasonable" tower height has been chosen, based upon the available cost estimates, practicality of access, and sufficient field performance. Within this range, *tower cost is a constant.* The range which was chosen is quite narrow: 60 meters to 80 meters. Above about 80 meters, access (for both humans and cogen water piping) becomes more difficult; below about 60 meters, the system incurs unnecessary performance penalties due to poor field geometry (e.g. blocking and shading). In chapter 5, a **single tower height is chosen for all models**, thus minimizing any possible distortions of a system-to-system cost.

Price Estimation: There are very few solar thermal plant design studies which incorporate a tower this small. One exception is the 600 kWe Israeli SCOT system, which includes a lightweight, 49 meter tower which carries a 190 m^2 reflector on the top, shaped like an inverted dome (Kribus *et al* 1997). Although the weight of the mirror and associated support structures are not given, 15 kg/m^2 seems like a reasonable minimum, meaning that this tower must support at least 3 tons – considerably lighter (and simpler) than the MPT system. The SCOT tower is estimated to cost $46,000.

The wind power industry provides further indications of tower cost, with the advantage that large modern wind turbines are *heavier* than the MPT. Research by Gipe (1997) indicates that towers for wind installation run around 20% of installed system cost. The

[50] There is evidence that tower cost does not vary linearly with height; for example, a 130 meter tower designed for the PHOEBUS project may cost up to $5 million (Grasse 1991); this figure is 40-50 times what is expected for the MPT, although the tower is only twice as tall.

D.O.E.'s Renewable Energy Annual 1996 (DOE 1997a) establishes $1,250/kWe as a typical cost for modern wind turbine systems. 50-60 meters is a common hub height for today's 500 kWe machines; a "light" model of these machines might weigh under 100 tons but many will weigh more. Thus a 50 meter tower capable of supporting 100 tons can be expected to cost around $125,000 in the wind industry. A study by Cohen at Princeton Economic Research Inc. (PERI) predicts a cost of $185,000 for a 70 meter tower bearing a 1 MWe turbine, to be built in 2005[51] (Cohen 1998).

A figure of $200,000 has been used throughout the MPT model for a 60-80 meter tower. This price represents a conservative figure exceeding both the ~3 ton Israeli tower at ~$50,000 and the ~100 ton wind towers at $125,000-$185,000. The final choice of a uniform tower height is discussed in section **V.3**.

IV.2.3 Heliostats

Heliostat cost dominates system capital outlay and, in all but the most optimistic future projections, LEC. Significant advances have been made in heliostat technology in recent years, and the choice of drum-type, stretched membrane heliostats for the MPT reflect this progress. However, there will need to be several more significant evolutionary periods before costs become low enough to catapult solar thermal from a mere fraction of a percent of electric production to a major market share. One of the first of these is likely to be a transition away from thin glass mirrors which are bonded onto the steel drums, as in the current system, to reflective foils forming the surface of the drum itself (e.g. Beninga 1997; Weinrebe *et al* 1996). Another improvement which will reduce costs depends upon the manufacture of wider sheets of the current steel membrane material: the SAIC dishes produced today require a number of expensive welds across the drum to join

[51] Although a tower of this height, at this price, does not appear in Cohen's analysis until 2005, the intervening technological developments are related to the turbine, not to the tower itself. There is no indication in the PERI study that unit tower costs are expected to fall substantially between now and 2005.

steel strips edge to edge. If the entire drum could be fabricated out of one or two much wider strips, production costs would fall substantially (Mancini 1997).

On the performance side, the improvements will be much more modest. Current heliostats boast reflectivity around 90%; it should be possible to improve this to 93 or 95% at some point in the future, judging by some of the more advanced modules under manufacture today. An incremental improvement of similar magnitude may be available by changing the mounting orientation of the heliostats, so that one of the two axes points directly at the receiver, as opposed to the traditional altitude/azimuth system. This idea, which allows the heliostats to incorporate built-in astigmatic corrections, has been proposed by researchers at Israel's Weizmann Institute (Zaibel *et al* 1995).

Current heliostat prices (installed) are above \$200 / m^2. As a general rule of thumb, this cost must fall to half its current level to ensure the future viability of solar thermal power. Thus a rather broad range (\$50 to \$200) of heliostat prices has been considered for the results presented in chapter 5. Table **IV-1** lists a number of recent heliostat prices found in modeling exercises, manufacturer's claims, and actual project construction:

Table IV-1: Various Heliostat Price Estimates, in Dollars per Square Meter

Project	*Price*	*Context*	*Source*
SCOT/CC	\$248	Based on recent Israeli "manufacturer cost quotes"	Kribus *et al* (1997)
PHOEBUS	\$175	Study for a 30 MWe Hot Air Plant in Jordan	Grasse (1991)
year 2000	\$182	30 MWe plant / 500 units a year production rate	Kolb (1997)
SAIC	\$120	Estimate for SAIC's "large production run scenario"	SAIC (1997a)
year 2005	\$99	100 MWe plant / 3000 units a year	Kolb (1997)
year 2010	\$75	200 MWe plant / 10,000 units a year	*ibid*
year 2020	\$70	200 MWe plant / 50,000 units a year	*ibid*

IV.2.4 Receiver

Pricing the MPT receiver introduces considerable uncertainty, because at least two designs (window and cavity) are candidates and both must be considered "still on the drawing board" for the size range proposed here. Nonetheless, researchers at the

Weizmann Institute in Israel maintain that the current 50 kWt DIAPR receiver (windowed, operating up to 30 bars and 1300 C) "can be upscaled to 1 MWt using current manufacturing capabilities, and to larger sizes with some investment in manufacturing capabilities." (Kribus *et al* 1997) The same study specifies an approximate receiver cost of $64 per kWt for a 600 kWe system and, at the other end of the scale, $48 / kWt for a 34 MWe system.

Uncertainties prevent a meaningful cost distinction between the windowed (DIAPR-type) receiver and the shell-and-can (ASDB-type) receiver. Rather a cost range from $40/kWt to $80/kWt appears to be realistic for both types. As the results were developed for chapter 5, it became apparent that variation in receiver cost had a minor effect on overall system economics, so a fixed price of **$60/kWt was used for all** MPT model runs. Considerable uncertainty attends this figure, but it seems adequately conservative when compared to the Israeli estimates.

IV.2.5 TERC Concentrator

The cost of the TERC concentrator is estimated based upon its surface area (*SCONA).* As mentioned in chapter 3, the TERC can be well approximated over the vast majority of its surface by a simple cone; it is only the inner sections next to the receiver which must be very carefully molded. The specific cost is determined as follows:

- The TERC cost is never cheaper than the heliostats, but it is assumed that it varies in much the same manner, according to production experience and advancing technology. Thus in chapter 5, when LEC is plotted against heliostat cost, the cost of the TERC is also varying.

- The Israeli SCOT system includes a large, tower-mounted reflector which, while not the same size or shape as the TERC, represents a similar set of design parameters.

The SCOT study estimates a total (installed) cost of $276,000 for a 190 m^2 hyperbolic reflector and a set of similarly sized CPC collectors at ground level (total mirrored area of about 400 m^2) (Kolb *et al* 1997). The resulting specific cost of (276,000 / 400 =) $690 / m^2 must be taken as a very crude estimate. In the same study, the heliostat cost for this system is $248 / m^2. The MPT model estimates the installed TERC cost (which turns out not to be a very significant component of system cost) by using the ratio (2.8) between these two figures:

$$\text{TERC cost} = \textit{SCONA} * \text{Heliostat cost (\$/m}^2\text{)} * 2.8$$

IV.2.6 Gas Turbine, Recuperator, & Generator

IV.2.6.1 Open Cycle Cogeneration System

The specific cost of the two open-cycle machines (GT3 and GT4) has already been introduced in chapter 3: $530 per kWe for the GT3 and $450 per kWe for the GT4. These prices include the generators, but do *not* include installation costs. Total *installed* cost for an Allison 501KB5 (upon which the GT4 is based) is expected to run about $3.5 million ($897/kWe) for a cogeneration application, including all gas compressors, electrical connections, and heat recovery steam generator (Wenglarz 1997). The latter will be replaced by a pressurized hot water heater to exploit the tower siphon advantages of such a system (see section **III.2.6.3.1**), and to reduce the overall bulk of equipment in the tower. The GT3 (based on the Allison 501KB3) is essentially the same turbine with less expensive blades and a few minor modifications, but with the same installation requirements; thus the only price difference is the original $300,000 gap between the turbines themselves (Wenglarz 1997). Multiplying by the respective engine sizes (2.8 MWe and 3.9 MWe) yields total installed capital costs for these open cycle machines as follows:

GT3: $3.2 million ($1,143 / kWe)

GT4: $3.5 million ($897 / kWe)

An allowance of $50,000 (or approximately 3% of the original turbine price) is added to these figures to account for the cost of two added flanges: one which ducts compressed air to the solar receiver and a second which receives air from the receiver back into the (possibly modified) combustion chamber. This estimate is based on Allison's experience with very similar modifications on a 501 engine undertaken as part of a DOE experimental coal power initiative (Wenglarz 1997).

Note that the cost of circulating piping for cogeneration is not included in the MPT model, because the favorable assumption is made that the MPT replaces or augments the heat source in an already constructed hot water circulation system.[52] This assumption is consistent with the overall approach to the cogeneration application, which represents the "first competitive systems"; i.e. those which can be placed in the more favorable cogeneration locations. It is expected that, as systems such as the MPT become more common and the cost of solar components falls, the MPT design will become viable in cogeneration applications where capital costs are more significant.

IV.2.6.2 Recuperated Cycle System

Greater cost uncertainty exists for the RGT than for GT3 or GT4. A figure of $700 / kWe has been selected for the RGT. This estimate is loosely based on the much smaller Allied Signal recuperated engine, for which $500 / kWe represents the low-end cost estimate of a considerable range (see section **IV.3.3** below). Placing the 2-4 MWe RGT cost near the lower end of the range for a 50 kWe machine does not seem overly optimistic in light of the large scale economies evident for extremely small gas turbines. Adding to the conservative nature of this estimate is the realization that the ASDB price includes the

receiver. Finally, note that the RGT cost is approximately 70% of the open-cycle cogen turbines, which seems reasonable in light of the much lower turbine inlet temperatures and pressure ratios.

IV.3 Dish / Brayton Component Costs

IV.3.1 Land

The collected ASDB units will occupy essentially the same land area as the MPT, although their greater modularity will facilitate deployment over difficult terrain such as rooftops. However, the treatment of land cost is the same in both systems: it is neglected on the grounds that it forms a highly variable yet most likely minor part of the total capital outlay.

IV.3.2 Dish Reflectors

A central feature of the strategy pursued here is to equalize reflector costs between the power tower and dish systems so that their other merits might serve as a basis for comparison. To achieve this end, a standard, round, drum-type mirror facet is common to both systems: the MPT heliostats carry six such facets, while the ASDB dishes have fifteen. It is further assumed that the mounting expenses are essentially equivalent, per square meter of mirrored area, and that these costs are included in the heliostat prices in table **IV-1**, above. This balance-of-system equivalence is predicated on the following observations: While the dishes, which are larger, will require in total approximately one-half as many tracking drives as will the heliostats, these drives must be somewhat larger. In addition, the dish mounting is of a somewhat more complex form, and must include a support arm for the engine and receiver.

---

[52] Note that the installed cost *includes* an allowance for a heat recovery system in the turbine exhaust, HRSG or otherwise.

The range of dish costs allowed in the system evaluation is the same as the range of heliostat costs: from $50 to $200 per square meter. Note that these costs are based on the actual mirror area, *not* the summed aperture of the mirrors (which is slightly smaller due to curvature) nor the actual aperture of the dish (which is much larger due to spaces between the facets).

IV.3.3 Power Conversion Modules

In the case of the dish systems, the cost of the receiver and recuperated gas turbine is combined into a single figure for the "power conversion module". Allied Signal has not provided any estimate of the power module cost. Instead, a price range is constructed here by analogy with dish Stirling systems, which are nearer to commercialization. It must be remembered that the Brayton systems are intended to be more durable, more easily serviceable, and more easily used with natural gas than the Stirling systems, but not necessarily cheaper. Thus, it seems fair to establish a price range for the ASDB modules which resembles the range for Stirling modules.

SAIC currently manufacturers a dish/Stirling system which they hope to introduce to the broader market over the next several years. This system uses a dish composed of round drum facets, just like the ASDB system as modeled here.[53] SAIC estimates total system cost for a 25 kWe system as follows[54]:

Table IV-2: SAIC Cost Estimates for 25 kWe Dish / Stirling System

Annual Production	*Price per Watt Electric*	*Total System Price*
100 units	$5.40	$135,000
5000 units	$1.90	$47,500
25000 units	$1.40	$35,000

Source: SAIC (1997b)

[53] As previously mentioned, the actual dish which Allied Signal chooses to include may not be of this type.
[54] Unfortunately, the materials from which these figures are taken do not provide more detailed information; e.g. cost of individual components, financing assumptions, etc.

These systems have a mirrored area of 180 square meters. SAIC's "large production run scenario" from table **IV-2** specifies a mirror cost of $\$120/m^2$, yielding a dish price of $21,600. Subtracting this figure from the price for 25,000 annual units from table **IV-2** leaves $13,400 to account for the power conversion module, or roughly $500/kWe. Viewing this figure alongside the comparable cost of much larger gas turbines (in table **III-2**) reveals it to be optimistic, particularly as it includes receiver costs.

The figure of $500/kWe, derived above, represents an advanced production scenario and is only appropriate as the lower end of the range for the ASDB power module. The upper end of the range has been established by using the SAIC cost estimate for 100 units in conjunction with a more "current" mirror price of $\$250/m^2$; the resulting module cost is $3600/kWe. The ASDM module is somewhat simpler than the Stirling module, and will be easier to produce at low volumes because many of the parts are already familiar, and, in some case, can be obtained off-the-shelf. In light of these differences and to avoid unrealistic speculation, the upper limit on the ASDB power conversion modules has been reduced to $2000/kWe.

IV.4 Gas Costs

IV.4.1 Price Projections

The cost modeling allows natural gas prices to vary over a reasonable range in order to examine the system LEC under various conditions. The system does not model gas prices dynamically through time, as this method will not enhance accuracy over periods longer than a few years due to uncertainties in gas pricing models.

The model uses the "industrial" price estimates[55] from the 1998 Annual Energy Outlook (AEO) published by the Department of Energy (DOE 1997b). The basic range is established by assuming that the technology in the MPT and ASDB concepts will be "current" for perhaps 15 years; thus a low figure of $10.64/MWht (from the year 2000) and a high figure of $11.55/MWht (year 2012) are both relevant. The AEO includes various high and low growth scenarios in addition to the reference case; typically these allow a price fluctuation of around 20%. Applying this boundary to both the high and low estimates for individual years, and rounding to the nearest dime, a total range is determined for natural gas prices in the model: from $8.50/MWht ($2.50/mmBTU) to $13.90/MWht ($4.10/mmBTU).[56] The base case gas price will be $10/MWht, except for the less conservative "buy-down" analysis in section **V.8**, where the medium gas price is $11/MWht, with "low" and "high" cases at $10 and $12, respectively. (The effects of a carbon tax and of price risk upon the cost of gas are also examined briefly in **V.8**.)

IV.4.2 Cogeneration Savings

As discussed in chapter 3, the cogeneration model is constructed in such a way that the benefits can be accounted for in terms of gas savings; these savings are presented with the other results in chapter 5. It is assumed that the heat which is provided in the turbine exhaust would otherwise be provided by a gas burner at the same location, and that the efficiency of heat transfer between the exhaust stream and the hot water will be comparable to the heat transfer between the gas burner and water. It has been acknowledged that these are favorable assumptions which represent the "low-hanging"

---

[55] These figures are published in 1996 dollars per 1000 cubic feet, and have been converted into MWht, LHV using a conversion factor of 900 btu LHV / cu foot = 0.264 MWht / 1000 cu feet.

[56] The model uses **fixed gas prices** which are, in effect, levelized gas prices discounted at the same rate as the capital expenses (These could also be viewed as lower gas prices discounted at a lower rate, or gradually increasing gas prices discounted at a somewhat higher rate; the difference is academic because the gas prices are not explicitly levelized in the main analysis. This omission is justified by two realities: a) gas price projections are very flat in comparison with the base case 10% discount rate and b.) the uncertainty in prices is large enough to justify using a fixed price instead of a dynamic one. However, in chapter 5, a "fuel risk adjusted" case will be briefly presented in which the discount rate for the gas price is *much lower* than the capital discount rate, following the method of Awerbuch (1992). Use of the lower discount rate retains the same constant gas price through time, but raises the net present value (and levelized cost) considerably. See section **V.8.3** and the spreadsheet page "Fuel Risk" in the appendices for more detail on this case.

fruit for the cogeneration application, neglecting those sites in which a circulating fluid system is not already in place. However, the great range of possible installation costs under any assumption compels this study to confine itself to the most favorable sites. In any case, these sites should be the first to host an MPT system as such a system becomes economically viable; only as capital costs fall further will the MPT be considered for sites where additional capital outlay is associated with cogeneration.

The model outputs for the cogen version of the MPT include a figure (*AGS,* annual gas savings) for the gas which is replaced by turbine exhaust heat on an annual basis. This is multiplied by the current cost of fuel and deducted from the annual operating cost before the "post-cogen" LEC is calculated; the output tables in chapter 5 also include an LEC without cogen effects.

IV.5 Levelized Cost Calculation Method

The calculation of the levelized cost of energy followed here is a somewhat simplified version of a model which is fairly standard across the electric power industry. The capital costs of all the components are summed to yield the total capital cost (TCC). A real discount rate (RDR) is assumed, as is a project lifetime (PL). The capital charge rate (CCR), which represents the fraction of capital which is charged to the project in each calendar year, is then calculated from these latter two parameters as follows:

$$CCR = RDR / (1 - (1 + RDR)^{-PL})$$

The CCR represents loan payments (capital + interest) on the project cost, or more generally, the time-value of the money spent. Insurance is also added to the CCR (see below). Simplifications for the current model include a fixed discount rate and placement of the capital outlay at a single point in time, rather than spreading it out over the first few years of project life.

Multiplying the CCR by the TCC yields the annual capital cost (ACC). To this must be added annual operating expenses, including employment, scheduled and unscheduled maintenance, and most importantly, the cost of fuel.

The MPT base case scenario includes a 10% RDR and an additional 0.5% in insurance costs per annum. A lifetime of 20 years is used in both cases, yielding a CCR of 12.25%. The effect of CCR variance away from this base case value is examined in chapter 5.

IV.5.1 Operation & Maintenance

IV.5.1.1 Non-fuel Costs

It is common to separate the fuel from the other operating expenses and lump the remainder into a single figure calculated as fraction of the plant capital cost. This method recognizes that many of the operating costs will be specific to the location, while others will vary significantly from year to year. The following table summarizes these operating cost estimates for a variety of solar power projects:

Table IV-3: Non-Fuel O&M Cost Estimates as a Fraction of Capital Cost

Project	*Annual O&M*	*Context*	*Source*
PHOEBUS	1.3%	Study for a 30 MWe hot air plant in Jordan	Grasse (1991)
SEGS	1.0%	30-100 MWe trough-type plants in California	Klaiss *et al* (1990)
year 2000	1.5%	30 MWe hybrid plant	Kolb (1997)
year 2005	1.0%	100 MWe hybrid plant	Kolb (1997)
year 2010	1.2%	200 MWe solar-only plant	*ibid*
year 2020	1.0%	200 MWe solar-only plant	*ibid*

The data in table **IV-3** appear to show a weak economy of scale on O&M costs, but all of the estimates fall between 1.0% and 1.5%. Recognizing that all of the listed projects are

significantly larger than the MPT or ASDB systems, the O&M cost has been raised to 2.0% of the capital cost for both systems.[57]

IV.5.1.2 Fuel Costs

Fuel costs are found by multiplying the total fuel needs for a year's operation by the cost of fuel, which varies within the range developed in section **IV.4.1**, above. The spreadsheet model directly outputs the annual fuel needs as the variables *TAGR* (true annual gas required, for the MPT) and *ASDBTAGR* (for the ASDB). In the case of the MPT with cogeneration, the annual fuel needs are reported normally, and an operating cost is credited separately for the fuel which is "saved" by the cogeneration (see section **IV.4.2**, above, and chapter 5).

However, before *either* the annual fuel need *or* the annual electrical output is calculated, both must be multiplied by an annual availability to reflect system outages and maintenance periods.

IV.5.2 Availability and Annual Capacity Factor

In the modeling described in chapter 3, the systems are treated as if they were functioning at all times during the year; the capacity factor is 1.0. This reflects the approach with regard to solar position, ambient temperature, cogeneration loads, and so forth: no explicit periods are defined for which the system is "off-line". Such periods will certainly exist, although the highly reliable nature of the gas turbine technology employed will minimize them.[58]

---

[57] Establishing different O&M charge rates for the two systems (ASDB and MPT) would be misleading in view of present uncertainties; both systems incur a charge of 2% of their capital cost, per annum.

[58] Aeroderivative gas turbines, such as the Allison units modeled here, are among the most reliable of all prime movers.

An availability of 95% is generally considered to be an accurate expectation for modern gas turbines. This figure has been used as an annual capacity factor, but it is only applied to the model results in an aggregate sense, *after* they have been calculated for a full year. Thus, the amount of gas consumed is reduced by 5%, the amount of power produced is reduced by 5%, and the amount of gas "saved" through cogeneration is reduced by 5%. There is no effect upon solar fraction or solar efficiency.

The output tables in chapter 5 duly note that a 95% annual CF has been applied.

IV.5.3 Effect of Distributed Production

One of the major advantages to constructing a system at the 2-4 MWe scale is that costs associated with distribution of power from a central station can be avoided. These smaller systems can be placed at or near the sources of demand; if excess power is generated it must be redistributed on the grid (or "sold back" to the grid in the case of private ownership), but proper sizing will minimize this quantity.

There is no intention here to explore the details of the distributed power benefit, upon which a different value will be placed by different utilities in different regions. Rather, the goal has been to present the LEC of the systems so that utilities and other potential operators could evaluate their potential in light of their small size and deployment flexibility. In an effort to give some idea of how at least one utility might value this flexibility, a "distributed power bonus" of $750 per kWe of installed capacity has been subtracted from the capital cost and a new "distribution-adjusted LEC" has been calculated as separate step. This figure was derived from a study conducted by Arizona Public Service; the study actually estimates a benefit of "up to $1000/kWe" (Smith 1994); $750 was chosen as in an effort to establish a less extreme figure.[59] Chapter 5 presents

[59] The Pacific Energy Group (in Walnut Creek, CA) and NREL are in the process of developing a software tool called "Quickscreen" which will allow utilities to calculate the total benefits (both avoided costs and electric revenues) from distributed generation. The program then calculates a break-even purchase price for

both the actual LEC and this "distribution-adjusted LEC"; the latter may in some cases be more suitable when comparison is made with a central station power.

IV.5.4 Cost Summary

Table **IV-4** presents a complete summary of all the costs introduced in this chapter. After the annual capital cost (ACC) is determined, the non-fuel O&M costs (OMC) and the annual fuel costs (AFC) are added to it. (In the cogen scenario, the cogen fuel savings are deducted from the annual fuel costs at this point.) The resulting total annual cost (TAC) is divided by the total annual output, which is simply the gas turbine rating times the annual capacity factor times the number of hours in a year. All operations are carried out in watts (thermal or electric), and figures are adjusted to yield a final LEC in cents/kWh:

Annual Fuel Cost:	AFC = TAGR * FPRICE * 0.95
Annual Capital Cost:	ACC = CCR * TCC
Annual Maintenance Cost:	OMC = 2% * TCC
Total Annual Cost:	TAC = ACC + OMC + AFC
Levelized Energy Cost:	LEC = TAC / (*GTRATING* * 8760 * 0.95)

---

the utility. The beta release of Quickscreen comes with several built-in examples, including case studies for Arizona Public Service; the city of Austin, TX; Sacramento Municipal Utility District; Pacific Gas & Electric; etc., etc. Most of the quickscreen calculations are not relevant to this study, because they are intended to determine the "revenue-neutral" break-even cost of adding a distributed resource, not the relative tradeoff between the distributed resource and central generation. However, the first three user inputs in the program ask for the avoided substation, sub-transmission, and bulk-transmission costs, as determined for each project. The examples do not indicate the size of the distributed installation and are, in any case, very site-specific (e.g. the avoided substation cost, which is given in $ instead of $/kW, is a function of the particular station which that particular utility would have to build in a particular location if distributed generation is not used instead.)

The five or six examples in the program, while varying widely, do lend support to the figure of $750 / kWe which is used here. The sum of the three avoided costs mentioned covers an enormous range; from a high of $7,450 / kWe to a low of $15 / kWe, but most values are between $500 and $1,000 / kWe. Of course, these cases are, for the most part, selected to highlight the benefits of distributed production, and this benefit will not apply in all areas. For this reason (as indicated in the text), the distributed benefit is *not* included in any of the figures in chapter 5 (but does appear as a final line in the tables of complete results).

Table IV-4: Cost Summary for MPT and ASDB Systems

Item	*Unit*	*MPT Cost*	*ASDB Cost*
Tower	$	200,00	
Land	$	0	0
Reflectors	$ / m^2	50 - 200	50 - 200
TERC	$ / m^2	280% of Reflector Cost	
Receiver	$ / kWt	40 - 80	
Complete 3 MWe Cogen Engine	$ / kWe	1143	
Complete 4 MWe Cogen Engine	$ / kWe	897	
Complete 2-4 MWe Recuperated Engine	$ / kWe	700	
Receiver Ducting	$	50,000	
Receiver/Engine	$ / kWe		500 - 2000
O & M	$ / year	2% of Capital Cost	2% of Capital Cost
Fuel	$ / MWht LHV $ / mmBTU LHV	8.50 - 13.90 2.50 - 4.10	8.50 - 13.90 2.50 - 4.10
Distribution Bonus	$ / kWe	**$750**	**$750**
Annual CF		0.95	0.95
Capital Charge	% / year	12.25	12.25

CHAPTER 5: RESULTS

Note: Most tables and figures for this chapter are placed at the end to smooth the text.

V.1 General Approach to Results

The spreadsheet models created for the MPT (mini power tower) and the ASDB (Allied Signal dish Brayton) systems contain dozens of parameters. It was not practical (nor, in some cases, meaningful) to optimize the systems over all of these parameters. Instead, the modeling follows a two-step process: as a first step, both qualitative and quantitative arguments are made to establish a *base case* physical configuration. Once this format is established, a select group of physical (e.g. system size; receiver configuration), economic (e.g. cost of gas; cost of mirrors), and geographic conditions are varied and the effects recorded in charts and graphs.

In the case of the MPT, only a small number of the total possible parameters are addressed here. These include the choice of the gas turbine cycle, height of the tower, the spacing of the heliostats, the field rim angle, the use of a TERC and/or window, the temperature of the receiver, and a range of economic variables. An effort has been made to focus on the most influential variables but the resulting exclusions are necessarily somewhat arbitrary; some of these excluded parameters are the size and number of the heliostat facets, the reflectivity of the mirrors, the geometric form of the aperture (e.g. elliptical instead of circular), the reflectivity and transmittance of the window, the use of liquid fuels, steam bottoming cycles, and non-constant field conditions of any kind (such as variable spacing between rows, variable size facets, etc.). Of these exclusions (many of which could be addressed within the current computer model or through minor alterations) some are appropriate topics for further study (see section **V.11**) while others are insignificant.

By contrast, the ASDB system is much more clearly defined by the manufacturer's specifications, and thus parameter variance for the dishes is mostly limited to geographic location. Alternative turbine inlet temperatures are also briefly examined, in addition to economic variations similar to those applied to the MPT.

Beginning with section **V.3**, results will be presented in a series of graphs and tables. Each section will address a particular set of these figures. Although a sequential reading will develop the complete picture in the most methodical fashion, each section is intended to be clear enough on its own to allow for individual reading.

V.2 Choice of Locations

Four locations, all within the United States, were chosen as application sites for the STEPs. These locations determine not only the strength of the sun's beam and its position in the sky, but also the efficacy of cogeneration. All of the data for all four locations was collected from a single database maintained by NREL (1997); by choosing all locations within the United States the comparability of the data was ensured (as was rough equality of economic conditions). The NREL data includes figures for average daily solar flux, and average, high, and low temperatures for each month of the year as well as annual summary data on heating and cooling degree-days. The use of this data to construct a cogeneration capacity factor (*CCF*) and annual solar map (in conjunction with a latitude-driven geometric model) has been described in detail in chapter 3.

The four locations were Dagget, CA, Pueblo, CO, Tampa, FL, and Atlantic City, NJ. These four were chosen not to represent the entire nation but rather to cover an approximate "better half" for solar power applications. It is important to recall that both the MPT and the ASDB rely upon the *direct beam* portion of the solar flux; thus Tampa, which is further south than Pueblo but at a much lower altitude and with more cloudy

weather, produces significantly less solar input. The average daily direct-beam flux for all four locations is as follows:

Table V-1: Average Daily Solar Fluxes and Cogen Capacity Factors for Four Locations

Location (lat °N)	*Average Flux, kwh/m²/day*	*Heating Degree Days, Annual, 18.3 C base*	*Cooling Degree Days, Annual, 18.3 C base*	*Cogen Capacity Factor (chap.3)*
Atlantic City (40)	3.8	2872	459	0.62
Tampa (28)	4.5	403	1887	0.49
Pueblo (38)	6.1	3007	541	0.66
Dagget (35)	7.5	1106	1659	0.42

Source: NREL 1997 (Flux, HDD, CDD); "STEPS" Excel program (CCF)

Dagget is an outstanding place for solar applications and is the primary location in most of the results which follow: base case results are given for all four locations but parameter variance is restricted to Dagget for the sake of clarity. The reader will easily be able to extract the variance results to the other locations by comparing the base case performances.

Dagget-type conditions can only be expected over a fairly small part of the country: the southernmost portions of California and Arizona. However, the latitude of Dagget is still fairly high – 35° – and for international applications there should be many comparable sites (in, for example, North Africa). The other three locations are more representative of general U.S. conditions. Pueblo is fortunate because its elevation completely offsets its northern location; it is comparable to areas further to the south such as parts of Texas, Oklahoma, and New Mexico. The Tampa site, and especially the Atlantic City site, produce conditions which could be replicated over most of the country with the exception of very northern, cloudy areas.

The location has an effect not just upon the solar beam but upon the thermal characteristics, critical for the cogeneration application. The thermal system modeled here includes both heating and cooling, but is *sized* according to the cooling demand. After the maximum cooling load is determined (see chapter 3 for complete details), the combined capacity factor is found by summing the capacity factor for this maximum load over both

cooling *and* heating conditions (after adjustment for an efficiency differential between cooling and heating modes). Thus the cogen application will be favored in climates which offer either a great deal of heating (Pueblo) or a great deal of cooling (Dagget; Tampa) but will be less potent in more temperate areas (Atlantic City). The variations in combined capacity factor (*CCF*)are not enormous, but they are enough to affect the geographic comparison somewhat (see section **V.5.2**) – of course, these concerns are largely irrelevant for the ASDB and recuperated MPT.[60] The *CCF*'s for each location are constant across all models and are summarized above in **table V-1**.

V.3 Optimal Configurations

The optimization process is a prelude to the main results, which begin in section **V.4**. System optimization was conducted via a mixture of quantitative and qualitative thinking, and is by no means finely tuned. However, the systems, as modeled, are not expected to differ substantially from the "ideal" system which could be constructed by varying component composition, size, and positioning, within the constraints of overall scale and application mode (e.g. a 2MWe system with recuperation; a 4MWe system with cogen). The discussion in this section refers mainly to the MPT systems; the ASDB system is much more simple and is largely defined by Allied Signal receiver and engine specifications.

The spreadsheet model is constructed in such a way that a great many more field construction and operation parameters can be varied than are actually varied in the results presented here. Tables in the next few subsections summarize both variable and fixed parameters, and the complete spreadsheet appears in Appendix **C**.

[60] The ASDB and the MPT are somewhat sensitive to the ambient temperature – modeled as a constant year-round average – in that colder areas will exhibit better gas turbine efficiency. However, this effect is of lesser importance than differences in the solar flux. It should be noted that a cold, clear location (e.g. a desert, considered as a 24-hour thermal environment) will be the very best for hybrid gas turbine STEPs.

V.3.1 Base Case Values of Variable Parameters

The parameters which *are* allowed to vary were chosen either because of their large impact upon system performance (e.g. TERC vs. no TERC; receiver temperature) or upon system cost (e.g. mirror prices). Table **V-2** presents the "variable" parameters. A subset of these parameters, relating to MPT field layout, appear here but were actually loosely optimized and then fixed in a "first-round" of results; these parameters appear *both* in this table *and* in the one which follows in section **V.3.3**, listing "fixed" parameters. (It was necessary to standardize the field layout in order to present the remaining results intelligibly.) The establishment of the MPT field layout is discussed in the next section.

V.3.2 Establishing the Standard MPT Field Layout

Figures **V-1a,b,c,d** present the basic tradeoff inherent in heliostat field construction: the taller the tower becomes, the larger the field for a given rim angle. However, as the field grows, it occupies more land area, and the average distance between heliostat and tower increase, resulting in greater optical spread and the need for a larger, and less efficient, aperture (and/or TERC). This effect can be balanced by placing the heliostats closer together, but then the blocking and shading losses become a problem.

Figs. **V-1** present the total number of heliostats, size of the TERC, and blocking & shading efficiency as functions of both the tower height (*THEIGHT*) and the heliostat spacing (*XFOOT, YFOOT*). The figures are collected for a 2.3 MWe open-cycle plant at the Dagget location. This plant size does not and need not directly correspond to either of the base cases which make up the bulk of the results – 2 MWe recuperated and 4 MWe open cycle. However, the number of heliostats in this plant (ranging from 200 to 250 depending upon configuration) is close enough to the plant sizes eventually modeled (196 heliostats for 2MWe Recup; 326 for 4MWe cogen) to enable meaningful decisions about field construction strategy.

The construction rim angle (*CRA*) has been set at 45°, the maximum figure for which the available TERC data (i.e. Gordon & Ries 1993) can be interpreted with confidence, and also near the apparent point of diminishing returns for this type of secondary. The rim angle was left as a variable so as to enable a reduction in TERC dimensions (and increase in concentration) by reducing it; however, it quickly became apparent that the penalty in field shape (forcing a longer, narrower, and less efficient ellipse) would not be worth the TERC savings. This situation is a result of the low tower heights, which are necessary for other reasons (see below). With a much taller tower, a smaller rim angle might be practical; conversely, if a TERC is not used at all then a larger rim angle offers a slight advantage (a few of the model "variations" eliminate the TERC and increase the *CRA* to 55°; see section **V.5.3**).

The regions of tower height (60-80 meters) and heliostat spacing (12 to 20 meters) have been carefully chosen[61]. The tower heights appear to represent the maximum region within which excessive tower cost can be avoided;[62] this range is not entirely different from wind power analogues, and is also low enough to fit within the water pressure constraints for the cogeneration application (see chapter 3). By contrast, the heliostat spacing can be more readily optimized geometrically with our incurring serious cost

[61] The actual spacing values themselves are somewhat arbitrary; because a vast number of arrangements are possible, including many irregular and non-rectangular patterns not even addressed here, and it seemed undesirable to give the impression of precise optimization in this area. Furthermore, the optimal spacing pattern will be strongly influenced by local weather patterns (e.g. morning and evening cloudiness makes some of the blocking & shading irrelevant), need for field access, land availability, etc. Thus the five points chosen on the graph represent good coverage of the range from too tight (12 meters) to too loose (20 meters), but are not intended to be exhaustive. The first two points seek to examine one particular tradeoff between x (north-south) and y (east-west) spacing and do so successfully (the trade-off is essentially even in all respects), but both of these arrangements are too tight. The (16,14) spacing which is chosen is not intended to represent an absolute optimum under the current model, but further optimization would be *unrealistic* in view of the many other factors which must effect spacing. In particular, non-constant spacing should be considered in any further work with this model; see section **V.11**.

[62] As discussed in chapter 4, there is no explicit function for tower cost as a function of height; rather a single, somewhat conservative estimate has been made and held constant across all MPT systems (which also have a constant tower height of 70 meters; see end of this section). Without a cost constraint on tower height, the optimum value soars far beyond a realistic range (well over 100 meters) for such a small system, but the 70 meter figure eventually chosen seems like a much more realistic maximum.

constraints; the range in the figures has been chosen to span the region of optimum spacing. The following trends are evident from the graphs:

Figure V-1a: The total number of heliostats required is substantially lower with taller towers, but these savings diminish both as the towers rise and as the heliostats are spaced further apart. For the 80 meter tower, wider spacing eventually means *more* heliostats because the field becomes larger and less efficient, but for the 60 meter tower the wider spacing decreases the number of heliostats because the gain in blocking & shading efficiency outweighs the geometric effect of a field enlargement. Put another way, wider spacing is good up to a point, after which it hurts; moreover, the optimal spacing depends upon tower height because taller towers offer a higher angle to the receiver and thus can tolerate more tightly packed heliostat fields.

Figure V-1b: Blocking & shading efficiency (the fraction of light neither shaded not blocked) also increases dramatically with tower height and heliostat spacing, and again these returns diminish as height and spacing increase. This trend is of course necessary to produce the observed results with regard to heliostat numbers.

Figure V-1c: The TERC size exhibits the *opposite* trend: it increases with tower height and field spacing, thus limiting the trend towards higher towers and more widely spaced (and thus larger) heliostat fields. It is difficult to make a precise judgment, but it appears that the larger TERCs shown on the graph would begin to incur significant extra penalties for structural reinforcement and general practicality. (If this system did not have a TERC secondary, then the increase would be in the aperture size instead, and the associated costs would be re-radiation instead of the need for a larger structure). As detailed in section **IV.2.5**, The surface area of the TERC is charged at a rate equal to 280% of the rate for heliostats, based upon a comparison with the Israeli SCOT system (Kolb *et al* 1997); however, the mirror on the smaller SCOT system is 190 m^2 and the TERCs on figure **V-1c** run above 500 m^2 (for an 80 meter tower with widely spaced heliostats).

Choice of a 70 meter tower with (16,14) spacing: Diminishing returns, higher costs, and an unwieldy TERC all argue against the 80 meter tower, while an unacceptably large field and high blocking & shading losses disadvantage the 60 meter tower.[63] A 70 meter tower seems the optimum choice here. Examining the 70 meter data (particularly in figs **V-1a** and **V-1b**) for spacing efficiency reveals an apparent peak at the (16,14) mark – with heliostats 16 meters from their neighbors to the east and west and 14 meters from their neighbors to the north and south. (See note[61] for an essential discussion of the spacing data.) In order to facilitate comparison between different regions and turbine cycles without tedious re-optimization, and at the same time avoid introducing variable but unknown tower expenses, a standard tower height (70 m) and heliostat spacing (16 m, 14 m) was adopted for *all* MPT systems modeled here. The results which follow represent a *general guideline* of system performance and cost under different conditions, but it would be essential to complete a more detailed site-oriented optimization for each and every particular opportunity which might arise for the MPT.

Figure **V-1d** presents bird's-eye views of four different heliostat fields. Each is constructed with a 70 meter tower, (16,14) spacing, and a rim angle of 45 degrees (except for the "no TERC" case at the bottom, with a rim angle of 55 degrees) but the locations and power cycles vary as indicated.

[63] Nonetheless a 60 meter tower might be preferable, with a wider heliostat spacing, if the cost increment between 60 and 70 meters turned out to be substantial in an actual application. However, the arguments in favor of a higher tower become even stronger in weaker solar regimes (i.e. most locations other than Dagget) because total field size must be enlarged to reach the same power levels attained in the ideal regime. Thus a toss-up between between 60 and 70 meters at the Dagget location argues in favor of a 70 meter (or higher) standard elsewhere.

V.3.3 Fixed Parameters

In table **V-3**, the MPT field construction parameters discussed in sections **V.3.1** and **V.3.2** (including *CRA*, *THEIGHT, XFOOT, YFOOT*) are listed along with the rest of the fixed parameters. None of the parameters in the table are allowed to change in any of the models which follow. The sole exception to this is *CRA*, which is increased from 45° to 55° for those MPT runs which do not employ a TERC. The table lists explanations for the other fixed variables, some of which are worthy of further investigation in future studies.

V.4 Overview: Complete Result Tables

Once values are selected for the variable input parameters, the spreadsheet model, ("STEPS.xls") is "run" through a year of solar data for a given location. (See section **III.1.1** for description of how the solar data is compiled for these runs). The spreadsheet tracks various output parameters, including annual totals and averages, and collects all of the significant figures into a single column on a separate results page. In figures **V-2(a-e)** a series of columns have been arranged side-by-side to allow direct comparison of different model runs.

V.4.1 Complete MPT Results

There are 3 pages of complete MPT results; each page contains six unique model runs. On the first page, figure **V-2a**, we see "base" cases of both the recuperated and cogeneration application at various system scales, as well as gas-only cases, but all of the results are for the Dagget location. Based on these results, the 4MWe cogen and 2MWe recup were chosen for experimentation in other locations and with component changes. The second page, figure **V-2b**, shows these two configurations in the other three locations (the gas-only case is omitted in other locations because the results will be virtually

identical to those at Dagget). The final page, figure **V-2c**, returns to Dagget but explores some *component* variations.

It is important to understand the "base case" economic assumptions maintained for all of these runs, as distinct from the "component variations" which are introduced in the third figure. **All of the runs have identical economic conditions**; the only differences are in the physical variables (such as field size, number of heliostats, etc) which must be adjusted for each application in order to equalize the power output across all of the cases running on the same cycle (i.e. recup or cogen). The leveling was done to facilitate comparison, but does of course result in larger fields in, e.g., Atlantic City and smaller fields in, e.g., Dagget. Thus, differences in the *output* results (especially levelized cost of energy, LEC) are *solely* the result of differences in location and power cycle and do *not* reflect any economic effects as a function of scale. The major exception to this is the comparison on the first page between the 3MWe and 4MWe cogeneration cases; here, the scale *is* different and the turbine price (per unit energy) is in fact lower for the 4MWe engine (see section **III.2.6.1**). However, for all of the later runs, the less competitive 3MWe plant was eliminated and only the 4MWe cogen (and 2MWe recup) are studied from this point on.

The format of figures **V-2** would be too cumbersome for the more detailed economic comparison which follows in sections **V.6** and **V.7**. System efficiency as a function of scale, location, and component configuration is explored with stiarstep diagrams in section **V.5**.

V.4.2 Complete ASDB Results

The ASDB system is at a further stage of development and is more well-defined than the MPT. Furthermore, the cluster of individual dishes which are combined to simulate an MPT-size plant is completely insensitive to scale as modeled here; a 1MWe dish field and

a 4MWe dish field will have exactly the same LEC (provided they are in the same location, of course). Thus the dish results are less extensive than the MPT results.

Figures **V-2d** and **V-2e** present the dish results; the first page explores the effects of geography, while the second presents several component variations at the Dagget location, in a fashion analogous to section **V.2.1** above. Unlike the MPT, the ASDB results *do* contain one instance of economic variation: cases DD4ce and DD4ee, which explore the effect of changing the engine/receiver unit's price from $1,000 (base case) to $500 (DD4ce) or $2,000 (DD4ee). This change does not effect any of the performance results, of course, but its effect is clearly visible on the bottom lines (LEC calculations). Creating these cases was necessary in order to introduce this important area of uncertainty, which is unique to the ASDB system: in the case of the MPT, the engine dominates the power conversion system cost but is derived from well-known commercial products. The economic variations which are explored in sections **V.6** and **V.7** below do not place ASDB engine cost on the axis of any graph; rather these three cases (base case $1,000; DD4ce $500; DD4ee $2,000) are each plotted as a separate line (where relevant) when other parameters (such as mirror cost) are varied. See later sections for further clarification of this approach.

V.5 Efficiency: Stairstep Diagrams

The "stairstep" diagram is a valuable tool for quickly understanding the performance of solar power systems, and the differences between alternative configurations. The figures presented here each contain two series of bars; each bar represents an efficiency between 0 and 100%. The bars in the darker row indicate the net *annual* energy transmission efficiency of each component in the system; the lighter bars track the cumulative effect of these components. The very last bar represents the net *annual* solar-to-electric efficiency of the system.

Note that the stairsteps only represent the performance of the systems in *hybrid* mode; i.e. when the sun is shining. All of these system are in fact *dominated* by their gas-only modes (inspect the solar fractions on the tables in section **V.4** or, for a clearer view, see figs **V-4b,c,d** in the next section), in which the solar components are irrelevant and the gas turbine efficiency will be a couple of points higher (in the case of the MPT; compare *GASEFF* to *GTEFF* on the tables in section **V.4**). Nonetheless, as *solar* systems, it is the hybrid-mode efficiency of the systems which is important; to be economically viable, these systems must produce thermal energy from sunlight at a price comparable, per thermal unit, to the price of natural gas.

Finally, note that the electric generator efficiency is fixed for all cases and therefore included in the gas turbine efficiency (and indeed, in the variables *GTEFF* and *GASEFF*).

V.5.1 MPT Efficiency: Effects of System Scale and Cycle

Figure **V-3a** contains four stairsteps, all of them from Dagget. On top are 3 MWe systems, first cogen and then recuperation. These 3MWe systems were both abandoned in favor of either a larger (in the case of cogen) or smaller (in the case of recup) version: the adjusted systems appear below and their higher net efficiency is immediately apparent. The reasons differ in each case: for the cogen system, the 4MWe size allows a substantially more efficient and less expensive (per unit power) engine, while in the recuperated case, the engine is identical and instead the weaker effect of a smaller (and more efficient, for the 70 meter tower) heliostat field dominates. Note the large difference in blocking & shading efficiency for the recuperated cases; this is not as prominent on the cogen side because the difference in field size is not as dramatic, and because the recuperated fields are generally larger than the cogen fields for a given field size (due to higher SF as a result of lower TIT).

The recuperated cases appear to have a substantial efficiency advantage over the cogen cases, largely because of their higher turbine efficiencies. It is crucial to remember that the net LEC of the cogen systems is very favorably impacted by the gas savings from turbine exhaust heat recovery, and that this **heat recovery is not represented in the stairstep diagrams**.

V.5.2 MPT Efficiency: Effects of Location

Figure V-3b contains six stairsteps in three pairs of two, each pair representing one of the remaining three locations arranged in descending order of solar resource (Pueblo, Tampa, Atlantic City). The efficiency tends to decline with solar resource because the fields become less efficient as they grow in size (again, examine the blocking & shading figures). In the cases of Tampa and Dagget, significant efficiency losses are also evident in the gas turbines, where the higher annual ambient temperature is taking its toll.

Surprisingly, the most efficient location, at least for the recuperated cycle, is *not* Dagget, but Pueblo. An excellent solar resource (about 80% of Dagget's; see table **V-1**) combines with very low ambient temperatures to produce a net annual solar-to-electric efficiency of 22.4%, just edging out Dagget's 22.2%. In the cogen case, the situation is flipped, and Dagget's 16.8% just tops Pueblo's 16.4%. (Again, note that these figures are not adjusted for heat recovery savings; they use open-cycle turbine efficiencies).

Higher efficiency does *not* necessarily translate into lower LEC. The better solar resource at Dagget will ensure that the recuperated MPT is cheaper there than in Pueblo, despite the nearly identical efficiencies. However, in the cogen case, the excellent thermal environment at Pueblo (extreme temperatures year-round) means a higher cogen CF and, as it happens, the lowest LEC of any MPT system modeled here, including those at Dagget (see section **V.6**).

V.5.3 MPT Efficiency: Effects of Component Variation

Figure V-3c contains stairstep diagrams for four component variations on the 2MWe recuperated system at Dagget. In the first two of these, the TERC is removed and two much larger apertures are placed on the receiver: 5 meters and 7 meters in diameter. In the third case, the window is removed (with the TERC restored), while in the final case, both the window and the TERC are removed (with a 5 meter aperture).

It seems apparent (see chapter 3) that both the TERC and the window are important and achievable elements in the MPT design, so their removal, which introduces a number of new optimization problems, is not the focus of extensive investigation here. It is evident from the top half of figure **V-3c** that, as long as a window is left in place, then creating quite a large aperture (7 meters) will allow efficiency to climb back near the levels achieved with the TERC (20% instead of 22.2%). This performance is possible because the window blocks most of the re-radiation, and has in addition very low external reflectance. These properties are much more realistic for the TERC-assisted system (aperture diameter 1.76 meters) than for the non-TERC system (aperture diameter 5-7 meters, possibly composed of multiple receivers). There seems little doubt that the TERC's fabrication and installation cost would be worth the extra two points in efficiency when combined with the unknown savings in window design and construction.

On the other hand, removal of the window (see "2 MWe recup no window") while preserving the TERC has far less drastic consequences. The aperture remains the same, and the annual re-radiation losses only rise from 1% to 2.6%. These radiation losses are so small relative to most other solar power systems for one reason only: the TERC allows a *much* smaller aperture than standard central receivers. This case contains an important revelation: if it is significantly cheaper and/or easier to design a receiver *without* a window, then that course of action should be considered in a system which includes a TERC. It is not entirely clear, however, that it is indeed easier to design a windowless receiver: the window allows volumetric absorption into pressurized air, which must

otherwise be contained behind a solid, heat-transferring wall – see the discussions on receivers in sections **I.1.4.3** and **III.2.4**.

In the final case from figure **V-3c**, both the TERC *and* the window are removed, and radiation losses leap to 17.3% with a 5 meter aperture (losses would be unacceptable with a 7 meter aperture). Overall efficiency drops to 14.4%, a figure not unthinkable for many conventional power tower designs but considerably below those acceptable for the MPT.

The message from figure **V-3c** is clear: **the MPT must have either a TERC or a windowed receiver (but not necessarily both) to maintain its advantages**.

V.5.4 ASDB Efficiency

Figure V-3d presents stairsteps for the ASDB systems. It is immediately apparent that the solar-to-electric efficiency of the dish systems is on a level with the MPT. Dish performance is impacted by location through two mechanisms, which off-set in some cases: re-radiation is higher (as a fraction of input) in weaker solar regimes[64], and turbine performance is again stronger in cooler climates. Pueblo, *not* Dagget, provides the most efficient setting, but (as with the MPT) Dagget will boast a somewhat lower LEC because of the stronger solar resource.

Component-by-component comparison reveals an important result: the **geometric efficiency** of the dishes (94.3 %) is only slightly higher than the geometric efficiency of the MPT fields (90-92%). In the case of the dishes, this figure refers to the difference in dish aperture (presented to the sun) and actual dish surface area (larger because the dish is curved and thus the drum-type facets are tilted with respect to the sun; both calculations

[64] This effect (higher radiation losses in weaker regimes, because of the larger ratio between re-radiation, which is not a function of the solar regime, and total radiation, which is) becomes more visible in the ASDB than in the MPT because the very small aperture and insulating window of the latter system strongly dampen re-radiation, making variation in it nearly undetectable.

concern only the mirror facets). In the case of the MPT, the geometric efficiency represents cosine losses incurred in the same fashion: the mirrors are always somewhat tilted with regard to the sun because they must reflect its image to a third point, the receiver (of course, the calculations for the MPT are vastly more complex than those for the ASDB, because the sun position is constantly moving in the system's frame of reference; see chapter 3). When this project was initiated, it was assumed that the geometric efficiency of a heliostat field would be greatly, rather than marginally, inferior to that of a dish. However, the MPT has several unique design characteristics which have reduced geometric losses (some of these reductions come at the price of increased blocking & shading, so the two must really be considered together when comparing final results with a dish system). These design characteristics include: an oval field located to the north of the tower in latitudes high enough that the sun always stays on the south side of the tower; a relatively compact field; and a constant rim angle around the edge of the field (which produces the oval shape, a projection of a circular acceptance cone onto an inclined plane).

The blocking & shading and aperture efficiency of the dish are set to 100%. Ideally, the SAIC type of dish does not have any shading because the mirror facets can be placed so that none overlap the region at the back of the dish where sunlight is blocked by the receiver/engine unit. As for the aperture, the dish is a compact and symmetrical system in which there is little advantage to cutting off any portion of the main body of the solar flux[65]. Of course, in both cases the efficiencies will not literally reach 100%, but the figure is used here to convey the idea that losses from these sources will be insignificant. Re-radiation is a much more significant area of loss for the dishes, and in this case the aperture of the ASDB has been generously sized (a conservative choice) resulting in re-radiation losses of 10-15% in comparison with 1-3% for the MPT. See section **III.3** for more details on the ASDB model.

[65] It makes sense in a dish to cut off the "corona" around the sun, and in doing so the sun's edge will inevitably be nicked as well. Thus 100% aperture acceptance will be technically impossible, but real systems can closely approach this figure. Moreover, a generous aperture diameter allows some of the exaggerations in aperture efficiency to be counteracted by re-radiation losses.

V.6 Capital Cost: Relative Contributions of Components

Figure **V-4a** illustrates the (installed) capital costs, broken down into the major physical components, for the base case MPT systems. It is immediately evident from the figure that the gas turbine power plant (which included the generator) represents the dominant capital cost in all systems (61% for the Dagget 4 MWe cogen plant; 49% for the 2MWe recuperated plant in the same location). The heliostat field contributes the bulk of the remaining cost (24% for the 4MWe cogen plant; 29% for the 2MWe recuperated plant).

The large fraction of capital consumed by the gas turbine has very little impact upon the accuracy of comparisons between the MPT and gas-only plants, because both share the same turbine. Moreover, the turbine (at least for the cogen MPT) is established, commercially-available technology which is not expected to diminish in price as quickly as some of the solar components (particularly the heliostats). Thus, when calculating the diminishing costs of the MPT over time (see section **V.8**), or when testing the sensitivity to economic conditions (see section **V.7**), the analysis can be focused upon the solar components with the understanding that the turbine costs, while large, are relatively invariant; moreover, whatever variance *does* occur in turbine costs will affect both solar *and* gas-only systems.

The degree of commercial readiness is not the same for all components. While the turbine and tower are priced at today's costs, the mirrors (heliostats and TERC) and solar receiver are priced at a level which assumes some prior production experience. The MPT "base case", which is priced in fig **V-4a,** represents neither a "first" plant nor a "break-even" plant, but rather a plant somewhere along the way. In section **V-8**, costs for a first plant (at today's prices) are estimated, and a hypothetical experience curve is used to find the total cost of "buying down" the component costs until the first break-even plant is reached (a plant which is commercially competitive with a gas-only plant).

V.7 Levelized Cost

V.7.1 Variation of LEC with Configuration and Location

Figure **V-4b** presents LEC and SF (solar fraction) for all of the model runs under the base case economic conditions (these conditions are specified at the top of the figure). Figures **V-4c** and **V-4d**, which follow, present selected cases for enlarged and direct comparison, but do *not* add any new information. In fact, all of the information in these three figures can be found on the tabular complete results figures from section **V.4**.

The levelized energy cost is an annual figure, covering both gas-only and hybrid periods of operation, and is taken after cogeneration savings (if any) are accounted for but before the bonus for distributed production; in other words, these are the actual costs which would be incurred for these systems, in these locations, under these economic conditions.

The following general remarks are worth reviewing. Bear in mind that the gas-only cases and all component variations were only conducted at Dagget to keep the results manageable; the remaining figures in this series facilitate comparison of the Dagget-only variations (fig **V-4d**), as distinct from geographic effects on the base case model (fig **V-4c**).

- Although it appears (see bottom of fig **V-4b**) that the cheapest systems are solar (and not the two gas-only Dagget cases) this is *not* an entirely accurate inference. The cheapest system of all is an ASDB located in Dagget, with a receiver/engine capital cost of $500 / kwt instead of the baseline figure of $1,000 used by all the other systems. (Note that the most expensive system, by far, is an ASDB system with a $2,000 / kWt unit). This system represents technologically-driven cost reductions which cannot be expected in the immediate future. The second cheapest system, the Pueblo 4 MWe cogen plant, is benefiting from a superb cogeneration environment in

Pueblo; if a gas-only cogen plant were constructed there it would also benefit from this environment, and its LEC would be lower than the solar plant by about the same margin as the gas-only LEC at Dagget is lower than its solar analog (some .21 cents / kwh, for a gas-only cogen LEC at Pueblo of about 3.61). *However*, the cogen environment will not effect the recuperated plants, and the Pueblo cogen solar plant will *remain cheaper* than a Pueblo recuperated gas-only plant. This is, unfortunately, comparing apples and oranges: the real point is that cogen is clearly superior in Pueblo to recuperation, regardless of energy source.

- Of the four locations, recuperation is only superior (in LEC terms) in Dagget. Despite good cycle efficiency, **recuperation suffers because of its much (50%) higher solar fraction** – in an economic regime with cheaper solar components (or with incentives for solar fraction), recuperation becomes more competitive with cogeneration, as illustrated in section **V.7.2** below.

- **Overall, the recuperation and cogeneration applications are surprisingly similar in LEC,** revealing that factors other than turbine cycle (e.g. site availability, development of technology, solar fraction) are more likely be decisive.

- In light of the caveats in the first paragraph of this list, it is evident that gas-only plants (in these small-scale, distributed power applications) are marginally cheaper than their solar-assisted counterparts, even under fairly optimistic economic conditions for solar. The LEC differences are as follows for the Dagget location: cogen system, gas 5% cheaper; recup system, gas 7% cheaper. **These gas-only margins are small, and as developed in section V.8 below, they disappear if mirror prices drop somewhat more than expected, or if gas prices rise.**

V.7.1.1 LEC for Basic Systems

Figure **V-4c** focuses on the basic systems ("principal model runs"), discarding the component variations and gas-only cases in order to highlight the differences between cogen, recup, and dish systems, and how those differences are affected by location.

As we have already seen, the cogen application in Pueblo is the most economical system by a clear margin – some 7.5% cheaper than the recuperated plant in Dagget (the latter has almost twice the solar fraction, 30% vs. 17%).

- In every location, the dish system is more expensive (by 0.2 to 0.4 cents/kwh) than *either* of the MPT systems. It must be recognized, however, that the dish price is very strongly dependent on the capital cost of the receiver/engine unit, and as other figures in this chapter show, these relationships can be easily inverted by the uncertainty range of that cost. Moreover, the dish has deployment advantages (modularity; independence; indifference to variable terrain) which cannot be disregarded. **Only in the best cogen locations, such as Pueblo, can these results be interpreted as a demonstration of economic superiority for the MPT when compared to the dish / Brayton system.**

- The differences between locations are not as grave as one might have predicted based upon inequities in the solar resource (this damping effect is largely because of the hybrid nature of these plants). For example, the Atlantic City cogen plant is actually cheaper than some of the alternative configurations in Tampa (cogen, recup, dish), Pueblo (dish), and even Dagget (dish). Comparison across the same type of system reveals that the total cost increases from the best to worst location are 11% for the dish, 12% for the recuperated MPT, and 17% for the cogen MPT. These modest spreads, while not detracting from the image of the southwest as prime solar territory, **argue strongly in favor of including most of the rest of the country for possible consideration as well.**

V.7.1.2 LEC for Systems with Component Variations

Figure **V-4d** includes only systems located in Dagget in order to highlight the effects of component variations. The sharp variance of the ASDB LEC with receiver/engine unit cost has already been noted. Other observations from this figure include:

- **Changes in receiver or turbine inlet temperatures of 50 or 100 C can have small but noticeable effects upon solar fraction and LEC.** In particular, reducing the receiver temperature (from a baseline of 800 C) by 50 degrees in the cogen MPT cuts the solar fraction from 19% to 16% and the LEC from 4.18 to 4.15. Raising this temperature by 50 degrees increases solar fraction to 21% and LEC to 4.21. In the dish case, a 117 C reduction in TIT has very little effect upon solar fraction but raises the LEC from 4.37 to 4.81 as a result of decreased turbine efficiency. By contrast, an 83 C rise in TIT reduces the dish system's LEC to 4.18; this gain is hypothetical, however, because it is not clear what cost penalties (in the form of new material requirements; e.g. ceramics) might be incurred by this higher TIT.

- As might be expected from the impact on system efficiency (see section **V.5.3**), removal of either the TERC or the window from the MPT system increases LEC marginally, from 4.15 (for the base case 2MWe recup system) to 4.16 (no TERC & 7 m aperture, and no window & 5 m aperture) or to 4.22 (no TERC; 5 meter aperture). **However, the loss of these components isn't strongly felt until *both* are missing,** when LEC jumps to 4.39 (no TERC & no window & 5 m aperture).

- As expected, the 3MWe cogen plant cannot compete with the 4MWe plant, solely because the former has a significantly more expensive engine. This point of this demarcation may be an artifact of the choice of engines used for the MPT model, but it seems evident that some such demarcation will exist *somewhere*: as system scale diminishes, **a point will be reached where gas turbine cost moves sharply**

upward, or efficiency moves sharply downward, or both. See sections **III.2.6.1** and **IV.2.6.1** for additional clarification.

V.7.2 Variance of LEC with Fuel Price, Mirror Price, Capital Charge Rate

Three economic parameters seem paramount in determining the competitiveness of current and future hybrid solar plants: mirror cost, gas cost, and capital charge rate (cost of capital). Graphs were prepared to explore the variance in LEC with each of these economic parameters. For clarity, the graphs are limited to seven base case systems at Dagget: three ASDB systems (varying only in engine cost: $500, $1,000, or $2,000), two gas-only systems (cogen and recup) and two MPT systems (cogen and recup). Variance at other locations can be inferred from these graphs; moreover, to the extent that such graphs can be used to find the "point of first competition" for solar plants, it is appropriate to focus on a high-resource location such as Dagget. (Please refer to section **V.8** for an explicit treatment of "break-even conditions" for STEPs)

Each graph presents the variance of a single economic variable; the other two (and all additional parameters) must be held constant. This is made clear on the figures. (Section **V.8** presents a graph upon which *both* gas price *and* mirror price are variant.)

V.7.2.1 LEC and Fuel Price

Figure **V-5a** plots the LEC of seven systems against gas price. The dark, dashed lines representing the ASDB systems make clear once again how critical the impact of receiver/engine price is on the relative placement of the ASDB with regard to the MPT.

- **It is evident from the figure that gas price *per se* has almost no effect upon the relative placement of the recuperated and cogen cases**, despite the dramatic difference in solar fraction (cogen 19%, recup 30%). Remarkably, the gas displaced in

the cogen system by exhaust heat matches almost exactly the gas displaced in the recuperated system by increased solar fraction, with the result that both systems require essentially the same net amount of gas per kwh. Equal gas requirements, together with (approximately) equal LEC means equal sensitivity to gas cost, and neither gains an advantage as gas price fluctuates.[66]

- **As gas prices reach the upper end of their expected range over the next 20 years or so** (see section **IV.4.1**), **both MPT systems become competitive at a mirror price of $100 / m^2**. This is evident from the convergence of all four cases near the right edge of figure **V-5a**.

V.7.2.2 LEC and Mirror Price

Figure **V-5b** is similar to **V-5a** except that gas price is now constant (at $10 / MWht) and mirror price is the variable. Again, the placement of the ASDB systems is solely dependent upon the capital cost of the key component.

- While the cogen system is superior at today's mirror prices, **it is evident that as mirror prices fall, the recuperated system gains the advantage, and most importantly, this crossover occurs *before* parity with gas-only systems is reached**. As mirror price falls, the slight efficiency advantage of the recuperated system prevails despite its larger solar fraction, which becomes less and less of a handicap. All of the above notwithstanding, **one should avoid reading too much into the relative positions of the cogen and recuperated MPT**; the systems are very close, well within the limits of error and uncertainty of this study.

---

[66] In section **V.8**, when mirror cost is also varied, LEC is no longer equal between the two systems, and thus different gas sensitivities develop even though the requirements are the same, because the gas cost makes up a different fraction of the whole in each system. These observations, while interesting, are not key results in either section.

- **As mirror prices reach the lower end of their expected range** (for the foreseeable future), **both MPT systems become competitive** at a gas price of $10 / MWht ($2.94 / mmBTU). As before, the systems converge at the edge of the graph.

V.7.2.3 LEC and Capital Charge Rate

- **Figure V-5c** completes the trio, and contains a single intriguing observation: **if the cost of capital were to fall below 7%, then the MPT systems would be competitive** with gas at the base case assumptions ($100/m^2 mirrors and $10/MWht gas). This dramatic realization is a result of the capital intensity of solar power projects and requires two caveats: first, the base case assumptions for mirror cost have not yet been reached by the industry; second, the cost of capital as modeled here must include all managerial overhead and project start-up costs (but *not* O&M).

V.7.3 Implied Solar LEC for the MPT

It is possible to combine the LEC for the hybrid MPT's with their corresponding solar fractions and compare with the results from the gas-only plants to derive a "solar LEC". This calculation (see table **V-4**) attempts to represent the levelized cost for that portion of the systems output which derives from sunlight, as opposed to the cost for that portion which derives from natural gas. It must be stressed, however, that from the outset the overall design of the system has relied upon synergy between the gas and solar energy sources, and therefore the solar LEC *could not be achieved in the absence of gas.* In other words, the solar LEC cannot be taken to represent the cost of energy from a solar-only MPT because, at present, no such design exists. However, they can be used to compare with *other* solar-only energy sources, such as photovoltaics. Such comparisons will readily demonstrate that the MPT would provide some of the cheapest solar energy available anywhere.

Table V-4: Implied Solar LEC for the MPT at Dagget, CA:

Plant	*Solar Fraction*	*LEC, c/kWh*	*Gas-Only LEC*	*Implied Solar LEC*
4 MWe Cogen	19%	4.59	4.23	**6.12**
2 MWe Recup	30%	4.56	4.07	**5.70**

V.8 MPT Break-Even Conditions and Buy Down Cost

V.8.1 Relation between Gas and Mirror Prices

Figure V-6a summarizes much of the foregoing discussion, and identifies goals for current heliostat R&D. The graph should be thoughtfully considered because it represents a departure from the graphs in section **V.7**. Mirror price is on the horizontal axis with gas price on the vertical axis. Any point along the slanting lines, each representing one of the two MPT systems, defines a mirror price and a gas price which, *together*, create conditions of economic parity ("break-even") between a gas-only system and the MPT. Thus as mirror prices fall, the MPT can tolerate lower and lower gas prices and remain competitive; as mirror prices rise, the MPT requires higher and higher gas prices to compete.

The MPT lines do not run below $\$50/m^2$ nor above $\$200/m^2$, because these appear to be reasonable limits upon mirror cost in the foreseeable future. The heavy horizontal lines on the graph represent the minimum and maximum gas prices in the model, but the MPT lines *are* allowed to cross these because the range of gas prices in the model is much narrower than the range of mirror prices, and it was felt that the top portion of the graph contributed to its clarity. The ASDB systems are omitted here because a direct gas-only analogy does not exist for them and it is more accurate to think only of the MPT. The gas-only systems are also omitted, because their inclusion would be illogical.

Focusing on the area between the minimum and maximum gas price lines, which can be considered as the "zone of reasonable expectation", we see that things will begin to get interesting for the MPT as heliostat prices fall past $100. At this point, a high gas price will be required for economic parity, but this requirement rapidly diminishes as heliostat prices fall towards $50. At today's gas prices (about $11/MWht), **heliostat costs need to reach about $60/m^2;** a price point representing between 1/4 and 1/3 of today's heliostat costs. However, **improvements in gas turbine cost or efficiency would make an enormous impact here as well;** for the 4 MWe cogen plant in Dagget, **the gas turbine represents over 60% of the capital cost,** while the mirrors make up 24%.

V.8.2 Cost of Buying Down the MPT

The reduction of per-unit production costs as a function of cumulative manufacturing experience is a well-studied phenomenon. The resulting "experience curves" are typically characterized by a "progress ratio" (PR) which expresses the manufacturing cost as a percentage of what it was when only ½ as many total units had been produced. Thus, an 85% PR means that for every doubling in cumulative production, the price will be reduced by 15%.

A progress ratio approach has been used in this section to estimate the *total* cost of bringing the MPT far enough down the experience curve that it competes with natural gas plants *of the same size* on a basis of economic parity. As previously noted, the "base case" MPT costs presented here do not correspond to a "first" plant, nor do they correspond to a "break-even" plant, in which price parity with gas-only plants has already been reached. In order to calculate the total cost of bringing the MPT down the experience curve, through the point which represents the base case of this study, and onward to the break-even point, a number of assumptions and simplifications must be made:

- The gas turbine and tower costs in the base case are used in all plants, because these costs represent commercially available components. The cost of these components is not expected to be significantly impacted by the MPT, at least in the near term.

- The receiver cost in the base case is used in all plants, because to much uncertainty surrounds this component to allow the construction of a meaningful experience curve. Fortunately, the receiver represents a small portion of the total capital cost (under 10%; see figure **V-4a**).

- Only the mirror cost (affecting the heliostat field and the TERC) is placed on the experience curve. The selection of mirror cost accesses the most promising area for technological improvement, as well as the largest component of the incremental cost of adding solar capability to a gas turbine plant. Restricting progress down the curve to this component alone is conservative, but in many ways makes a stronger and clearer statement about the priorities for R&D in this area. Regardless, no other components lend themselves to accurate modeling at the present time.

- A progress ratio of 85% is used for mirror costs, and this ratio is applied based upon the number of MPT plants which have been built, beginning with the *third* such plant. This configuration represents a compromise between several other options, including a.) basing the curve upon the total number of heliostats ever built (perhaps 3-4 thousand), which ignores the change in technology and scale which is required for the MPT drum-type modules, or b.) basing the curve upon the number of MPT plants beginning with the first plant, which would overestimate the effect of the first few plants on production costs. The choice of 85% is necessarily somewhat arbitrary but appears modest when compared to the progress ratio of the photovoltaic industry, which is around 80%.

- Additional R&D and overhead costs are charged to the first two plants. The first plant incurs a 100% charge; i.e. the capital cost of the plant is doubled. The second plant incurs a 50% charge. These charges loosely reflect industry experience and expectations (e.g. Kolb 1997).

- The analysis is limited to the 4 MWe Dagget Cogen plant, for simplicity.

Figure **V-6b** presents results for the application described above; additional assumptions and parameters are detailed on the figure.[67] Although not shown on the figure, it is of interest to note that the *incremental* capital cost (i.e. that portion of the total cost which is due to the addition of solar power) of the first plant is between $7.5 and $8.0 million for all of the cases. This figure represents the added cost of the solar components ($2.5 - $3 million) as well as the R&D charge introduced above. The comparable gas-only plant is assumed to incur no R&D charges; thus its capital cost is invariant over the whole length of the experience curve and is equal to $3.5 million.

Experience curves are very powerful, but their use involves a high degree of uncertainty. Nonetheless, the figure demonstrates that *either* a carbon tax of $50 / ton *or* arrangement of 8% financing (real discount rate; includes inflationary effects) could bring the total buy-down cost of the MPT to less than $60 million. (Including the true price risk of natural gas, as calculated by some analysts, could do even more for the MPT. See the next section for a discussion of the "Fuel Risk Adjusted" case on figure **V-6b**.) In the process, some 100 to 150 plants would be built, supplying 400 - 600 MWe of distributed electric power, 20% of it produced from sunlight. This calculation *does not assume any favorable movement of natural gas prices.* When this $60 million is compared with the estimated $400 billion which the United States spends on energy each year (or with the annual sum which the world invests in new energy projects, also about $400 billion), it seems a small price to pay. Even without a carbon tax or special financing, the buy-down

[67] Note that the "medium" gas price here is $11/MWht, while the base case price is $10/MWht. The base case is designed to be more conservative than the buy-down graph (fig **V-6b**).

cost of the MPT could be in the range of $127 million, still only *three one-hundredths of one percent* of the larger picture.

Bringing small renewable technologies such as the MPT to the break-even point is cheap.[68] This result should not come as a surprise, for several reasons. Most significantly, movement down the experience curves depends upon amassing a larger number of *units*, and small-scale plants naturally produce a faster growth in total number of units than do larger plants. In effect, with a small-scale technology, one learns by doing, because the up-front costs are not so overwhelming that the first plant cannot be built while the technology is still maturing. Furthermore, as pointed our by R Williams at PU/CEES[69], small renewable plants are designed from the outset to be safe and clean, so the large sums and regulatory sags which other projects incur because of concerns about safety (e.g. nuclear) or emissions clean-up (e.g. coal) can be avoided entirely.

V.8.3 Adjusting the Economics of the MPT for Fuel Price Risk

This section briefly explores the implications for the MPT of some of the work on fuel price risk carried out by Shimon Awerbuch and others (e.g. Felder 1996; Wenger *et al* 1997). The thrust of Awerbuch's argument (Awerbuch 1992; Awerbuch *et al* 1996) is as follows: The standard practice of discounting future fuel purchases at the same rate as capital outlays considerably underestimates the real cost of these fuel purchases if risk is taken into account. In particular, the price of natural gas is "counter-cyclical":[70] it tends to move in a direction opposite to that taken by capital markets and by the economy in general. This means that the owners of gas plants are exposed to double jeopardy: in

[68] It should be noted again that the break-even point, in this context, refers to price parity with gas-only plants *of the same size*. Such plants are not uncommon, and many more are expected to be built in the years ahead. Another way to look at this is as follows: if we assume a location in which the benefits of distributed production are sufficient to establish price parity between small gas-only plants and large central station plants which would otherwise have to be built, then the buy down costs presented here, if expended, would allow the replacement of these small gas-only plants with solar-assisted plants of the same size; i.e. MPT's.
[69] Princeton University's Center for Energy and Environmental Studies.
[70] According to Awerbuch (1992), coal and oil are also counter-cyclical but to a significantly lesser extent.

times of economic slowdown and reduced profits, they will have to contend with *rising* gas costs.

Awerbuch quantifies the tendency of natural gas prices to follow the general market by calculating a "beta" for natural gas; this is the same measure found in the financial markets and frequently used to express information about, e.g., common stocks. A large positive beta indicates close tracking of the market, a zero beta indicates no correlation, and a negative beta indicates counter-cyclical behavior. Awerbuch uses data from New York State to calculate a beta for natural gas of -1.0.

The correct discount rate (as determined by the market, which is for this purpose assumed to be efficient) for natural gas cannot be observed explicitly, maintains Awerbuch, because of a lack of market instruments which could reflect it.[71] As an alternative, he makes use of the beta: by examining the market's treatment of investments with a similar beta (in this case, -1.0), the correct discount rate for natural gas can be determined by analogy.

The resulting risk-adjsuted discount rate for gas, based on the NYS beta, was *0%!* In other words, Awerbuch found that the price risk of natural gas was so high that future expenditures *could not be discounted at all.* For expenditures which had previously been discounted at 10%, this reduction makes a profound difference in the levelized cost for the fuel. Awerbuch's results also include a "low risk" case in which a beta of -0.5 is used instead[72], resulting in a gas discount rate of about 5%.

Figure **V-6b,** described in the last section, contains a case for which the "low risk" discount rate of 5% has been applied to the fuel costs, raising these from the "medium case" of $11/MWht to $16.10/MWht. This leap has a dramatic effect on MPT economics, as evidenced in the figure: the buy-down cost becomes *one-sixth* of what would be

[71] It is not entirely clear why some information cannot be gathered by observing the spread on futures contracts, etc., but these instruments are not mentioned in Awerbuch (1992) or Awerbuch *et al* (1996).

without the risk-adjustment, and one-half of what it would be without the risk adjustment but with a large ($50/ton C) carbon tax. The magnitude of these changes is consistent with those which Awerbuch reports.[73] **Table V-5** displays the effects of risk adjustment on real, discounted, and levelized fuel prices for the MPT's 20 year nominal lifetime. The reader is left to judge the wisdom of these dramatic figures; however, Awerbuch's basic argument is fundamentally sound and should not be neglected (even if used in an attenuated form) in future economic studies of renewables.

V.9 Summary of Results

This section recapitulates the foregoing discussions, but does not introduce any new data. Prior sections provide support for all of the declarations found here.

V.9.1 Choice of STEP system: MPT vs. ASDB

- The MPT system is cheaper than the ASDB as modeled here, but if the engine/receiver cost of the ASDB (an uncertain quantity) is reduced, the relative performance changes rapidly.

- In excellent cogeneration locations, the MPT (which has this capability) will probably be a stronger choice than the ASDB (which does not), if the landscape is conducive to the MPT.

- The ASDB has the highest solar fractions (23%-32% depending upon location), closely followed by the recup MPTs (23%-30%) and more distantly by the cogen MPTs (14%-19%).

---

[72] Awerbuch (1992) proposed this lower figure in a conservative effort to translate his results from New York to Colorado.

[73] Awerbuch (1992) calculates a 309% increase in LEC for a combined cycle plant under his base case and a roughly 200% increase in LEC under the "low risk" case.

- The geometric efficiency of the ASDB (94%) is not as superior to that of the MPT (90-92%) as was originally thought. In this respect as in others, the MPT is unique among power towers.

V.9.2 STEPs vs. Gas-Only Plants of Similar Size and Configuration

- Gas-only plants are from 7-9% cheaper than equivalently sized MPTs if heliostat price is $\$100/m^2$, gas price is \$10/MWht, and capital charge rate is 12.25% per annum with an additional 2% for O&M.

- The competitiveness of ASDB systems depends upon the receiver/engine cost, but at the baseline assumption of \$1,000 / kwt, the ASDB systems are some 10-15% more expensive than gas-only. Comparison is difficult because there is no gas-only analog for the ASDB.

- As heliostats fall into the $\$60\text{-}\$90/m^2$ range, the MPT systems should become competitive. *If a carbon tax, low discount rate, or fuel price risk adjustment is taken into account, then the MPT could compete at heliostat prices as high as* $\$190/m^2$.

- The cost of buying down the MPT until it reaches economic parity with a gas-only plant of the same size may be as low as \$50-\$100 million, and could take as few as 100-150 plants. If fuel price risk is taken into account using Awerbuch's method, then the buy-down could be as cheap as \$20 million, requiring only 35 plants.

V.9.3 Choice of Location with and without Cogeneration

- Differences in solar resource are much less important for hybrid plants than for solar-only plants, particularly where renewable energy incentives might exist.

- The LEC spread from best to worst location is in the range of 10-20%; this is considerably *less than current regional variance* in the cost of electricity.

- Cogeneration can create more favorable conditions in a region with a good solar resource and extreme temperatures year-round (such as Pueblo, CO) than in a region with a superb solar resource and somewhat more moderate temperatures (such as Dagget, CA).

- With price parity almost within reach in the United States (at least, for small distributed applications), it seems probable that both MPT and ASDB plants may be financially competitive *today* in countries with significantly higher gas prices. A gas price of $20 / MWht ($5.88 / mmBTU) would make an MPT system competitive at mirror prices up to $175 / m^2!

V.10 Conclusions

This study set out to examine the viability of gas-assisted solar thermal power plants at a relatively unexamined size range (2-4 MWe). A "mini power tower" (MPT) was constructed in the imagination by combining a number of cutting-edge solar thermal technologies, including heliostats from SAIC Inc., a TERC secondary from the theoretical literature, and a windowed receiver from the Weizmann Institute in Israel. Extensive computational modeling was required to simulate the behavior of the MPT under varying solar conditions. A cogeneration module was added, in order to examine the effects of

this increasingly-popular synergy on a hybrid solar system. In a parallel effort, Allied Signal's dish / Brayton system (ASDB), currently in the early stages of commercial development, was modeled on the same footing as the MPT to enable direct comparison.

The results were good. The MPT is a very high-performance member of its class. Its advanced technology does not rely on improbable gimmicks, and it is resilient to a broad range of minor changes in system configuration. In the near future, the MPT should be able to produce electricity at a levelized cost that is nearly equal to that obtained in a similarly-sized gas-only plant. A combination of reasonable public incentives and incremental technological improvement could easily push the balance in favor of the solar-assisted plant. The MPT is much smaller than other central receivers, making it more versatile to deploy, yet it boasts superior efficiency. It will be highly visible, making a clear environmental statement to the public on behalf of its owners, yet its price tag is only $5 million.

No matter how successful the MPT is as a concept, a number of technological challenges must be faced before it becomes a reality. Of its core technologies (heliostats, TERC, receiver, engine), only the engine is a fully commercial product. Also encouraging, the heliostats are nearing full-scale production, and pose no problem in terms of feasibility; rather, price reductions will be the key to this area. By contrast, the receiver is still in the prototype stage, and at a smaller scale (although several might be combined in parallel, an idea currently being pursued at Weizmann in Israel). Finally, the TERC is a drawing-board concept and has yet to be demonstrated in practice.

The ASDB, if it can be built according to Allied Signal's plans, will also be a formidable entry into this field. Its solar performance appears to match that of current dish / Stirling designs, while its compatibility with natural gas is very likely to be superior. Durability and ease of maintenance will be critical areas to watch as this technology unfolds. Relative to the MPT, the ASDB appears likely to be more expensive, at least in the early

stages, and it cannot be readily adapted for cogeneration. However, the ASDB is certainly more versatile than the MPT, and can be deployed at a much smaller scale.

The graphs in this chapter have presented numbers with two or even three significant figures. This level of accuracy reflects the computer-model origins of the data, but is not appropriate for determining the potential of a new and untested technology. It is enough that the MPT is "nearly" competitive with gas-only designs at a heliostat price of "about" $\$100/m^2$; it is not meaningful to judge the technology more closely at this stage. Often, and particularly when only domestic applications are considered, these extra digits after the decimal can be misinterpreted as demonstrating the viability or hopelessness of a particular technology. In the case of the MPT or the ASDB, deployment in other countries, and particularly in developing countries, introduces a whole new parameter space, like turning the "coarse" knob on a microscope. If we back up from the graphs and take this global perspective, this study appears to show that both STEP systems would be valuable additions in many parts of the world, even under today's economic conditions.

V.11 Directions for Further Research

A study of this kind raises more questions than it answers. Some of these new questions have been compiled here and divided into three principle areas: technical background, modeling methodology, and application data.

V.11.1 Further Research in Technical Background

The technical background of both systems provides a rich mine of unexplored and under-explored subjects. These include:

- **The further optimization of the TERC**, and more importantly, the manufacturing methods necessary to create one on the scale required for the MPT (which is of course modest for a central receiver). Gordon & Ries (1993) suggest that the outside area might be approximated by a cone, and then only the inner surfaces need be precision ground. How difficult is this grinding? What will it cost? How will the resulting structure be mounted on the tower? What will the wind-load on it be? How will it be accessed for cleaning? How realistic is the 93% TERC reflectivity used herein?

- **The precise nature and cost of the MPT receiver.** Work in this area is ongoing at the Weizmann Institute, where a larger receiver may eventually be composed of smaller DIAPR-scale (50 kWt) receivers in parallel, separated by additional secondary reflectors. How large can a single windowed receiver be? How do window costs vary with size? How accurate are the window properties as modeled here? How much will this receiver cost? What will be its maximum operating temperature? Its optimum operating temperature? How long will it last?

- **The price curve for SAIC type heliostats**, including any effects caused by reducing the heliostat size from 22 facets to 6 facets. Will the long-term average reflectivity of these heliostats improve? (90% is used here as a modern day figure). Will the mirrors be deleted altogether in favor of a reflecting film? What are the potential savings from eliminating the mirrors? How long will the film last?

- **The ASDB engine.** As the program at Allied Signal develops, do the specifications used here remain accurate? What about the cost, which is demonstrated here to be

both uncertain and critical? Can a higher TIT be used without negatively impacting lifetime and/or cost? Many of these questions cannot be answered without full cooperation from Allied Signal, if they can be answered at all; until the program is further along, this area is mostly guesswork.

- **The MPT recuperated engine.** Small recuperated turbines are a growing area of interest for a number of applications. How accurate is the performance model developed here? Will these engines be clearly superior to their open-cycle counterparts at this scale (without cogen), as it currently appears?

- **The MPT tower.** Tower cost is estimated loosely in this model based on analogs with the wind industry because an insufficient number of central receivers has been built in this size range. How will the cost of the tower vary with height, load, and access requirements? How will the width of the tower vary with these parameters? Are there possible synergies for the tower – such as deploying a wind turbine on top, some distance above the receiver?

Finally, although the bulk of this section is devoted to further research on the MPT and the ASDB, there is at least one alternative system which should be explicitly mentioned:

- **The linked-dish array (LDA).** It now appears that the geometric advantages of the dish vs. the central receiver (especially the MPT) may not be large enough to justify the LDA concept, but if several major components of the MPT presented major development problems, the LDA might resurface. What are the options for a flexible but tightly sealed joint between the pipe and the dish? How large must the pipes be to keep the pressure losses down? Will these lead to unacceptable thermal losses? Unacceptable costs? Can a current receiver design be used on the dishes or will a new design be necessary?

V.11.2 Further Research in Modeling Methodology

There are a number of ways in which the current model is limited, and there are even some capabilities within the model which have not been fully exploited. Areas for further modeling research include:

- **More radical variations in MPT system scale.** This study aimed at the apparent low end of system scale: the point at which gas turbine cost turned sharply upward, and gas turbine efficiency turned sharply downward. This point appeared around 4 MWe. Are smaller, high-efficiency gas turbines under development? What are the advantages in building a much smaller MPT system? What about a 10 MWe MPT? Is the field efficiency the same? How large must the tower be? What does this do to the cogen application?

- **Variable spacing of the heliostat field.** The current MPT model deploys heliostats in even rows, but some degree of improved efficiency will be available if the distance between heliostats is not constant. (This will require a number of changes to the way the program create and keeps tracks of heliostats.) How big will the improvements be? Would varying the size of the heliostats also contribute? How much variance is required? What will it cost?

- **Inclined plane transformations.** The current MPT model uses an averaging approach to the projection of the heliostat image onto the TERC (and from there onto the receiver). All three surface planes (heliostat, TERC, receiver) are oriented differently from each other, and the heliostat plane has a unique orientation *for each heliostat at each time of the day!* Furthermore, each heliostat has a different aim point on the TERC, and each area of the projected image has a different solar concentration (higher in the center). It is not expected that the current method, which averages

between the best and worst sun positions (see chapter 3 for details) introduces serious errors, but complete validation would be useful.

- **More realistic simulation of focusing errors.** The current MPT model introduces an "average" focusing error into each heliostat, but an alternative approach would be to distribute errors "randomly" through the field to each heliostat. What should the distribution of these errors look like? Is the current estimate sufficiently conservative? Will these errors change with system lifetime? With ambient temperature?

- **Complete solar modeling of the ASDB dish.** In the current ASDB model, the Allied Signal specs, which include radiation losses, are used to determine the aperture size, and admittance is basically assumed to be 100%. Software exists (at Sandia labs and elsewhere) for explicit ray-trace type modeling of an entire dish (made up of a variable number of individual facets) to calculate the aperture acceptance as a function of diameter. What is the optimum value for this parameter? What is the effect on the accuracy of the current results?

V.11.3 Further Research in Application Data

Only four applications are covered in this study, and even with these four, opportunities exist for more extensive data. Application research possibilities include:

- **A study of land availability and cost.** The MPT is not large as solar plants go, but it still covers several football fields. How significant will land cost (currently neglected) be for a typical cogen system? A recup system? How flat will this land be? Can the system be installed in unusual places, such as the roof of a shopping mall? What is the regional availability and price of "wasteland?" How do land costs affect the price comparison between the MPT and the ASDB, which is more modular?

- **A more sophisticated cogen model.** This is a complex area; the current model is carefully constructed but relies upon monthly averaged data and, more importantly, is designed to be "blind" to what lies beyond the power plant: the model does not include information on the number and location of chiller/heater units, and includes only a coarse estimate (10%) for the net thermal losses in the hot water lines running between the power plant and the HVAC units. Developing a cogen model which was tailored to particular locations, or which could accept a broader range of application parameters, might prove quite interesting. Can the apparent superiority of a location such as Pueblo be validated? Are there even better areas? How important is physical proximity between the solar plant and the HVAC units? What are the *incremental* costs of using a centralized solar cogen system instead of individually-fired units? (In the model, indirectly-fired units are assumed).

- **Daily modeling of ambient temperature.** Ambient temperature affects gas turbine performance and cogeneration capacity factor. Changes in this area are not expected to be large, but the current model uses an annual average ambient temperature because the solar data is tabulated by sun position in order to effect a 20-fold increase in execution time (see section **III.1.1**). As computer speeds increase, it will be feasible to run this model on a PC hour-to-hour through the year *without* tabulating solar position; of course, hourly temperature data (which is available for many locations) will be necessary. (The model is only manageable in its current form on a Pentium II equipped machine, but given the pace of processor advances, it will no longer be a particularly slow program in a year or two).

- **Extension of application research to other countries.** All of the above questions can be applied internationally, and some of the results may be markedly different. Furthermore, the solar performance of the system will be somewhat different at lower latitudes, and the system design may require modification. Should some of the

heliostat field be placed south of the tower at lower latitudes? How much? What are the implications for heliostat spacing? For tower height?

- **Integration with energy market trends.** The results figures in section **V.4** include a "distribution-adjusted" LEC on a final line. This represents the LEC after a $750 / kWe credit (about 0.9 cents/kWh under base case assumptions; see figs. V-2) is taken for remote power production. How accurate is this figure in different locations? Are there other "bonuses" which should be included, such as a "bonus" for renewable energy production, or a "bonus" for cogeneration? What about a "bonus" for corporate image, in the event of a corporate owner (e.g. in an industrial park)? What is the current cost of capital for a project like this, as a function of location? As a function of ownership? What state, federal, and international organizations might sponsor such a project?

FIG V-1a:
Total Number of Heliostats as a Function of Heliostat Spacing and Tower Height
(2.3 MWe open cycle at Dagget; clear radius around tower = 15 meters; rim angle = 45 degrees)

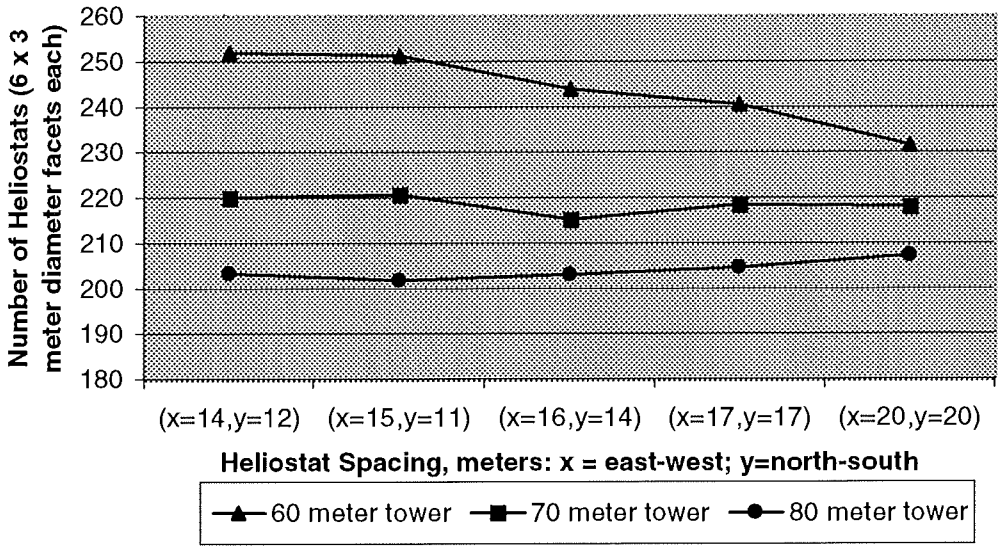

FIG V-1b:
Blocking & Shading Efficiency as a Function of Heliostat Spacing and Tower Height
(2.3 MWe open cycle at Dagget; clear radius around tower = 15 meters; rim angle = 45 degrees)

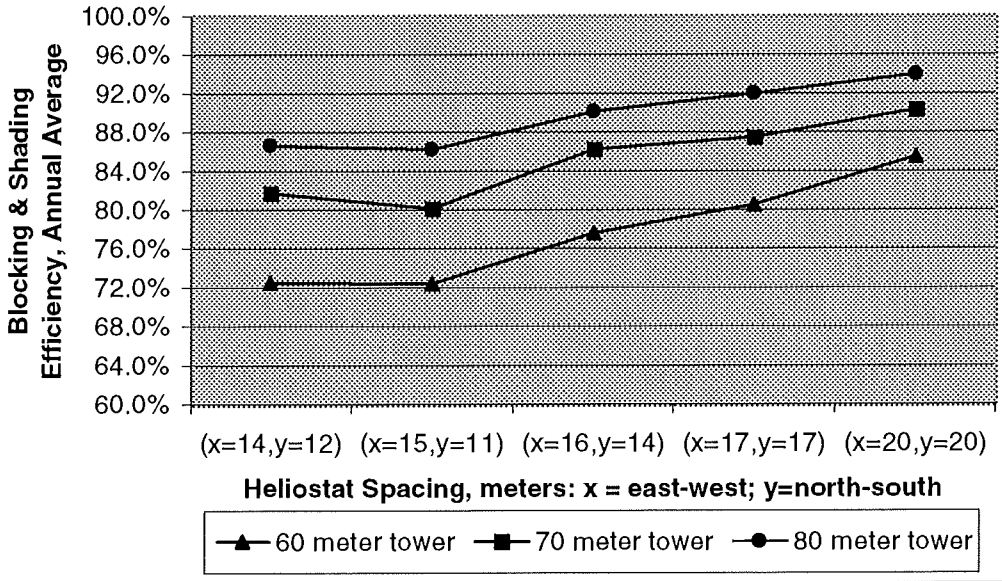

FIG V-1c:
TERC Size as a Function of
Heliostat Spacing and Tower Height
(2.3 MWe open cycle at Dagget; clear radius around tower
= 15 meters; rim angle = 45 degrees)

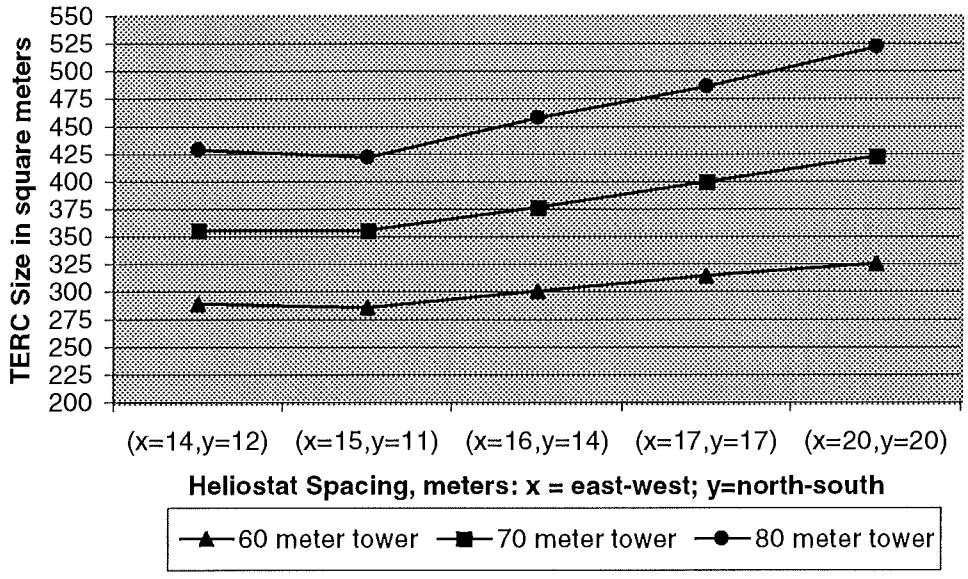

Figure V-1d: Heliostat Fields

(small squares in clearing at bottom represent tower)

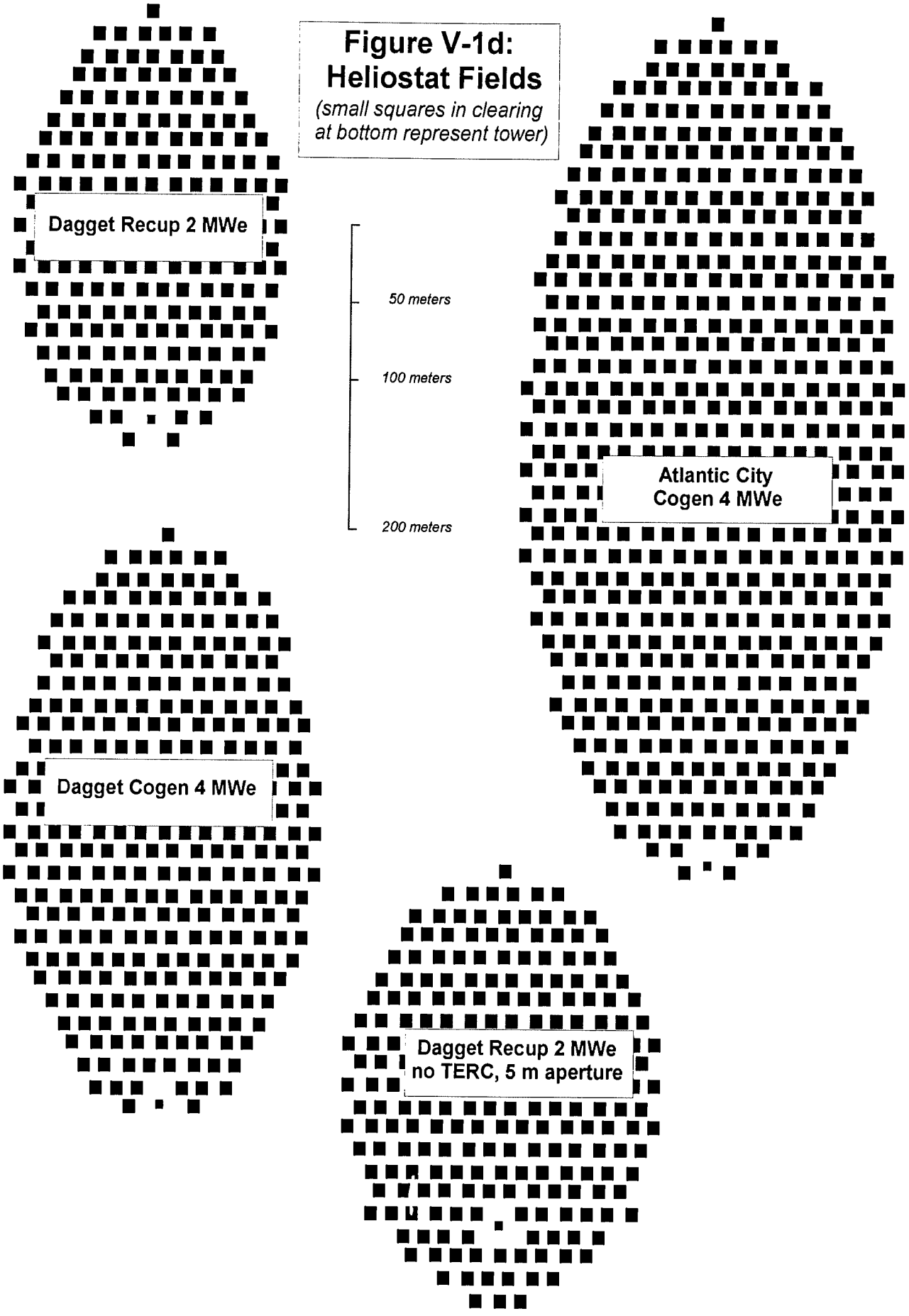

Table V-2: Complete Listing of VARIABLE Model Input Parameters

Name	*Description*	*Range*	*Explanation*
(Both Systems)			
LAT	latitude	28-40 deg N	Depends upon the four locations
INSOL	insolation	0-1000 W/m^2	An output of the model, section **III.1.1**
PHIS	solar elevation	0-80 deg	An output of the model, section **III.1.1**
THS	solar azimuth	70-290 deg	An output of the model, section **III.1.1**
AT	ambient temp, annual avg	10-20 C	A function of location; NREL (1997)
(MPT Systems)			
THEIGHT	tower height	60-80 m	See Section **V.3.2**
XFOOT	east-west h-stat spacing	14-20 m	See Section **V.3.2**
YFOOT	north-south h-stat spacing	12-20 m	See Section **V.3.2**
FRAD	field long (N-S) axis	up to 550 m	Depends upon system rating, solar flux
SECCON	toggle for using a TERC	on or off	TERC is desirable in most systems
WINDOW	toggle for using a window	on or off	Window is desirable in most systems
DIFEED	diameter of aperture	5-7 m	Only applies without a TERC[74]
MAXTEMP	maximum receiver temp	750-850 C	Fixed at 800 C for most runs
MODE	specifies turbine cycle	"ogt" or "rgt"	open cycle cogen or recuperated
NHSTAT[75]	total number of heliostats	up to 560	Depends upon system rating, solar flux
(ASDB Systems)			
ASDBTIT	turbine inlet temperature	700-900 C	Most runs at spec value of 817 C
(Economics)			
MPRICE	price of h-stats *or* dishes	50-200 $/m^2	Base case $100; see section **IV.2.3**
FPRICE	price of fuel both systems	8-14 $/MWht	LHV; derived in section **IV.4.1**
EPRICE	price of ASDB rec/eng	$500-2k /kwt	Base Case $1000/kwt; see **IV.3.3**
CAPRATE	annual capital charge rate	12.25%	See section **IV.6**

[74] If a TERC is in place, the aperture is determined automatically by the concentration ratio of the TERC (see section **III.2.5**), and is much smaller (1-2 meters) than the 5-7 meters necessary without the TERC. The exact sizes may be found under the variable *DIAPE2* in figures **V-2** in section **V.4**.

[75] NHSTAT is not a model input (it is determined by *FRAD, THEIGHT, XFOOT, YFOOT, and CRA*) but is included here anyway because of its centrality.

Table V-3: Complete Listing of FIXED Model Input Parameters

Name	*Description*	*Value*	*Explanation*
(MPT Systems)			
THEIGHT	tower height	70 m	Also in "variable" table; see section **V.3.2**
XFOOT	east-west h-stat spacing	16 m	Also in "variable" table; see section **V.3.2**
YFOOT	north-south h-stat spacing	14 m	Also in "variable" table; see section **V.3.2**
CRA	field rim angle at receiver	45 deg	Also in "variable" table; see section **V.3.2**
MTHW	half-width of the tower	3 m	Minimal shading; allows internal access
MDIAM	diameter of mirror facets	3 m	See section **III.2.2**
MNUM	# of mirrors per heliostat	6	Reduced for the MPT; see section **III.2.2**
PRAD	clear radius around tower	15 m	Allows for access and machinery
ROE	reflectivity of mirrors	90%	Standard figure for heliostats
TERC	choice of TERC design	1	Always use TERC "#1" (45 deg *CRA*)
TROE	reflectivity of the TERC	93%	See chapter 3, section **III.2.5**
SHA	solar half-angle	.01 rads	Constant figure; valid in all locations
MWREF	max window reflectivity	5%	With FAARA, determines net reflectivity
FAARA	full acceptance rim angle	20 degs	With MWREF, determines *EWREF*[76]
WTFEED	window transmittance	38.2 %	IR re-radiation transmittance; see **III.2.4**
ECLC	convection coefficient	0 W/m^2K	Convection losses are small and neglected
PR	ogt comp pressure ratio	10.1; 9.3	Larger: 4MWe ogt; smaller: 3MWe ogt
RPR	rgt comp pressure ratio	2.7	See text for this and *PR*, section **III.2.6**
TIT	ogt turbine inlet temp	1077; 1027	Larger: 4MWe ogt; smaller: 3MWe ogt
RTIT	rgt turbine inlet temp	817	See text for this and *TIT*, section **III.2.6**
Cn/Tn/RCn/RTn	isentropic efficiencies	various	Determined by turbine model sec. **III.2.6**
GREFF	electric generator eff	95%	Various references; e.g. GTW (1997)
REGEN	recuperator effectiveness	90%	See section **III.2.6.2**
RPDROP	recup high-pressure drop	3%	Supported by (**TK**)
RPDROP2	recup low-pressure drop	3%	Supported by (**TK**)
TOWDROP	pressure drop in receiver	5%	See section **III.2.4**
RETLOSS	temp drop on water return	10%	Arbitrary but intended as conservative
CHILLOUT	chiller unit outlet temp	165 C	Supported by Thompson (1997)
(ASDB Systems)			
ASDBHP	compressor pressure ratio	2.33	From Allied Signal specs
ASDBREGEN	recuperator efficiency	90%	Inferred from Allied Signal specs
ASDBPRDROP	recup high-pressure drop	0.084 bar	From Allied Signal specs
ASDBPRDROP2	recup low-pressure drop	0.029 bar	From Allied Signal specs
ASDBARP	pressure exiting receiver	2.196 bar	From Allied Signal specs
ASDBCn/Tn	isentropic efficiencies	.705/.905	Tweaked until matched AS specs; **III.3.3**
ASDBGREFF	generator efficiency	94.5%	Inferred from Allied Signal specs
DROE	dish reflectivity	90%	Technological equivalence with heliostats
DRAPE	receiver aperture diameter	0.409 m	Inferred from Allied Signal specs
DAPE	mirror aperture proj area	100 m^2	Inferred from AS specs & from model
DAREA	actual mirror surface area	106.1 m^2	Larger than *DAPE* (structural curvature)
(Economics)			
RPRICE	receiver price, MPT	$60 / kwt	Left at midpoint of range; effect is minor
DVALUE	value of distributed prod	$750/kWe	see sec **IV.6.3**; effect reported separately
O&M	annual O&M charge rate	2%	see section **IV.6.1.1**; minor effect

[76] EWREF, which is the reflectivity of the window to *incoming solar* radiation, is a function of each field geometry and thus is not listed in the parameter table. EWREF is always less than MWREF (usually much less). See section **III.2.7.3** for a discussion of how the window reflectivity was modeled.

FIGURE V-2a

MPT BASE CASES in Dagget:

Variable	*Description*	*Units*	DC3	DC4	DR2	DR3	DC4go	DR2go
			Dagget	Dagget	Dagget	Dagget	Gas Only	Gas Only
INPUTS:			Cogen 3MW	Cogen 4MW	Recup 2MW	Recup 3MW	Cogen 4MW	Recup 2MW
SPOT	**Physical Location**		Dagget	Dagget	Dagget	Dagget	Dagget	Dagget
LAT	North Latitude	*deg*	35	35	35	35	35	35
FRAD	**Extreme Field Radius**	*meters*	350	380	267	375		
PRAD	Clear Radius Around Tower	*meters*	15	15	15	15		
CRA	Field Rim Angle at Receiver	*deg*	45	45	45	45		
THEIGHT	Receiver (tower) Height	*meters*	70	70	70	70		
MODE	**Recuperated or Open+Cogen**		OpenCog	OpenCog	Recup	Recup	OpenCog	Recup
XFOOT	East-West Heliostat Spacing	*meters*	16.0	16.0	16.0	16.0		
YFOOT	North-South Heliostat Spacing	*meters*	14.0	14.0	14.0	14.0		
SECCON	Yes if a TERC Secondary is used		YES	YES	YES	YES		
WINDOW	Yes if a Quartz Window is used		YES	YES	YES	YES		
MAXTEMP	Receiver Maximum Outlet Temp	*deg C*	800	800	800	800		
CF	Capacity Factor		95%	95%	95%	95%	95%	95%
	Economic Variable Inputs:							
MPRICE	**Mirror Price, w/ Mounting & Drives**	*$ / m^2*	100	100	100	100		
RPRICE	Receiver Price	*$ / kWt*	60	60	60	60		
FPRICE	**Fuel Price (by lower heating value)**	*$/MWht*	10	10	10	10	10	10
CAPRATE	Capital Charge Rate		12.25%	12.25%	12.25%	12.25%	12.25%	12.25%
DVALUE	Value of Distributed Production	*$ / kWe*	750.00	750.00	750.00	750.00	750.00	750.00
OUTPUTS:								
	Heliostats and Aperture:							
NHSTAT	Number of Heliostats in the Field		288	326	196	309	0	0
TOTA	Total Mirrored Area	*m^2*	12,215	13,826	8,313	13,105	0	0
DIAPE1	Aperture of TERC (if applicable)	*meters*	19.85	20.05	19.13	20.02		
DIAPE2	Aperture of Receiver	*meters*	1.83	1.84	1.76	1.84		
SCONA	Surface Area of TERC Secondary	*m^2*	401	409	372	408		
	Energy Yield:							
HOURS	Annual Hours of Solar Operation	*hours*	4,065	4,065	4,065	4,065	0	0
ANNEMW	Ideal Available; Avg over HOURS	*MWt*	8.15	9.23	5.55	8.75		
ANNTBBMW	Xmitted, absent Blckng or Shdng; ""	*MWt*	6.68	7.55	4.57	7.16		
ANNTMW	Actual Transmitted to Receiver, ""	*MWt*	5.37	5.89	3.99	5.61		
ANNRMW	Passing the Aperture, ""	*MWt*	5.18	5.69	3.85	5.41		
ANNRADMW	Lost Through Re-radiation; ""	*MWt*	0.02	0.02	0.04	0.04		
ANNDMW	Delivered to the Turbine Inlet; ""	*MWt*	5.16	5.66	3.81	5.37		
PKDMW	Annual Maximum Delivered	*MWt*	7.73	8.47	5.75	8.04		
HGTRATING	**Engine Rating, based on PKDMW**	*MWe*	2.81	3.91	2.00	2.80	3.91	2.00
	Solar Efficiencies (Annual Figures):							
ROE	Net Mirror Reflectivity		90.0%	90.0%	90.0%	90.0%		
ANNUAL	Geometric Eff Less Blckng or Shdng		91.0%	90.9%	91.5%	91.0%		
ANNBEFF	**Blocking and Shading Efficiency**		80.4%	78.0%	87.2%	78.3%		
APEEFF	Receiver Aperture Efficiency		96.6%	96.6%	96.6%	96.6%		
RECEFF	Receiver Efficiency		99.6%	99.6%	99.0%	99.2%		
STEFF	**Net Solar to Thermal Eff**		63.3%	61.3%	68.7%	61.4%		
GTEFF	**Engine Efficiency in Hybrid (Solar) Mode**		24.9%	27.4%	32.3%	32.3%		
HEFF	**Net Solar to Electric Efficiency, MPT**		15.7%	16.8%	22.2%	19.9%		
	Solar Fraction:							
TOTHEAT	Annual Heat Req. at the Turbine Inlet	*MWht*	92,072	116,201	49,512	69,183	114,039	47,810
HEAT	Annual Heat Supplied by MPT	*MWht*	19,939	21,860	14,719	20,741	0	0
HSF	**Fraction of Power from Solar**		21.7%	18.8%	29.7%	30.0%	0.0%	0.0%
	Gas Performance:							
GASEFF	**Efficiency in Gas only Mode**		25.9%	28.5%	34.8%	34.8%	28.5%	34.8%
HADJEFF	Combined Net (Gas+Solar > Electric) Eff		22.6%	25.0%	29.7%	28.3%	28.5%	34.8%
	Cogeneration:							
CCF	Comb Heating+Cooling Annual CF		42.3%	42.3%	42.3%	42.3%	42.3%	42.3%
CGREFF	Annual Waste Heat Gas Replacement Rate		32.7%	32.4%	0.0%	0.0%	32.4%	0.0%
TAGR	Total Gas Required Annually, LHV	*MWht*	72,133	94,341	34,793	48,442	114,039	47,810
AGS	Gas Saved Annually by Cogen, LHV	*MWht*	22,038	26,531	0	0	26,531	0
AGR	Adjusted Gas Required: TAGR-AGS	*MWht*	50,095	67,810	34,793	48,442	87,508	47,810
CADJGEFF	Cogen Adjusted Gas-Only Eff.		34.1%	37.1%	34.8%	34.8%	37.1%	34.8%
CADJEFF	Cogen Adjusted Net Energy Eff.		28.8%	31.6%	29.7%	28.3%	37.1%	34.8%
	Capital Costs:							
Tower	Tower	*$1,000*	200.0	200.0	200.0	200.0	0.0	0.0
Mirrors	Mirrors	*$1,000*	1,221.5	1,382.6	831.3	1,310.5	0.0	0.0
TERC	TERC	*$1,000*	112.2	114.5	104.2	114.1	0.0	0.0
Receiver	Receiver (includes ducting)	*$1,000*	463.8	507.9	345.2	482.3	0.0	0.0
Engine	Gas Turbine Engine	*$1,000*	3,210.4	3,503.7	1,400.2	1,956.5	3,503.7	1,400.2
	Annual Costs & LEC							
O&M	O&M (at 2% of capital cost)	*$1k / yr*	104.2	114.2	57.6	81.3	70.1	28.0
ACC	**Annual Capital Cost**	*$1k / yr*	638.0	699.3	352.9	497.8	429.2	171.5
Fuel Cost	**Annual Gas Cost: TAGR * FPRICE**	*$1k / yr*	721.3	943.4	347.9	484.4	1140.4	478.1
Electricity	Net Electricity Yield; HGTRATING*CF	*MWh*	23,375	32,506	16,647	23,260	32,506	16,647
Raw LEC	**Raw LEC**	*c/kWh*	6.26	5.40	4.56	4.57	5.04	4.07
Cogen Fuel	Cogen Fuel Savings; AGS * FPRICE	*$1k / yr*	(220.4)	(265.3)	0.0	0.0	(265.3)	0.0
Cogen LEC	**Cogen Adjusted LEC**	*c/kWh*	5.32	4.59	4.56	4.57	4.23	4.07
Distribution	Annualized Distribution Bonus	*$1k / yr*	(258.1)	(358.9)	(183.8)	(256.8)	(358.9)	(183.8)
Cog & Dis LEC	**Cogen & Distribution Adjusted LEC**	*c/kWh*	4.21	3.48	3.45	3.47	3.12	2.97

FIGURE V-2b

MPT BASE CASES in other locations:

(4MWe + Cogen if not indicated)

Variable	*Description*	*Units*	PC4	PR2	TC4	TR2	AC4	AR2
			Pueblo	Pueblo	Tampa	Tampa	Atlantic City	Atlantic City
INPUTS:			Cogen 4MW	Recup 2MW	Cogen 4MW	Recup 2MW	Cogen 4MW	Recup 2MW
SPOT	Physical Location		Pueblo	Pueblo	Tampa	Tampa	tlantic City	tlantic City
LAT	North Latitude	*deg*	38	38	28	28	39.5	39.5
FRAD	Extreme Field Radius	*meters*	420	290	550	378	555	375
PRAD	Clear Radius Around Tower	*meters*	15	15	15	15	15	15
CRA	Field Rim Angle at Receiver	*deg*	45	45	45	45	45	45
THEIGHT	Receiver (tower) Height	*meters*	70	70	70	70	70	70
MODE	Recuperated or Open+Cogen		OpenCog	Recup	OpenCog	Recup	OpenCog	Recup
XFOOT	East-West Hellostat Spacing	*meters*	16.0	16.0	16.0	16.0	16.0	16.0
YFOOT	North-South Hellostat Spacing	*meters*	14.0	14.0	14.0	14.0	14.0	14.0
SECCON	Yes if a TERC Secondary is used		YES	YES	YES	YES	YES	YES
WINDOW	Yes if a Quartz Window is used		YES	YES	YES	YES	YES	YES
MAXTEMP	Receiver Maximum Outlet Temp	*deg C*	800	800	800	800	800	800
CF	Capacity Factor		95%	95%	95%	95%	95%	95%
	Economic Variable Inputs:							
MPRICE	Mirror Price, w/ Mounting & Drives	*$ / m^2*	100	100	100	100	100	100
RPRICE	Receiver Price	*$ / kWt*	60	60	60	60	60	60
FPRICE	Fuel Price (by lower heating value)	*$/MWht*	10	10	10	10	10	10
CAPRATE	Capital Charge Rate		12.25%	12.25%	12.25%	12.25%	12.25%	12.25%
DVALUE	Value of Distributed Production	*$ / kWe*	750.00	750.00	750.00	750.00	750.00	750.00
OUTPUTS:								
	Heliostats and Aperture:							
NHSTAT	Number of Heliostats in the Field		373	214	550	319	560	309
TOTA	Total Mirrored Area	*m^2*	15,819	9,076	23,326	13,529	23,750	13,105
DIAPE1	Aperture of TERC (if applicable)	*meters*	20.29	19.35	20.88	20.04	20.90	20.02
DIAPE2	Aperture of Receiver	*meters*	1.87	1.78	1.92	1.84	1.92	1.84
SCONA	Surface Area of TERC Secondary	*m^2*	419	381	444	408	444	408
	Energy Yield:							
HOURS	Annual Hours of Solar Operation	*hours*	4,047	4,047	4,095	3,926	4,040	3,880
ANNEMW	Ideal Available; Avg over HOURS	*MWt*	8.71	5.00	9.25	5.59	8.22	4.72
ANNTBBMW	Xmitted, absent Blckng or Shdng; ""	*MWt*	7.14	4.13	7.51	4.59	6.73	3.90
ANNTMW	Actual Transmitted to Receiver, ""	*MWt*	5.35	3.52	5.10	3.66	4.46	3.07
ANNRMW	Passing the Aperture, ""	*MWt*	5.17	3.40	4.93	3.53	4.31	2.97
ANNRADMW	Lost Through Re-radiation; ""	*MWt*	0.02	0.04	0.02	0.04	0.02	0.04
ANNDMW	Delivered to the Turbine Inlet; ""	*MWt*	5.15	3.36	4.90	3.49	4.29	2.93
PKDMW	Annual Maximum Delivered	*MWt*	8.46	5.58	8.50	5.83	8.43	5.56
HGTRATING	Engine Rating, based on PKDMW	*MWe*	3.89	2.00	3.93	2.01	3.88	1.99
	Solar Efficiencies (Annual Figures):							
ROE	Net Mirror Reflectivity		90.0%	90.0%	90.0%	90.0%	90.0%	90.0%
ANNUAL	Geometric Eff Less Blckng or Shdng		91.1%	91.8%	90.2%	91.2%	91.0%	91.9%
ANNBEFF	Blocking and Shading Efficiency		74.9%	85.2%	67.9%	79.7%	66.3%	78.7%
APEEFF	Receiver Aperture Efficiency		96.6%	96.6%	96.6%	96.6%	96.6%	96.6%
RECEFF	Receiver Efficiency		99.6%	98.9%	99.5%	98.9%	99.5%	98.7%
STEFF	Net Solar to Thermal Eff		59.1%	67.2%	53.0%	62.5%	52.2%	62.0%
GTEFF	Engine Efficiency in Hybrid (Solar) Mode		27.7%	33.4%	27.3%	32.0%	27.7%	33.4%
HEFF	Net Solar to Electric Efficiency, MPT		16.4%	22.4%	14.5%	20.0%	14.5%	20.7%
	Solar Fraction:							
TOTHEAT	Annual Heat Req. at the Turbine Inlet	*MWht*	114,349	48,096	117,327	50,063	113,970	47,886
HEAT	Annual Heat Supplied by MPT	*MWht*	19,787	12,919	19,066	13,026	16,459	10,786
HSF	Fraction of Power from Solar		17.3%	26.9%	16.3%	26.0%	14.4%	22.5%
	Gas Performance:							
GASEFF	Efficiency in Gas-only Mode		28.8%	35.8%	28.4%	34.5%	28.8%	35.8%
HADJEFF	Combined Net (Gas+Solar > Electric) Eff		25.3%	30.7%	24.4%	28.9%	25.0%	30.5%
	Cogeneration:							
CCF	Comb Heating+Cooling Annual CF		66.4%	66.4%	49.4%	49.4%	62.3%	62.3%
CGREFF	Annual Waste Heat Gas Replacement Rate		50.2%	0.0%	38.0%	0.0%	47.1%	0.0%
TAGR	Total Gas Required Annually, LHV	*MWht*	94,562	35,177	98,261	37,037	97,511	37,100
AGS	Gas Saved Annually by Cogen, LHV	*MWht*	40,266	0	31,484	0	37,672	0
AGR	Adjusted Gas Required: TAGR-AGS	*MWht*	54,296	35,177	66,777	37,037	59,839	37,100
CADJGEFF	Cogen Adjusted Gas-Only Eff.		44.9%	35.8%	39.0%	34.5%	43.4%	35.8%
CADJEFF	Cogen Adjusted Net Energy Eff.		37.3%	30.7%	32.0%	28.9%	35.6%	30.5%
	Capital Costs:							
Tower	Tower	*$1,000*	200.0	200.0	200.0	200.0	200.0	200.0
Mirrors	Mirrors	*$1,000*	1,581.9	907.6	2,332.6	1,352.9	2,375.0	1,310.5
TERC	TERC	*$1,000*	117.3	106.7	124.2	114.4	124.4	114.1
Receiver	Receiver (includes ducting)	*$1,000*	507.5	334.8	510.3	349.6	505.7	333.8
Engine	Gas Turbine Engine	*$1,000*	3,490.9	1,401.4	3,523.2	1,404.2	3,478.7	1,396.5
	Annual Costs & LEC							
O&M	O&M (at 2% of capital cost)	*$1k / yr*	118.0	59.0	133.8	68.4	133.7	67.1
ACC	Annual Capital Cost	*$1k / yr*	722.5	361.4	819.6	419.1	818.8	411.0
Fuel Cost	Annual Gas Cost; TAGR * FPRICE	*$1k / yr*	945.6	351.8	982.6	370.4	975.1	371.0
Electricity	Net Electricity Yield; HGTRATING*CF	*MWh*	32,387	16,661	32,686	16,694	32,274	16,602
Raw LEC	Raw LEC	*c/kWh*	5.51	4.63	5.92	5.14	5.97	5.11
Cogen Fuel	Cogen Fuel Savings; AGS * FPRICE	*$1k / yr*	(402.7)	0.0	(314.8)	0.0	(376.7)	0.0
Cogen LEC	Cogen Adjusted LEC	*c/kWh*	4.27	4.63	4.96	5.14	4.81	5.11
Distribution	Annualized Distribution Bonus	*$1k / yr*	(357.6)	(183.9)	(360.9)	(184.3)	(356.3)	(183.3)
Cog & Dis LEC	Cogen & Distribution Adjusted LEC	*c/kWh*	3.17	3.53	3.86	4.03	3.70	4.01

FIGURE V-2c

MPT COMPONENT VARIATIONS:

(R2 is Recup 2; C4 is Cogen 4. All Dagget)

Variable	*Description*	*Units*	DR2nt5	DR2nt7	DR2nw	DR2nt5nw	DC4hr	DC4lr
			No TERC	No TERC	No Window	No TERC &	850 C Rece	750 C Rece
INPUTS:			R2, 5 M dia	R2, 7 M dia	R2	No Win R2	C4	C4
SPOT	**Physical Location**		Dagget	Dagget	Dagget	Dagget	Dagget	Dagget
LAT	North Latitude	*deg*	35	35	35	35	35	35
FRAD	**Extreme Field Radius**	*meters*	230	200	267	280	434	340
PRAD	Clear Radius Around Tower	*meters*	15	15	15	15	15	15
CRA	Field Rim Angle at Receiver	*deg*	55	55	45	55	45	45
THEIGHT	Receiver (tower) Height	*meters*	70	70	70	70	70	70
MODE	**Recuperated or Open+Cogen**		Recup	Recup	Recup	Recup	OpenCog	OpenCog
XFOOT	East-West Heliostat Spacing	*meters*	16.0	16.0	16.0	16.0	16.0	16.0
YFOOT	North-South Heliostat Spacing	*meters*	14.0	14.0	14.0	14.0	14.0	14.0
SECCON	Yes if a TERC Secondary is used		NO	NO	YES	NO	YES	YES
WINDOW	Yes if a Quartz Window is used		YES	YES	NO	NO	YES	YES
MAXTEMP	Receiver Maximum Outlet Temp	*deg C*	800	800	800	800	850	750
CF	Capacity Factor		95%	95%	95%	95%	95%	95%
	Economic Variable Inputs:							
MPRICE	**Mirror Price, w/ Mounting & Drives**	*$ / m^2*	100	100	100	100	100	100
RPRICE	Receiver Price	*$ / kWt*	60	60	60	60	60	60
FPRICE	**Fuel Price (by lower heating value)**	*$/MWht*	10	10	10	10	10	10
CAPRATE	Capital Charge Rate		12.25%	12.25%	12.25%	12.25%	12.25%	12.25%
DVALUE	Value of Distributed Production	*$ / kWe*	750.00	750.00	750.00	750.00	750.00	750.00
OUTPUTS:								
	Heliostats and Aperture:							
NHSTAT	Number of Heliostats in the Field		226	201	198	289	387	274
TOTA	Total Mirrored Area	*m^2*	9,585	8,525	8,397	12,257	16,413	11,621
DIAPE1	Aperture of TERC (if applicable)	*meters*	5.00	7.00	19.13	5.00	20.37	19.77
DIAPE2	Aperture of Receiver	*meters*	5.00	7.00	1.76	5.00	1.87	1.82
SCONA	Surface Area of TERC Secondary	*m^2*	n/a	n/a	372	n/a	422	398
	Energy Yield:							
HOURS	Annual Hours of Solar Operation	*hours*	3,896	3,851	4,065	3,743	4,065	4,065
ANNEMW	Ideal Available; Avg over HOURS	*MWt*	6.63	5.96	5.60	8.77	10.96	7.76
ANNTBBMW	Xmitted, absent Blckng or Shdng; ""	*MWt*	5.38	4.81	4.61	7.13	8.94	6.36
ANNTMW	Actual Transmitted to Receiver, ""	*MWt*	4.78	4.35	4.02	6.10	6.61	5.18
ANNRMW	Passing the Aperture, ""	*MWt*	4.03	4.28	3.90	4.74	6.39	5.00
ANNRADMW	Lost Through Re-radiation; ""	*MWt*	0.31	0.60	0.10	0.82	0.03	0.02
ANNDMW	Delivered to the Turbine Inlet; ""	*MWt*	3.73	3.68	3.80	3.92	6.36	4.98
PKDMW	Annual Maximum Delivered	*MWt*	5.81	5.76	5.76	5.92	9.48	7.47
HGTRATING	**Engine Rating, based on PKDMW**	*MWe*	2.02	2.00	2.00	2.06	3.90	3.92
	Solar Efficiencies (Annual Figures):							
ROE	Net Mirror Reflectivity		90.0%	90.0%	90.0%	90.0%	90.0%	90.0%
ANNUAL	Geometric Eff Less Blckng or Shdng		90.1%	89.7%	91.5%	90.3%	90.6%	91.1%
ANNBEFF	**Blocking and Shading Efficiency**		88.9%	90.6%	87.2%	85.6%	74.0%	81.4%
APEEFF	Receiver Aperture Efficiency		84.4%	98.3%	96.9%	77.7%	96.6%	96.6%
RECEFF	Receiver Efficiency		92.4%	86.1%	97.4%	82.7%	99.6%	99.6%
STEFF	**Net Solar to Thermal Eff**		56.2%	61.9%	67.8%	44.7%	58.0%	64.2%
GTEFF	**Engine Efficiency in Hybrid (Solar) Mode**		32.3%	32.3%	32.3%	32.3%	27.4%	27.4%
HEFF	**Net Solar to Electric Efficiency, MPT**		18.2%	20.0%	21.9%	14.4%	15.9%	17.6%
	Solar Fraction:							
TOTHEAT	Annual Heat Req. at the Turbine Inlet	*MWht*	49,897	49,505	49,614	50,840	116,014	116,585
HEAT	Annual Heat Supplied by MPT	*MWht*	13,792	13,478	14,667	13,934	24,548	19,220
HSF	**Fraction of Power from Solar**		27.6%	27.2%	29.6%	27.4%	21.2%	16.5%
	Gas Performance:							
GASEFF	**Efficiency in Gas-only Mode**		34.8%	34.8%	34.8%	34.8%	28.5%	28.5%
HADJEFF	Combined Net (Gas+Solar > Electric) Eff		27.7%	28.9%	29.5%	25.2%	24.3%	25.6%
	Cogeneration:							
CCF	Comb Heating+Cooling Annual CF		42.3%	42.3%	42.3%	42.3%	42.3%	42.3%
CGREFF	Annual Waste Heat Gas Replacement Rate		0.0%	0.0%	0.0%	0.0%	32.4%	32.4%
TAGR	Total Gas Required Annually, LHV	*MWht*	36,105	36,027	34,947	36,906	91,467	97,366
AGS	Gas Saved Annually by Cogen, LHV	*MWht*	0	0	0	0	26,488	26,619
AGR	Adjusted Gas Required: TAGR-AGS	*MWht*	36,105	36,027	34,947	36,906	64,978	70,747
CADJGEFF	Cogen Adjusted Gas-Only Eff.		34.8%	34.8%	34.8%	34.8%	37.1%	37.1%
CADJEFF	Cogen Adjusted Net Energy Eff.		27.7%	28.9%	29.5%	25.2%	30.4%	32.6%
	Capital Costs:							
Tower	Tower	*$1,000*	200.0	200.0	200.0	200.0	200.0	200.0
Mirrors	Mirrors	*$1,000*	958.5	852.5	839.7	1,225.7	1,641.3	1,162.1
TERC	TERC	*$1,000*	0.0	0.0	104.2	0.0	118.2	111.3
Receiver	Receiver (includes ducting)	*$1,000*	348.3	345.7	345.9	355.4	568.6	448.3
Engine	Gas Turbine Engine	*$1,000*	1,413.1	1,402.6	1,403.1	1,441.7	3,498.0	3,515.3
	Annual Costs & LEC							
O&M	O&M (at 2% of capital cost)	*$1k / yr*	58.4	56.0	57.9	64.5	120.5	108.7
ACC	**Annual Capital Cost**	*$1k / yr*	357.7	343.1	354.4	394.8	738.2	666.0
Fuel Cost	**Annual Gas Cost; TAGR * FPRICE**	*$1k / yr*	361.1	360.3	349.5	369.1	914.7	973.7
Electricity	Net Electricity Yield; HGTRATING*CF	*MWh*	16,800	16,674	16,681	17,140	32,453	32,613
Raw LEC	**Raw LEC**	*c/kWh*	4.63	4.55	4.57	4.83	5.46	5.36
Cogen Fuel	Cogen Fuel Savings; AGS * FPRICE	*$1k / yr*	0.0	0.0	0.0	0.0	(264.9)	(266.2)
Cogen LEC	**Cogen Adjusted LEC**	*c/kWh*	4.63	4.55	4.57	4.83	4.65	4.54
Distribution	Annualized Distribution Bonus	*$1k / yr*	(185.5)	(184.1)	(184.2)	(189.2)	(358.3)	(360.1)
Cog & Dis LEC	**Cogen & Distribution Adjusted LEC**	*c/kWh*	3.52	3.45	3.46	3.73	3.54	3.44

FIGURE V-2d ASDB BASE CASES

Variable	*Description*	*Units*	DD3	DD4	PD4	TD4	AD4
			Dagget	Dagget	Pueblo	Tampa	Atlantic City
INPUTS:			3MWe	4 MWe	4 MWe	4MWe	4 MWe
SPOT	Physical Location		Dagget	Dagget	Pueblo	Tampa	Atlantic City
LAT	North Latitude	*degrees*	35	35	38	28	39.5
MODE	Recuperated or Open+Cogen		Recup	Recup	Recup	Recup	Recup
ASDBTIT	Turbine Inlet Temp for the ASDB Engine	*deg C*	816	816	816	816	816
CF	Capacity Factor		95%	95%	95%	95%	95%
	Economic Variable Inputs:						
MPRICE	Mirror Price, Including Mounting & Drives	*$ / m^2*	100	100	100	100	100
RPRICE	Engine/Receiver Combined Price	*$ / kWe*	1000	1000	1000	1000	1000
FPRICE	Fuel Price (by lower heating value)	*$/MWht*	10	10	10	10	10
CAPRATE	Capital Charge Rate		12.25%	12.25%	12.25%	12.25%	12.25%
DVALUE	Value of Distributed Production	*$ / kWe*	750.00	750.00	750.00	750.00	750.00
OUTPUTS:							
	Matching with MPT scales:						
# Dishes	Number of Pooled ASDB Systems		118	164	174	236	234
Comb Area	Total Mirrored Area over all dishes	*m^2*	12,514	17,392	18,453	25,028	24,816
	Energy Yield:						
ASDBHOURS	Annual Hours of Solar Operation	*hours*	4,065	4,065	4,047	3,792	3,697
ANNASDBEMW	Ideal Power Available; Avgd over Hours	*MWt*	8.36	11.62	10.17	10.71	9.37
ANNASDBDMW	Power Delivered to the Turbine Inlet; ""	*MWt*	6.39	8.89	7.67	7.86	6.77
ASDBPKDMW	Annual Max Power Delivered, All Dishes	*MWt*	9.42	13.09	12.59	13.25	12.60
ASDBRATING	Pooled Rating of ASDB Systems	*MWe*	2.80	3.89	3.87	3.90	3.87
	Solar Efficiencies:						
DROE	Net Facet Reflectivity		90.0%	90.0%	90.0%	90.0%	90.0%
DEFF/DROE	Geometric Dish Effic. (from curvature)		94.3%	94.3%	94.3%	94.3%	94.3%
ANNASDBREFF	Annual ASDB Receiver Efficiency		90.1%	90.1%	88.8%	86.5%	85.2%
ASDBSTEFF	Annual Solar to Thermal Eff		76.5%	76.5%	75.4%	73.4%	72.3%
ASDBGTEFF	Gas Turbine Efficiency (at all times)		29.7%	29.7%	30.7%	29.4%	30.7%
ANNASDBEFF	Annual Solar to Electric Effic., ASDB		22.8%	22.8%	23.2%	21.6%	22.2%
	Solar Fraction & Hybrid Performance:						
ASDBHEATREQ	Annual Total Heat Req. at Turbine Inlet	*MWht*	78,373	108,925	104,773	110,287	104,868
ASDBHEATPROV	Annual Heat Supplied by Solar	*MWht*	24,695	34,321	29,470	28,309	23,789
ASDBSF	Fraction of Annual Power from Solar		31.5%	31.5%	28.1%	25.7%	22.7%
ASDBADJEFF	Combined Net (Gas+Solar > Electric) Eff.		27.1%	27.1%	28.2%	26.9%	28.3%
ASDBTAGR	Gas required annually to fuel the systems	*MWht*	53,678	74,604	75,302	81,978	81,079
	Capital Costs:						
Mirrors	Mirrors	*$1,000*	1,251.4	1,739.2	1,845.3	2,502.8	2,481.6
Engine/Receivers	Complete Power Conversion Units	*$1,000*	2,801.2	3,893.2	3,871.3	3,900.5	3,872.6
	Annual Costs & LEC						
O&M	O&M (at 2% of capital cost)	*$1k/yr*	81.1	112.6	114.3	128.1	127.1
ACC	Annual Capital Cost	*$1k/yr*	496.4	690.0	700.3	784.4	778.4
Fuel Cost	Annual Gas Cost; ASDBTAGR * FPRICE	*$1k/yr*	536.8	746.0	753.0	819.8	810.8
Electricity	Net Electricity Yield; ASDBRATING*CF	*kWh*	23,312	32,399	32,217	32,460	32,228
Raw LEC	Raw LEC	*c/kWh*	4.78	4.78	4.87	5.34	5.33
Distribution	Annualized Distribution Bonus	*$1k/yr*	(257.4)	(357.7)	(355.7)	(358.4)	(355.8)
Dist Adj LEC	Distribution Adjusted LEC	*c/kWh*	3.68	3.68	3.76	4.23	4.22

FIGURE V-2e ASDB VARIATIONS

Variable	*Description*	*Units*	DD4ce	DD4ee	DD4ht	DD4lt
			Dagget	Dagget	Dagget	Dagget
INPUTS:			Cheap Eng	Xpns Eng	High TIT	Low TIT
SPOT	Physical Location		Dagget	Dagget	Dagget	Dagget
LAT	North Latitude	*degrees*	35	35	35	35
MODE	Recuperated or Open+Cogen		Recup	Recup	Recup	Recup
ASDBTIT	Turbine Inlet Temp for the ASDB Engine	*deg C*	816	816	900	700
CF	Capacity Factor		95%	95%	95%	95%
	Economic Variable Inputs:					
MPRICE	Mirror Price, Including Mounting & Drives	*$/m^2*	100	100	100	100
RPRICE	Engine/Receiver Combined Price	*$/kWe*	500	2000	1000	1000
FPRICE	Fuel Price (by lower heating value)	*$/MWht*	10	10	10	10
CAPRATE	Capital Charge Rate		12.25%	12.25%	12.25%	12.25%
DVALUE	Value of Distributed Production	*$/kWe*	750.00	750.00	750.00	750.00
OUTPUTS:						
	Matching with MPT scales:					
# Dishes	Number of Pooled ASDB Systems		164	164	164	164
Comb Area	Total Mirrored Area over all dishes	*m^2*	17,392	17,392	17,392	17,392
	Energy Yield:					
ASDBHOURS	Annual Hours of Solar Operation	*hours*	4,065	4,065	4,065	4,065
ANNASDBEMW	Ideal Power Available; Avgd over Hours	*MWt*	11.62	11.62	11.62	11.62
ANNASDBDMW	Power Delivered to the Turbine Inlet; ""	*MWt*	8.89	8.89	8.58	9.22
ASDBPKDMW	Annual Max Power Delivered, All Dishes	*MWt*	13.09	13.09	12.73	13.48
ASDBRATING	Pooled Rating of ASDB Systems	*MWe*	3.89	3.89	4.08	3.46
	Solar Efficiencies:					
DROE	Net Facet Reflectivity		90.0%	90.0%	90.0%	90.0%
DEFF/DROE	Geometric Dish Effic. (from curvature)		94.3%	94.3%	94.3%	94.3%
ANNASDBREFF	Annual ASDB Receiver Efficiency		90.1%	90.1%	87.0%	93.6%
ASDBSTEFF	Annual Solar to Thermal Eff		76.5%	76.5%	73.8%	79.4%
ASDBGTEFF	Gas Turbine Efficiency (at all times)		29.7%	29.7%	32.1%	25.6%
ANNASDBEFF	Annual Solar to Electric Effic., ASDB		22.8%	22.8%	23.7%	20.4%
	Solar Fraction & Hybrid Performance:					
ASDBHEATREQ	Annual Total Heat Req. at Turbine Inlet	*MWht*	108,925	108,925	105,921	112,181
ASDBHEATPROV	Annual Heat Supplied by Solar	*MWht*	34,321	34,321	33,121	35,621
ASDBSF	Fraction of Annual Power from Solar		31.5%	31.5%	31.3%	31.8%
ASDBADJEFF	Combined Net (Gas+Solar > Electric) Eff.		27.1%	27.1%	28.9%	23.7%
ASDBTAGR	Gas required annually to fuel the systems	*MWht*	74,604	74,604	72,800	76,560
	Capital Costs:					
Mirrors	Mirrors	*$1,000*	1,739.2	1,739.2	1,739.2	1,739.2
Engine/Receivers	Complete Power Conversion Units	*$1,000*	1,946.6	7,786.4	4,083.9	3,455.0
	Annual Costs & LEC					
O&M	O&M (at 2% of capital cost)	*$1k/yr*	73.7	190.5	116.5	103.9
ACC	Annual Capital Cost	*$1k/yr*	451.5	1166.9	713.3	636.3
Fuel Cost	Annual Gas Cost; ASDBTAGR * FPRICE	*$1k/yr*	746.0	746.0	728.0	765.6
Electricity	Net Electricity Yield; ASDBRATING*CF	*kWh*	32,399	32,399	33,986	28,753
Raw LEC	Raw LEC	*c/kWh*	3.92	6.49	4.58	5.24
Distribution	Annualized Distribution Bonus	*$1k/yr*	(357.7)	(357.7)	(375.2)	(317.4)
Dist Adj LEC	Distribution Adjusted LEC	*c/kWh*	2.82	5.39	3.48	4.13

FIGURE V-3a: Stairsteps (Dagget)

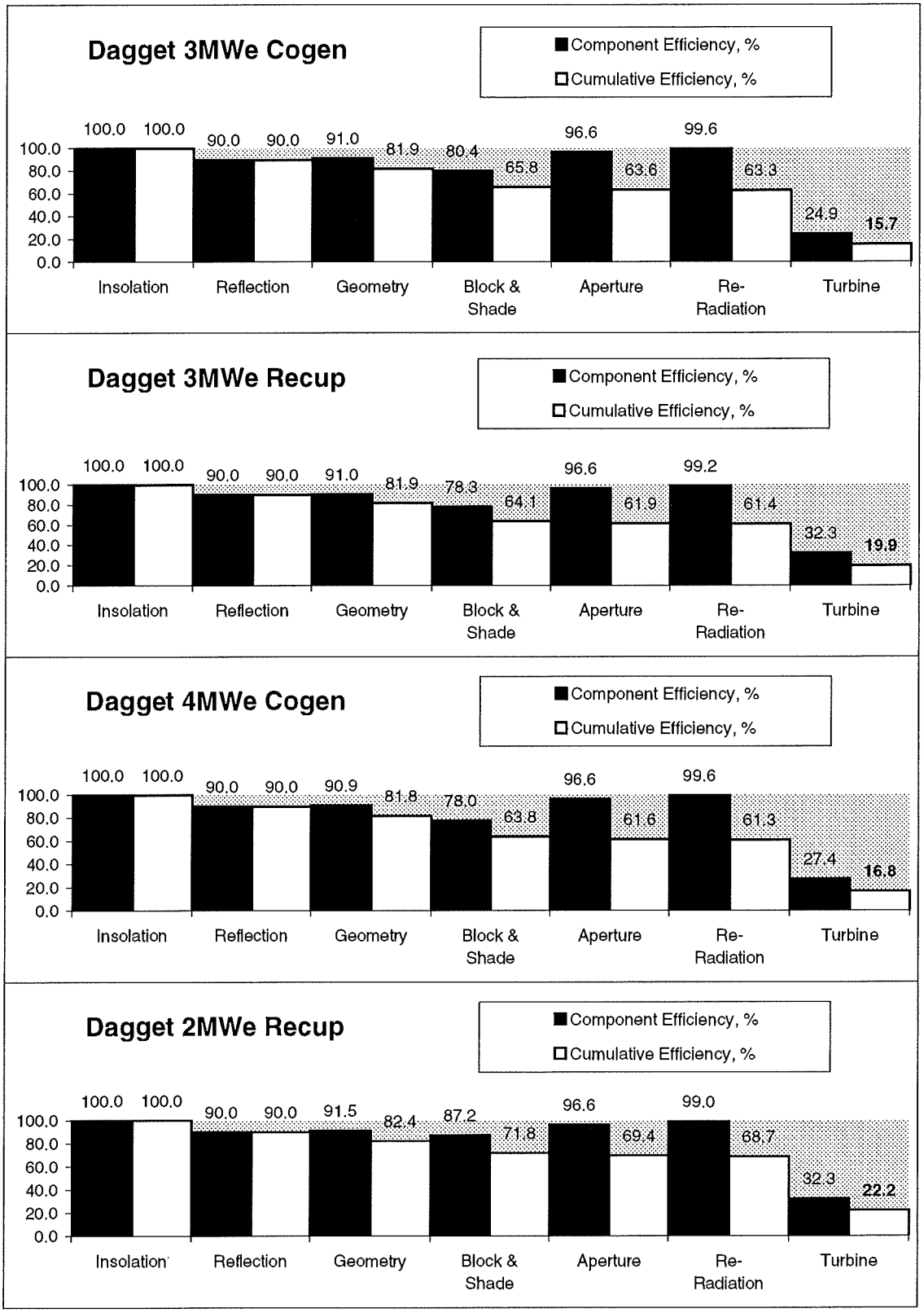

FIGURE V-3b: Stairsteps (Geographic Variations)

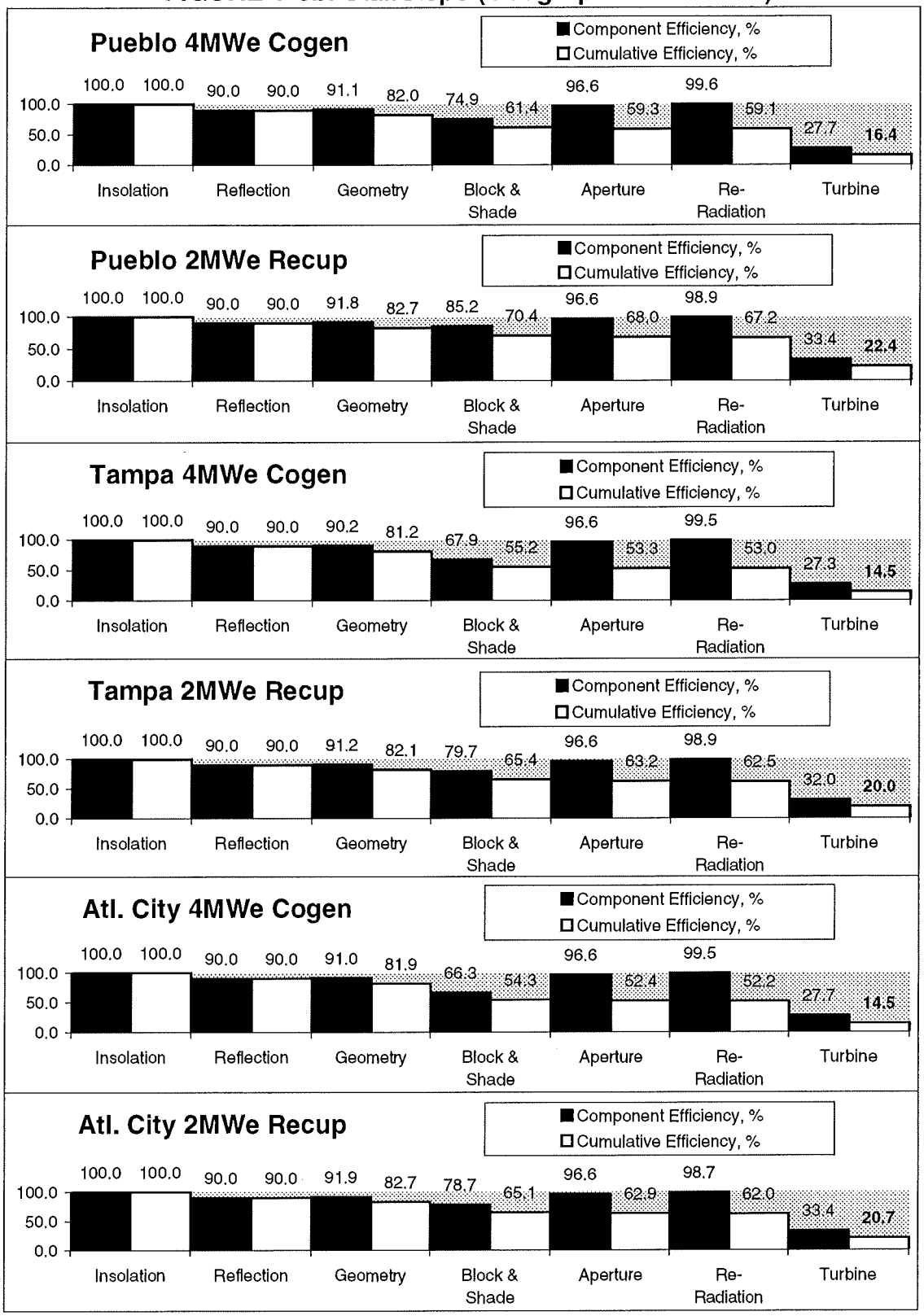

FIGURE V-3c: Stairsteps (Dagget Variations)

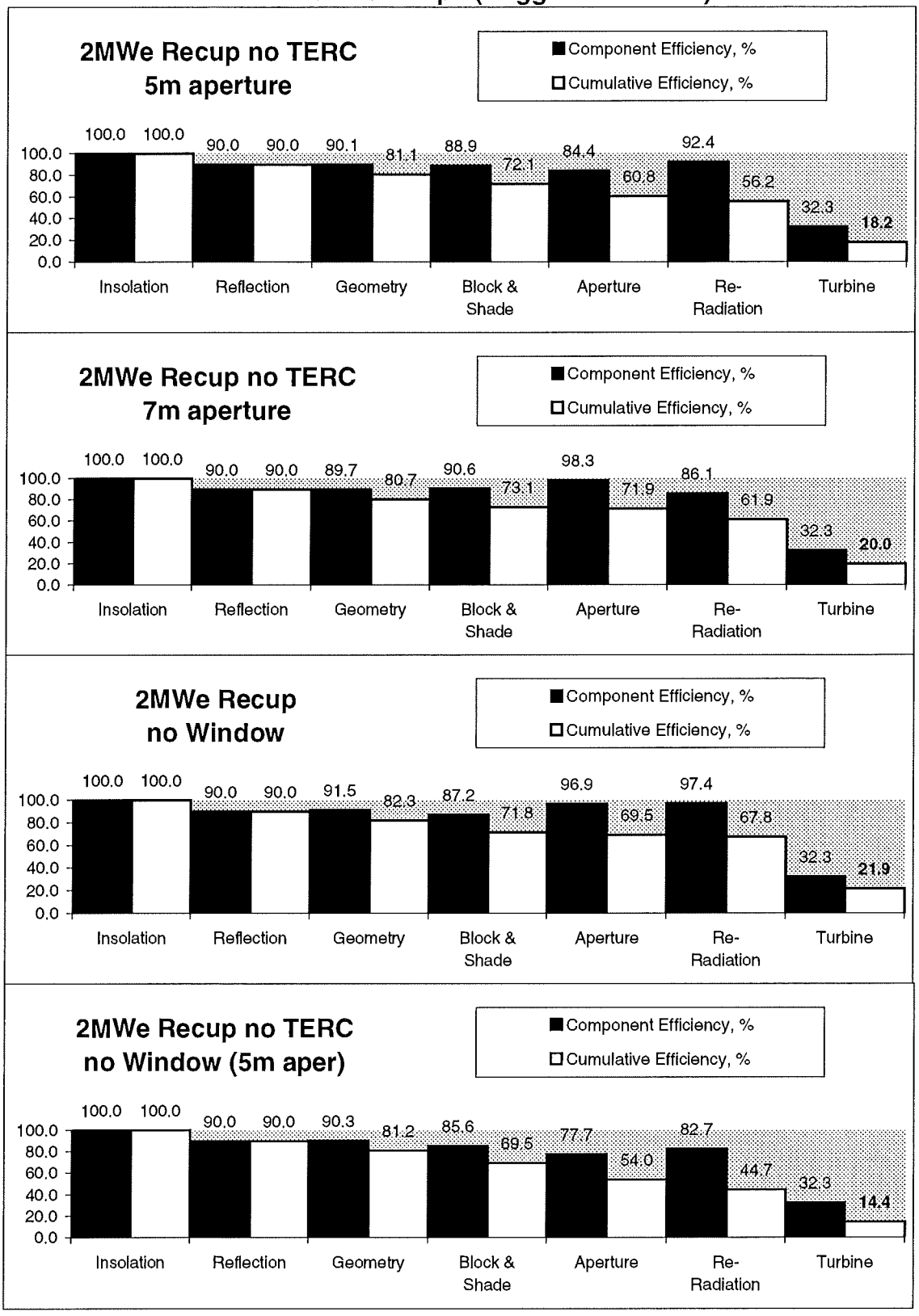

FIGURE V-3d: Stairsteps (Dish Systems)

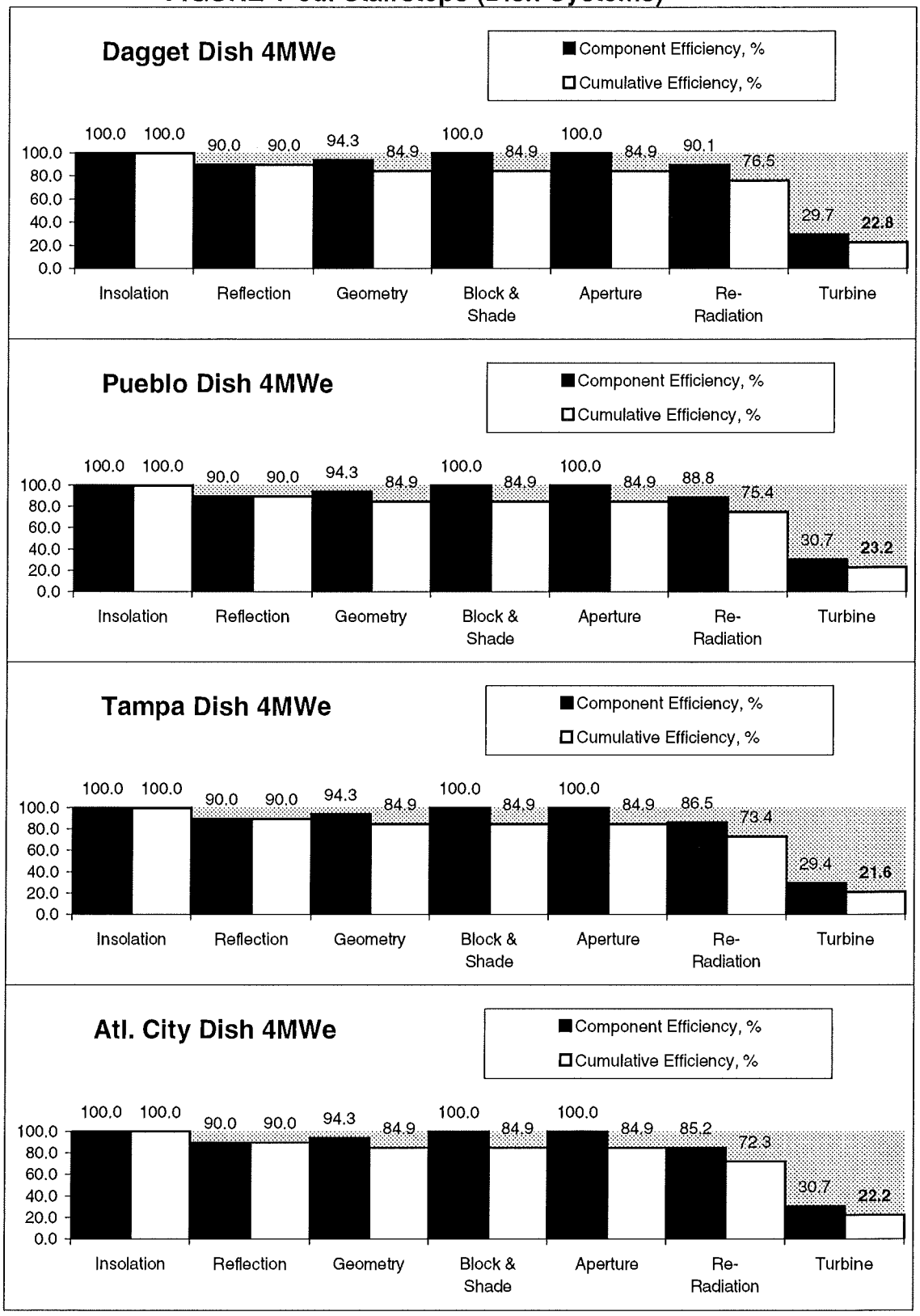

Figure V-4a: Capital Cost by Component

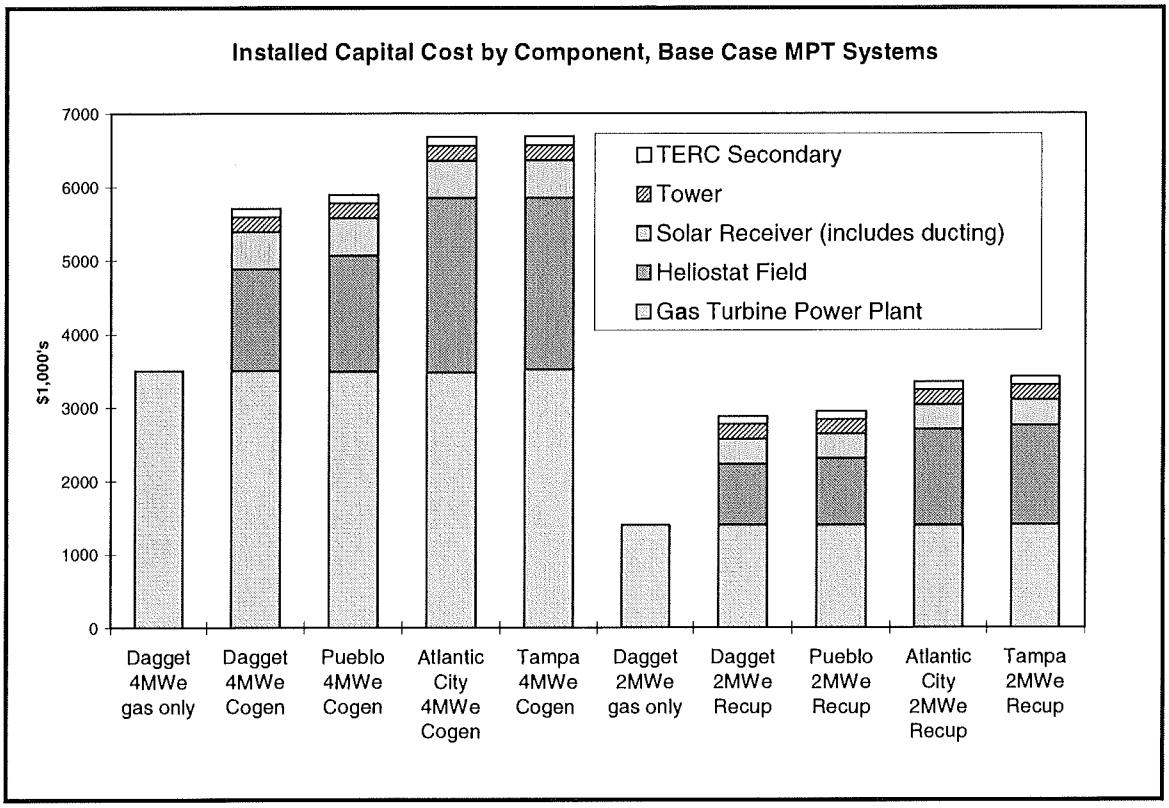

***Note**: The "base case" plant represents neither a "first plant" nor a "break-even" plant (see text).*

FIGURE V-4b:
All Model Runs
Levelized Energy Cost (post-cogen) & Solar Fraction

Base Case (Mirrors $100/m^2; Recvr. $60/kwt; Gas $10/MWht; CCR 12.25%; O&M 2%)

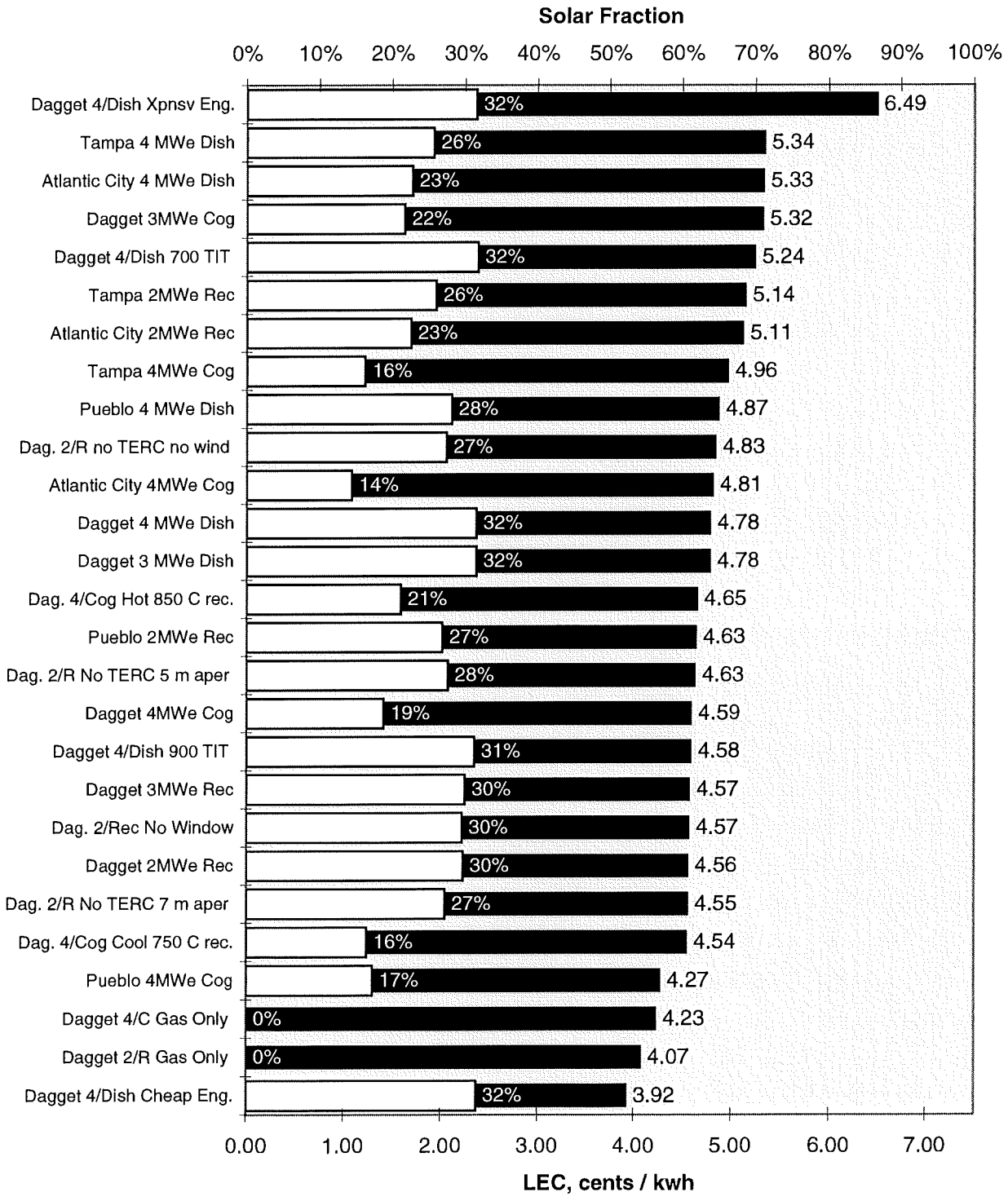

FIGURE V-4c:
Principal Model Runs
Levelized Energy Cost (post-cogen) & Solar Fraction
Dishes in White, Cogen in Gray, Recup in Black
Base Case (Mirrors $100/m^2; Recvr. $60/kwt; Gas $10/MWht; CCR 12.25%; O&M 2%)

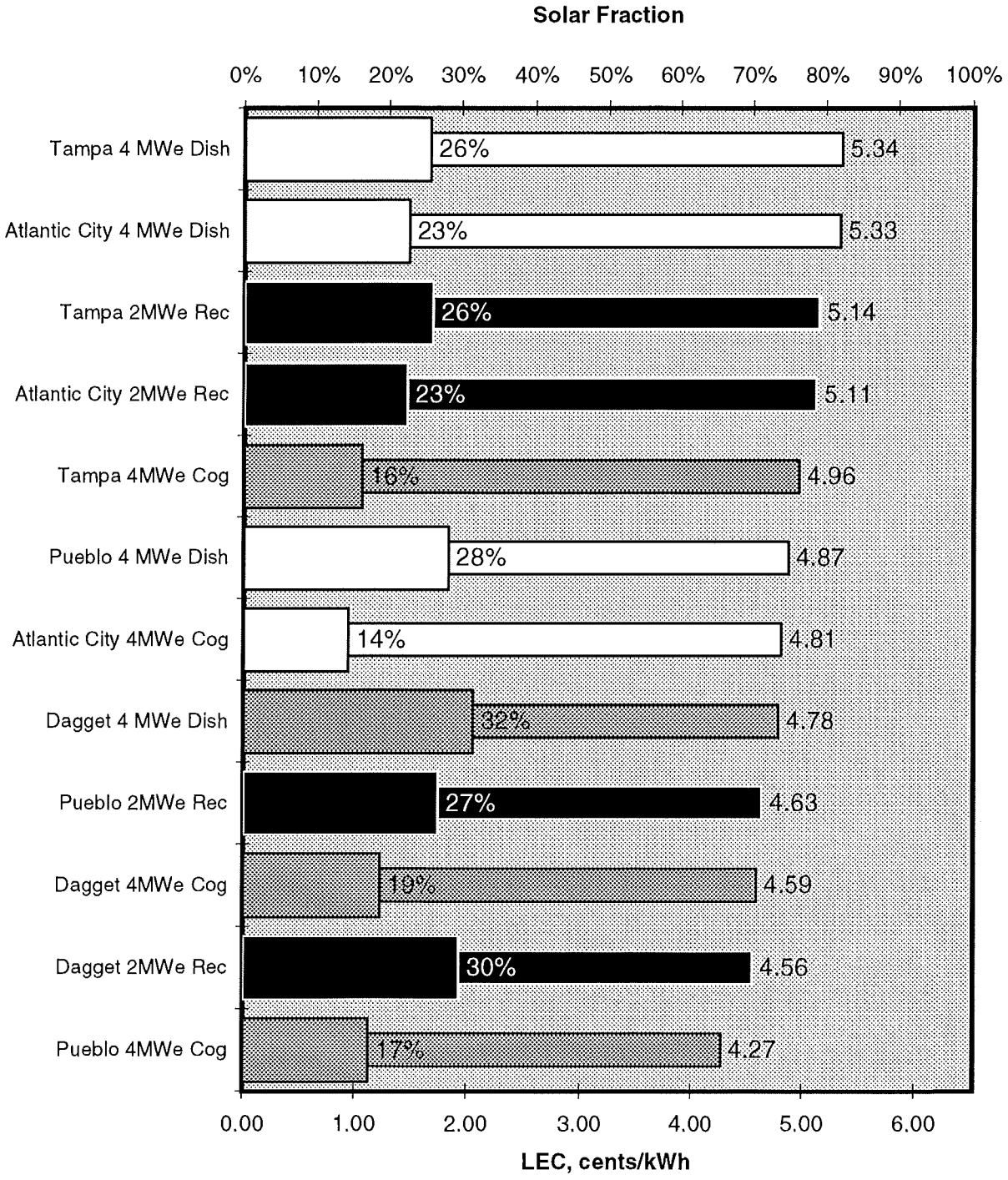

FIGURE V-4d:
Dagget Variations
Levelized Energy Cost (post-cogen) & Solar Fraction
Dishes in White, Cogen in Gray, Recup in Black
Base Case (Mirrors $100/m^2; Recevr. $60/kwt; Gas $10/MWht; CCR 12.25%; O&M 2%)

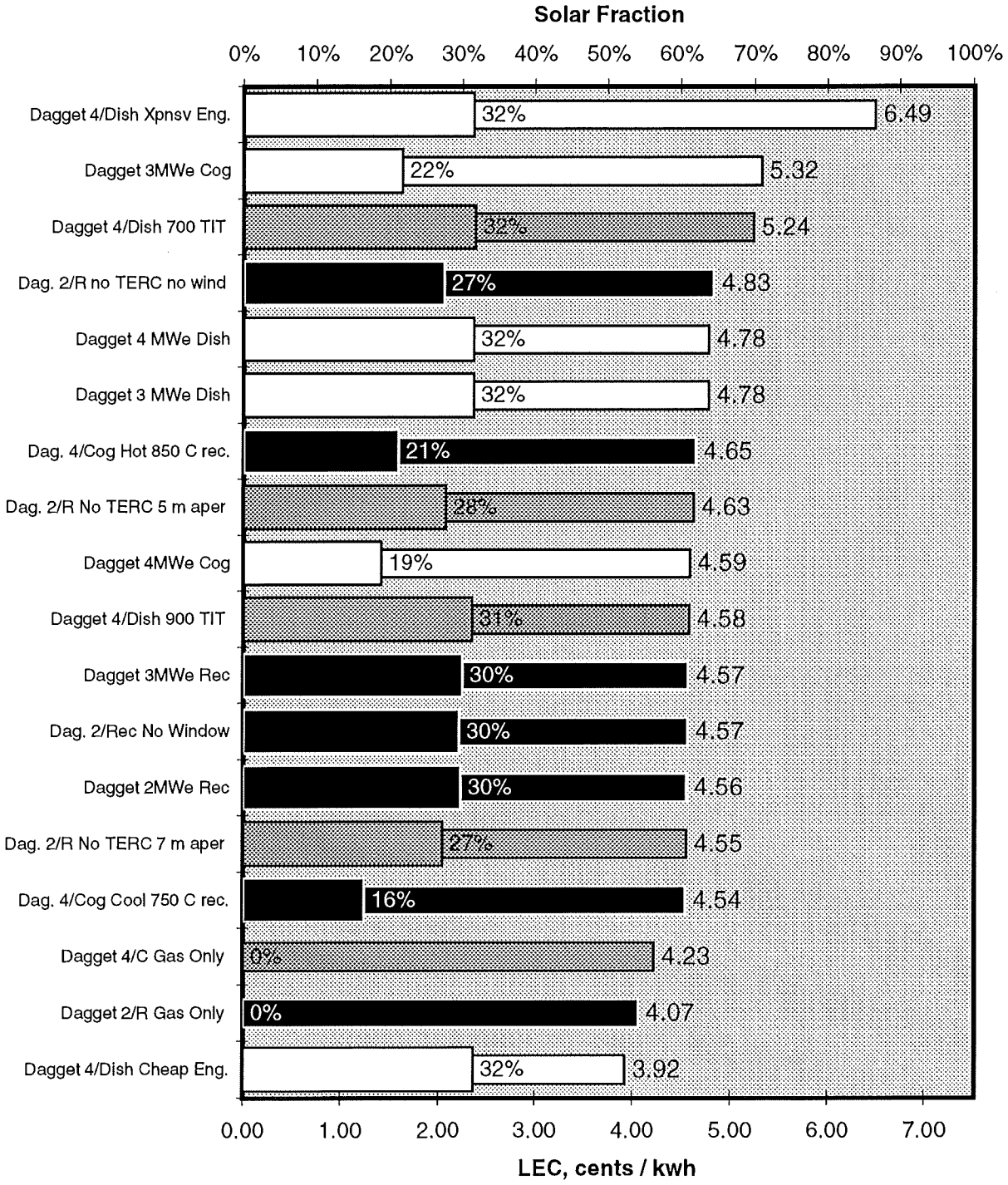

FIGURE V-5a
LEC (post-cogen) as a Function of Gas Price at Dagget

Base Case Assumptions:
(Mirrors $100/m^2; Receiver $60/kWt; 12.25% CCR + 2% O&M; 95% CF; etc.)

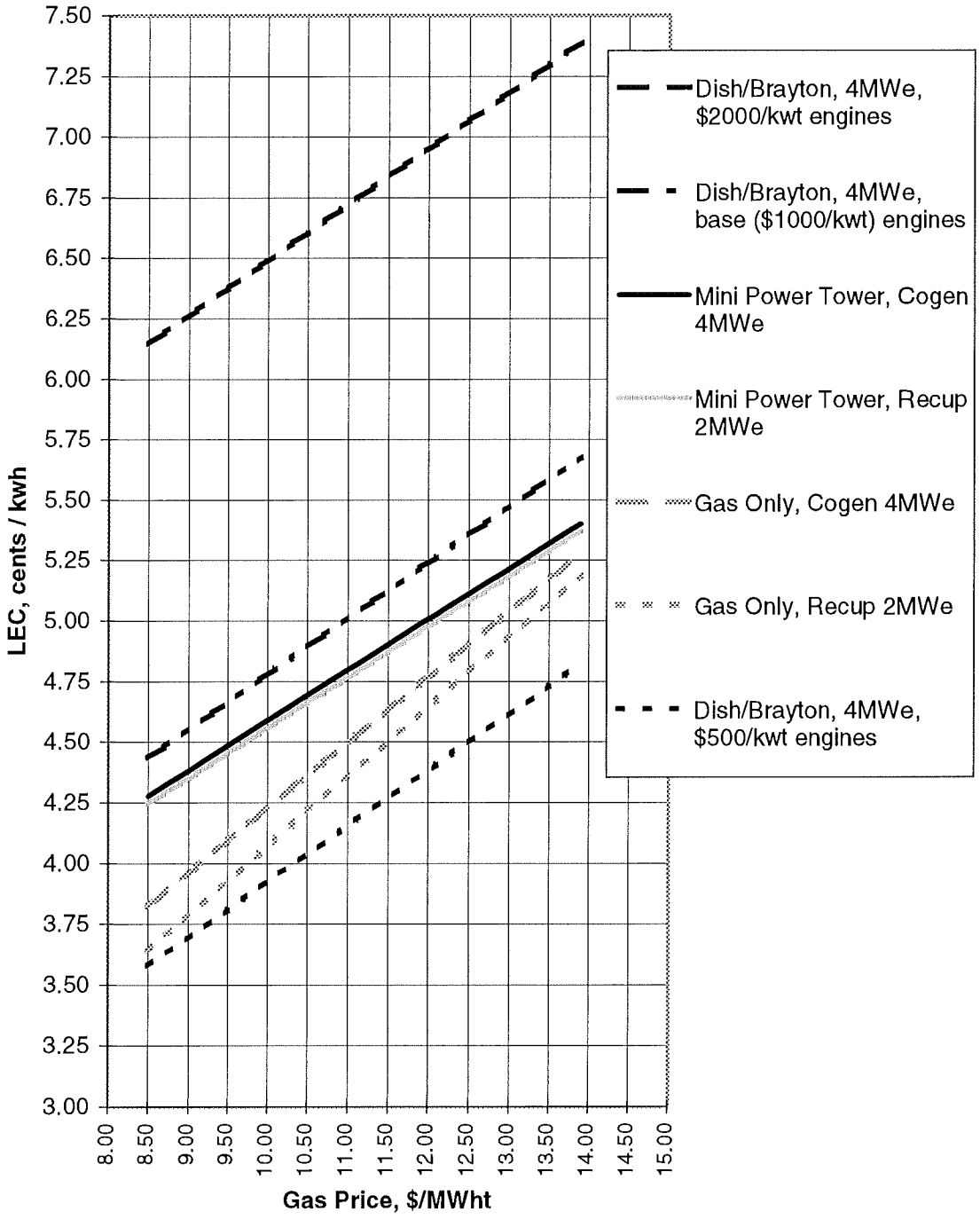

FIGURE V-5b
LEC (post-cogen) as a Function of Mirror Price at Dagget

Base Case Assumptions:
(Gas $10/MWht LHV; Receiver $60/kWt; 12.25% CCR + 2% O&M; 95% CF)

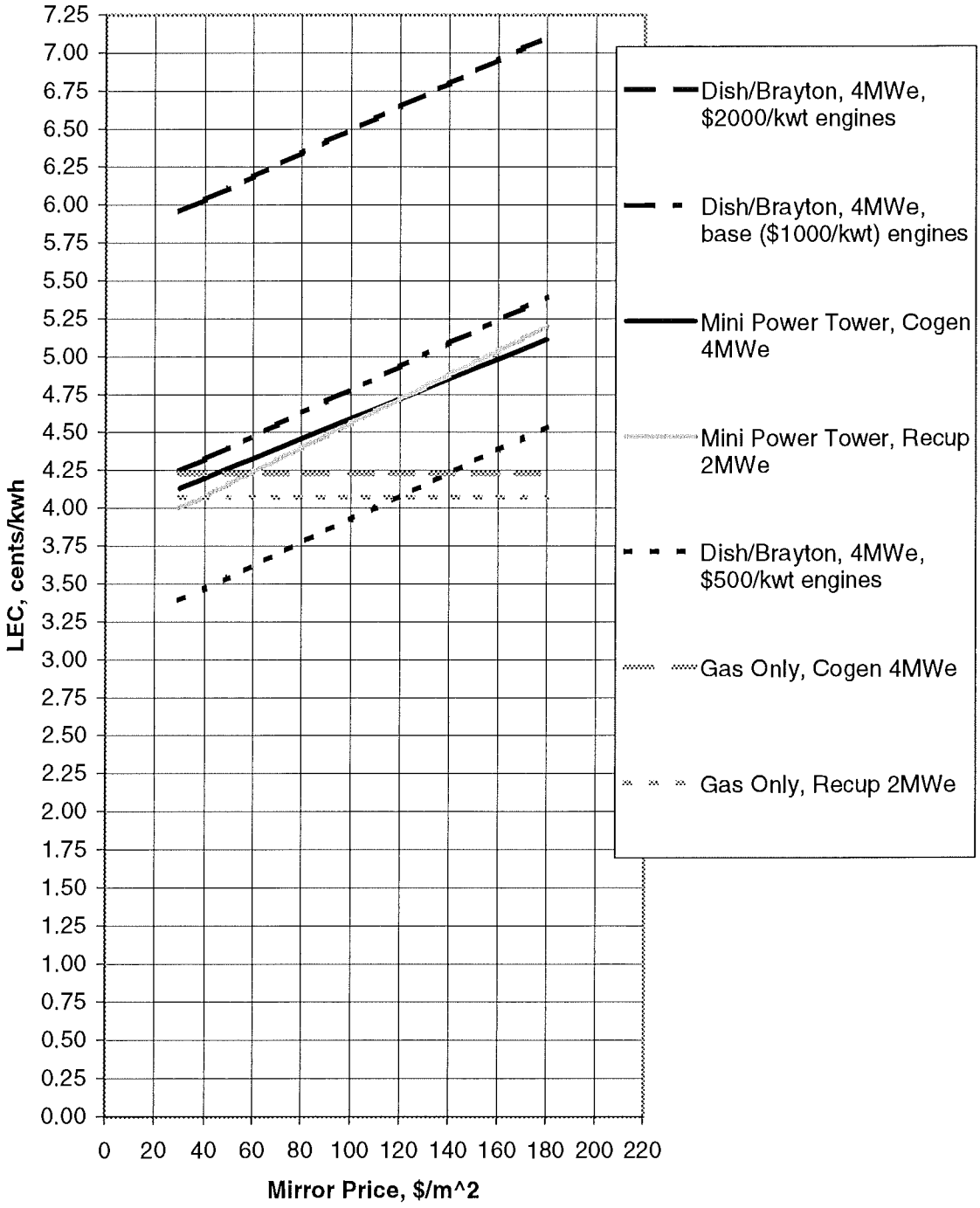

FIGURE V-5c
LEC (post-cogen)
as a Function of Capital Charge Rate at Dagget

Base Case Assumptions:
(Gas $10/MWht LHV; Mirr. $100/m^2; Receiv. $60/kWt; 2% O&M; 95% CF)

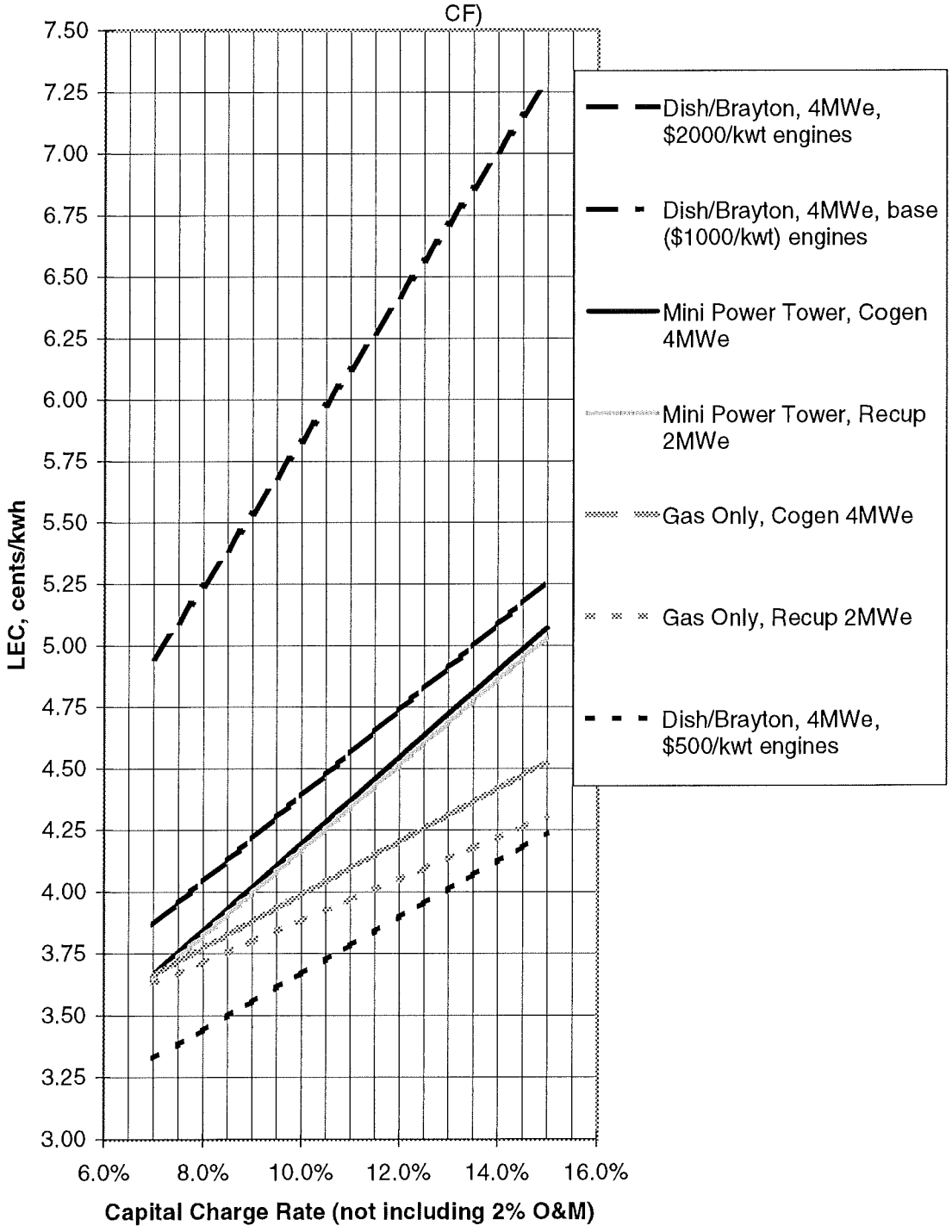

FIGURE V-6a
Break Even Lines for MPT Systems at Dagget

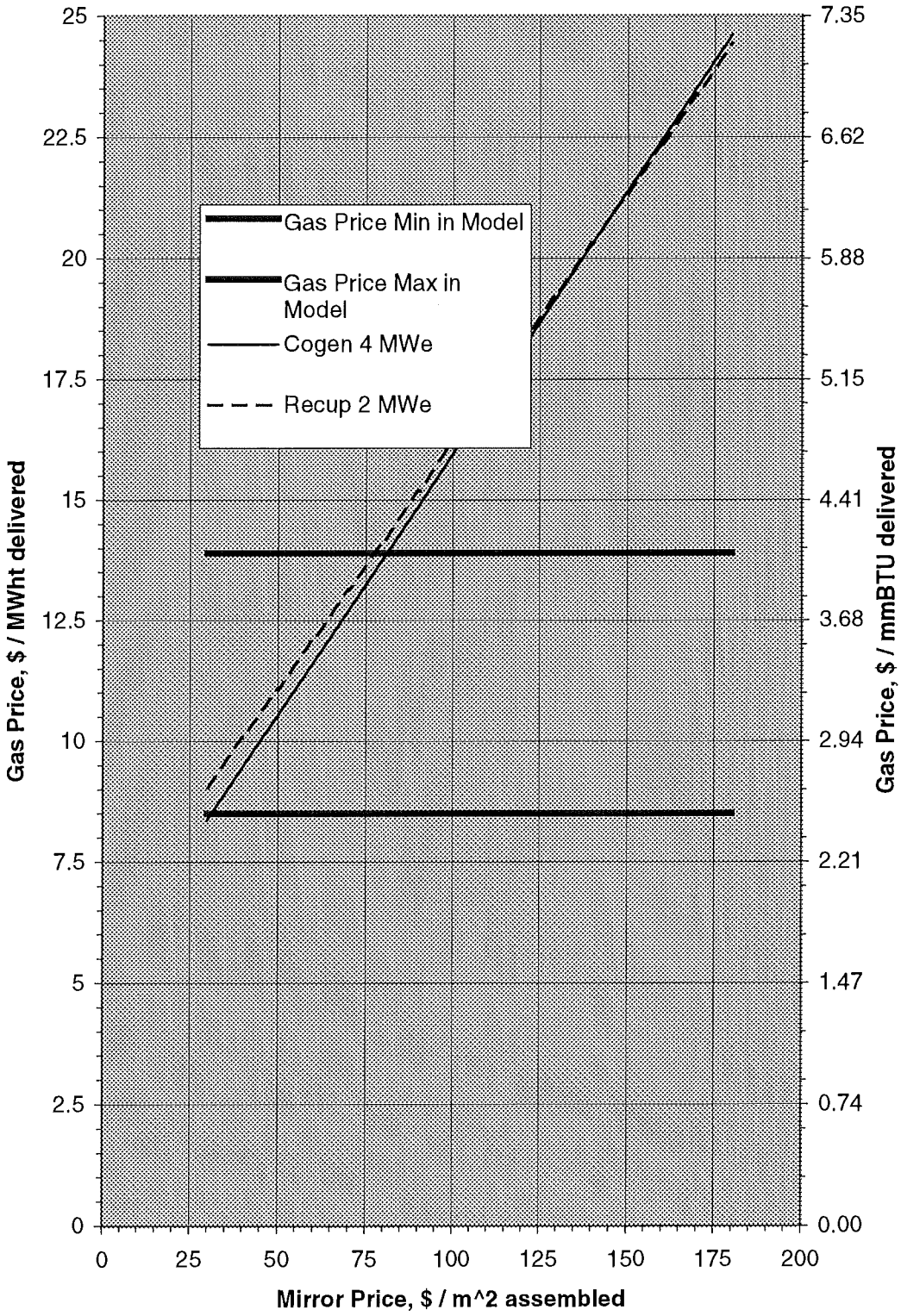

Figure V-6b:
Total Cost of Buying Down the MPT Until Reaching Energy Cost Parity with Gas Only Plants of the Same Size

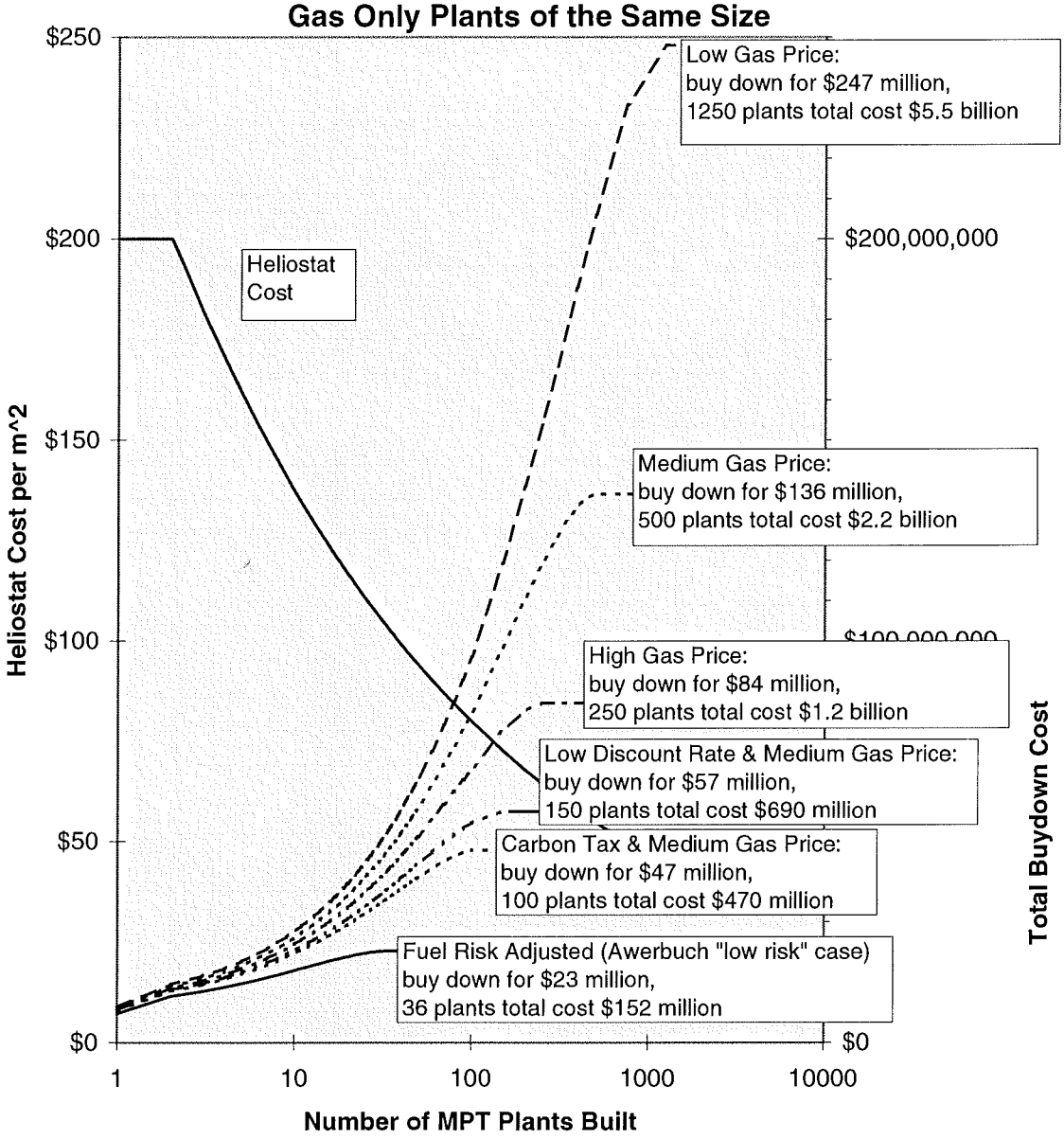

Base Case Dagget 4 MWe Cogen MPT assumptions throughout: 12.25% CCR (10% DR + 0.5% insurance); 2% O&M; $60/kWt receiver; 95% CF; etc. An 85% progress ratio, based on the number of MPT plants built, is used for the heliostat and TERC prices; *all other components prices (tower, turbine, and receiver) remain fixed* (see text). Starting heliostat price is $200 / m^2. Experience curve does not take effect until the third plant is built. A 100% (of total capital cost) R&D and program startup charge is assessed on the first plant, and a 50% R&D charge is assessed on the second plant; subsequent plants are not charged for R&D.

Gas Prices are fixed for the entire production period and are thus levelized costs across all plants:
High= $12/Mwht ($3.53/mmBTU); Medium= $11/MWht ($3.24/mmBTU); Low= $10/Mwht ($2.94/mmBTU)
"Low Discount Rate" (for construction capital) = 8% (vs. 10% base case) "Carbon Tax"=$50/ton carbon

Fuel Risk Adjustment is similar to the "low risk" (more conservative) case from Awerbuch (1992): The tendency of gas prices to move against the market is reflected by a 5% DR for gas instead of the usual 10%, resulting in an adjusted levelized fuel cost of $16.10 (instead of $11.00) per MWht, a 46% increase. If the baseline Awerbuch case (0% gas DR) is used instead, then the adjusted cost of fuel becomes $25.80 and the buydown cost is equal to the R&D charges only!

Table V-5:

Effect of Awerbuch's Risk Adjustment on 20 Years of Natural Gas Prices

Year	*Actual Cost, per MWht*	*Net Present Value at Gas DR = 10%*	*5%*	*0%*
1	$11.00	$10.00	$10.48	$11.00
2	$11.00	$9.09	$9.98	$11.00
3	$11.00	$8.26	$9.50	$11.00
4	$11.00	$7.51	$9.05	$11.00
5	$11.00	$6.83	$8.62	$11.00
6	$11.00	$6.21	$8.21	$11.00
7	$11.00	$5.64	$7.82	$11.00
8	$11.00	$5.13	$7.45	$11.00
9	$11.00	$4.67	$7.09	$11.00
10	$11.00	$4.24	$6.75	$11.00
11	$11.00	$3.86	$6.43	$11.00
12	$11.00	$3.50	$6.13	$11.00
13	$11.00	$3.19	$5.83	$11.00
14	$11.00	$2.90	$5.56	$11.00
15	$11.00	$2.63	$5.29	$11.00
16	$11.00	$2.39	$5.04	$11.00
17	$11.00	$2.18	$4.80	$11.00
18	$11.00	$1.98	$4.57	$11.00
19	$11.00	$1.80	$4.35	$11.00
20	$11.00	$1.64	$4.15	$11.00
NPV (per MWht/year):		$93.65	$137.08	$220.00
CCF (at Capital DR = 10%):		11.7%	11.7%	11.7%
LEC (per MWht):		**$11.00**	**$16.10**	**$25.84**

V.12 Closing Personal Remark

This project completes the requirements for the Master of Science degree in Mechanical Engineering at Princeton University. As such, it is perhaps 70% a learning experience and 30% a work with meaningful implications. Of the learning fraction, some of the lessons were of a general nature, useful to any engineer or scientist: lessons about technology development and assessment, R&D objectives, and problem redefinition. Other lessons, of a more specific nature, are perhaps too evident in the finished product: lessons about the intricacies of MS-Excel, the tedious complexity of central receiver systems, and the fine details of solar plant modeling. Both sets of learning have been enriching, and have lent me confidence both within and without the field of engineering.

As for the external implications, it is the hope of this researcher that his work may develop a potency in the real world which is only hinted at on the computer. My "Mini Power Tower" is a cobbling together of ideas, none of them conspicuously radical, most of them belonging to other people, until an abstraction is created which possesses a number of quite pleasing properties. I hope that others will also, to some degree, admire these properties, so that one day the abstraction can become something more.

References

Note: World Wide Web references carry the date upon which the page was accessed.

Abele, M *et al* (1996) Design and Test Results of a Receiver-Reactor for Solar Methane Reforming *Solar Engineering (ASME Conference Proceedings 1996)* pp. 339-346.

Allied Signal (1997) "Receiver Design: Baseline System Design Point Performance" Allied Signal Aerospace (presentation materials; Sandia Labs summer 1997).

Awerbuch, S *et al* (1996) Capital Budgeting, Technological Innovation and the Emerging Competitive Environment of the Electric Power Industry *Energy Policy* **V** 24 **N** 2 pp. 195-202.

Awerbuch, S (1992) "Direct Testimony of Shimon Awerbuch, Ph. D." to the Public Utilities Commission, State of Colorado (docket Co. 91R-642EG, pre-filed Feb. 14, 1992). Reprint by the Colorado Solar Energy Industries Association.

Beninga *et al* (1995) Design, Testing, and Commercialization Plans for the SAIC/STM 20 kWe Solar Dish/Stirling System. *IECEC (ASME Conference 1995)* pp. 487-489.

Beninga, K J (1997) "Solar Power Technologies" Science Applications International Corporation (SAIC Science and Technology Trends series; company paper).

Bohn, M S *et al* (1995) Combined-Cycle Power Tower *Solar Engineering Vol. 1 (ASME Conference 1995)* pp. 597-605.

Buck, R *et al* (1994) Development of a Volumetric Receiver-Reactor for Solar Methane Reforming *Solar Engineering (ASME Conference Proceedings 1994)* pp. 73-78.

Buck, R *et al* (1996) Receiver Development for a Dish-Brayton System *Solar Engineering (ASME Conference Proceedings 1996).*

Carrier (1997) "Chiller: Absorption" *http://wwwd.carrier.com* Nov 1997.

Cohen, E H *et al* (1998) "Recent Improvements and Performance Experience at the Kramer Junction SEGS Plants" *http://www.kjcsolar.com/ASMEF961.html* Jan 1998.

Cohen, H, *et al* (1996) Gas Turbine Theory (4^{th} ed.) Essex, England: Longman Group.

Cohen, J (1998) "Summary of Large HAWTS in Windfarms Technology Characterization" Princeton Economic Research, Inc. (NREL subcontractee).

CREST (1997) Center for Renewable Energy and Sustainable Technology *http://solstice.crest.org.*

De Laquil, P D *et al* (1993) "Solar Thermal Electric Technology" in Johansson, T B *et al* (eds.) (1993) Renewable Energy: Sources for Fuels and Electricity Washington DC: Island Press.

DOE (1997a) Renewable Energy Annual 1996 (April 1997) *http://www.eia.doe.gov* Dec 1997.

DOE (1997b) Early Release of the Annual Energy Outlook 1998 *http://www.eia.doe.gov* Dec 1997.

DOE (1998) Comprehensive Electricity Competition Plan.

Felder, F A (1996) Integrating Financial Theory Methods in Electricity Resource Planning *Energy Policy* **V** 24 **N** 2 pp. 149-154.

Gallup, D R and J B Kesseli (1994) A Solarized Brayton Engine Based on Turbo-Charger Technology and the DLR Receiver. *AIAAA 94* pp. 1719-1724

Gas-Turbines.com (1997a) "Kawasaki Heave Industries Ltd. M1a-11" *http://www.gas-turbines.com* Oct 1997.

Gas-Turbines.com (1997b) "Prices (listed by) Output" *http://www.gas-turbines.com* Oct 1997.

GEC (1997) "GEC Alsthom European Gas Turbines, Turbine Range: Hurricane" *http://www.gecalsthom.egt.co.uk* Oct 1997.

Gipe, P (1997) "Trends in Wind Turbine Towers" *http://keynes.fb12.tu-berlin.de/luftraum/konst/towertrends.html* Dec 1997.

Gordon, J M & H Ries (1993) Tailored Edge-ray Concentrators as Ideal Second Stages for Fresnel Reflectors *Applied Optics* **V** 32 **N** 13 pp. 2243-2251.

Gould, W R *et al* (1996) The Solar Two Power Tower Project Status and Operating Experience to Date *Solar Engineering (ASME Conference Proceedings 1996).*

Grasse, W (1991) PHOEBUS – International 30 MWe Solar Tower Plant *Solar Energy Materials* **V** 24 pp. 82-94.

GTW (1994) Gas Turbine World: The 1993-1994 Handbook Fairfield, CT: Pequot Publishing.

GTW (1997) Gas Turbine World: Performance Specs 1996-1997 (Volume 16) *Gas Turbine World.*

Heller, P *et al* (1994) Development of a Volumetric Received for a Dish-Brayton System *Joint Solar Engineering Conference (ASME Conference 1994)* pp. 561-566.

ICGTI (1997a) "Allison Engine Company Model 501-KB3" *http://www.icgti.org*

ICGTI (1997b) "Allison Engine Company Model 501-KB5" *http://www.icgti.org*

IES (1997) "IES Models for Baseload and Cogeneration Applications – Performance Data" *http://www.in2nett.com/ies* Dec 1997.

Incropera, F P and D P DeWitt (1990) Fundamentals of Heat and Mass Transfer (3rd ed.) New York: Wiley & Sons.

Jones, S A (1996) Annual Performance Prediction for Off-axis Aligned Lugo Heliostats at Solar Two *Solar Engineering (ASME Conference 1996)* pp. 133-138.

Jones, S A *et al* (1995) Recent Results on the Optical Performance of Solar Two Heliostats *Solar Engineering Vol I (ASME Conference 1995)* pp. 581-589.

Karni, J *et al* (1995) The DIAPR: A High-pressure, High-temperature Solar Receiver *Solar Engineering (ASME Conference 1995)* pp. 591-595.

Klaiss *et al* (1990) "Costs & Revenues of Renewable Electricity Production Systems" DLR Stuttgart (working paper exact date unknown).

Kolb, G J (1997) "Power Tower Technical Characterization" Working Paper.

Kribus, A (1994) Optical Performance of Conical Windows for Concentrated Solar Radiation *Journal of Solar Energy Engineering* **V** 116 pp. 47-52.

Kribus, A *et al* (1997) A Solar-Driven Combined Cycle Power Plant *Journal of Solar Energy* "accepted March 1997."

Levitan, R *et al* (1991) Closed-loop Operation of a Solar Chemical Heat Pipe at the Weizmann Institute Solar Furnace *Solar Energy Materials* **V** 24 pp. 464-477.

Levy, M *et al* (1992) Chemical Reactions in a Solar Furnace 2: Direct Heating of a Vertical Reactor in an Insulated Receiver. Experiments and Computer Simulations *Solar Energy* **V** 48 pp. 395-402.

Mancini, T (1997) Private Communication with Tom Mancini at Sandia National Labs Aug 1997.

Muir, J F *et al* (1994) Solar Reforming of Methane in a Direct Absorption Catalytic Reactor on a Parabolic Dish: I – Test and Analysis *Solar Energy* **V** 52 pp. 467-477.

Noble, J E *et al* (1995) Test Results from a 10 kWe Solar / Natural Gas Hybrid Pool Boiler Receiver *IECEC (ASME Conference Proceedings 1995).*

NREL (1997) Summary Solar Radiation and Climate Data *http://solstice.crest.org* Nov 1997.

Ogden, J (1988) "Alternative Cooling Technologies for Commercial Buildings: A New Jersey Case Study" Princeton University CEES Working Paper.

PIX (1997) "Photographic Information eXchange" Joint DOE/NREL Project *http://www.nrel.gov/data/pix* Jan 1998.

Rabl, A (1985) Active Solar Collectors and Their Applications New York: Oxford.

RCLSGI (1997) "Heat Pump Theory" Robinson Computer Lab, Ohio State University *http://rclsgi.eng.ohio-state.edu/~christ/~r/~ceat/~theory.html*

Rutgers (1997) "The Busch Cogeneration Project" *http://www.rci.rutgers.edu* Nov 1997.

SAIC (1997a) "Low Cost Heliostats for Power Tower Systems" Science Applications International Corporation (brochure).

SAIC (1997b) "Solar Dish/Stirling Power Systems" Science Applications International Corporation (brochure).

SAIC (1997c) "Solar Detoxification of Soil System" Science Applications International Corporation (brochure).

Segal, A and M Levy (1993) Solar Chemical Heat Pipe in Closed Loop Operation: Mathematical Model and Experiments *Solar Energy* **V** 51 pp. 367-376.

Schiel, W *et al* (1994) Evaluation of the 9-KWe Dish / Stirling System of Schlaich Bergermann und Partner using the Proposed IEA Dish / Stirling Performance Analysis Guidelines. *American Institute of Aeronautics and Astronautics* 1994 (IECEC?) conference proceedings pp. 1725-1729.

Smith (1994) Value of Solar Thermal & PV to Arizona Public Service Company *ASME Solar Engineering 1994* v 1 p 617.

Stine, W and R Diver (1997) "A Compendium of Solar Dish / Stirling Technology" *http://solstice.crest.org* Dec 1997.

Sunlab (1996) "Solar Two: Utility-Scale Power from the Sun" Sunlab: a joint project of NREL and Sandia Lab (brochure dated Feb 1996).

Thompson, M (1997) Private Communication with Mike Thompson at Trane, Inc., Nov 1997.

Trane (1996) "Trane Horizon Absorption Series: Two-Stage Steam Fired Absorption Water Chillers 380-750 Tons" The Trane Company (company publication ABS-DS-4).

Weinrebe, G *et al* (1996) On the Performance of the ASM 150 Stretched Membrane Heliostat *Solar Engineering (ASME Conference 1996)* pp.113-117.

Wenger, H *et al* (1997) A Case Study if Utility PV Economics *Solar Engineering (ASES / ASME Conference 1997).*

Wenglarz, R (1997) Private Communication with Richard Wenglarz at the Allison Engine Company, Dec 1997.

White, F M (1994) Fluid Mechanics (3^{rd} ed.) New York: McGraw-Hill.

Yazaki (1984) "Yazaki Gas and Solar Air Conditioning Equipment" Yazaki (brochure).

Zaibel, R *et al* (1995) An Astigmatic Corrected Target-Aligned Heliostat for High Concentration *Solar Energy Materials and Solar Cells* **V** 37 pp. 191-202.

APPENDIX A: Selected Equations and Functions

A.1: Gas Turbine Equations

The gas turbine modeling is described in chapter 3 of the text. It follows standard (theoretical) thermodynamics. Gas properties vary, but only on an *average* basis (that is, the gas properties for a given process, whether compression, expansion, or heat transfer, are determined by the average of the beginning and ending temperatures and compositions for that process). Following Gas Turbine Theory (Cohen *et al* 1996 p. 57), Cp and γ are given fixed values, but these values are different for compression and expansion processes, as shown below. For heat transfer and combustion processes, two parametric relationships were devised based upon figure 2.15 (p.59) in Cohen *et al*; one relationship is derived using an average inlet temperature of 900 K to represent recuperated combustion chambers, and the other is derived using an average inlet temperature of 700 K to represent open-cycle combustion chambers. Both relationships assume 98% combustion, again following Cohen *et al*. These functions are COMBUSTR and COMBUSTO and they are also detailed below.

Notation:

P_C = Compressor Pressure Ratio, pre-defined
P_T = Turbine Pressure Ratio, pre-defined.

Note: there is a pressure drop in the MPT in solar operation, and in the ASDB at all times. This drop means that P_T does not always equal P_C. (In addition, there are recuperator pressure drops in the RGT MPT and in the ASDB, further reducing P_T relative to P_C). Furthermore, in the MPT, the gas turbine temperature and efficiency calculations yield two different sets of results, depending on whether the system is in hybrid (solar) mode or gas-only mode. These twin sets of results are explained in the text; no differentiation is necessary here, but it should be understood that η can take two values for the MPT.

γ = gas constant = 1.4 for compressors; 1.33 for turbines
$\lambda = (\gamma - 1) / \gamma$; λ_C = for compressor conditions; λ_T = for turbine conditions
Cp = specific heat = 1.005 for compressors (Cp_C); 1.150 for turbines (Cp_T)
η = thermal to mechanical efficiency
ρ = recuperator effectiveness (90% throughout for both ASDB and RGT MPT)

(all degrees K:)
AT = ambient temperature (t1), usually defined
CET = compressor exit temperature (t2), usually calculated
    CRET = compressed (high pressure) side recuperator exit temperature
TIT = turbine inlet temperature (t3), usually defined
TET = turbine exit temperature (t4), usually calculated
    RET = recuperator exit temperature, low pressure side

Heat input required during combustion processes:

Open cycle: COMBUSTO (t2,t3) = .98 * (1.29 * (t3-t2) - 21.5) kJ / kg
Recup cycle: COMBUSTR (t2,t3) = .98 * (1.29 * (t3-t2) - 43.0) kJ / kg

Open Cycle Calculations:

[A.1] $CET = AT * P_C^{\lambda_C}$

[A.2] Fuel Required = COMBUSTO(CET,TIT)

[A.3] $TET = TIT / P_T^{\lambda_T}$

[A.4] $\eta = [((TIT - TET) * Cp_T) - ((CET - AT) * Cp_C)] / (\text{Fuel Required})$

Recuperated Cycle Calculations:

[A.5] $CET = AT * P_C^{\lambda_C}$

[A.6] $CRET = CET + \rho * (TET - CET)$

[A.7] Fuel Required = COMBUSTR(CRET,TIT)

[A.8] $TET = TIT / P_T^{\lambda_T}$

[A.9] $RET = TIT - \rho * (TET - CET)$

[A.10] $\eta = [((TIT - TET) * Cp_T) - ((CET - AT) * Cp_C)] / (\text{Fuel Required})$

A.2 Natural Gas Heat Content

Lower Heating Value (water vapor in exhaust not condensed):

21,501 BTU/lb 50,012 kJ/kg

Higher Heating Value (including latent heat of water vapor in exhaust):

23,860 BTU/lb 55,499 kj/kg

A.3: Pipe Flow Equations

Pipe flow does not play a major role in the modeling; it is only relevant to appendix D, the (aborted) study of the LDA piping problem.

Notation:

ΔP = pressure drop in pipe, pascales
ρ = density of fluid (air) in the pipe, kg / m^3
d = diameter of the pipe, meters
f = Darcy friction factor, dimensionless
L = length of the pipe, meters
V = fluid velocity, m/s
g = gravitational constant (used for Moody chart unit conversions), 9.8 m/s^2
ε = pipe roughness, cm (see e.g. White 1994 for values as a function of material)
rr = relative roughness
μ = viscosity, s/m^2
Re = Reynold's number

In order to find total pressure drop using the Moody chart (found in any basic fluid mechanics text, e.g. White 1994), which is a compilation of empirical flow relationships for various regimes, the relative roughness and Reynold's number must be calculated:

[A.11] $Re = (V * d) / \mu$

[A.12] $rr = \varepsilon/d$

Entering the Moody chart with Re and rr, we will find f, the Darcy friction factor, which is related to the flow parameters as follows:

[A.13] $f = (2 * \Delta P * d) / (L * V^2 * \rho)$

Re-arranging for the pressure drop and converting to bars yields:

[A.14] $\Delta P, \text{bars} = (f * L * V^2 * \rho) / (2 * d * 100{,}000)$

APPENDIX B: Sun Position Table and Climate Data

This appendix contains two figures, found on the following pages:

Figure B-1: This figure is a sun position chart used for the annual performance calculations as described in the text. It is generated as part of the model; the latitude is input as a function of location (Dagget, Tampa, Pueblo, or Atlantic City) and then the model steps through an entire year in 165 minute increments. The sun positions are divided up into 5-degree by 5-degree squares of elevation (phi, zeroed at the horizon) and azimuth (theta, zeroed at due north).

Figure B-2: Climate data for the four locations. See chapter 3 for explanation and source.

FIGURE B-1

Range of Application: 25 to 60 degrees north latitude:
Daylight Hours: 4381 hours

TEMPORAL RESOLUTION: 365 DAYS / 15 MINUTE INCREMENT
CURRENT LATITUDE: 35 deg N

365 **PHI*:** Table Tot: 1

TABLE IS NORMALIZED

THETA*:	2.5	7.5	12.5	17.5	22.5	27.5	32.5	37.5	42.5	47.5	52.5	57.5	62.5	67.5	72.5	77.5
45																
55																
65																
75	0.006391															
85	0.009473	0.011242	0.003424													
95	0.007761	0.008046	0.011927	0.008731	0.00194											
105	0.007076	0.005193	0.005022	0.005764	0.008902	0.003367										
115	0.005364	0.011071	0.008046	0.007304	0.007647	0.011984	0.008902	0.002168								
125		0.001198	0.009644	0.008845	0.006962	0.006791	0.00759	0.011641	0.009815							
135				0.006505	0.005592	0.004337	0.004052	0.004394	0.005478	0.00856	0.002739					
145					0.009416	0.008274	0.006049	0.005649	0.005878	0.006734	0.010842	0.009073	0.000571			
155						0.009986	0.007361	0.005535	0.005136	0.005136	0.005421	0.006619	0.010386	0.006905		
165						0.001484	0.007475	0.003995	0.003253	0.003196	0.003081	0.00331	0.003709	0.005307	0.006848	
175							0.011242	0.006334	0.005022	0.004679	0.004451	0.004508	0.004622	0.005421	0.007647	0.00856
185							0.011242	0.006334	0.005022	0.004679	0.004451	0.004508	0.004622	0.005421	0.007647	0.00856
195						0.001484	0.007475	0.003995	0.003253	0.003196	0.003081	0.00331	0.003709	0.005307	0.006848	
205						0.009986	0.007361	0.005535	0.005136	0.005136	0.005421	0.006619	0.010386	0.006905		
215					0.009416	0.008274	0.006049	0.005649	0.005878	0.006734	0.010842	0.009073	0.000571			
225				0.006505	0.005592	0.004337	0.004052	0.004394	0.005478	0.00856	0.002739					
235		0.001198	0.009644	0.008902	0.006905	0.006791	0.00759	0.011641	0.009815							
245	0.005364	0.011071	0.008046	0.007304	0.007647	0.011984	0.008902	0.002168								
255	0.007076	0.005193	0.005022	0.005764	0.008902	0.003367										
265	0.007761	0.008046	0.011927	0.008731	0.00194											
275	0.009473	0.011242	0.003424													
285	0.006391															
295																
305																
315																

---

* the bins are centered at the values in the axis and abcissa

FIGURE B-2

Latitude	39.5	28	38	35
"EARTH" constant, found by trial & error (see text)	685	690	885	970
Place	Atlantic City	Tampa	Pueblo	Dagget
Average high, hottest month	29.2	32.3	33.9	39.9
Record high, hottest month	40.0	36.7	41.1	46.7
Average low, hottest month	18.3	23.6	16.2	23.3
Annual HDD (heating degree days, 18.3 C base)	2872	403	3007	1106
Annual CDD (cooling degree days, 18.3 C base)	459	1887	541	1659
AVERAGE DAILY FLUXES, BY MONTH:	Daily Flux, kwh	Daily Flux, kwh	Daily Flux, kwh	Daily Flux, kwh
1	2.9	4.0	4.8	5.4
2	3.4	4.5	5.2	5.9
3	3.9	5.1	5.7	6.9
4	4.2	5.9	6.5	8.1
5	4.3	5.4	6.6	8.9
6	4.7	4.5	7.6	9.7
7	4.5	4.0	7.4	9.0
8	4.4	3.9	6.9	8.7
9	4.1	3.8	6.6	8.2
10	3.9	4.5	6.2	7.3
11	3.0	4.3	4.9	6.0
12	2.6	4.0	4.6	5.4

AVG DAILY HIGH/LOW TEMPS BY MONTH:	High	Low	High	Low	High	Low	High	Low
1 (degrees C)	4.7	-5.9	21.0	10.0	7.4	-9.9	15.9	2.6
2	5.8	-4.7	21.9	10.9	10.4	-6.9	18.9	5.2
3	10.9	-0.4	24.8	13.6	14.0	-3.3	21.4	7.8
4	15.9	4.1	27.6	16.0	19.9	2.1	25.6	10.8
5	21.8	9.8	30.7	19.7	24.7	7.6	30.8	15.3
6	26.7	14.8	31.9	22.7	30.9	12.3	36.6	19.7
7	29.2	18.2	32.3	23.6	33.9	16.2	39.9	23.3
8	28.5	17.5	32.3	23.6	32.1	15.0	38.6	22.7
9	24.8	13.1	31.7	22.7	27.4	10.1	34.3	18.7
10	18.9	6.5	29.1	18.4	21.4	2.6	28.2	13.1
11	13.2	2.1	25.4	14.0	13.8	-4.3	20.8	6.9
12	7.4	-3.2	22.3	11.3	8.2	-9.2	15.8	2.6

APPENDIX C: Complete Spreadsheet Model

This appendix contains the complete spreadsheet model, minus the figures (which appear in the text) and the climate data and solar position table (which appear in appendix B). Thirteen elements remain:

1. "H" (a), the heliostat model input and output page
2. "H" (b), the complete listing of each heliostat and its properties (for a typical field)
3. "Blocks", the blocking page where the blockages for each heliostat are listed ("")
4. "TRC", the page where the TERC calculations are performed
5. "Engine", the page where the engine calculations are performed
6. "D", the dish model input and output page
7. "Func", containing functions created for this model
8. "H Prog", containing the programs (Visual Basic) for the Heliostat Model
9. "D Prog", containing the programs (Visual Basic) for the Dish Model
10. "S Prog", containing the programs (Visual Basic) for the Solar Position Table
11. "RGT", where the creation of the MPT RGT is developed mathematically
12. "Buy Down", where the MPT buy down costs are calculated
13. "Fuel Risk", where the Awerbuch fuel risk adjustment is calculated

NOTE: These pages are miniaturized and are included here only for thoroughness. The text is intended to read clearly **without any need to refer to this appendix**.

Heliostat Field Simulation

All angles are relative to 0 degrees at due NORTH

INPUTS:

	THEIGHT	**70**	meters	Tower Height ***changing THEIGHT (or any new field) requires a new run of "Find Blockers"***
	MTHW	**3**	meters	Mean Tower Half-Width (radius). Tower shading is based on a rectangular model.
	MDIAM	**3**	meters	diameter of heliostat modules -- these are perfectly round and focused on the receiver.
	MNUM	**6**		# of modules per heliostat. Must be even
	HAREA	42.41	m^2	Total heliosat area. The heliostat is focused ("canted") on the receiver less a 5% error.
	HX	9.03	meters	X dimension of SAIC-type heliostat defined above. 5 per side> 2 rows, 10 > 3 rows, 20 > 4
	HY	9	meters	Y dimension of SAIC-type heliostat defined above
	XFOOT	**16**	meters	Footprint, max: **twice HX** Balance against blocking and shading
	YFOOT	**14**	meters	Footprint, suggestion: HY+2m. Balance against blocking.
	FRAD	**200**	meters	Field Radius (really just the outer limit of distances from the tower to scan for inclusion.)
	PRAD	**15**	meters	Plant Radius (blank space in the middle of field)
	CRA	**45**	degrees	Rim Angle Used in Field construction, as seen from due north bearing (180 = round field)
	ROE	**90%**		Mirror Specular Reflectivity
	SECCON	**1**	(switch)	If =1, a secondary TERC is used. TERC used is **only valid for RIM around 40 degrees**
	WINDOW	**1**	(switch)	If = 1, a windowed receiver is in use, and EWREF is nonzero
	DIFEED	**5.00**		Diameter Feed for non-secondary systems -- in effect only if SECCON != 1
	TERC	**1**	(switch)	If = 1, the 49.6 degree TERC is used... if = 2, the 35 degree TERC is used.
	TROE	**93.0%**		Reflectivity of the TERC
	SHA	**0.0100**	radians	Includes mirror errors. The true Solar Half Angle is 4.7 mrads. Quite important.
3.91891	MAXTEMP	**750**	C	Max Operating temperature of receiver in celsius, with phi~75, theta~180
4.17255	RECCAL	7.463	MWt	corresponding net DMW for calibration. **Automatically set by annual program.**
2.188	MWREF	**5.0%**		Max Window Reflectivity: this is at 0 degrees rim angle and decreases linearly with rim angle.
132	FAARA	**20**	degrees	Full Acceptance Rim Angle -- beyond this, EWREF is 0. See Kribus (1994) "Optical Performance..."
0.81376	WTFEED	**38.20%**		Average Window Transmittance in the IR. Set constant at BelowCut(4,600,1000) or model won't run
341.66	ECLC	**0.00**	W/mK	Effective Convection Loss Coefficient over the window or aperture of size DIAPE2.
	PHIS	**77.5**	degrees	phi, solar degrees above horizon
	THS	**175**	degrees	theta, solar degrees from due north = 0
		c/o EARTH	970	Earth Constant (copied from Sun page)
		coSOLCON	1350	Solar Constant (copied from Sun page)
		c/o SPOT	Dagget	(copied from Sun page)

Engine Control:

	MODE	**ogt**		(One of: OGT=open gas turbine with cogen, RGT=regenerated gas turbine)
	PR	**10.1**		Compression Ratio
	RPR	**2.7**		Compression Ratio, RGT
	TIT	**1077**	C	Gas Turb Inlet Temp:
	RTIT	**817**	C	Gas Turbine Inlet Temp, RGT
	Cn	**78.2%**		Compressor Isentropic Effic
	Tn	**89.2%**		Turbine Isentropic Effic
	RCn	**73.2%**		Same as above, but
	RTn	**93.4%**		these are for the MPT RGT turbine
	GREFF	**95.0%**		Generator Efficiency
	REGEN	**90.0%**		Recuperator Effectiveness
	TOWDROP	**5.0%**		Combined tower ducting (if any) and receiver pressure drop for heliostat MPT system.
	RETLOSS	**10.0%**		Return line loss, as a fraction of the difference between chiller output and ambient. Used to find WIT.
	CHILLOUT	**165**	C	Chiller Water Exit Temperature.
	RPDROP	**3%**		Regenerator pressure drop, high pressure side, percentage
	RPDROP2	**3%**		Regenerator pressure drop, low pressure side, percentage

These figures are in the gas-only mode:

To mimic:

	Cn	Tn	TIT	HP	Discharge	n, post-gen	at AT=
KW/M1A-1	0.710	0.893	910	9.3	459	23.4	15
501 KB5	0.782	0.892	1077	10.1	549	28.7	15
501 KB3	0.924	0.818	1016	9.3	566	26.0	15
MPT RGT	0.732	0.934	817	2.7	191	35.4	15

Once again, Cn includes all and any inlet losses, filters, etc, and also represents pressure losses in the engine (because Tn is determined first in this case)

c/o GASEFF: 28.50% w/o generator: 30.0% c/o AT: 19.8 C

PHASE 1 OUTPUTS (instant values -- from field building):

Shading Constants For This Field: (northern lats only)

			Adj. S:		bearing	from ths	range	b	hor frac	a	v frac	shaded
			8.33	SH1	270.0	95.0	16.0	15.9	0.0%	1.4	0.0%	0.0%
				SH2	209.7	34.7	16.1	9.2	0.0%	13.2	0.0%	0.0%
				SH3	150.3	24.7	16.1	6.7	19.0%	14.6	0.0%	0.0%
				SH4	90.0	85.0	16.0	15.9	0.0%	1.4	0.0%	0.0%

AVHZBS	46.3%		Average horizontal blocking and shading overlap (if there is one at all, depending on vertical). Also known as MHO.
ATTBASE	0.719		Attenuation Base - this is derived from earth and solar constants and is raised to 1/sin(phis) in various places to calculate insolation
NHSTAT	132		# of heliostats
TOTA	5598	m^2	Total maximum aperture area; this is also the **total mirror area** of the heliostats
EMW	5.387	MWt	Light falling on this area of flat mirrors, with atmospheric attenuation, in a 1 kW max regime
YCENT	33.7	meters	point on Y-axis which marks the "center" of the field **as seen from the tower.** Puts top hstat at CRA
RCENT	77.7	meters	Range to the center, as the center is seen from the tower.
RIM	45.0	deg	Rim angle used (maximum of N/S or E/W. Equalizing these will help -- round aperture)
ARA	31.8	deg	Average Rim Angle (geometric average)
EWREF	0.29%		Effective Window Reflectivity for this field.
EWTRA	38.2%		Effective Window Transmittance (in the IR bands) for re-radiation. Equal to 100% if there is no window.
TBBMW	4.493	MWt	Transmitted Before Blocking & Shading (including tower shading) is counted
TMW	4.337	MWt	Transmitted MWt (strikes the receiver but not necessarily admitted)
BEFF	96.5%		Blocking&Shading Efficiency: this is the fraction of light not shaded (by mirrors or tower) before mirrors nor blocked after mirrors
EFF	92.7%		Optical efficiency (hstats versus an ideal dish without blockage from the focal point receiver - does **not** include roe or heliostat blockage)
c/o DIAPE1	18.33	meters	Outer (Secondary) Aperture Diameter
c/o DIAPE2	1.69	meters	Inner (Absorber) Aperture Diameter
c/o SCOND	6.99	meters	depth of TERC
c/o SCONA	341.66	m^2	area of secondary concentrator (TERC)
ETREF	3.15%		Effective Terc Reflective Losses; funtion of TROE and T_DIR
RMW	4.188	MWt	INSTANT Received MWt: this passes the aperture. includes misses, window reflections, and TERC reflections.
EFF2	96.6%		Aperture Efficiency (instant efficiency of the outer aperture at this angle. **Includes** Reflection Losses on the Secondary (TERC)
RECTEMP	586	deg C	Maximum instant receiver exit temperature. Based on rectemp calibration above.
RADMW	0.016	MWt	Re-radiated megawatts; does not include any convection losses at window/aperture DIAPE2
EFF3	77.46%		(instant solar to thermal efficiency at this aperture and angle. Mirror area basis)
	77.46%		(check using efficiencies)

PHASE 2 OUTPUTS (from annual calculations):

HOURS	4065	hours	Time when sun is up AND positive heat flow is possible; used for totaling calculations	-80.00	-24.00
ANNEMW	7.756	MWt	Annual Insolation falling on FLAT mirrors, time-weighted average		
ANNTBBMW	6.360	MWt	Annual Transmitted MWt, before tower shdaing, mirror shading, and miror blocking	28148.67	m^2
ANNTMW	5.176	MWt	Actual Transmitted MWt, reaching the receiver	10000.33	
ANNRMW	4.998	MWt	Annual Average Megawatts actually passing the aperture. Includes aperture misses and reflections.	2.814773	m^2, limit
PKDMW	7.472	MWt	Peak Delivered Megawatts: annual RMW peak less RADMW	1.893114	diape2 in limit
ANNRADMW	0.021	MWt	Annual average megawatts re-radiated from the aperture	4.021105	m^2, 70% limit
ANNDMW	4.977	MWt	Annual Average Delivered Megawatts	2.262704	diape2 at 70% limit
HEAT	20231	MWHt	Total, net, annual delivered heat		
ANNBEFF	81.4%		ANNUAL Blocking & Shading Efficiency, fraction of transmitted light which is not blocked nor shaded.		
ANNUAL	91.1%		ANNUAL Heliostat Efficiency, **not** including mirror reflectivity **not** including blocking & shading		
APEEFF	96.6%		ANNUAL Aperture Efficiency.		
RECEFF	99.6%		ANNUAL Receiver Efficiency.		
STEFF	64.2%		ANNUAL Solar to Thermal Efficiency. Does not include convection. MIRROR AREA BASIS		
(check)	64.2%		(same thing, power based instead of multiplying efficiencies)		
HEFF	17.6%		**ANNUAL Solar to Electric Efficiency, Mirror Area Basis**		
HGTRATING	3.919	MWe	Gas **T**urbine Rating		
TOTHEAT	122,721	MWHt	Total heat required, based upon HGTRATING, GASEFF, GTEFF, and HOURS		
HSF	16.5%		Heliostat Annual Solar Fraction (at turbine inlet)		
HADJEFF	25.6%		Adjusted "Raw Form to Electric" Efficiency to reflect combined solar and gas operations.		
WIT	150	C	Water Inlet Temperature at Heat Recovery System.		
FLCGREFF	77%		Instant cogen gas replacement efficiency, at full-load (assumes that heat trasfer effectiveness = burner effectiveness)		
CGREFF	32.4%		Cogen Gas Replac. Effic; fraction of turbine exhaust heat which replaces gas on an annual basis		
CADJEFF	32.6%		Cogeneration Adjusted "Raw Form" Efficiency. Tricky but accurate		
CADJGEFF	37.1%		Cogeneration Adjusted Efficiency, When Running in Gas Only Mode		
TAGR	102,490	MWht, LH\	True Annual Gas Requirement before any cogenration adjustment		
AGS	28,020	MWht, LH\	Annual Gas Savings from cogeneration, if any		
AGR	74,470	MWht, LH\	Annual Gas Requirement, after cogeneration adjustment, if any		
AGSPER	27.3%		Annual Gas Savings from Cogen, as a percentage of total gas originally needed		
c/o MODE	ogt		(copied from Dish Model; ogt = open cycle rgt = recuperated cycle)		
c/o GASEFF	28.5%		Gas Turbine Efficiency, copied from Engine Model, Gas-only operation		
c/o GTEFF	27.4%		Gas Turbine Efficiency, copied from Engine Model, Solar & Hybrid operation		
c/o CCF	42.3%		Cogeneration Capacity Factor; Computed in Solar Data Spreadsheet ***DO NOT CHANGE THESE FORMULAE WITHOUT CHANGING THE PROGRAMMING TOO!***		

It is imperative that the entire row below the header row be left blank for table clearing!!

Hstat #	x	y	Range, m	TH, degs	Towr Angl	Cos (Eps)	Epsilon	Rim, deg	Shaded	Blocked	XMIT,KWt	adj focus - m	fs m	ft m	corr hs m	corr ht m	Area of Elli m	Rect. appr Area Cov.	Received KWt	Before Blocking BB,KWt
1	0.00	200.00	200.00	180.00	19.29	0.526	58.26	45.00	0.0%	10.0%	28.86	201.30	230.45	175.84	6.273	7.396	36.436	100.0%	28.86	32.08
2	-40.00	186.00	190.25	167.86	20.20	0.539	57.41	44.83	0.0%	15.3%	27.30	192.59	219.57	168.92	5.985	7.108	33.415	100.0%	27.30	32.22
3	-24.00	186.00	187.54	172.65	20.47	0.544	57.04	44.10	0.0%	11.0%	28.73	190.17	216.44	167.09	5.850	6.964	31.999	100.0%	28.73	32.27
4	-8.00	186.00	186.17	177.54	20.61	0.546	56.91	43.72	0.0%	9.0%	29.38	188.95	214.91	166.13	5.785	6.894	31.325	100.0%	29.38	32.29
5	8.00	186.00	186.17	182.46	20.61	0.544	57.01	43.72	0.0%	9.0%	29.37	188.95	215.02	166.05	5.790	6.899	31.374	100.0%	29.37	32.28
6	24.00	186.00	187.54	187.35	20.47	0.539	57.35	44.10	0.0%	10.9%	28.70	190.17	216.76	166.85	5.865	6.979	32.150	100.0%	28.70	32.22
7	40.00	186.00	190.25	192.14	20.20	0.531	57.91	44.83	0.0%	15.2%	27.26	192.59	220.10	168.51	6.011	7.133	33.671	100.0%	27.26	32.14
8	-48.00	172.00	178.57	164.41	21.41	0.554	56.33	44.12	0.0%	15.9%	27.24	182.21	206.69	160.64	5.607	6.724	29.611	100.0%	27.24	32.38
9	-32.00	172.00	174.95	169.46	21.81	0.563	55.76	43.06	0.0%	11.9%	28.62	179.01	202.52	158.24	5.427	6.531	27.836	100.0%	28.62	32.47
10	-16.00	172.00	172.74	174.69	22.06	0.567	55.44	42.38	0.0%	8.2%	29.85	177.07	200.02	156.74	5.320	6.416	26.809	100.0%	29.85	32.51
11	0.00	172.00	172.00	180.00	22.15	0.568	55.41	42.14	0.0%	8.2%	29.84	176.41	199.26	156.19	5.288	6.381	26.501	100.0%	29.84	32.52
12	16.00	172.00	172.74	185.31	22.06	0.564	55.67	42.38	0.0%	8.2%	29.82	177.07	200.23	156.58	5.331	6.426	26.905	100.0%	29.82	32.48
13	32.00	172.00	174.95	190.54	21.81	0.556	56.20	43.06	0.0%	12.1%	28.47	179.01	202.94	157.91	5.448	6.551	28.031	100.0%	28.47	32.40
14	48.00	172.00	178.57	195.59	21.41	0.545	56.98	44.12	0.0%	15.8%	27.19	182.21	207.32	160.15	5.639	6.754	29.913	100.0%	27.19	32.28
15	-56.00	158.00	167.63	160.48	22.66	0.570	55.28	43.57	0.0%	16.0%	27.32	172.58	194.81	152.88	5.268	6.380	26.398	100.0%	27.32	32.54
16	-40.00	158.00	162.98	165.79	23.24	0.582	54.44	42.10	0.0%	12.2%	28.68	168.51	189.50	149.85	5.037	6.132	24.257	100.0%	28.68	32.66
17	-24.00	158.00	159.81	171.36	23.65	0.590	53.87	41.03	0.0%	8.8%	29.86	165.75	185.92	147.76	4.883	5.966	22.881	100.0%	29.86	32.74
18	-8.00	158.00	158.20	177.10	23.87	0.593	53.64	40.47	0.0%	6.9%	30.52	164.35	184.16	146.67	4.808	5.886	22.227	100.0%	30.52	32.78
19	8.00	158.00	158.20	182.90	23.87	0.591	53.77	40.47	0.0%	6.9%	30.50	164.35	184.26	146.59	4.814	5.891	22.273	100.0%	30.50	32.76
20	24.00	158.00	159.81	188.64	23.65	0.584	54.24	41.03	0.0%	9.0%	29.74	165.75	186.22	147.52	4.900	5.982	23.020	100.0%	29.74	32.69
21	40.00	158.00	162.98	194.21	23.24	0.573	55.03	42.10	0.0%	12.1%	28.64	168.51	190.01	149.45	5.065	6.158	24.495	100.0%	28.64	32.57
22	56.00	158.00	167.63	199.52	22.66	0.558	56.09	43.57	0.0%	15.8%	27.28	172.58	195.53	152.31	5.307	6.417	26.746	100.0%	27.28	32.42
23	-64.00	144.00	157.58	156.04	23.95	0.583	54.31	43.28	0.0%	15.3%	27.67	163.81	184.10	145.75	4.976	6.086	23.784	100.0%	27.67	32.68
24	-48.00	144.00	151.79	161.57	24.76	0.600	53.13	41.32	0.0%	11.6%	29.04	158.79	177.54	142.03	4.687	5.776	21.261	100.0%	29.04	32.85
25	-32.00	144.00	147.51	167.47	25.39	0.612	52.24	39.75	0.0%	8.7%	30.10	155.11	172.76	139.28	4.480	5.552	19.535	100.0%	30.10	32.98
26	-16.00	144.00	144.89	173.66	25.79	0.620	51.72	38.72	0.0%	5.9%	31.10	152.86	169.87	137.56	4.356	5.419	18.543	100.0%	31.10	33.05
27	0.00	144.00	144.00	180.00	25.92	0.621	51.63	38.37	0.0%	6.0%	31.09	152.11	168.97	136.93	4.319	5.379	18.245	100.0%	31.09	33.06
28	16.00	144.00	144.89	186.34	25.79	0.616	51.99	38.72	0.0%	6.1%	30.99	152.86	170.07	137.40	4.368	5.431	18.630	100.0%	30.99	33.01
29	32.00	144.00	147.51	192.53	25.39	0.605	52.77	39.75	0.0%	8.6%	30.06	155.11	173.15	138.96	4.503	5.575	19.715	100.0%	30.06	32.90
30	48.00	144.00	151.79	198.43	24.76	0.589	53.90	41.32	0.0%	11.4%	29.00	158.79	178.14	141.55	4.722	5.809	21.542	100.0%	29.00	32.74
31	64.00	144.00	157.58	203.96	23.95	0.569	55.29	43.28	0.0%	15.0%	27.65	163.81	184.92	145.11	5.022	6.130	24.179	100.0%	27.65	32.54
32	-72.00	130.00	148.61	151.02	25.22	0.595	53.49	43.34	0.0%	14.2%	28.15	156.05	174.75	139.36	4.740	5.852	21.784	100.0%	28.15	32.80
33	-56.00	130.00	141.55	156.70	26.31	0.617	51.90	40.84	0.0%	9.8%	29.80	150.02	166.84	134.89	4.386	5.472	18.852	100.0%	29.80	33.03
34	-40.00	130.00	136.01	162.90	27.23	0.635	50.59	38.65	0.0%	7.0%	30.87	145.32	160.73	131.39	4.118	5.183	16.766	100.0%	30.87	33.21
35	-24.00	130.00	132.20	169.54	27.90	0.647	49.66	37.00	0.0%	5.3%	31.58	142.11	156.58	128.97	3.939	4.990	15.438	100.0%	31.58	33.33
36	-8.00	130.00	130.25	176.48	28.26	0.653	49.25	36.10	0.0%	3.9%	32.08	140.47	154.52	127.70	3.852	4.895	14.809	100.0%	32.08	33.39
37	8.00	130.00	130.25	183.52	28.26	0.651	49.40	36.10	0.0%	3.9%	32.06	140.47	154.62	127.62	3.858	4.901	14.851	100.0%	32.06	33.37
38	24.00	130.00	132.20	190.46	27.90	0.641	50.12	37.00	0.0%	5.2%	31.55	142.11	156.87	128.73	3.958	5.007	15.565	100.0%	31.55	33.27
39	40.00	130.00	136.01	197.10	27.23	0.625	51.31	38.65	0.0%	6.9%	30.84	145.32	161.22	130.99	4.149	5.212	16.985	100.0%	30.84	33.11
40	56.00	130.00	141.55	203.30	26.31	0.604	52.87	40.84	0.0%	9.6%	29.73	150.02	167.53	134.33	4.429	5.513	19.176	100.0%	29.73	32.89
41	72.00	130.00	148.61	208.98	25.22	0.578	54.66	43.34	0.0%	13.7%	28.15	156.05	175.66	138.63	4.794	5.904	22.230	100.0%	28.15	32.63
42	-80.00	116.00	140.91	145.41	26.42	0.603	52.92	43.89	0.0%	9.6%	29.71	149.47	166.96	133.81	4.571	5.692	20.435	100.0%	29.71	32.88
43	-64.00	116.00	132.48	151.11	27.85	0.631	50.87	40.82	0.0%	7.2%	30.80	142.35	157.63	128.55	4.146	5.234	17.046	100.0%	30.80	33.17
44	-48.00	116.00	125.54	157.52	29.14	0.656	49.02	37.92	0.0%	3.8%	32.15	136.55	150.07	124.24	3.810	4.871	14.574	100.0%	32.15	33.42
45	-32.00	116.00	120.33	164.58	30.19	0.675	47.55	35.46	0.0%	2.6%	32.73	132.25	144.52	121.03	3.567	4.607	12.906	100.0%	32.73	33.61
46	-16.00	116.00	117.10	172.15	30.87	0.686	46.65	33.78	0.0%	2.4%	32.93	129.60	141.14	119.01	3.421	4.449	11.955	100.0%	32.93	33.73
47	0.00	116.00	116.00	180.00	31.11	0.689	46.45	33.18	0.0%	3.1%	32.72	128.71	140.06	118.28	3.377	4.400	11.669	100.0%	32.72	33.75
48	16.00	116.00	117.10	187.85	30.87	0.682	47.00	33.78	0.0%	2.4%	32.87	129.60	141.32	118.86	3.434	4.461	12.033	100.0%	32.87	33.68
49	32.00	116.00	120.33	195.42	30.19	0.666	48.22	35.46	0.0%	2.5%	32.70	132.25	144.89	120.71	3.592	4.632	13.068	100.0%	32.70	33.52
50	48.00	116.00	125.54	202.48	29.14	0.643	49.97	37.92	0.0%	3.5%	32.13	136.55	150.65	123.77	3.848	4.907	14.832	100.0%	32.13	33.29
51	64.00	116.00	132.48	208.89	27.85	0.615	52.05	40.82	0.0%	6.7%	30.79	142.35	158.41	127.91	4.198	5.283	17.416	100.0%	30.79	33.00
52	80.00	116.00	140.91	214.59	26.42	0.584	54.29	43.89	0.0%	9.2%	29.68	149.47	167.97	133.01	4.635	5.753	20.939	100.0%	29.68	32.68
53	-72.00	102.00	124.85	144.78	29.28	0.641	50.16	41.43	0.0%	3.1%	32.24	135.98	150.14	123.16	3.981	5.077	15.872	100.0%	32.24	33.27

54	-56.00	102.00	116.36	151.23	31.03	0.673	47.70	37.79	0.0%	0.0%	33.59	129.00	141.05	117.99	3.567	4.629	12.969	100.0%	33.59	33.59
55	-40.00	102.00	109.56	158.59	32.57	0.701	45.53	34.37	0.0%	0.0%	33.87	123.51	133.95	113.89	3.251	4.285	10.941	100.0%	33.87	33.87
56	-24.00	102.00	104.79	166.76	33.74	0.720	43.91	31.61	0.0%	0.0%	34.07	119.72	129.08	111.03	3.037	4.053	9.669	100.0%	34.07	34.07
57	-8.00	102.00	102.31	175.52	34.38	0.730	43.12	30.04	0.0%	0.4%	34.02	117.77	126.63	109.53	2.932	3.939	9.071	100.0%	34.02	34.16
58	8.00	102.00	102.31	184.48	34.38	0.727	43.33	30.04	0.0%	0.4%	34.01	117.77	126.72	109.45	2.939	3.945	9.107	100.0%	34.01	34.14
59	24.00	102.00	104.79	193.24	33.74	0.713	44.50	31.61	0.0%	0.0%	33.99	119.72	129.35	110.80	3.058	4.073	9.780	100.0%	33.99	33.99
60	40.00	102.00	109.56	201.41	32.57	0.689	46.45	34.37	0.0%	0.0%	33.75	123.51	134.41	113.51	3.285	4.318	11.138	100.0%	33.75	33.75
61	56.00	102.00	116.36	208.77	31.03	0.657	48.89	37.79	0.0%	0.0%	33.44	129.00	141.71	117.44	3.614	4.674	13.268	100.0%	33.44	33.44
62	72.00	102.00	124.85	215.22	29.28	0.622	51.57	41.43	0.0%	2.6%	32.21	135.98	151.01	122.44	4.041	5.134	16.295	100.0%	32.21	33.07
63	-80.00	88.00	118.93	137.73	30.48	0.644	49.94	42.81	0.0%	1.3%	32.85	131.10	144.61	118.85	3.905	5.019	15.395	100.0%	32.85	33.30
64	-64.00	88.00	108.81	143.97	32.75	0.684	46.83	38.51	0.0%	0.0%	33.70	122.91	133.94	112.79	3.407	4.478	11.980	100.0%	33.70	33.70
65	-48.00	88.00	100.24	151.39	34.93	0.722	43.82	34.10	0.0%	0.0%	34.08	116.15	125.19	107.76	3.007	4.043	9.547	100.0%	34.08	34.08
66	-32.00	88.00	93.64	160.02	36.78	0.752	41.23	30.00	0.0%	0.0%	34.38	111.06	118.66	103.95	2.715	3.724	7.940	100.0%	34.38	34.38
67	-16.00	88.00	89.44	169.70	38.05	0.771	39.52	26.95	0.0%	0.0%	34.57	107.90	114.65	101.55	2.538	3.531	7.039	100.0%	34.57	34.57
68	0.00	88.00	88.00	180.00	38.50	0.777	39.06	25.79	0.0%	0.0%	34.62	106.82	113.34	100.68	2.484	3.470	6.769	100.0%	34.62	34.62
69	16.00	88.00	89.44	190.30	38.05	0.766	39.99	26.95	0.0%	0.0%	34.51	107.90	114.82	101.39	2.553	3.545	7.107	100.0%	34.51	34.51
70	32.00	88.00	93.64	199.98	36.78	0.742	42.12	30.00	0.0%	0.0%	34.28	111.06	119.02	103.64	2.744	3.751	8.084	100.0%	34.28	34.28
71	48.00	88.00	100.24	208.61	34.93	0.707	45.03	34.10	0.0%	0.0%	33.93	116.15	125.73	107.30	3.050	4.083	9.781	100.0%	33.93	33.93
72	64.00	88.00	108.81	216.03	32.75	0.666	48.28	38.51	0.0%	0.0%	33.52	122.91	134.69	112.17	3.464	4.532	12.327	100.0%	33.52	33.52
73	80.00	88.00	118.93	222.27	30.48	0.622	51.55	42.81	0.0%	0.9%	32.77	131.10	145.59	118.05	3.976	5.086	15.884	100.0%	32.77	33.07
74	-72.00	74.00	103.25	135.78	34.14	0.687	46.63	40.27	0.0%	0.0%	33.73	118.50	129.04	108.82	3.348	4.438	11.671	100.0%	33.73	33.73
75	-56.00	74.00	92.80	142.88	37.03	0.734	42.75	35.04	0.0%	0.0%	34.20	110.43	118.59	102.83	2.856	3.901	8.751	100.0%	34.20	34.20
76	-40.00	74.00	84.12	151.61	39.77	0.777	39.00	29.58	0.0%	0.0%	34.62	103.96	110.29	98.00	2.474	3.484	6.768	100.0%	34.62	34.62
77	-24.00	74.00	77.79	162.03	41.98	0.810	35.92	24.57	0.0%	0.0%	34.94	99.42	104.51	94.57	2.239	3.197	5.622	100.0%	34.94	34.94
78	-8.00	74.00	74.43	173.83	43.24	0.826	34.26	21.34	0.0%	0.0%	35.10	97.07	101.57	92.76	2.195	3.055	5.267	100.0%	35.10	35.10
79	8.00	74.00	74.43	186.17	43.24	0.824	34.56	21.34	0.0%	0.0%	35.07	97.07	101.66	92.69	2.188	3.062	5.261	100.0%	35.07	35.07
80	24.00	74.00	77.79	197.97	41.98	0.801	36.76	24.57	0.0%	0.0%	34.86	99.42	104.76	94.35	2.236	3.219	5.653	100.0%	34.86	34.86
81	40.00	74.00	84.12	208.39	39.77	0.763	40.24	29.58	0.0%	0.0%	34.49	103.96	110.72	97.62	2.512	3.520	6.944	100.0%	34.49	34.49
82	56.00	74.00	92.80	217.12	37.03	0.716	44.27	35.04	0.0%	0.0%	34.02	110.43	119.21	102.29	2.909	3.952	9.028	100.0%	34.02	34.02
83	72.00	74.00	103.25	224.22	34.14	0.665	48.33	40.27	0.0%	0.0%	33.51	118.50	129.88	108.12	3.416	4.503	12.079	100.0%	33.51	33.51
84	-80.00	60.00	100.00	126.87	34.99	0.678	47.30	43.12	0.0%	0.0%	33.65	115.96	126.59	106.22	3.415	4.538	12.170	100.0%	33.65	33.65
85	-64.00	60.00	87.73	133.15	38.59	0.735	42.70	37.45	0.0%	0.0%	34.21	106.62	114.48	99.30	2.821	3.889	8.619	100.0%	34.21	34.21
86	-48.00	60.00	76.84	141.34	42.33	0.791	37.75	31.00	0.0%	0.0%	34.75	98.75	104.36	93.43	2.339	3.360	6.173	100.0%	34.75	34.75
87	-32.00	60.00	68.00	151.93	45.83	0.839	32.96	24.08	0.0%	0.0%	35.22	92.71	96.68	88.90	2.160	2.966	5.032	100.0%	35.22	35.22
88	-16.00	60.00	62.10	165.07	48.42	0.872	29.33	17.79	0.0%	0.0%	35.53	88.89	91.89	86.00	2.102	2.724	4.497	100.0%	35.53	35.53
89	0.00	60.00	60.00	180.00	49.40	0.882	28.17	14.89	0.0%	0.0%	35.63	87.59	90.30	84.95	2.078	2.647	4.320	100.0%	35.63	35.63
90	16.00	60.00	62.10	194.93	48.42	0.865	30.07	17.79	0.0%	0.0%	35.47	88.89	92.05	85.85	2.086	2.739	4.487	100.0%	35.47	35.47
91	32.00	60.00	68.00	208.07	45.83	0.827	34.24	24.08	0.0%	0.0%	35.10	92.71	97.01	88.60	2.127	2.997	5.008	100.0%	35.10	35.10
92	48.00	60.00	76.84	218.66	42.33	0.773	39.35	31.00	0.0%	0.0%	34.58	98.75	104.87	92.98	2.387	3.406	6.387	100.0%	34.58	34.58
93	64.00	60.00	87.73	226.85	38.59	0.713	44.48	37.45	0.0%	0.0%	34.00	106.62	115.19	98.69	2.886	3.950	8.952	100.0%	34.00	34.00
94	80.00	60.00	100.00	233.13	34.99	0.653	49.19	43.12	0.0%	0.0%	33.40	115.96	127.54	105.44	3.494	4.613	12.660	100.0%	33.40	33.40
95	-72.00	46.00	85.44	122.57	39.33	0.721	43.88	41.26	0.0%	0.0%	34.07	104.93	113.12	97.33	2.931	4.038	9.296	100.0%	34.07	34.07
96	-56.00	46.00	72.47	129.40	44.01	0.787	38.08	34.51	0.0%	0.0%	34.72	95.72	101.26	90.48	2.340	3.388	6.226	100.0%	34.72	34.72
97	-40.00	46.00	60.96	138.99	48.95	0.851	31.65	26.56	0.0%	0.0%	35.34	88.18	91.66	84.84	2.119	2.873	4.783	100.0%	35.34	35.34
98	-24.00	46.00	51.88	152.45	53.45	0.903	25.40	17.66	0.0%	0.0%	35.83	82.78	84.85	80.75	2.047	2.514	4.043	100.0%	35.83	35.83
99	-8.00	46.00	46.69	170.13	56.30	0.932	21.27	9.35	0.0%	0.0%	36.10	79.94	81.33	78.56	2.011	2.332	3.684	100.0%	36.10	36.10
100	8.00	46.00	46.69	189.87	56.30	0.928	21.83	9.35	0.0%	0.0%	36.06	79.94	81.41	78.49	2.003	2.340	3.681	100.0%	36.06	36.06
101	24.00	46.00	51.88	207.55	53.45	0.893	26.75	17.66	0.0%	0.0%	35.73	82.78	85.08	80.53	2.021	2.539	4.031	100.0%	35.73	35.73
102	40.00	46.00	60.96	221.01	48.95	0.835	33.39	26.56	0.0%	0.0%	35.18	88.18	92.06	84.46	2.076	2.914	4.752	100.0%	35.18	35.18
103	56.00	46.00	72.47	230.60	44.01	0.766	39.98	34.51	0.0%	0.0%	34.52	95.72	101.86	89.95	2.400	3.445	6.493	100.0%	34.52	34.52
104	72.00	46.00	85.44	237.43	39.33	0.696	45.87	41.26	0.0%	0.0%	33.83	104.93	113.94	96.63	3.007	4.111	9.710	100.0%	33.83	33.83
105	-64.00	32.00	71.55	116.57	44.37	0.764	40.21	39.76	0.0%	0.0%	34.49	95.09	101.26	89.30	2.509	3.605	7.104	100.0%	34.49	34.49
106	-48.00	32.00	57.69	123.69	50.51	0.839	32.92	31.97	0.0%	0.0%	35.22	86.17	89.85	82.64	2.116	2.960	4.920	100.0%	35.22	35.22
107	-32.00	32.00	45.25	135.00	57.12	0.910	24.51	22.60	0.0%	0.0%	35.89	79.19	81.03	77.38	2.027	2.471	3.935	100.0%	35.89	35.89
108	-16.00	32.00	35.78	153.43	62.93	0.961	16.07	11.80	0.0%	0.0%	36.37	74.68	75.42	73.95	1.980	2.165	3.367	100.0%	36.37	36.37
109	0.00	32.00	32.00	180.00	65.43	0.978	12.16	1.14	0.0%	0.0%	36.52	73.12	73.53	72.71	1.961	2.065	3.180	100.0%	36.52	36.52

110	16.00	32.00	35.78	206.57	62.93	0.953	17.59	11.80	0.0%	0.0%	36.30	74.68	75.57	73.80	1.962	2.182	3.362	100.0%	36.30	36.30
111	32.00	32.00	45.25	225.00	57.12	0.895	26.44	22.60	0.0%	0.0%	35.76	79.19	81.34	77.09	1.990	2.507	3.918	100.0%	35.76	35.76
112	48.00	32.00	57.69	236.31	50.51	0.819	34.97	31.97	0.0%	0.0%	35.03	86.17	90.35	82.19	2.061	3.013	4.877	100.0%	35.03	35.03
113	64.00	32.00	71.55	243.43	44.37	0.740	42.30	39.76	0.0%	0.0%	34.25	95.09	101.96	88.69	2.582	3.674	7.450	100.0%	34.25	34.25
114	-56.00	18.00	58.82	107.82	49.96	0.801	36.73	39.18	0.0%	0.0%	34.86	86.86	91.52	82.44	2.177	3.272	5.594	100.0%	34.86	34.86
115	-40.00	18.00	43.86	114.23	57.93	0.883	27.94	30.91	0.0%	0.0%	35.64	78.48	80.87	76.16	2.040	2.645	4.239	100.0%	35.64	35.64
116	-24.00	18.00	30.00	126.87	66.80	0.954	17.40	21.46	0.0%	0.0%	36.31	72.35	73.19	71.52	1.978	2.201	3.419	100.0%	36.31	36.31
117	-8.00	18.00	19.70	156.04	74.28	0.995	5.59	12.92	0.0%	0.0%	36.69	69.08	69.17	69.00	1.949	1.972	3.018	100.0%	36.69	36.69
118	8.00	18.00	19.70	203.96	74.28	0.991	7.65	12.92	0.0%	0.0%	36.65	69.08	69.24	68.93	1.939	1.981	3.017	100.0%	36.65	36.65
119	24.00	18.00	30.00	233.13	66.80	0.942	19.55	21.46	0.0%	0.0%	36.20	72.35	73.42	71.30	1.948	2.229	3.411	100.0%	36.20	36.20
120	40.00	18.00	43.86	245.77	57.93	0.865	30.10	30.91	0.0%	0.0%	35.47	78.48	81.26	75.79	1.991	2.692	4.210	100.0%	35.47	35.47
121	56.00	18.00	58.82	252.18	49.96	0.778	38.89	39.18	0.0%	0.0%	34.63	86.86	92.12	81.91	2.245	3.337	5.886	100.0%	34.63	34.63
122	-48.00	4.00	48.17	94.76	55.47	0.825	34.40	40.30	0.0%	0.0%	35.09	80.72	84.50	77.11	2.096	3.088	5.083	100.0%	35.09	35.09
123	-32.00	4.00	32.25	97.13	65.26	0.906	25.08	32.77	0.0%	0.0%	35.85	73.22	75.01	71.47	2.005	2.500	3.937	100.0%	35.85	35.85
124	-16.00	4.00	16.49	104.04	76.74	0.966	14.88	25.69	0.0%	0.0%	36.42	68.32	68.90	67.75	1.961	2.128	3.277	100.0%	36.42	36.42
125	16.00	4.00	16.49	255.96	76.74	0.958	16.65	25.69	0.0%	0.0%	36.34	68.32	69.05	67.60	1.939	2.148	3.272	100.0%	36.34	36.34
126	32.00	4.00	32.25	262.87	65.26	0.890	27.12	32.77	0.0%	0.0%	35.71	73.22	75.32	71.18	1.962	2.540	3.915	100.0%	35.71	35.71
127	48.00	4.00	48.17	265.24	55.47	0.804	36.51	40.30	0.0%	0.0%	34.88	80.72	85.00	76.66	2.040	3.148	5.043	100.0%	34.88	34.88
128	-40.00	-10.00	41.23	75.96	59.50	0.824	34.52	43.70	0.0%	0.0%	35.08	77.18	80.82	73.70	2.080	3.116	5.091	100.0%	35.08	35.08
129	-24.00	-10.00	26.00	67.38	69.62	0.892	26.82	38.14	0.0%	0.0%	35.73	70.94	72.93	69.00	2.004	2.596	4.087	100.0%	35.73	35.73
130	24.00	-10.00	26.00	292.62	69.62	0.880	28.33	38.14	0.0%	0.0%	35.61	70.94	73.16	68.78	1.970	2.629	4.067	100.0%	35.61	35.61
131	40.00	-10.00	41.23	284.04	59.50	0.805	36.35	43.70	0.0%	0.0%	34.90	77.18	81.23	73.33	2.022	3.171	5.037	100.0%	34.90	34.90
132	0.00	-24.00	24.00	360.00	71.08	0.854	31.40	44.63	0.0%	0.0%	35.36	70.30	73.02	67.68	2.013	2.882	4.557	100.0%	35.36	35.36

132 Counts a maximum of 6 blocking heliostats

Source Hstat#	sin (TA)/ Adj S	Net Blockage	TA, rads	Adj S	Blocks... total #	Hstat #	a	b	frac. of s	Hstat #	a	b	frac. of s
1	0.042	0.100	0.34	7.86	2	4	14.0	-8.0	12.2%	5	14.0	8.0	12.2%
2	0.044	0.153	0.35	7.89	1	9	15.4	4.9	46.6%				
3	0.044	0.110	0.36	7.91	1	10	14.9	6.1	32.2%				
4	0.044	0.090	0.36	7.91	2	10	13.6	-8.6	5.5%	11	14.3	7.4	18.9%
5	0.044	0.090	0.36	7.91	2	12	13.6	8.6	5.5%	11	14.3	-7.4	18.9%
6	0.044	0.109	0.36	7.90	1	12	14.9	-6.1	32.2%				
7	0.044	0.152	0.35	7.87	1	13	15.3691	-4.9	46.6%				
8	0.046	0.159	0.37	7.93	1	16	15.6351	3.9	56.6%				
9	0.047	0.119	0.38	7.96	1	17	15.2	5.3	41.0%				
10	0.047	0.082	0.39	7.97	1	18	14.7	6.7	26.6%				
11	0.047	0.082	0.39	7.97	2	18	14.0	-8.0	12.2%	19	14.0	8.0	12.2%
12	0.047	0.082	0.39	7.96	1	19	14.7	-6.7	26.6%				
13	0.047	0.121	0.38	7.94	1	20	15.2	-5.3	42.2%				
14	0.046	0.158	0.37	7.91	1	21	15.6	-3.9	56.6%				
15	0.048	0.160	0.40	7.97	1	24	15.9	2.9	68.8%				
16	0.049	0.122	0.41	8.00	1	25	15.5	4.3	52.1%				
17	0.050	0.088	0.41	8.02	1	26	15.0	5.8	35.5%				
18	0.050	0.069	0.42	8.03	2	26	13.6	-8.7	4.4%	27	14.4	7.3	20.0%
19	0.050	0.069	0.42	8.03	2	28	13.6	8.7	4.4%	27	14.4	-7.3	20.0%
20	0.050	0.090	0.41	8.01	1	28	15.0	-5.8	36.6%				
21	0.049	0.121	0.41	7.98	1	29	15.5	-4.3	52.1%				
22	0.049	0.158	0.40	7.94	1	30	15.9	-2.9	68.8%				
23	0.051	0.153	0.42	8.01	1	33	16.0	1.6	82.1%				
24	0.052	0.116	0.43	8.05	1	34	15.8	3.2	65.4%				
25	0.053	0.087	0.44	8.08	1	35	15.4	4.8	47.7%				
26	0.054	0.059	0.45	8.10	1	36	14.8	6.4	28.8%				
27	0.054	0.060	0.45	8.10	2	36	14.0	-8.0	12.2%	37	14.0	8.0	12.2%
28	0.054	0.061	0.45	8.09	1	37	14.8	-6.4	30.0%				
29	0.053	0.086	0.44	8.06	1	38	15.4	-4.8	47.7%				
30	0.052	0.114	0.43	8.02	1	39	15.8	-3.2	65.4%				
31	0.051	0.150	0.42	7.97	1	40	16.0	-1.6	1				
32	0.053	0.142	0.44	8.04	1	43	16.1	0.2	1				
33	0.054778	0.098	0.46	8.092431	1	44	16.0	1.8	1				
34	0.056236	0.070	0.48	8.137235	1	45	15.7	3.5	1				
35	0.057292	0.053	0.49	8.167906	1	46	15.2	5.3	0				

36	0.057863	0.039	0.49	8.181515	2	46	13.5	-8.8	0	47	14.5	7.1	21.1%
37	0.057899	0.039	0.49	8.176461	2	48	13.5	8.8	0	47	14.5	-7.1	21.1%
38	0.057398	0.052	0.49	8.152885	1	48	15.2	-5.3	0				
39	0.056406	0.069	0.48	8.112647	1	49	15.7	-3.5	1				
40	0.055006	0.096	0.46	8.058882	1	50	16.0	-1.8	1				
41	0.053298	0.137	0.44	7.995323	1	51	16.1	-0.2	1				
42	0.055217	0.096	0.46	8.057149	1	53	16.1	-1.4	1				
43	0.057479	0.072	0.49	8.127628	1	54.0	16.1	0.2	1				
44	0.059471	0.038	0.51	8.188936	1	55.0	16.0	203.9%	1				
45	0.061052	0.026	0.53	8.236135	1	56.0	15.6	398.9%	1				
46	0.062084	0.024	0.54	8.264536	1	57.0	15.0	601.2%	0				
47	0.062469	0.031	0.54	8.270764	2	57.0	14.0	-800.0%	0	58.0	14.0	800.0%	12.2%
48	0.062166	0.024031	0.538792	8.253688	1	58	14.96179	-6.01205	0.343871				
49	0.06121	0.024717	0.52687	8.214785	1	59	15.62333	-3.98893	0.565724				
50	0.059699	0.035034	0.508657	8.157721	1	60	15.99505	-2.03921	0.776484				
51	0.057765	0.067038	0.486082	8.087379	1	61	16.12271	-0.24154	0.976151				
52	0.055551	0.091796	0.461057	8.008792	1	62	16.06684	1.362559	0.854132				
53	0.059996	0.030788	0.510994	8.151314	1	64	16.05102	-1.53782	0.831947				
54	0.062624	0	0.541576	8.231444	1	65	16.12217	0.275005	0.976151				
55	0.064875	0	0.568535	8.299042	1	66	15.95433	2.33656	0.743206				
56	0.066547	0	0.588947	8.347313	1	67	15.46016	4.580787	0.499168				
57	0.067461	0.003964	0.600025	8.37025	1	68	14.58267	6.88083	0.244038				
58	0.067508	0.003795	0.600025	8.364358	1	68	14.58267	-6.88083	0.244038				
59	0.066686	0	0.588947	8.329863	1	69	15.46016	-4.58079	0.499168				
60	0.065097	0	0.568535	8.270671	1	70	15.95433	-2.33656	0.743206				
61	0.062917	0	0.541576	8.19308	1	71	16.12217	-0.275	0.976151				
62	0.060346	0.026113	0.510994	8.104031	1	72	16.05102	1.537822	0.831947				
63	0.062171	0.013292	0.531987	8.158917	1	74	15.74054	-3.4979	0.621187				
64	0.065509	0	0.57166	8.258908	1	75	16.02768	-1.76452	0.809762				
65	0.068567	0	0.609602	8.350061	0								
66	0.07108	0	0.64194	8.423581	0								
67	0.072764	0	0.664056	8.470101	0								
68	0.073391	0	0.671963	8.482252	2	78	14	-8	0.122019	79	14	8	0.122019
69	0.072873	0	0.664056	8.457385	0								
70	0.071291	0	0.64194	8.39872	0								
71	0.068864	0	0.609602	8.314062	0								
72	0.065874	0	0.57166	8.213022	1	82	16.02768	1.764515	0.809762				
73	0.062589	0.009207	0.531987	8.104452	1	83	15.74054	3.497899	0.621187				
74	0.067897	0	0.595797	8.264984	1	85	15.613	-4.02916	0.554631				

75	0.071854	0	0.64625	8.380814	0				
76	0.075396	0	0.694042	8.48386	0				
77	0.078128	0	0.732708	8.561406	0				
78	0.079655	0	0.754728	8.600735	0				
79	0.079719	0	0.754728	8.593778	0				
80	0.078315	0	0.732708	8.540917	0				
81	0.07569	0	0.694042	8.45088	0				
82	0.072234	0	0.64625	8.336782	0				
83	0.06834	0	0.595797	8.211456	1	93	15.613	4.029162	0.554631
84	0.069559	0	0.610726	8.244255	1	95	14.8	-6.4	0.299501
85	0.074406	0	0.673478	8.382453	0				
86	0.079081	0	0.738867	8.515972	0				
87	0.083113	0	0.79989	8.630211	0				
88	0.085918	0	0.845157	8.706826	0				
89	0.086976	0	0.86217	8.72949	0				
90	0.086067	0	0.845157	8.69181	0				
91	0.083394	0	0.79989	8.601134	0				
92	0.079468	0	0.738867	8.474442	0				
93	0.074872	0	0.673478	8.330318	0				
94	0.070077	0	0.610726	8.183296	1	104	14.8	6.4	0.288408
95	0.075914	0	0.686392	8.348248	1	96	13.48314	8.614228	0.04437
96	0.08166	0	0.768058	8.507724	0				
97	0.087094	0	0.854326	8.65881	0				
98	0.091502	0	0.932947	8.779872	0				
99	0.094051	0	0.982558	8.845376	0				
100	0.094139	0	0.982558	8.83716	0				
101	0.091753	0	0.932947	8.755871	0				
102	0.087479	0	0.854326	8.620704	0				
103	0.082143	0	0.768058	8.457667	0				
104	0.076463	0	0.686392	8.288378	1	103	13.48314	-8.61423	0.055463
105	0.082741	0	0.774419	8.451652	0				
106	0.089408	0	0.881517	8.631227	0				
107	0.095485	0	0.996887	8.79493	0				
108	0.099918	0	1.098307	8.911679	0				
109	0.101624	0	1.142018	8.949369	0				
110	0.100114	0	1.098307	8.894213	0				
111	0.095849	0	0.996887	8.761518	0				
112	0.089898	0	0.881517	8.58426	0				
113	0.083313	0	0.774419	8.393657	0				

114	0.089631	0	0.871954	8.541567	0
115	0.097024	0	1.011033	8.733736	0
116	0.103315	0	1.165905	8.896498	0
117	0.107085	0	1.296494	8.989291	0
118	0.107196	0	1.296494	8.979936	0
119	0.103631	0	1.165905	8.869394	0
120	0.097498	0	1.011033	8.691275	0
121	0.090211	0	0.871954	8.486608	0
122	0.095821	0	0.968108	8.597458	0
123	0.103382	0	1.13908	8.785361	0
124	0.109068	0	1.33941	8.924231	0
125	0.109302	0	1.33941	8.905164	0
126	0.10381	0	1.13908	8.74918	0
127	0.096385	0	0.968108	8.547112	0
128	0.100251	0	1.038493	8.594796	0
129	0.107079	0	1.21516	8.754536	0
130	0.107424	0	1.21516	8.726443	0
131	0.100766	0	1.038493	8.550918	0
132	0.109177	0	1.240499	8.664326	0

Values from control:

c/o TERC	1	(1 = 49.6 degree max; 2 = 35.0 degree max)
c/o CRA	45.0 degrees	
c/o TROE	93.0%	(reflectivity)
c/o RCENT	77.7 meters	

hstat imag 1.554 at center, full diameter

Values Set Here:

Degrade	**80%**	Degredation of Gordon&Ries concentration faction for gaps and errors in their paper or my understanding
T1 slope	**1.19**	Yields DIAPE2 if DIAPE 1 & SCOND are known. Slope is width/depth for *one-half* of the secondary, not counting aperture width
T2 slope	**0.66**	same, for terc2 (narrow field)

radius area Cratio

Calculations and Values for Return: 77.69131 18962.46 12071.47

T1DIR	**55%**	The fraction of rays which do not strike the secondary but pass straight to the aperture
T2DIR	**35%**	same, for terc2 (narrow field)
CMAX	10000.3 NOT USEI	Concentration Limit (multiple of cos-adjusted field at this rim angle: 2piL^2(1-cos(CRA))/cos(CRA)
ABSMIN	1.57 m^2	Thermodynamically smallest possible absorber, after Gordon & Ries
CACH	70%	Achieved concentration, after degrade, from table below
SCOND	6.99 meters	Depth of secondary.
DIAPE2	1.69 meters	Diameter of the absorber aperture (it's possible this is supposed to be a constant for each terc type -- but this is okay, too...)
DIAPE1	18.33 meters	This is the receiver (or outer secondary) aperture; = DIFEED *only* if SECCON = 0
(utility)	11.97 meters	Length down sleeve of complete cone; utility
SCONA	341.7 m^2	Area of secondary. Calculated as if for a conical TERC

CRA	Concentration/max		Depth Fraction		Direct Hits Only Conc/Max	
	T1	T2	T1	T2	T1	T2
19.5	*26%*	46%	*0.0053*	0.02	*14%*	16%
21.9	*31%*	55%	*0.0059*	0.03	*17%*	19%
24.5	*34%*	60%	*0.0065*	0.04	*19%*	21%
26.3	*38%*	65%	*0.0072*	0.05	*21%*	23%
27.6	*39%*	67%	*0.0077*	0.06	*21%*	23%
28.5	*41%*	69%	*0.0084*	0.07	*23%*	24%
29.2	*43%*	71%	*0.0089*	0.08	*24%*	25%
29.6	*45%*	72%	*0.0096*	0.09	*25%*	25%
30.3	46%	73%	0.0100	0.10	25%	26%
35.9	63%		0.0200		35%	
38.9	71%		0.0300		39%	
40.8	78%		0.0400		43%	
42.2	82%		0.0500		45%	
43.2	84%		0.0600		46%	
43.9	86%		0.0700		47%	
44.5	87%		0.0800		48%	
45.0	88%		0.0900		48%	
45.4	89%		0.1000		49%	

*figures in italics are extrapolation only; they are NOT part of the Gordon & Ries chart

Here's the Engine for the MPT System; ASDB Engine Below...

Copies:	*Turbine eff*	0.892	*Comp. eff:*	0.782	Mode:	ogt	Ambient:	19.81507
	RPDrop	0.030	*RPDrop2*	0.030	Regen	0.900	Tower Dp:	0.05

RGT or OGT:	bar	K	C	efficiency:	
t1 (amb.)		293	20		
p2 (h.pr.)	10.100				
t2 / CRIT		643	370		compressed regenerator inlet temperature
CREP	10.100				
ENGCRET		643	370		This is the regenerator exit temperature if there are no receiver pressure drops
CRET'		643	370		This is actual regenerator exit temperature
p3/ARP	9.595				The second regenerator pressure drop is *not* included here
t3		1350	1077		
t4		822	549		This is as if there **were** regenerator pressure losses but **no** receiver losses
t4' / RIT		830	557		This is the actual figure for TET
TET		822	549	*vs 549 KB:*	This is the low-pressure regenerator (system discharge) temperature **without** receiver effects
TET' ("TET")		830	557		This is the low-pressure regenerator (system discharge) temperature
c/o GREFF				95.0%	
GT n	(GASEFF)	(including generator		28.50%	This is the GT efficiency **with** regenerator drop but **without** receiver drop
GT n'	(GTEFF)	efficiency...)		27.39%	**This is the GT efficiency in solar mode**
GT n'/n				0.961	
%c				66.3%	
%c'				67.4%	

ASDB Engine Model:		*0.905*		*0.705*		
Copies:	*Turbine eff*	0.905	*Comp. eff:*	0.705		
	Reg. P Dp	0.084	*Reg. Eff:*	0.900		
	LP P Dp:	0.029				

	bar	K	C	*spec values*	
t1 (amb.)		293	20		
p2 (h.pr.)	2.330				
t2 / CRIT		406	133	*vs 127*	compressed regenerator inlet temperature
ASDBCRE	2.246				
ASDBCRET		932	659	*vs 591*	compressed regenerator outlet temperature
CRET'		927			Regen exit temp if there were no receiver pressure drops
p3	2.196				The second regenerator pressure drop is *not* included here
t3		1173	900	*vs 816*	
t4		985	712		*As if there **were** pressure losses in the regenerator, but **not** in the receiver*
t4' = RIT		990	717	*vs 646*	*Using the actual p3, instead of p2*
RET		465	192	*vs 179*	System Discharge
p3/p2				0.942	
c/o ASDBGREFF				94.5%	
GT n				33.3%	This is the GT efficiency without a pressure drop in the receiver
GT n'	(ASDBGTEFF)			32.1%	**This is the GT efficiency**
					This is within .3 percentage points (1%) of the Sandia specs! When the right Tamb is used (24 C adjusted CIT)...
GT n'/n				0.963	

ASDB MODEL

(Complete except for: engine model, insolation model)

INPUTS:

Background Conditions:

c/o AT	19.8	C	Ambient Temperature; copied from solar data worksheet. Annual DAYTIME average
INSOL	**962.25**	W/m^2	Current insolation; this is the input slot for the solar year data when model is run dynamically

ASDB Model & Benchmarks:

*These figures taken or inferred from Sandia specs

	0.322	kg/s	*ASDB flow rate / dish Average Volume Flow in Receiver 0.288224 m^3/s
ASDBHP	2.33	bar	*ASDB pressure
ASDBREGEN	90.0%		*Regeneration efficiency; heat gained over heat available. Inferred from Sandia specs
ASDBTIT	900	C	*Turbine Inlet Temperature
ASDBRPDROP	0.084	bar	*Recuperator Pressure Drop, High pressure side
ASDBRPDROP2	0.029	bar	*Recuperator Pressure Drop, Low pressure side
ASDBARP	2.196	bar	*Return pressure, post recuperator, post receiver
ASDBCn	70.5%		*These have been tweaked until the Sandia spec results (temps and effs) are matched;
ASDBTn	90.5%		* these are not given in the specs. Cn includes inlet housing, filters, etc.
ASDBGREFF	94.5%		*Generator Efficiency

Dish Modeling (currently based on ASDB specs, without explicit dish receiver modeling)

DROE	**0.90**		Dish Reflectivity
REFTEMP	711	C	*Temperature of ASDB specs; used to determine DRAREA. T4Average of inlet and outlet
REFLOSS	6.98	kW	*Losses at assumed 1 kW flux
DRAPE	0.409	meters	*Receiver aperture diameter, inferred from the above reference conditions. Used to calculate DRAREA.
DRAREA	0.131	m^2	Used for losses in dish table
DAPE	100	m^2	*Dish aperture, inferred from ASDB specs for a 1kW max regime a DROE of .9 (not in specs)
(utility)	1.0613		Conversion Factor for Spherical Approximation. radius 7 meters focus 7.5 meters.
DAREA	106.1	m^2	Dish mirror surface area; snaps to a multiple of 3.0 m facets.
(calculated)	15.0	facets	Number of facets per dish
(calculated)	163.4	m^2	Total Surface Area of Entire Dish Structure

RESULTS:

ASDB System - Instant Results:

	ASDBEMW	0.1021	MWt	Equivalent Energy: Falls on a flat, ideal two-axis tracker
0.942951	DEFF	84.9%		Dish Geometric Efficiency; a constant equal to the cosine losses * dish reflectivity
0.848656	ASDBRMW	0.0867	MWt	Power Received into the receiver
0.900	ASDBRECTEMP	884	C	Receiver Exit Temperature; calculated iteratively
	ASDBRADMW	0.0091	MWt	Power re-radiated from the receiver
	ASDBREFF	89.5%		Receiver Efficiency for D/E systems; a pure function of insolation and operating temperature
	ASDBDMW	0.0776	MWt	This is passed into the air for a single ASDB system
	c/o ASDBGTEFF	32.1%		Allied Dishes Net Heat-to-Electric Engine Efficiency; compare with GTEFF
	ASDBEFF	24.4%		INSTANT SOL > ELEC EFFICIENCY FOR DISH / ENGINE, MIRROR AREA BASIS

ASDB Systems - Annual Results

ASDBHOURS	4065	hours	Operating Hours. Different for ASDB b/c different cut-out conditions.
ANNASDBEMW	0.071	MWt	Annual Average Equivalent MWt, mirror area basis
ANNASDBDMW	0.052	MWt	MW into air for a field of ASDB systems, annual average
ASDBPKDMW	0.078	MWt	Peak MW delivered to heat engine, field of ASDB systems
ANNASDBREFF	87.0%		Annually averaged receiver efficiency, ASDB systems
ASDBSTEFF	73.8%		Annually averaged solar to thermal efficiency, ASDB system. Includes REFF & DEFF
ANNASDBEFF	23.7%		**ANNUAL SOL > ELEC EFFICIENCY FOR DISH / ENGINE, MIRROR AREA BASIS**
(calculated)	25.1%		(Aperture Basis)
ASDBHEATREQ	680	MWHt	Annual heat required for this dish field, assuming CF = 1 in hybrid mode
ASDBHEATPROV	213	MWHt	Annual heat provided by solar input
ASDBTAGR	467	MWHt	True Annual Gas Required for CF = 1.0
ASDBSF	31.3%		Solar Fraction for the ASDB systems
ASDBRATING	0.025	MWe	Sum electrical weighting for the collection of ASDB systems
ASDBADJEFF	28.9%		Adjusted Efficiency: solar and gas combined. Gas is higher b/c no receiver, cosine, or reflective losses
c/o ASDBGTEFF	32.1%		

```
Public Function logn(x)
logn = Application.Ln(x)
End Function


'Public Function funky(x)
'   Set P = Application.Worksheets("Blocks").range("BSOUT").Offset(x, 3)
'   funky = 0
'   For i = 1 To P.Value
'     vblock = (1 - P.Offset(0, (i - 1) * 4 + 2) * Sin(P.Offset(0, -2)) / P.Offset(0,
 -1))
'     If vblock < 0 Then vblock = 0
'     funky = funky + vblock * P.Offset(0, (i - 1) * 4 + 4)
'   Next i
'End Function

Public Function acos(x)
  acos = Application.acos(x)
End Function

'Rim Angle Function
Public Function RAF(x, y, THEIGHT, YCENT, RCENT)
  R = (x ^ 2 + y ^ 2) ^ 0.5
  RAF = (180 / 3.1415927) * (acos(1 - 0.5 * (x ^ 2 / (THEIGHT ^ 2 + R ^ 2) + (YCENT
/ RCENT - y / (THEIGHT ^ 2 + R ^ 2) ^ 0.5) ^ 2 + (THEIGHT / RCENT - THEIGHT / (THEIG
HT ^ 2 + R ^ 2) ^ 0.5) ^ 2))).
End Function

Public Function atan2(x, y)
  atan2 = Application.atan2(x, y)
End Function

Public Function cadja(a, ell)
  a = (3.1415927 / 180) * a
  cadja = 0
  For i = 0 To a Step 0.0001
    cadja = cadja + (Tan(i) + Tan(i) ^ 3) * 0.0001 * Cos(i)
  Next i
  cadja = cadja * 3.1415927 * 2 * ell ^ 2
End Function

'Cp is now a function. See below for the curve fit used
'This was derived somewhat arbitrarily but is good to less than 1% throughout range

Public Function cp(t)
  cp = 1.004 + 0.0001 * t ^ 1.09
End Function

Public Function t4avg(x, y)
  t4avg = ((y ^ 5 - x ^ 5) / (5 * (y - x))) ^ 0.25
End Function

Public Function max(x, y)
  If x >= y Then
  max = x
```

```
  Else: max = y
  End If
End Function

Public Function min(x, y)
  If x <= y Then
  min = x
  Else: min = y
  End If
End Function

' Tower Shading Function:
Public Function TSF(R, tht, MTHW, THEIGHT, HX, HY, PHIS, THS)
  If R < THEIGHT / Tan((3.1415927 / 180) * (PHIS)) Then
    TSF = min(max(0, MTHW - max(-1 * MTHW, R * Sin((3.1415927 / 180) * (Abs(tht - TH
S))) - (0.5 * (HX + HY)) / 2)) / (0.5 * (HX + HY)), 1)
  Else
    TSF = 0
  End If
End Function

'Functions Combustr and combusto for regenerated and open cycle combustion
'these are relations derived from Cohen et al fig. 2.15
't3 and t4 are the inlet and outlet temperatures at the burner
'the function returns the amount of fuel heat (kj/kg) required to raise the air
'temperature the desired amount; used for efficiency calculations
'combustr assumes an inlet temperature of 900 K
'combusto assumes an inlet temperature of 700 K
'note that the functions have been linearized and the raw temperatures
'don't matter (so C and K are both fine); only the difference is used
Public Function COMBUSTR(t3, t4)
  COMBUSTR = 0.98 * (1.29 * (t3 - t4) - 21.5)
End Function

Public Function COMBUSTO(t3, t4)
  COMBUSTO = 0.98 * (1.29 * (t3 - t4) - 43)
End Function

'Function BelowCut: t1,t2 define a linear temperature range. Function
'returns the fraction of radiation from this temperature range which is
'at wavelengths below cut
Function BelowCut(cut, t1, t2)
 ' Warning: only intended for receiver temperatures (300 K - 1100 K)
 ' Doesn't consider wavelengths below .1 microns
  C1 = 374200000
  C2 = 14390
  Total = 0
  Included = 0

  For tem = t1 To t2 Step (t2 - t1) / 10
    For lam = 0.1 To 100 Step 0.02
      Power = C1 / (lam ^ 5 * (2.7183 ^ (C2 / (lam * tem)) - 1))
      Total = Total + Power
      If lam < cut Then
        Included = Included + Power
      End If
    Next lam
  Next tem
  BelowCut = Included / Total
End Function
```

```
Sub Generate_Field()   'generates heliostat field

  Set control_panel = Worksheets("H")

  THEIGHT = control_panel.Range("THEIGHT")
  xfoot = control_panel.Range("XFOOT")
  yfoot = control_panel.Range("YFOOT")
  FRAD = control_panel.Range("FRAD")
  PRAD = control_panel.Range("PRAD")
  CRA = control_panel.Range("CRA")
  YCENT = control_panel.Range("YCENT")
  RCENT = control_panel.Range("RCENT")

  Set PHIS = control_panel.Range("PHIS")
  Set THS = control_panel.Range("THS")
  Set NHSTAT = control_panel.Range("NHSTAT")
  Set TOTA = control_panel.Range("TOTA")
  Set EMW = control_panel.Range("EMW")
  Set TMW = control_panel.Range("TMW")
  Set EFF = control_panel.Range("EFF")
  Set place = control_panel.Range("START")

  'Application.ScreenUpdating = False 'About twice as fast when enabled!

  ' Turn off calculation to speed up formula insertion
  Application.Calculation = xlManual

  'Completely Erase the Current Table -- must be a whole blank row above it!
  Clean_Table

  Application.Goto Reference:="NHSTAT"
  'Initialize Field Creation Variables:
  NHSTAT.Value = 0
  y = FRAD
  x = 0
  R = (x * x + y * y) ^ 0.5
  'Place entry cursor on hstat number column of first row in new table
  Set place = place.Offset(2, 0)
  'Begin Heliostat Creation
  While y >= (-1 * FRAD)
    'current locator Is in bounds, place a (centered) heliostat on it:
    ' but only if it falls within the allowed rim angle:'
    If Cos((3.1415927 / 180) * CRA) < (1 - 0.5 * (x ^  2 / (THEIGHT ^ 2 + R ^ 2) + (Y
CENT / RCENT - y / (THEIGHT ^ 2 + R ^ 2) ^ 0.5) ^ 2 + (THEIGHT / RCENT - THEIGHT / (
THEIGHT ^ 2 + R ^ 2) ^ 0.5) ^ 2)) Then
      NHSTAT.Value = NHSTAT.Value + 1
      place.Value = NHSTAT.Value
      place.Offset(0, 1).Value = x
      place.Offset(0, 2).Value = y
      place.Offset(0, 3).Value = R
      place.Offset(0, 4).FormulaR1C1 = "=DEGREES(ATAN2(RC[-2],RC[-3]))+180"
      Set place = place.Offset(1, 0)
    End If
    'Increment and Relocate Pointer -- this is messy; improve?:
    x = x + xfoot
    R = (x * x + y * y) ^ 0.5
    While y >= (-1 * FRAD) And (R > FRAD Or R < PRAD)
      x = x + xfoot
      R = (x * x + y * y) ^ 0.5
      While R < PRAD        ' Pass across inner circle
```

```
        x = x + xfoot
        R = (x * x + y * y) ^ 0.5
      Wend
      If R > FRAD And x > 0 Then
        y = y - yfoot
        'using 5.5 instead of 5 ensures a stagger between rows...
        'the 5 itself is just to ensure that we move out far enough on the
        'circle for the next pass -- in very large fields, this may not be enough
        x = -1 * x - 5.5 * xfoot
        R = (x * x + y * y) ^ 0.5
      End If
    Wend 'We may have found a new qualifying place for an hstat
  Wend 'If we drop out of this, we are below the entire field radius
  ' Now add the remaining formulas and find the simple results:
  ' Set Placemark on the Tower Angle Column:
  Set place = control_panel.Range("START")
  Set place = place.Offset(1, 5)
  ' Set angles alpha and beta:
  'a = (3.1415927 / 180) * THS All of these lines are direct calculation,
  'b = (3.1415927 / 180) * PHIS and we need to put in the formula instead
  Application.Goto Reference:="RECENTER"
  For i = 1 To NHSTAT
    place.Offset(i, 0).FormulaR1C1 = "=DEGREES(ATAN(THEIGHT/RC[-2]))"
    place.Offset(i, 1).FormulaR1C1 = "=1-.5*((cos(radians(RC[-1]))*cos(radians(RC[-2
]))  - cos(radians(PHIS))*cos(radians(THS)))^2 + (cos(radians(RC[-1]))*sin(radians(RC
[-2])) - cos(radians(PHIS))*sin(radians(THS)))^2 + (sin(radians(RC[-1])) - sin(radia
ns(PHIS)) )^2)"
    place.Offset(i, 2).FormulaR1C1 = "=DEGREES(ACOS(RC[-1]))"
    place.Offset(i, 3).FormulaR1C1 = "=DEGREES(ACOS(1-0.5*(RC[-7]^2/(THEIGHT^2+RC[-5
]^2)+(YCENT/RCENT-RC[-6]/SQRT(THEIGHT^2+RC[-5]^2))^2+(THEIGHT/RCENT-THEIGHT/SQRT(THE
IGHT^2+RC[-5]^2))^2)))"
    place.Offset(i, 4).FormulaR1C1 = "=MAX(IF(R[-1]C[-7]=RC[-7],SH1,0)+IF(RAF(RC[-8]
-(XFOOT/2),RC[-7]-YFOOT,THEIGHT,YCENT,RCENT)<CRA,SH2,0)+IF(RAF(RC[-8]+(XFOOT/2),RC[-
7]-YFOOT,THEIGHT,YCENT,RCENT)<CRA,SH3,0)+IF(R[1]C[-7]=RC[-7],SH4,0),  TSF(RC[-6],RC[
-5], MTHW, THEIGHT, HX, HY, PHIS, THS))"
    place.Offset(i, 5).FormulaR1C1 = "=offset(BSOUT,RC[-10],2)"
    place.Offset(i, 6).FormulaR1C1 = "=MAX(0,(1-MAX(RC[-1],RC[-2])-((1-AVHZBS)/(3*AV
HZBS)*MIN(RC[-1],RC[-2]))))*cos(radians(RC[-4]/2))*HAREA*.001*coSOLCON*ATTBASE^(1/SI
N(RADIANS(PHIS)))*ROE"
    place.Offset(i, 7).FormulaR1C1 = "=.95*RC[-9]/cos(radians(rc[-7]))"
    place.Offset(i, 8).FormulaR1C1 = "=RC[-1]/cos(radians(RC[-6]/2))"
    place.Offset(i, 9).FormulaR1C1 = "=RC[-2]*cos(radians(RC[-7]/2))"
    place.Offset(i, 10).FormulaR1C1 = "=(1+(2/3.1415927)*(1/cos((3.1415927/180)*rc[-
7])-1))*(ABS(RC[-2]-RC[-12]/cos(radians(rc[-10])))*(AVERAGE(HX,HY)/RC[-2])+2*SIN(SHA
)*RC[-12]/cos(radians(rc[-10])))"
    place.Offset(i, 11).FormulaR1C1 = "=(1+(2/3.1415927)*(1/cos((3.1415927/180)*rc[-
8])-1))*(ABS(RC[-13]/cos(radians(rc[-11]))-RC[-2])*AVERAGE(HX,HY)*cos(radians(RC[-9]
/2))/RC[-2]+2*SIN(SHA)*RC[-13]/cos(radians(rc[-11])))"
    place.Offset(i, 12).FormulaR1C1 = "=3.1415927*(RC[-2]/2)*(RC[-1]/2)"
    place.Offset(i, 13).FormulaR1C1 = "=IF(DIAPE1>MAX(RC[-3]:RC[-2]),1,IF(DIAPE1<MIN
(RC[-3]:RC[-2]),(3.1415927*DIAPE1*DIAPE1*0.25)/RC[-1],MIN(RC[-3]:RC[-2])*DIAPE1/(RC[
-3]*RC[-2])))"
    place.Offset(i, 14).FormulaR1C1 = "=RC[-1]*RC[-8]"
    place.Offset(i, 15).FormulaR1C1 = "=cos(radians(RC[-13]/2))*HAREA*.001*coSOLCON*
ATTBASE^(1/SIN(RADIANS(PHIS)))*ROE"
  Next i
  Find_Blockers
  Hcalc
End Sub
```

```
Sub Annual_Efficiency()   'Convolves Hstat field through solar year

  Set control_panel = Worksheets("H")
  Set input_panel = Worksheets("S")

  Set PHIS = control_panel.Range("PHIS")
  Set THS = control_panel.Range("THS")
  Set hours = control_panel.Range("HOURS")

  Set reccal = control_panel.Range("RECCAL")
  Set EMW = control_panel.Range("EMW")
  Set TMW = control_panel.Range("TMW")
  Set TBBMW = control_panel.Range("TBBMW")
  Set RMW = control_panel.Range("RMW")
  Set RADMW = control_panel.Range("RADMW")
  Set PKDMW = control_panel.Range("PKDMW")
  Set place = input_panel.Range("TAB1_HEAD")
  Set DH = input_panel.Range("Lighthours")
  Set ANNEMW = control_panel.Range("ANNEMW")
  Set ANNTMW = control_panel.Range("ANNTMW")
  Set ANNRMW = control_panel.Range("ANNRMW")
  Set ANNRADMW = control_panel.Range("ANNRADMW")
  Set ANNTBBMW = control_panel.Range("ANNTBBMW")

  'Turn off automatic calculation to enhance speed:
  Application.Calculation = xlManual
  'Set all annual sums to zero:
  ANNEMW.Value = 0
  ANNTMW.Value = 0
  ANNTBBMW.Value = 0
  ANNRMW.Value = 0
  ANNRADMW.Value = 0

  hours.Value = 0
  PKDMW.Value = 0

  'Application.ScreenUpdating = False

  'Set receiver temperature / delivered megawatts calibration:
  PHIS.Value = 80   'This seems to be about optimal for lat ~ 35
  THS.Value = 180
  'Three iterations ought to be enough to calibrate fairly well:
  Hcalc
  reccal.Value = RMW.Value - RADMW.Value
  Hcalc
  reccal.Value = RMW.Value - RADMW.Value
  Hcalc
  reccal.Value = RMW.Value - RADMW.Value
  For i = 1 To 18
    For j = 1 To 14 ' Instead of 1 to 28 to exploit am/pm symmetry
      If place.Offset(j, i).Value > 0 Then
        PHIS.Value = i * 5 - 2.5
        THS.Value = (j + 4) * 10 - 5
        Hcalc
        'Don't count hours when the losses are larger than the gains:
        If RMW.Value > RADMW.Value Then
          If (RMW.Value - RADMW.Value) > PKDMW.Value Then PKDMW.Value = (RMW.Value -
RADMW.Value)
          sfact = place.Offset(j, i).Value * 2  'This is the sun time factor for the
sun position
            ' The 2 is added in the above line as a symmetry correction
```

```
            hours.Value = hours.Value + sfact * DH.Value
            ANNRADMW.Value = ANNRADMW.Value + sfact * RADMW.Value
            ANNEMW.Value = ANNEMW.Value + sfact * EMW.Value
            ANNTBBMW.Value = ANNTBBMW.Value + sfact * TBBMW.Value
            ANNTMW.Value = ANNTMW.Value + sfact * TMW.Value
            ANNRMW.Value = ANNRMW.Value + sfact * RMW.Value
          End If
        End If
      Next j
    Next i
    'Now we must recorrect the averages to reflect the "cut-out" hours:
    If hours.Value > 0 Then
      ANNRADMW.Value = ANNRADMW.Value * (DH.Value / hours.Value)
      ANNEMW.Value = ANNEMW.Value * (DH.Value / hours.Value)
      ANNTBBMW.Value = ANNTBBMW.Value * (DH.Value / hours.Value)
      ANNTMW.Value = ANNTMW.Value * (DH.Value / hours.Value)
      ANNRMW.Value = ANNRMW.Value * (DH.Value / hours.Value)
    End If
    'Turn Calculation back to Automatic:
    Application.Calculation = xlAutomatic
    Hcalc
    'Record_Results
End Sub

Sub Find_Blockers()

    Set controlp = Worksheets("H")
    Set OP = Worksheets("Blocks")

    Set P = controlp.Range("BSSTART")
    Set PHIS = controlp.Range("PHIS")
    Set THS = controlp.Range("THS")
    Set NHSTAT = controlp.Range("NHSTAT")
    Set HX = controlp.Range("HX")
    Set HY = controlp.Range("HY")
    Set O = OP.Range("BSOUT")

    Set P = P.Offset(1, 0)
    SMAX = 0.5 * (HX.Value + HY.Value)

    Dim n_array(10)
    Dim a_array(10)
    Dim b_array(10)
    Dim f_array(10)
    Dim temp(10)

    Application.Calculation = xlManual

    clear_blocks

    Set O = O.Offset(0, 2)

    For i = 1 To NHSTAT
      OP.Range("BSOUT").Offset(-3, 0).Value = i
      O.Offset(i, -2).Value = i
      Set P = P.Offset(1, 0)
      blocknum = 0
      aMax = SMAX / Sin((3.1415927 / 180) * (P.Offset(0, -16).Value))
      For j = max(1, i - 3) To min(NHSTAT, i + 60)
        If i <> j Then
          BLoc = 180 + (180 / 3.1415927) * atan2((P.Offset(0, -19).Value - P.Offset(j
```

```
- i, -19).Value), (P.Offset(0, -20).Value - P.Offset(j - i, -20).Value))
        kappa = P.Offset(0, -17).Value - BLoc
        a = Cos((3.1415927 / 180) * kappa) * ((P.Offset(0, -20).Value - P.Offset(j -
 i, -20)) ^ 2 + (P.Offset(0, -19).Value - P.Offset(j - i, -19)) ^ 2) ^ 0.5
        If Abs(kappa) > 0.01 Then b = Tan((3.1415927 / 180) * kappa) * a Else b = 0
        If a < aMax And Abs(b) < SMAX And Abs(kappa) < 90 Then
          blocknum = blocknum + 1
          n_array(blocknum) = j
          a_array(blocknum) = a
          b_array(blocknum) = b
          f_array(blocknum) = 0
        End If
      End If
    Next j
    offstep = 3
    For k = 1 To blocknum
      If offstep = 2 Then offstep = 3 Else offstep = 2
      For l = offstep To blocknum Step 2
        If a_array(l) < a_array(l - 1) Then
          temp(1) = n_array(l)
          temp(2) = a_array(l)
          temp(3) = b_array(l)
          n_array(l) = n_array(l - 1)
          a_array(l) = a_array(l - 1)
          b_array(l) = b_array(l - 1)
          n_array(l - 1) = temp(1)
          a_array(l - 1) = temp(2)
          b_array(l - 1) = temp(3)
        End If
      Next l
    Next k

    For k = -1 * (SMAX / 2) To (SMAX / 2) Step 0.1
      BN = 1
      Done = 0
      Do
        If Abs(b_array(BN) - k) < (SMAX / 2) Then
          f_array(BN) = f_array(BN) + (0.1 / SMAX)
          Done = 1
        End If
        BN = BN + 1
      Loop Until Done = 1 Or BN > blocknum
    Next k
    O.Offset(i, 3).Value = blocknum
    O.Offset(i, 2).FormulaR1C1 = "=HY * Cos(Radians(OFFSET(START,1+RC[-4],7)/ 2))"
    O.Offset(i, 1).Value = (3.1415927 / 180) * P.Offset(0, -16)
    O.Offset(i, -1).FormulaR1C1 = "=sin(RC[2])/RC[3]"
    O.Offset(i, 0).FormulaR1C1 = "=RC[7]*MAX(0,1-RC[5]*RC[-1])+RC[11]*MAX(0,1-RC[9]*
RC[-1])+RC[15]*MAX(0,1-RC[13]*RC[-1])+RC[19]*MAX(0,1-RC[17]*RC[-1])+RC[23]*MAX(0,1-R
C[21]*RC[-1])+RC[27]*MAX(0,1-RC[25]*RC[-1])"
    For k = 1 To blocknum
      O.Offset(i, (k - 1) * 4 + 4).Value = n_array(k)
      O.Offset(i, (k - 1) * 4 + 5).Value = a_array(k)
      O.Offset(i, (k - 1) * 4 + 6).Value = b_array(k)
      O.Offset(i, (k - 1) * 4 + 7).Value = f_array(k)
      n_array(k) = 0
      a_array(k) = 0
      b_array(k) = 0
    Next k
  Next i
  Application.Calculation = xlAutomatic
```

```
  Application.Goto Reference:="temp"
  Hcalc
End Sub

Sub Clean_Table()
    'Now clear the main table:
    Application.Goto Reference:="START"
    ' The main table starts TWO rows below the "Start" Range
    ActiveCell.Offset(2, 0).Range("A1").Select
    ' This will delete EVERY CONTIGUOUS CELL in the table region
    Selection.CurrentRegion.Select
    Selection.ClearContents
    ActiveCell.Offset(-2, 0).Range("A1").Select
End Sub

Sub clear_blocks()
    Application.Goto Reference:="BSOUT"
    ActiveCell.Offset(1, 0).Range("A1").Select
    ' This will delete EVERY CONTIGUOUS CELL in the table region
    Selection.CurrentRegion.Select
    Selection.ClearContents
    Application.Goto Reference:="BSOUT"
End Sub

Sub Draw_Picture()

  Set TL = Worksheets("Pic").Range("TOPLEFT")
  Set HP = Worksheets("H").Range("START")
  FRAD = Worksheets("H").Range("FRAD")
  NHSTAT = Worksheets("H").Range("NHSTAT")
  MTHW = Worksheets("H").Range("MTHW")
  HX = Worksheets("H").Range("HX")
  HY = Worksheets("H").Range("HY")
  'Locate left-most heliostat:
  Application.Calculation = xlManual
  leftedge = 0
  For i = 1 To NHSTAT
    If HP.Offset(i + 1, 1).Value < leftedge Then leftedge = HP.Offset(i + 1, 1).Valu
e
  Next i
  cent = -1 * leftedge + 10

  Application.Goto Reference:="TOWERVIEW"  'For viewing only
  Range("TOWERVIEW") = "X"
  Application.ScreenUpdating = False
  Selection.SpecialCells(xlConstants, 2).Select
  Selection.ClearContents
  Selection.Interior.ColorIndex = xlNone
 'Draw Tower:

  For i = (cent - MTHW) / 3 To (cent + MTHW - 1) / 3
    For j = (FRAD + 10 - MTHW) / 3 To (FRAD + 10 + MTHW - 1) / 3
      TL.Offset(Int(j), Int(i)) = "T"
      TL.Offset(Int(j), Int(i)).Select
      With Selection.Interior
        .ColorIndex = 3
        .Pattern = xlSolid
        .PatternColorIndex = xlAutomatic
      End With
    Next j
  Next i
```

```
  'Draw Hstats:
  Application.Goto Reference:="TOPLEFT"  'For viewing only
  Application.ScreenUpdating = False
  For i = 1 To NHSTAT
    x = HP.Offset(i + 1, 1).Value
    y = HP.Offset(i + 1, 2).Value
    xhw = HX / 2
    yhw = HY / 2
    For j = (cent + x - xhw) / 3 To (cent + x + xhw - 1) / 3
      For k = (FRAD + 10 - y - yhw) / 3 To (FRAD + 10 - y + yhw - 1) / 3
        TL.Offset(Int(k), Int(j)) = "H"
        TL.Offset(Int(k), Int(j)).Select
        With Selection.Interior
          .ColorIndex = 1
          .Pattern = xlSolid
          .PatternColorIndex = xlAutomatic
        End With

      Next k
    Next j
  Next i
  Application.ScreenUpdating = True
  Application.Calculation = xlAutomatic
End Sub

' Martin's explicit recalculation
Sub RecalcWorkBook()
    Dim wh As Worksheet
    For Each wh In Application.ActiveWorkbook.Worksheets
        wh.Calculate    ' Recalculate
    Next wh
End Sub

'Ted's Targeted Heliostat Recalculation
Sub Hcalc()
  'Worksheets("Control").Calculate
  'Worksheets("H").Calculate
  'Worksheets("Blocks").Calculate
  'Worksheets("TRC").Calculate
  'Worksheets("Engine").Calculate
  Calculate
  'Worksheets("H").Calculate
  'Worksheets("Iter").Calculate
  'Application.Goto Reference:="RECTEMP"
  'ActiveCell.FormulaR1C1 = _
   '     "=CRET+((RMW-IF(ISERROR(RADMW),0.2,RADMW))/RECCAL)*(MAXTEMP-CRET)*cp(AVERAG
E(CRET,MAXTEMP))/cp(AVERAGE(CRET,RECTEMP))"
End Sub


Sub Record_Results()
'
' Record_Results Macro
' Macro recorded 12/30/97 by Ted Caplow
'

'
    Application.Goto Reference:="RESULTS"
    ActiveCell.Range("a1:a67").Select
    Selection.Copy
```

```
    ActiveCell.Offset(-3, 0).Select
    Selection.End(xlToRight).Select
    Selection.End(xlToRight).Select
    ActiveCell.Offset(3, 1).Range("a1").Select
    Selection.PasteSpecial Paste:=xlValues, Operation:=xlNone, SkipBlanks:= _
        False, Transpose:=False
    Selection.PasteSpecial Paste:=xlFormats, Operation:=xlNone, SkipBlanks:= _
        False, Transpose:=False
    Application.Goto Reference:="RESULTS"
    ActiveCell.Range("a68:a76").Select
    Selection.Copy
    ActiveCell.Offset(-70, 0).Select
    Selection.End(xlToRight).Select
    Selection.End(xlToRight).Select
    ActiveCell.Offset(70, 1).Range("a1").Select
    Selection.PasteSpecial Paste:=xlFormulas, Operation:=xlNone, SkipBlanks:= _
        False, Transpose:=False
    Selection.PasteSpecial Paste:=xlFormats, Operation:=xlNone, SkipBlanks:= _
        False, Transpose:=False
    ActiveCell.Offset(-70, 0).Range("a1").Select
End Sub
```

```
Sub Annual_Calcs()    'Convolves Dish field through solar year

  Set control_panel = Worksheets("D")
  Set input_panel = Worksheets("S")
  Set second_panel = Worksheets("Control")

  Set INSOL = control_panel.Range("INSOL")
  Set place = input_panel.Range("TAB1_HEAD")
  Set DH = input_panel.Range("Lighthours")

  Set ASDBHours = control_panel.Range("ASDBHOURS")
  Set ASDBDMW = control_panel.Range("ASDBDMW")
  Set ASDBeMW = control_panel.Range("ASDBEMW")
  Set ANNASDBEMW = control_panel.Range("ANNASDBEMW")
  Set ANNASDBDMW = control_panel.Range("ANNASDBDMW")
  Set ASDBPKDMW = control_panel.Range("ASDBPKDMW")

  EARTH = second_panel.Range("EARTH")
  solcon = second_panel.Range("SOLCON")
    'Turn off automatic calculation to enhance speed:
  Application.Calculation = xlManual

  'Set all annual sums to zero:
  ANNASDBDMW.Value = 0
  ANNASDBEMW.Value = 0
  ASDBPKDMW.Value = 0
  ASDBHours.Value = 0

  colsum = 0

  For i = 1 To 18
    colsum = 0
    For j = 1 To 28
      If place.Offset(j, i).Value > 0 Then colsum = colsum + place.Offset(j, i).Valu
e
    Next j
    If colsum > 0 Then
      INSOL.Value = solcon * (EARTH / solcon) ^ (1 / Sin((i * 5 - 2.5) * (3.1415927
/ 180)))
      Calculate
      'First, check for "system cut-out" conditions:
      If ASDBDMW.Value > 0 Then
        If ASDBDMW.Value > ASDBPKDMW.Value Then ASDBPKDMW.Value = ASDBDMW.Value
        ASDBHours.Value = ASDBHours.Value + colsum * DH.Value
        ANNASDBEMW.Value = ANNASDBEMW.Value + colsum * ASDBeMW.Value
        ANNASDBDMW.Value = ANNASDBDMW.Value + colsum * ASDBDMW.Value
      End If
    End If
  Next i
  'Now we must readjust all of the totals to reflect the cut-out hours:
  ANNASDBEMW.Value = ANNASDBEMW.Value * (DH.Value / ASDBHours.Value)
  ANNASDBDMW.Value = ANNASDBDMW.Value * (DH.Value / ASDBHours.Value)

  'Turn Calculation back to Automatic:
  Application.Calculation = xlAutomatic
  Calculate
End Sub
```

```
Sub Record_ASDB()
'
' Record_ASDB Macro
' Macro recorded 1/2/98 by Ted Caplow
'

'
    Application.Goto Reference:="ASDBRESULTS"
    ActiveCell.Range("a1:a45").Select
    Selection.Copy
    ActiveCell.Offset(-3, 0).Select
    Selection.End(xlToRight).Select
    Selection.End(xlToRight).Select
    ActiveCell.Offset(3, 1).Range("a1").Select
    Selection.PasteSpecial Paste:=xlValues, Operation:=xlNone, SkipBlanks:= _
        False, Transpose:=False
    Selection.PasteSpecial Paste:=xlFormats, Operation:=xlNone, SkipBlanks:= _
        False, Transpose:=False
    ActiveCell.Offset(-3, 0).Range("a1").Select
End Sub
```

```
Sub Generate_Solar_Year()    'generates two tables:
    'one with normalized elev/azim frequencies
    'one with same frequencies weighted for atmospheric attenutation
    'both are a sole function of latitude

  Clear_Solar_Table

  Set control_panel = Worksheets("Control")
  Set output_panel = Worksheets("S")

  LAT = control_panel.Range("LAT")
  LAT = 6.2832 * (LAT / 360)
  ink = control_panel.Range("step")
  ink2 = control_panel.Range("step2")
  earthcon = control_panel.Range("EARTH")
  solcon = control_panel.Range("SOLCON")

  Set monthplace = control_panel.Range("MONTH")
  Set place = output_panel.Range("TAB1_HEAD")
  Set Message = output_panel.Range("Message")
  Set LH = output_panel.Range("LIGHTHOURS")

  LH.Value = 0

  Application.Calculation = xlManual
  Application.Goto Reference:="MONTH"    'for view control only

  For i = 1 To 12
    monthplace.Offset(i, 2).Value = 0
  Next i

  For days = 1 To 365 Step ink
    Mnth = Int(days / 30.42) + 1
    SINDEC = -1 * Sin(0.4093) * Cos(6.2832 * (days + 10) / 365.25)
    COSDEC = (1 - SINDEC ^ 2) ^ 0.5
    For Clock = 0 To (24 - ink2) Step ink2
      hours = Clock + ink2 / 2
      HANG = 6.2832 * (hours / 24)
      If HANG < 3.1416 Then THETA = HANG + 3.1416
      If HANG >= 3.1416 Then THETA = HANG - 3.1416
      COSZEN = Cos(LAT) * COSDEC * Cos(HANG) + Sin(LAT) * SINDEC
      If COSZEN > 1 Then COSZEN = 1
      ZEN = (180 / 3.1415927) * acos(COSZEN)
      PHI = 90 - ZEN
      THETA = 360 * (THETA / 6.2832)
      'Now we have phi and theta in degrees and can place them as we choose:
      'If it's daylight, then place entry in matrix, add to hour counter:
      If PHI > 0 And THETA > 40 Then
        XOFF = Int(PHI / 5) + 1
        YOFF = Int(THETA / 10) - 3
        place.Offset(YOFF, XOFF).Value = place.Offset(YOFF, XOFF) + 1
        monthplace.Offset(Mnth, 2).Value = monthplace.Offset(Mnth, 2).Value + 0.001
* solcon * (earthcon / solcon) ^ (1 / Sin((3.1415927 / 180) * PHI)) * ink * ink2 / 3
0.4
        LH.Value = LH.Value + (ink * ink2)
      End If
    Next Clock
    place.Offset(-1, 0).Value = days
```

```
  Next days
  Calculate
  'Now normalize the table:
  Total = output_panel.Range("TABTOT")
  For i = 1 To 18
    For j = 1 To 28
      If place.Offset(j, i).Value > 0 Then
        place.Offset(j, i).Value = place.Offset(j, i).Value / Total
      End If
    Next j
  Next i
  Message.FormulaR1C1 = "Table is NOT weighted for attenuation"
  'Include_Attenuationc  NO!! This was a very confusing approach. Stick with
  '                      time fractions, not power fractions.
  Application.Calculation = xlAutomatic
End Sub



Sub Include_Attenuation() 'Adds atmospheric attenuation weighting to solar data

  Set output_panel = Worksheets("S")

  Set place = output_panel.Range("TAB1_HEAD")
  Set Message = output_panel.Range("Message")

  For i = 1 To 18
    For j = 1 To 28
      ZEN = 90 - (i * 5 - 2.5)
      ZEN = 6.2832 * (ZEN / 360)
      If place.Offset(j, i).Value > 0 Then
        place.Offset(j, i).Value = place.Offset(j, i).Value * Cos(ZEN)
      End If
    Next j
  Next i
  'Now normalize the table:
  Total = output_panel.Range("TABTOT")
  For i = 1 To 18
    For j = 1 To 28
      If place.Offset(j, i).Value > 0 Then
        place.Offset(j, i).Value = place.Offset(j, i).Value / Total
      End If
    Next j
  Next i
  Message.FormulaR1C1 = "Table has been weighted for attenuation"
End Sub



'
' Clear_Solar_Table Macro
' Macro recorded 10/16/97 by Ted Caplow
'
'
Sub Clear_Solar_Table()
    Application.Goto Reference:="TAB1_HEAD"
    ActiveCell.Offset(1, 1).Range("A1:T28").Select
    Selection.ClearContents
    ActiveCell.Offset(-1, -1).Range("A1").Select
End Sub
```

There are two calculation methods for finding the RGT properties:

1. Based upon the ASDB RGT, and Stefano Consonni's suggestions:

Temperatures		Pressure Ratios:		Efficiencies	
Ambient:	15.0	Head:	2.33	C, isen	0.705
isen T2:	126.67	Tail:	2.13	T, isen	0.905
TIT:	900			C, poly	0.737
isen T4:	716.86			T, poly	0.896

Check with T2:
by poly: 126.67 * calculations follow Cohen et al p. 50-53
Check with T4:
by poly: 716.86

Consonni suggests adding 3-4 points (we choose 3) to the polytropic efficiencies to account for scale:
(Consonni also suggests using TIT 850 but I have maintained TIT 817 for solar fraction)
Pressure Ratio has been determined through manual optimization

MPT RGT:

Temperatures		Pressure Ratios:		Efficiencies	
Ambient:	15.0	Head:	2.70	C, isen	0.733
poly T2:	143.84	Tail:	2.540	T, isen	0.934
TIT:	817	(no receiver drop included)		C, poly	0.767
poly T4:	605.45			T, poly	0.926
				Regen	0.900

Check with T2: Regeneration Exit Temps:
by isen: 143.84 High P: 190.00
Check with T4: Low P: 559.29
by isen: 605.45

Net efficiency:
Cp corrected: 37.34%

Results:
36.2% at 800 C and 2.6 bar *Ambient 19.8*
37.7% at 850 C and 2.7 bar *These are pretty fair numbers... these are before generator, gasonly*

2. Method: derive polytopic efficiencies from the Allison turbines, and use those without modification
not yet pursued

									Dagget 4 MWe Cogen (Copy of Varync breakeven function to fiddle with gas co			Dagget 2 M
									Mirror Cost	$/MWht	$/mmBTU	$/MWht
				$10 gas					45.05	10.00	2.94	10.58
				$11 gas					54.3	11.00	3.24	11.53
				$12 gas					63.5	12.00	3.53	12.47
									39.4	9.39	2.76	10.00
									49.1	10.44	3.07	11.00
									58.9	11.50	3.38	12.00
carbon content: 48.6 kg C/MWht (derived from Bob's 13.5 kg C/GJ)				$50 / ton carbon tax					76.7	13.43	3.95	13.82
				Awerbuch beta = -1.0, gas DR = 0%, Awerbuch base case					191	25.81	7.59	25.53
My method: use an 85% experience curve for the heliostats ONLY,				5% GAS DR; near Awerbach "low risk case"					101.5	16.11	4.74	16.36
based on the cumulative # of plants built.									25.8	7.92	2.33	8.61
Let 1/2 the plants be cogen and the other 1/2 recup (I will average the field sizes and the b-e points)									33.7	8.77	2.58	9.42
Use insights from Kolb to get a ratio for the first plant to its component costs. I will use 2:1									41.55	9.62	2.83	10.22
I will reduce this to 1.5:1 on the second plant (since this may also have R&D)									42.2	9.69	2.85	10.29
From the third plant on, it's component costs only.									51.9	10.74	3.16	11.28
Experience curve doesn't begin until the third plant.									61.7	11.80	3.47	12.29
									60	11.62	3.42	12.11
TOTAL BUY DOWN:	$247,949,404	$136,624,889	$84,531,852	$57,514,776	$47,888,411	$6,788,987	$22,781,554		72.3	12.95	3.81	13.37
STARTING HSTAT PRICE:	200								84.6	14.28	4.20	14.63
EXPERIENCE RATIO:	85%											

SYSTEM:	Dagget 4 MWe Cogen			8% RDR	$50 / ton carbc	Awerbuch bet	5% GAS DR; near Auerbach "low risk case"
GAS COST ($/MWht):	10	11	12	11	13.43	25.81	16.11
CARBON TAX ($/kg):							
B/E MIRROR COST ($/m^2):	45.05	54.3	63.5	72.3	76.7	191	101.5
HSTAT UNITS / PLANT	326	326	326	326	326	326	326
effective MIRROR AREA:	14,971	14,971	14,971	14,971	14,971	14,971	14,971
BALANCE OF PLANT COST:	$4,211,600	$4,211,600	$4,211,600	$4,211,600	$4,211,600	$4,211,600	$4,211,600

BUY DOWN COSTS:

plant	hstat cost	Lower Gas Price	Medium Gas Pric	Higher Gas Pri	Lower Discou	Carbon Tax an	Fuel Risk Adj	Fuel Risk Adjust	TOTAL BOP COST
1	$200	$8,851,113	$8,574,149	$8,298,683	$8,035,193	$7,903,449	$4,481,078	$7,160,887	$4,211,600
2	$200	$14,436,548	$13,951,861	$13,469,795	$13,008,688	$12,778,135	$6,788,987	$11,478,652	$8,423,200
3	$182	$16,484,765	$15,861,597	$15,241,797	$14,648,946	$14,352,520	$6,788,987	$12,681,756	$12,634,800
4	$170	$18,355,391	$17,593,742	$16,836,209	$16,111,613	$15,749,314	$6,788,987	$13,707,270	$16,846,400
5	$161	$20,096,284	$19,196,153	$18,300,887	$17,444,546	$17,016,375	$6,788,987	$14,603,050	$21,058,000
6	$155	$21,736,103	$20,697,489	$19,664,490	$18,676,404	$18,182,361	$6,788,987	$15,397,755	$25,269,600
7	$149	$23,293,770	$22,116,675	$20,945,943	$19,826,112	$19,266,197	$6,788,987	$16,110,310	$29,481,200
8	$145	$24,782,636	$23,467,059	$22,158,594	$20,907,018	$20,281,230	$6,788,987	$16,754,063	$33,692,800
9	$141	$26,212,577	$24,758,519	$23,312,320	$21,929,000	$21,237,339	$6,788,987	$17,338,891	$37,904,400
10	$137	$27,591,170	$25,998,630	$24,414,698	$22,899,633	$22,142,100	$6,788,987	$17,872,371	$42,116,000
11	$134	$28,924,392	$27,193,370	$25,471,705	$23,824,895	$23,001,490	$6,788,987	$18,360,480	$46,327,600
12	$131	$30,217,071	$28,347,567	$26,488,169	$24,709,614	$23,820,337	$6,788,987	$18,808,046	$50,539,200
13	$129	$31,473,177	$29,465,191	$27,468,060	$25,557,760	$24,602,611	$6,788,987	$19,219,039	$54,750,800
14	$127	$32,696,027	$30,549,560	$28,414,696	$26,372,651	$25,351,629	$6,788,987	$19,596,777	$58,962,400
15	$125	$33,888,434	$31,603,485	$29,330,887	$27,157,098	$26,070,203	$6,788,987	$19,944,070	$63,174,000
16	$123	$35,052,803	$32,629,372	$30,219,041	$27,913,507	$26,760,740	$6,788,987	$20,263,326	$67,385,600
17	$121	$36,191,220	$33,629,308	$31,081,243	$28,643,965	$27,425,325	$6,788,987	$20,556,630	$71,597,200
18	$119	$37,305,503	$34,605,109	$31,919,312	$29,350,288	$28,065,777	$6,788,987	$20,825,801	$75,808,800
19	$118	$38,397,255	$35,558,379	$32,734,848	$30,034,080	$28,883,696	$6,788,987	$21,072,439	$80,020,400
20	$117	$39,467,892	$36,490,534	$33,529,271	$30,696,757	$29,280,501	$6,788,987	$21,297,964	$84,232,000
21	$115	$40,518,680	$37,402,841	$34,303,844	$31,339,586	$29,857,457	$6,788,987	$21,503,639	$88,443,600
22	$114	$41,550,753	$38,296,431	$35,059,701	$31,963,698	$30,415,697	$6,788,987	$21,690,598	$92,655,200
23	$113	$42,565,132	$39,172,329	$35,797,865	$32,570,118	$30,956,244	$6,788,987	$21,859,864	$96,866,800
24	$112	$43,562,742	$40,031,457	$36,519,261	$33,159,768	$31,480,022	$6,788,987	$22,012,362	$101,078,400
25	$111	$44,544,425	$40,874,659	$37,224,729	$33,733,492	$31,987,873	$6,788,987	$22,148,932	$105,290,000
26	$110	$45,510,948	$41,702,700	$37,915,037	$34,292,055	$32,480,564	$6,788,987	$22,270,342	$109,501,600
27	$109	$46,463,015	$42,516,285	$38,590,889	$34,836,162	$32,958,799	$6,788,987	$22,377,296	$113,713,200
28	$108	$47,401,272	$43,316,060	$39,252,931	$35,366,459	$33,423,223	$6,788,987	$22,470,440	$117,924,800
29	$107	$48,326,314	$44,102,620	$39,901,758	$35,883,541	$33,874,433	$6,788,987	$22,550,369	$122,136,400
30	$106	$49,238,692	$44,876,517	$40,537,921	$36,387,960	$34,312,980	$6,788,987	$22,617,634	$126,348,000
31	$105	$50,138,918	$45,638,261	$41,161,932	$36,880,226	$34,739,373	$6,788,987	$22,672,747	$130,559,600
32	$104	$51,027,466	$46,388,327	$41,774,265	$37,360,814	$35,154,089	$6,788,987	$22,716,182	$134,771,200
33	$104	$51,904,777	$47,127,157	$42,375,361	$37,830,166	$35,557,568	$6,788,987	$22,748,380	$138,982,800
34	$103	$52,771,265	$47,855,163	$42,965,634	$38,288,694	$35,950,224	$6,788,987	$22,769,755	$143,194,400
35	$102	$53,627,315	$48,572,731	$43,545,469	$38,736,784	$36,332,442	$6,788,987	$22,780,692	$147,406,000
36	$102	$54,473,290	$49,280,224	$44,115,229	$39,174,799	$36,704,584	$6,788,987	$22,781,554	$151,617,600
37	$101	$55,309,528	$49,977,981	$44,675,253	$39,603,078	$37,066,990	$6,788,987	$22,781,554	$155,829,200
38	$100	$56,136,350	$50,666,321	$45,225,860	$40,021,940	$37,419,980	$6,788,987	$22,781,554	$160,040,800
39	$100	$56,954,057	$51,345,546	$45,767,351	$40,431,687	$37,763,855	$6,788,987	$22,781,554	$164,252,400
40	$99	$57,762,932	$52,015,939	$46,300,011	$40,832,602	$38,098,898	$6,788,987	$22,781,554	$168,464,000
41	$99	$58,563,244	$52,677,770	$46,824,109	$41,224,955	$38,425,378	$6,788,987	$22,781,554	$172,675,600
42	$98	$59,355,247	$53,331,291	$47,339,897	$41,608,998	$38,743,549	$6,788,987	$22,781,554	$176,887,200
43	$97	$60,139,182	$53,976,745	$47,847,617	$41,984,974	$39,053,652	$6,788,987	$22,781,554	$181,098,800
44	$97	$60,915,278	$54,614,358	$48,347,497	$42,353,109	$39,355,915	$6,788,987	$22,781,554	$185,310,400
45	$96	$61,683,750	$55,244,349	$48,839,755	$42,713,622	$39,650,555	$6,788,987	$22,781,554	$189,522,000
46	$96	$62,444,806	$55,866,922	$49,324,595	$43,066,717	$39,937,778	$6,788,987	$22,781,554	$193,733,600
47	$95	$63,198,641	$56,482,276	$49,802,216	$43,412,593	$40,217,782	$6,788,987	$22,781,554	$197,945,200
48	$95	$63,945,443	$57,090,597	$50,272,803	$43,751,436	$40,490,752	$6,788,987	$22,781,554	$202,156,800
49	$94	$64,685,391	$57,692,063	$50,736,536	$44,083,424	$40,756,868	$6,788,987	$22,781,554	$206,368,400
50	$94	$65,418,655	$58,286,845	$51,193,585	$44,408,728	$41,016,299	$6,788,987	$22,781,554	$210,580,000
60	$90	$72,427,298	$63,910,670	$55,440,078	$47,337,773	$43,286,620	$6,788,987	$22,781,554	$252,696,000
70	$87	$78,907,516	$69,006,070	$59,158,147	$49,738,393	$45,028,517	$6,788,987	$22,781,554	$294,812,000
80	$84	$84,951,734	$73,665,471	$62,440,215	$51,703,014	$46,334,414	$6,788,987	$22,781,554	$336,928,000
90	$82	$90,626,624	$77,955,544	$65,352,956	$53,298,307	$47,270,982	$6,788,987	$22,781,554	$379,044,000
100	$80	$95,982,374	$81,926,477	$67,946,557	$54,574,460	$47,888,411	$6,788,987	$22,781,554	$421,160,000
150	$73	$119,320,678	$98,340,693	$77,474,113	$57,514,776	$47,888,411	$6,788,987	$22,781,554	$631,740,000
200	$68	$138,190,685	$110,286,613	$82,533,373	$57,514,776	$47,888,411	$6,788,987	$22,781,554	$842,320,000
250	$64	$153,999,912	$119,171,752	$84,531,852	$57,514,776	$47,888,411	$6,788,987	$22,781,554	$1,052,900,000
300	$62	$167,508,957	$125,756,709	$84,531,852	$57,514,776	$47,888,411	$6,788,987	$22,781,554	$1,263,480,000
350	$60	$179,191,249	$130,514,914	$84,531,852	$57,514,776	$47,888,411	$6,788,987	$22,781,554	$1,474,060,000
400	$58	$189,368,110	$133,767,687	$84,531,852	$57,514,776	$47,888,411	$6,788,987	$22,781,554	$1,684,640,000
450	$56	$198,270,888	$135,746,378	$84,531,852	$57,514,776	$47,888,411	$6,788,987	$22,781,554	$1,895,220,000
500	$55	$206,073,487	$136,624,889	$84,531,852	$57,514,776	$47,888,411	$6,788,987	$22,781,554	$2,105,800,000
750	$50	$233,235,011	$136,624,889	$84,531,852	$57,514,776	$47,888,411	$6,788,987	$22,781,554	$3,158,700,000
1250	$44	$247,949,404	$136,624,889	$84,531,852	$57,514,776	$47,888,411	$6,788,987	$22,781,554	$5,264,500,000
1500	$42	$247,949,404	$136,624,889	$84,531,852	$57,514,776	$47,888,411	$6,788,987	$22,781,554	$6,317,400,000

(starting gas cost:)		$11	/MWht	(check math)
Gas Discount Rate:		5.0%		12.46221
Gas Increase Rate:		0.0%		**16.10187**
year	fuel price	NPV		
1	$11.00	$10.48	/MWht	0.952381
2	$11.00	$9.98	/MWht	0.907029
3	$11.00	$9.50	/MWht	0.863838
4	$11.00	$9.05	/MWht	0.822702
5	$11.00	$8.62	/MWht	0.783526
6	$11.00	$8.21	/MWht	0.746215
7	$11.00	$7.82	/MWht	0.710681
8	$11.00	$7.45	/MWht	0.676839
9	$11.00	$7.09	/MWht	0.644609
10	$11.00	$6.75	/MWht	0.613913
11	$11.00	$6.43	/MWht	0.584679
12	$11.00	$6.13	/MWht	0.556837
13	$11.00	$5.83	/MWht	0.530321
14	$11.00	$5.56	/MWht	0.505068
15	$11.00	$5.29	/MWht	0.481017
16	$11.00	$5.04	/MWht	0.458112
17	$11.00	$4.80	/MWht	0.436297
18	$11.00	$4.57	/MWht	0.415521
19	$11.00	$4.35	/MWht	0.395734
20	$11.00	$4.15	/MWht	0.376889

TOTAL NPV:	$137.08
WACC(discount rate):	10.0%
CCF: (for WACC)	11.7%
LEVELIZED COST OF GAS	**$16.10**
Specific to plant:	
Assumed Gas Price:	$11.00
Assumed NPV:	$93.65
Current NPV:	$137.08
Difference	$43.44
Incremental Gas Use:	19,698
Capital Adjustment:	$855,585

note: this isn't fair, b/c the LEC of all pla
if we accept that gas is so much more e

APPENDIX D: Further Discussion of the Linked Dish Array (LDA)

D.1 Linked Dish Array Modeling

Note: This section describes some of the modeling challenges presented by the LDA concept. A decision was made, based upon these challenges, to discontinue investigation into the LDA for the purposes of this study. Thus, chapters 4 and 5 are only concerned with the MPT and ASDB designs. The LDA material is only included here as a possible platform for future research.

Whenever the proposal of a linked-dish array is floated in the solar community, it is quickly met by a chorus of doubts concerning thermal transport. A handful of early failures (see chapter 2) have no doubt contributed to this effect, and there is certainly substance for concern. Due to their unparalleled focusing power, dish systems are able to run at higher temperatures than other solar technologies. If the collected heat must be bodily transported in sensible form, those high temperatures create the potential for drastic thermal losses enroute to the final destination (a central heat engine in the case of the LDA). Moreover, if the system operates at pressure, then pressure losses over the piping network must also be accounted for. Finally, the capital and ongoing costs of the pipe itself (and any associated insulation) will increase the levelized cost of energy for the entire project. It is no wonder that the first instinct of many is to doubt the feasibility of thermal transport in dish systems.

But just how insuperable are these piping problems? Certainly, the viability of the hot-air OLAA system rests heavily upon the issue of piping. The superior optical efficiency of the dish collector and the superior conversion efficiency of the central gas turbine will both be decisively undermined if the piping network which joins them is inadequate or prohibitively expensive. Clearly, the LDA cannot move forward without providing a reasonable solution to the piping problem. This section will discuss some aspects of OLAA design which relate to the piping problem, including a few worked examples. Based on the considerations, a decision was made to *discontinue the current investigation* of LDA's. This decision stems more from an abundance of technical uncertainties than from any decisively negative finding.

D.1.1 The Layout of the Linked-Dish Arrays

The LDA is composed of a centrally located heat engine & generator (power plant) amid a circular field of dish modules. The power plant is located in the middle, and the field is circular, because of the need to minimize the total distance between the dishes and the plant. Unlike heliostat fields, the optical function of each dish in the LDA field is unaffected by its placement relative to the central power plant; thus the minimizing configuration is a circle.

In the hot-air (OLAA) LDA, each dish has both an inlet and a discharge pipe. The dishes are arranged in series of perhaps 3-10 dishes, with this number being fixed throughout the field for any one system design. The first dish in each series receives air off of the compressor though the inlet pipe, heats the air, and passes it through the discharge pipe to the next dish in the series. The discharge pipe of the last dish in each series leads back to the combustion chamber at the central power plant. Fields with multiple series, such as those proposed in this work, operate in parallel: the compressed air is branched off and divided evenly among the lead dishes from each series, and discharge from all of the final dishes is mixed together before entering the combustion chamber for temperature boosting.

The air is steadily heated as it passes through each dish series, resulting in a decrease in density. (The pressure drops continuously throughout the process. In the later dishes, the air is much hotter and moving faster (due to reduced density and constant mass flow). For these reasons, it is essential that the final dishes be adjacent to the power plant, in order to minimize the total degree-meters of piping (one "degree-meter" is one meter of pipe traversed by fluid one degree above the ambient). Packing all of the final dishes around the plant implies arrangement of the penultimate dishes just behind them, and so on, resulting in an "inside-out" field arrangement, in which the flow initially passes through long pipes from the compressor to the lead dishes at the edge of the circle, then returns to the power plant dish by dish.

The spacing between the dishes in the circle, however, is not so straightforward. If the dishes are placed in maximum proximity, then each dish will be deeply shaded by its neighbors when the sun is on the horizon. This shading effect will be particularly acute in the East-West direction, and particularly weak in the North-South direction, because at the intended latitudes of application the sun is never near the horizon to the North or South. Thus each dish can be placed closer to it N-S neighbors than it can to its E-W neighbors.

Nearly complete freedom from shading could be achieved if the dishes were placed a great way apart, but the resulting increases in piping cost would be unacceptable. Thus it is necessary to space the dishes in such a way that any increase in spacing would not justify the increased piping required to span the increase. This objective creates an optimization problem of considerable complexity, as the total cost of increased piping depends upon a great many factors.

The physical coupling between the dish receiver and the piping network is the area of greatest uncertainty. The pipes are fixed on the ground, yet most parabolic dish designs are mounted on pivots at the midpoint of the dish itself; the receiver is located at the focal point and swings widely to track the sun. An inflexible pipe may be mounted on the dish structure to connect the receiver with inlet and outlet ports located on the back of the dish *near* the pivot point, but flexible hoses will be required to actually connect these ports to the pipes on the ground. These hoses must withstand high temperatures (600 - 800 C), be very well insulated, and last for thousands of slow flexing cycles. Although this task does

not appear to be technologically impossible, the required materials are not part of the general solar equipment set and may be expensive to design and manufacture. Alternative coupling methods (such as two rotating pipe joints set 90 degrees apart on the dish rim, combined with a different pivoting scheme, or a Cassegrain mount with a redesigned receiver) introduce similar or greater uncertainties.

D.1.2 Pressure Losses in Pipes

D.1.2.1 General Pressure Drop Considerations

Pressure losses in the piping network are equal in importance to thermal losses. Regardless of the strategy pursued, the higher the pressure losses, the more expensive the energy will be from the entire system. Assume that a currently available gas turbine has been chosen for solar modification by the OLAA scheme. If the solar field piping losses are too large, then the compressor for this turbine will need to be upgraded. The new compressor will not only cost more, but will also require more power and reduce the net system output. Worse yet, when the piping system is closed off by valves and the compressed air is ducted directly to the burner instead (nighttime operation), then the oversized compressor will be a poor match for the turbine selected. Conversely, if the turbine is not enlarged, then the daytime efficiency of the turbine will be diminished to the extent that the pressure in the combustion chamber is below its design point (derived for gas-only operation). Lower pressures means a higher exhaust temperature, a less efficient turbine, and diminished overall performance.

Ideally, the original compressor will be retained, and the pressure drop through the field will small enough that the adverse effect on turbine efficiency is only a percentage point or two. These losses will only affect hybrid operations (where the air is circulated through the field and then fired up to turbine inlet temperature with gas); after the field has been shut off, any additional gas burned over night will be at the design point efficiency of the turbine.

In configurations with a bottoming steam cycle (CC) would reduce the effect of pressure losses, because some of the excess heat passed into the turbine exhaust could be recovered: in a combined cycle plant, the steam turbine could be designed just slightly oversize so that, during hybrid operation, some of the excess heat in the turbine exhaust can be absorbed in the steam generator. The better part load performance of steam turbines, relative to gas turbines, makes this procedure worthwhile. However the system scale (2-4 MWe) contemplated here makes the economical inclusion of a steam turbine problematic.

Before turning to a more quantitative consideration of the consequences of pressure drop, the physical causes should also be outlined. The pressure drop, or head loss, in a horizontal pipe is a function of the fluid composition (including viscosity and density), pipe material, volume flow rate, pipe diameter, and pipe length. The OLAA system

definition leaves little choice as to the fluid type: air is to be used, although the viscosity will vary somewhat with temperature. The volume flow rate, diameter, and length are all interrelated in that they depend upon aspects of the field layout; for example, the number of dishes in each parallel series, or chain, between the compressor and the burner/turbine. For example, a longer chain will require a higher flow rate than shorter chain, to achieve the same field exit temperature. If the fluid density (controlled here by the pressure) is the same in both cases, then the higher flowrate will require a higher velocity, and incur much higher pressure losses. Alternatively, the pressure could be raised instead of the volume flowrate, thereby increasing the volume heat capacity of the flow and allowing for a longer dish series without increasing the velocity. Yet another alternative might involve enlarging the pipe diameter to reduce the velocity (and thus the pressure loss) while maintaining a high volume flowrate.

The validity of the OLAA piping concept comes down to the following question: Assuming that a reasonable pressure and flowrate have been chosen (i.e. compatible with the other parts of the system, such as receivers and turbine), will the pressure loss in the pipes be unacceptable? The following analysis details, in quantitative form, how this proof-of-concept calculation can be performed.

D.1.2.2 Quantitative Pressure Drop Analysis

Table **D-1** lists the input parameters for pressure loss, and the determinants of the total cost associated with the pipes. All of these variables must be included to in order to optimize the piping layout.

Table D-1: Selected Variables Affecting Pressure Drop and Net Piping Cost

Affecting Pressure Drop			**Affecting Net Piping Cost**		
Item	*Units*	*Power of Effect*	*Item*	*Units*	*Power of Effect*
Flow velocity	m^3/s	second	Pipe diameter	cm	more than linear
Pipe diameter	cm	linear	Pipe length	m	linear
Pipe length	m	linear	Loss from pressure drop	kWe/bar	linear[1]
Pipe roughness	mm	**linear or less**	Cost of insulation	$/m	linear
Fluid pressure	bar	fairly weak	Cost of pipe	$/m	linear
Fluid temp	K	very weak			

[1] The right-hand side of table **D-1** is fairly self-explanatory with the exception of the item "Loss from pressure drop" in kWe/bar. This rate, which represents the electricity which will not be generated for each bar of pressure loss in the piping field, must be determined separately for each power cycle, base pressure, *and pressure drop*. As discussed previously, the effect of pressure drops will be to reduce system efficiency and thus electrical output, but the nature of *this* reduction will not vary linearly with the pressure drop – rather, it must be calculated "on the fly" in the model and then used to determine the net costs. Of course, the variation of net cost with "loss from pressure drop" *will* be linear, because each kWe not manufactured can be viewed instead as a linear increase in piping costs. Thus table **D-1** lists this as a linear parameter but this should not create confusion.

The relationship between these variables is of crucial importance for the typical optimization problem. Suppose that you had a fixed mass flowrate, pipe length, pipe roughness, and fluid composition, and were trying to select the correct pipe size to reduce pressure losses to an acceptable level. (This is in fact the most fruitful way to think about the OLAA optimization). Pipe diameter becomes the key variable – but it's influence is far more important than the table above seems to suggest. As shown below, if mass flowrate is held fixed, then halving the pipe diameter has nearly a *fifth* power affect on the pressure drop – thus increasing it by a factor of thirty! (Actually, all of these powers *are* in table **III-x-x**: one from the diameter itself and four more from the all-important flow velocity, which is itself quadrupled by halving the pipe diameter: 1 + 2 x 2 = 5.)

Appendix **A** contains formulas for calculating the pressure drop in the field piping. Pressure calculations are achieved by means of the "Moody Chart" (White 1994 p. 318). The Moody chart is, in essence, a compilation of different flow formulae, each tailored to particular flow regimes (laminar, partly turbulent, fully turbulent). Most of the calculations here take place in the partly to fully turbulent regime (Reynold's numbers on the order of 100,000) due to the low viscosity of air, and in this regime the chart is thought to be accurate to within 15% (White 1994 p.317). In order to use the chart, the Reynold's number and the pipe roughness are required; with these inputs the chart yields the "Darcy friction factor", from which the pressure drop may be calculated directly. The greatest uncertainty is probably in the pipe "roughness" measurement, but this parameter has a weak effect (power of approximately $^1/_3$) on pressure loss in the regime of interest.

D.1.2.2.1 Worked Example

Suppose that at some point in the OLAA optimization procedure, the following set of conditions was specified:

Pressure: 14 bar
Temperature: 600 K
Flow rate: 1.25 kg / sec / dish-series
Pipe diameter: 10.0 cm

Let us further suppose that the flow passes through a 125 meter pipe on its way to the first dish, and then passes through seven dishes, each connected to the next by a 20 meter pipe. The last dish is connected by a 40 meter pipe to the combustion chamber. As the flow moves through the dishes, the pressure will drop and the temperature will rise. Because the mass flow is constant, both changes must result in a substantially higher velocity rate, which will increase the rate of pressure drop in a continuing cycle which will only be stopped when the flow reaches the combustion chamber.

Consider the first segment. Calculations based on the specified parameters quickly yield the following additional information:

Flow velocity: 18.95 m / sec

Viscosity: 3e-05 Nsec / m^2
Density: 8.4 kg / m^3

The viscosity is approximate, and is looked up in White (1994) using a temperature of 600 K, which is derived from the compression ratio and compressor efficiency (see **appendix A**). The density, velocity, viscosity, and diameter quickly give us:

Reynold's #: 530,600

In order to consult the Moody chart, we will also need the ratio between the "roughness" and the diameter, both expressed in length units. A typical roughness figure for commercial steel pipes is 0.046 mm (White 1994). Combining this figure with the diameter specified yields the:

Relative roughness: 0.0046

Consulting the Moody chart, we find that this Reynold's number and relative roughness yield:

Friction factor: 0.029

The friction factor formula (**appendix A**) can be use to yield the pressure drop if the pipe length, pipe diameter, flow velocity, and density are specified. In this case, the entrance pipe (125 meters) will incur the following pressure drop:

Pressure Drop, first 125 meters: 54.7 kPa = 0.55 bar

As noted, this is an isobaric, isothermal approximation based on inlet conditions, but the small size of the drop relative to the total pressure (just over 4%) justifies this approach for the level of accuracy required in this preliminary exploration. Two key questions can be addressed here in back-of-the envelope fashion:

What happens if the pipe's diameter is reduced?

If the diameter is *not* increased, approximately how large will the total pressure drop be, and what will be its effect on power plant performance?

D.1.2.2.2 Effect of Pipe Diameter Reductions

Consider first the effect of halving the pipe's diameter. This change will have probably have a roughly linear effect upon the pipe cost. However, as shown by the process calculation above and its accompanying formulas in Appendix **A,** the effect on pressure drop is far more dramatic: Halving the pipe diameter quadruples the flow velocity, doubles the Reynold's number, and halves the relative roughness. The latter has little effect, because as noted, the friction goes approximately as the cube root of roughness for

this flow regime (nearly but not quite fully turbulent). The Reynold's number dependence in this region is even weaker; in fact, doubling the Reynold's number in this case results in no more than a 10% change in friction factor. Thus we exit the Moody chart with a similar friction factor as before. However, the direct relationship between flow velocity and pressure drop, for a *fixed* friction factor, is quadratic (see formulas in **appendix A**). This means that quadrupling the velocity increases the pressure drop by a factor of sixteen. But that's not all; the formula for pressure loss also has a single inverse power of the diameter; by halving it, we add yet another doubling of the pressure drop. A final incremental adjustment (in this case, an increase of 28%) must be made to the friction factor before these five doublings are applied!

Thus halving the diameter results in an approximately 41-fold increase in the pressure drop. This is the key point about pipe sizing. To be precise, the following parameters have changed as a result of halving the pipe diameter:

Table D-2: Effect of Halving the Pipe Diameter, Specific Example

Item	Old Value	New Value	Units
Diameter	10	5	cm
Velocity	18.95	75.8	m / sec
Reynold's #	530,600	1.06 million	none
Relative roughness	0.0046	0.0092	none
Friction factor	0.029	.037	none
Pressure drop	.55	22.3	bar

Clearly, this new loss (22.3 bar) is grossly unacceptable, particularly when there are still 160 meters of pipe to go, which must operate at higher temperatures and thus lower densities and higher flowrates. (Needless to add, a pressure drop of this magnitude also invalidates the isobaric model).

Fortunately, the strong dependence of pressure drop on pipe diameter cuts the other way as well: losses can be dramatically reduced by quite modest enlargements in pipe size and cost. However, it should be noted that the receivers also incur pressure losses, and cannot be readily enlarged because of heat transfer and optical considerations.

D.1.2.2.3 Extension to Complete Loop

Suppose the fluid was to be heated to 1000 K in the dish field; it has begun at 600 K as a result of compression. Thus the average temperature in the field will be about 800 K; this is 1.33 times higher than the temperature we began with. This higher average temperature means a lower average density and thus a higher average flow velocity:

Initial Temp: 600 K Approximate Average Temp: 800 K

Initial Density: 8.4 kg/m^3	Approximate Average Density[2]: 6.3 kg/m^3
Initial Velocity: 18.95 m/s	Approximate Average Velocity: 25.2 m/s
	Adjusted for Second Power Significance: 26.0 m/s
Initial Vicosity: 3.0e-05 Nsec / m^2	Approximate Average Viscosity: 3.8e-05 Nsec / m^2

Continuing on this "approximate average" (AA) basis, we can calculate the pressure drop over the total remaining length (160 m) using the same procedure as before:

Reynold's #:	418,000	(a 21% reduction)
Friction factor:	0.30	(essentially the same)
Pressure drop:	1.02 bar	
Total pressure drop:	1.52 bar	(3 times the feed pipe pressure drop alone)

Our question becomes, what effect does a drop in pressure of 1.5 bar have upon the efficiency of a gas turbine which normally operates at 14 bar? Section **III.x.x** introduced the gas turbine modeling methodology which is common to the MPT and the LDA. **Figure III-x-x** presents theoretical results for turbines operating under the conditions required by the example problem presented in this section.

The worked example above, together with the data in the figures, indicate that a pressure drop on the order of 1.5 bars can be expected if a 14 bar compressor is coupled to a 10 cm piping network arranged in series of 7 dishes. This pressure loss may be unacceptable: open-cycle turbine efficiency drops from 30.2% to 27.5% (an 8.9% gas turbine power loss). It is important to note that these results are for operation at maximum (design point) insolation. In the evening or at night, when some or all of the compressor air bypasses the dish field and passes directly to the combustor, these power losses will not be felt. Using a rule-of-thumb annual solar fraction of 0.25, the net annualized power loss from the 3 bar pressure drop will be on the order of 2-3%.

Several measures could be taken to reduce the field pressure drop and the turbine efficiency penalty it causes. As we have seen, increasing the piping diameter will rapidly improve the pipe performance. However, when this was attempted, pressure drops in the individual receivers rapidly became the dominant restraint. A more successful strategy would be to reduce the number of dishes in the series from eight to three or four. Although helpful, this step will create complicate the field geometry, and does not solve the dish/pipe coupling problem nor the general insulation problem.

[2] This figure neglects the density decreases due to pressure drops and only addresses those caused by temperature. This procedure assumes the pressure drops are only incremental; as we will see, that is not the case, and the average density will be even lower, leading to a need for even larger pipes.

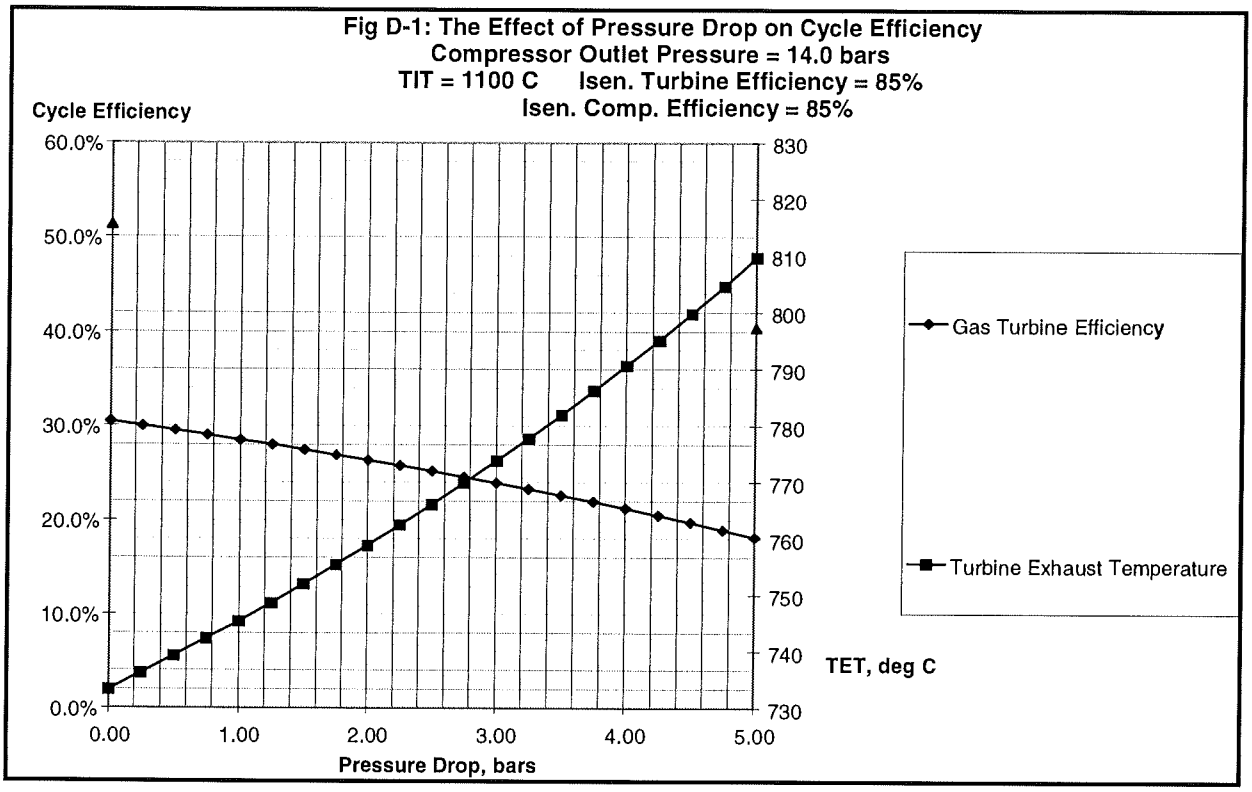

D.1.3 Decision to Suspend Further Investigation

Evaluation of the LDA pressure drop challenges, while no conclusive by any means, raised enough doubt (especially in light of the uncertainties surrounding the physical joint between piping and receiver) that a decision was made to devote more attention to the mini power tower (MPT) and dish engine (ASDB) designs and suspend investigation of the linked dish array. The next step would have been a careful analysis and proof-of-concept calculation for the thermal losses and associated insulation costs. It is expected that such an investigation would, like the pressure analysis, raise a number of doubts. However, the problems are complex rather than insuperable, and the theoretical advantages of a hot-air LDA (particularly as a hybrid system) remain, justifying further investigation by others should they wish to pursue it.